Strong Interaction Corrections to the Weak Radiative B-Meson Decay at Order $\mathcal{O}(\alpha_s^2)$ with Exact Dependence on the c-Quark Mass

Abdur Rehman

PhD dissertation under the supervision of
prof. dr hab. Mikołaj Misiak
at the Institute of Theoretical Physics, Faculty of Physics, University of Warsaw.

Warsaw, July 2015

Abstract

The process $\bar{B} \to X_s\gamma$ is known to provide important constraints on extensions of the Standard Model (SM). The present SM prediction for its CP- and isospin-averaged branching ratio reads $\mathcal{B}(\bar{B} \to X_s\gamma)^{\mathrm{SM}} = (3.36 \pm 0.23) \cdot 10^{-4}$. It agrees very well with the current experimental average $\mathcal{B}(\bar{B} \to X_s\gamma)^{\mathrm{exp}} = (3.43 \pm 0.22) \cdot 10^{-4}$. The experimental accuracy is expected to improve in a significant manner after the Belle-II experiment begins collecting data within the next few years. Consequently, theoretical calculations must also be upgraded to match the experimental precision.

A considerable contribution to the current theoretical uncertainty originates from the fact that some of the Next-to-Next-to-Leading-Order strong interaction corrections (called $K_{17}^{(2)}$ and $K_{27}^{(2)}$) have not yet been calculated for an arbitrary value of the charm and bottom quark mass ratio m_c/m_b. Instead, known results for these corrections at $m_c = 0$ and for $m_c \gg m_b/2$ serve as a basis for an interpolation in m_c, which introduces around $\pm 3\%$ uncertainty into $\mathcal{B}(\bar{B} \to X_s\gamma)^{\mathrm{SM}}$.

In order to remove this uncertainty, determining the exact dependence of $K_{17}^{(2)}$ and $K_{27}^{(2)}$ on the c-quark mass is necessary. In the language of Feynman diagrams with unitarity cuts, four-loop diagrams with two mass scales (m_c and m_b) need to be evaluated. The necessary ultraviolet counterterms involve three-loop two-mass-scale diagrams that must be calculated up to $\mathcal{O}(\varepsilon)$ in the dimensional regularization parameter ε.

In the present thesis, we evaluate [1] the exact dependence on the c-quark mass of all the necessary ultraviolet-counterterm diagrams that contribute to the yet-unknown parts of $K_{17}^{(2)}$ and $K_{27}^{(2)}$. These corrections originate from interferences of four-quark and photonic dipole operators. They are currently responsible for the main uncertainty in the perturbative contribution to $\mathcal{B}(\bar{B} \to X_s\gamma)^{\mathrm{SM}}$.

Apart from the calculation for arbitrary m_c, we also evaluate many of the necessary counterterm contributions at $m_c = 0$, and present them to all orders in ε wherever possible. Our results have contributed to the evaluation of the $m_c = 0$ boundary for the interpolation, and thus to the recently published updated phenomenological analysis of $\mathcal{B}(\bar{B} \to X_s\gamma)^{\mathrm{SM}}$ [2].

The thesis contains many technical details that have not been presented elsewhere, namely explicit expressions for all the relevant quantities in terms of the master integrals, as well as results for these integrals obtained using several different methods, involving Mellin-Barnes techniques and differential equations.

Contents

Chapter 1

Introduction

This thesis is based on the Standard Model (SM) [3–18] of elementary particle physics which describes our current knowledge of the three fundamental non-gravitational forces: strong, electromagnetic and weak. It is remarkable that all these three interactions are based on a common principle of gauge invariance, and successfully described by a local relativistic and renormalizable quantum field theory.[1] The mechanism of Electroweak Symmetry Breaking (EWSB) occurring at the scale $v \sim 248$ GeV is a main component of the SM. The scale v corresponds to the vacuum expectation value of the Higgs doublet that gives masses to the weak bosons $W^{\pm}$ and Z^0, leaving the spinless boson h^0 as the physical degree of freedom. In July 2012, the SM emerged as a complete theory in the sense that its last missing particle h^0 was experimentally found with mass around 126 GeV [20, 21].

The SM is an impressive theoretical achievement and one of the best successfully tested theories of contemporary physics. It has been investigated to a great precision at dedicated particle accelerator facilities [22]. In particular, the gauge sector of the SM has been extensively studied at the Large Electron-Positron (LEP) collider [23] at the European Organization for Nuclear Research (CERN), at the Stanford Linear Accelerator Center (SLAC), as well as at the Tevatron accelerator at the Fermi National Accelerator Laboratory (FNAL). These experiments have tested many SM observables reaching the accuracy of below per-mille level, becoming sensitive to loop quantum corrections of electroweak origin. Also, loop corrections due to Quantum Chromodynamics (QCD) played an important role in comparing theory predictions to the experimental results. Some of the noteworthy examples of relevant higher-order electroweak corrections occur in the case of the ρ-parameter [24–28], the muon decay and the Fermi constant G_F [29, 30], the Weinberg mixing angle extracted from leptonic observables [31], as well as anomalous magnetic moments of both the electron and the muon. In the anomalous magnetic moment cases, accuracies reaching one part in 10^9 [32] and one part in 10^6 [22] have been reached for the electron and muon, respectively. With such an accuracy, the anomalous magnetic moments (despite being leptonic quantities) become sensitive to strong interaction effects, which in the muonic case are the main limitation for further improving the accuracy on the theory side. Other examples of observables allowing for very precise comparisons between the SM predictions and data are the bound state spectra of positronium [33] and muonium. At present, no clear contradiction between the SM predictions

[1] See Ref. [19] for a sample list of textbooks on the SM and field theory.

and experimental data is observed, after supplementing the SM with neutrino masses stemming from dimension-five operators, as well as an extra weakly-interacting particle to describe Dark Matter (DM) in the Universe. There are a few measurements in which tensions with the SM predictions occur, but they either seem to be debatable or at least statistically allowed given the large number of observables considered.

Despite its success, one should keep in mind that the SM is likely only an effective theory that describes Nature at low energies, at or below the EWSB scale. At higher energies, beyond-SM degrees of freedom may become dynamical. Their possible existence could help us in better understanding the EWSB mechanism, neutrino masses and mixings, or the observed asymmetry between baryons and anti-baryons in the Universe. In general, a New Physics (NP) theory at the TeV scale or above is expected to satisfy the following requirements: (i) its gauge group should contain the $SU(3)_C \times SU(2)_L \times U(1)_Y$ of the SM, (ii) it should incorporate all the SM degrees of freedom either as fundamental or composite fields, and (iii) it should reduce to the SM in the low-energy limit. A search for Beyond-SM (BSM) theories is actively being carried out in two complementary ways, namely via direct production searches (high energy frontier) and via indirect searches (high intensity frontier). Both approaches require sincere theoretical predictions with quantifiable error estimates. In both of them, an important issue is to keep quantum effects under control, particularly the QCD ones. The main purpose of the Large Hadron Collider (LHC) are the direct searches at the TeV scale and beyond. So far, no direct evidence of NP has been found. At the same time, low energy measurements are becoming progressively accurate, increasing their potential of indirect searches. This requires higher precision on the theoretical side. In many cases, higher-order perturbative quantum corrections need to be calculated. It is particularly relevant for processes where virtual exotic particles might contribute to loop amplitudes. A well-known class of such processes are Flavor Changing Neutral Current (FCNC) decays which arise only at the one-loop level in the SM. An important difficulty in their case is that they involve quarks, so a good control over QCD effects is required to reach a percent-level accuracy.

The flavor structure of the SM is dictated by the Higgs-quark-antiquark Yukawa interactions which generate the quark masses when the Higgs field acquires its vacuum expectation value. The Yukawa coupling matrices contain a sizeable number of independent parameters. In the quark sector, these are the 6 physical masses of quarks and four parameters (3 angles and one phase) of the Cabibbo-Kobayashi-Maskawa (CKM) matrix [34, 35]. The CKM matrix describes the quark mass eigenstate mixing under weak interactions. Numerical values of these parameters are not predicted by the SM but rather have to be extracted from measurements before making any theoretical prediction.[2]

In the present thesis, we will focus on the quark flavor sector of the SM in the context of a subclass of B-meson decays, specifically the weak radiative B-meson decay. For definiteness, let us consider the mesons being bound states of the b quark and one of the light antiquarks ($\bar{u}$ or $\bar{d}$). The $b\bar{u}$ bound state is called B^-, and the $b\bar{d}$ bound state is called $\bar{B}^0$. Both of them will commonly be denoted by $\bar{B}$. We shall consider their weak radiative decays into a photon and any hadronic final state that contains no charmed ($C \neq 0$) particles, and has nonvanishing strangeness ($S \neq 0$), i.e. contains an unbalanced s quark. We shall sum over all the possible final states satisfying the above requirements,

[2] Some standard reviews of heavy flavor physics can be found in Refs. [36, 37].

which means considering an inclusive process. The branching ratio of this process is denoted by $\mathcal{B}\left(\bar{B} \to X_s\gamma\right)$. Its evaluation and/or measurement involves taking an average over $\bar{B} = B^-$ and $\bar{B} = \bar{B}^0$ (see Sec. 2.3 for more details).

Since the early 1990's, the decay $\bar{B} \to X_s\gamma$ has been one of the most frequently considered processes in flavor physics. It is well known as an invaluable and-well established means to constrain parameter spaces of BSM models. Being generated by the quark-level $b \to s\gamma$ FCNC transition in the SM, it receives dominant contributions from loop diagrams involving the W boson and up-type quarks. Sample Leading Order (LO) diagrams for $\bar{B} \to X_s\gamma$ in the SM, multi-Higgs doublet models and the Minimal Supersymmetric Standard Model (MSSM) are shown in Fig. 1.1. One can see that the SM contribution

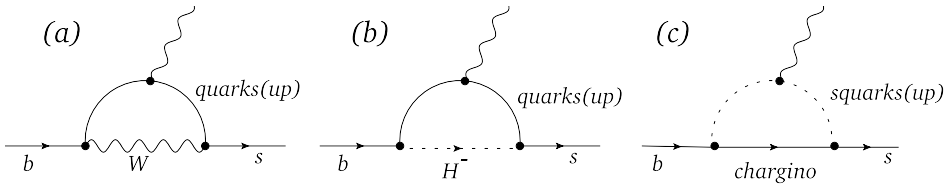

Figure 1.1: Sample LO diagrams for $\bar{B} \to X_s\gamma$ in the SM (a), multi-Higgs doublet model (b) and MSSM (c), respectively.

is of the same perturbative order as the possible BSM ones. Comparable contributions in the multi-Higgs doublet models can arise from loops with charged scalars as shown in Fig. 1.1(b). In the supersymmetric theories, chargino-squark loops shown in Fig. 1.1(c) often become important, even in scenarios with minimal flavor violation and moderate $\tan\beta$. In the SM, the considered decay receives an additional chirality suppression by a factor of m_b/m_W. Such a chirality suppression may be off-set in certain NP models like the MSSM with large $\tan\beta$ or left-right models. Therefore, constraints from $b \to s\gamma$ on such models are particularly severe [38, 39]. However, the power of $\bar{B} \to X_s\gamma$ for indirectly testing NP models depends on the accuracy of its measurements and precision of theoretical predictions.

Another application of $\bar{B} \to X_s\gamma$ that has frequently been discussed in the literature is constraining the Heavy Quark Effective Theory (HQET) [40] parameters that matter for extraction of the CKM elements $|V_{cb}|$ and $|V_{ub}|$ from the semileptonic B-meson decays. However, this application is now mostly of historical importance because of growing accuracy in the determination of these parameters from the semileptonic decays alone [41], and to intrinsic uncertainties generated by the charm-quark loop contributions to $\bar{B} \to X_s\gamma$.

As far as the measurements are concerned, the first observation of an exclusive hadronic process that is generated by $b \to s\gamma$, namely $B \to K^*\gamma$, was performed by the CLEO collaboration in 1993 [42]. Both at CLEO and at the so-called B-factories that started their operation in the late 1990's (Belle and Babar), electron-positron collisions at the center-of-mass energy overlapping with the $\Upsilon(4S)$ resonance were used to produce the B mesons. At Belle, a significant fraction of time was also spent at the $\Upsilon(5S)$ resonance, where B_s production in addition becomes kinematically allowed.

The current measurements of the CP- and isospin-averaged branching ratio of $\bar{B} \to X_s\gamma$ performed by CLEO [43], Belle [44,45] and Babar [46]- [50] contribute to the following

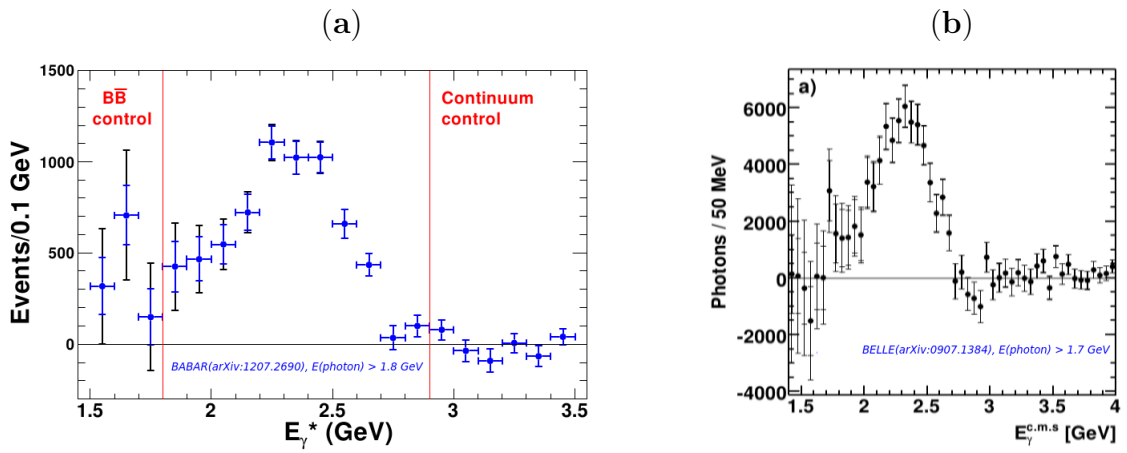

Figure 1.2: The measured photon energy spectra in $\bar{B} \to X_s\gamma$ as measured by the (a) Babar [46] and (b) Belle [44] experiments. The peaks are centered around $E_\gamma \simeq m_b/2 \simeq 2.35\,\text{GeV}$ which corresponds to the photon energy in the two-body partonic decay $b \to s\gamma$ with an approximately massless s quark.

world average [51]

$$\mathcal{B}\left(\bar{B} \to X_s\gamma\right)^{\text{exp}}_{(E_0=1.6)} = (3.43 \pm 0.21 \pm 0.07) \cdot 10^{-4}, \tag{1.1}$$

where the last error (± 0.07) originates from the photon spectrum modeling, while the first one (± 0.21) contains the remaining systematic errors together with the statistical one. This average, performed by the Heavy Flavor Averaging Group (HFAG), corresponds to including only photons whose energies E_γ are larger than E_0 in the B-meson rest frame, and E_0 is set to 1.6 GeV. The averaging involves an extrapolation[3] from measurements performed at $E_0 \in [1.7, 2.0]\,\text{GeV}$. A combination of the experimental results and their extrapolation to $E_0 = 1.6\,\text{GeV}$ are performed in the same step, to minimize model dependence. The experimental cuts at $E_0 \in [1.7, 2.0]\,\text{GeV}$ are necessary due to rapidly growing backgrounds at lower energies. On the other hand, theoretical predictions become less precise with growing E_0 (see below). Thus, an intermediate value of E_0 must be chosen for comparing theory with experiment. A conventional choice of $E_0 = 1.6\,\text{GeV}$ was proposed in Ref. [52], and it is being followed since then. The raw photon energy spectra in the inclusive measurements are shown in Fig. 1.2. One can see that the uncertainties grow for smaller photon energies in both plots. It is due to subtraction of a larger and more uncertain background. The background originates from the so-called continuum processes (i.e. e^+e^- collisions that produce no B mesons), as well as, e.g., radiatively decaying π^0 and η particles produced in purely hadronic B-meson decays.

It is worth to emphasize that at the LHCb (a hadronic collider) at CERN, only measurements of exclusive $b \to s\gamma$ decay modes are feasible. The advantage of B-factories is that radiative B decays can be studied both inclusively and exclusively. An important improvement in the accuracy of the inclusive $\mathcal{B}\left(\bar{B} \to X_s\gamma\right)$ measurement is expected at Belle II [53] which is being constructed at present, and scheduled to begin collecting data in October 2017. It aims at collecting 50 times more $e^+e^- \to \Upsilon(4S) \to B\bar{B}$ events than

[3] Further comments on this extrapolation can be found in Sec. 2.1.3.

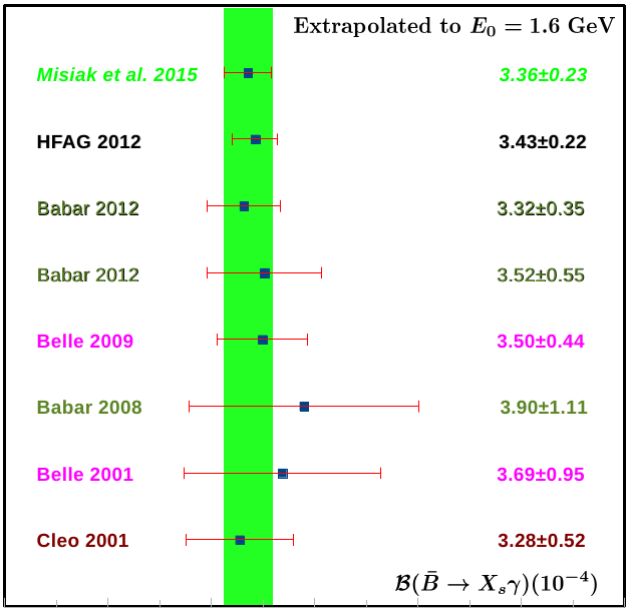

Figure 1.3: A summary of the $\mathcal{B}\left(\bar{B} \to X_s\gamma\right)$ measurements, and their comparison to the current SM prediction [2].

the previous B-factories taken together. Much larger statistics will allow to efficiently use the so-called hadronic tagging which practically removes the continuum background, and thus leads to a reduction of systematic errors, too.

On the theoretical side, the flavor changing weak interactions are described by the well-established Effective Field Theory (EFT) framework. Exploiting the Heavy Quark Expansion (HQE) within this framework, one shows [54–61] that the inclusive decay rate $\Gamma\left(\bar{B} \to X_s\gamma\right)$ is well approximated by the partonic decay rate[4]

$$\Gamma\left(\bar{B} \to X_s\gamma\right) = \Gamma\left(b \to X_s^{\text{partonic}}\gamma\right) + \delta\Gamma_{\text{nonp}}. \tag{1.2}$$

Here, X_s^{partonic} stands for $s, sg, sgg, sq\bar{q}, \ldots$ being partonic states with $q = u, d, s$ only. The detailed analysis of Ref. [61] results in an estimate of $\delta\Gamma_{\text{nonp}}/\Gamma\left(\bar{B} \to X_s\gamma\right)$ at the level of 0.05 or below, which is often expressed as the statement that "nonperturbative corrections" do not exceed 5% of the decay rate. The qualitative reason why the considered inclusive decay of the B meson can be very well described perturbatively is the fact that the b-quark mass m_b (or the B-meson mass $m_B \simeq 5.3\,\text{GeV}$) is much larger than the QCD confinement scale $\Lambda \sim m_B - m_b \sim 0.6\,\text{GeV}$, and that all the decay products are much lighter than m_b. It is also important that the numerically dominant contribution comes from processes where the b-quark decay and the photon emission occur practically at the same point, i.e. at distances much smaller than $1/\Lambda$.

Nonperturbative corrections in the considered case can be studied using the framework of HQET, as well as the Soft-Collinear Effective Theory (SCET). It is important to keep in mind that some of the nonperturbative effects are not suppressed by $\Lambda^2/m_{b,c}^2$ but only by $\Lambda^2/(m_b - 2E_0)^2$ or $\Lambda^2/(m_b^2 - 2m_bE_0)$ (see, e.g., Ref. [62]). Such a behavior is precisely the reason of the above-mentioned growth of theoretical uncertainties when E_0 tends to

[4] known also as the spectator model rate

Nonperturbative	5%	mostly $\mathcal{O}(\alpha_s\Lambda/m_b)$
Parametric	2%	$\alpha_s(M_Z)$, CKM, ...
Higher order	3%	tested by varying renormalization scales
m_c-interpolation	3%	matrix elements of $(\bar{s}c)_{V-A}(\bar{c}b)_{V-A}$ operators

Table 1.1: A breakdown of uncertainties in the current SM prediction for $\mathcal{B}(\bar{B} \to X_s\gamma)^{\rm SM}$ in Refs. [2, 64].

its perturbative kinematical endpoint of $m_b/2 \simeq 2.35\,\text{GeV}$. Therefore, extrapolating the experimental results down to a relatively low value of $E_0 = 1.6\,\text{GeV}$ (following the so-called shape function models with parameters fit to data) is advantageous with respect to performing the theory-experiment comparison directly at a higher value of E_0.

Both the perturbative and nonperturbative contributions are suitably studied within an effective theory obtained from the SM after decoupling the W boson and all the heavier particles. The effective weak interaction Lagrangian takes the form $\mathcal{L}_{\rm eff} \sim C_i Q_i$, where Q_i stand for operators containing the b quark and all the lighter fields, while C_i are the Wilson coefficients. The Renormalization Group (RG) improved perturbation theory is used to resum large logarithms of the form $(\alpha_s \ln m_W^2/m_b^2)^n$, $n = 0, 1, 2, \ldots$, which provides sufficient accuracy in the Wilson coefficient evaluation. The partonic decay rate (with $E_\gamma > E_0$) can be written in the following form

$$\Gamma(b \to X_s^{\rm partonic}\gamma) \;\sim\; C_i(\mu_b)C_j(\mu_b)G_{ij}(E_0,\mu_b) \tag{1.3}$$

where $\mu_b \sim m_b/2$ is the scale at which the Wilson coefficients are renormalized, while G_{ij} describe interferences between amplitudes generated by the operators Q_i and Q_j (see Chapter 2 for details). A summary of the Next-to-Leading Order (NLO) QCD calculations is given in Ref. [63], while the current status of the Next-to-Next-to-Leading Order (NNLO) QCD calculations is summarized in Refs. [2, 64]. Some additional information on the NNLO contributions can be found in Ref. [65].

The first NNLO estimate of the inclusive $\mathcal{B}\left(\bar{B} \to X_s\gamma\right)$ within the SM was given in 2006, in Ref. [66]. Very recently, we have provided in Ref. [2] an updated NNLO QCD prediction for the CP- and isospin-averaged branching ratio. The result reads

$$\mathcal{B}\left(\bar{B} \to X_s\gamma\right)^{\rm SM} = (3.36 \pm 0.23) \cdot 10^{-4} \tag{1.4}$$

for $E_0 = 1.6$ GeV. This SM prediction includes the NNLO QCD ($\mathcal{O}(\alpha_s^2)$) corrections and the $\mathcal{O}(\alpha_{em})$ electroweak ones. Its total error amounts to around 7% which is obtained by summing in quadrature four types of uncertainties shown in Tab. 1.1: (i) nonperturbative (5%), (ii) parametric (2%), (iii) higher-order ($\mathcal{O}(\alpha_s^3)$) perturbative (3%), (iv) the one stemming from m_c-interpolation ambiguity in the $\mathcal{O}(\alpha_s^2)$ correction (3%). The present status of $\mathcal{B}(\bar{B} \to X_s\gamma)$ is summarized in Fig. 1.3, with all the individual measurements extrapolated to $E_0 = 1.6\,\text{GeV}$ following the HFAG method [51].

The current experimental world average in Eq. (1.1) agrees very well with the SM prediction in Eq. (1.4). The SM result has moved towards the experimental value (as compared to Ref. [66]). In effect, a new bound on the charged Higgs boson mass in the two-Higgs-doublet-model II is now stronger. It reads $M_H^\pm > 480$ GeV at 95%C.L. and $M_H^\pm > 358$ GeV at 99%C.L. Similarly severe restrictions arise on parameters of the MSSM

and models alike. Such constraints can become particularly important when positive signals for new particles are seen at the LHC but ambiguities in measurements of their masses and couplings remain. For this reason, efforts towards improving accuracy of the branching ratio determination are undertaken on both the experimental and theoretical sides.

In the present thesis, we focus on a calculation that contributes to removing the fourth type of uncertainty in Tab. 1.1, namely the one due to the interpolation in m_c of the dominant m_c-dependent $\mathcal{O}(\alpha_s^2)$ corrections to the perturbative decay rate $\Gamma(b \to X_s^{\rm partonic}\gamma)$. These corrections are called $K_{17}^{(2)}$ and $K_{27}^{(2)}$. They are due to interferences of certain four-quark operators with the photonic dipole one.[5] Their evaluation for an arbitrary value of m_c is a very difficult task. In the language of Feynman diagrams with unitarity cuts, four-loop diagrams with two mass scales (m_c and m_b) need to be evaluated. The necessary ultraviolet counterterms involve three-loop two-mass-scale diagrams that must be calculated up to $\mathcal{O}(\varepsilon)$ in the dimensional regularization parameter ε.

So far, such calculations have been performed only for $m_c \gg m_b/2$ [67, 68] and for $m_c = 0$ [64]. They have served as a basis for the above-mentioned interpolation in m_c. The only way to remove the interpolation uncertainty is to perform these calculations again, this time for an arbitrary value of the charm quark mass.

Here, we evaluate [1] the exact dependence on the c-quark mass of all the necessary ultraviolet-couterterm diagrams that contribute to the yet-unknown parts of $K_{17}^{(2)}$ and $K_{27}^{(2)}$. Using the optical theorem, we express the relevant contributions to the decay rate in terms of imaginary parts of three-loop two-scale propagator diagrams. Chapter 3 is dedicated to presenting technical details of our calculations. One important element in our procedure is an automatized reduction using Integration By Parts (IBP) [69,70] of $\mathcal{O}(10^3)$ loop-integrals to a much smaller set of the so-called Master Integrals (MIs). We follow the Laporta algorithm [71] that has been implemented by different authors in several publicly available computer algebra codes, e.g., `AIR` [72], `FIRE` [73, 74] or `REDUZE` [75]. We have extensively used both the `Mathematica` and `C++` versions of `FIRE`.

Once the master integrals are found, the calculation of the MIs is necessary, which constitutes the most difficult task of the entire calculation. We mainly apply the Differential Equation (DE) method [76–78], while other methods are used for cross-checks only. In the DE method, the set of MIs is extended to make it closed under differentiation with respect to $z = m_c^2/m_b^2$, and a system of differential equations is numerically solved starting from initial conditions at large z. It cannot be done along the real axis due to presence of spurious singularities, but rather along an ellipse in the complex plane. The initial conditions are found using asymptotic expansions, which effectively reduces our three-loop two-scale problem to a two-loop single-scale one.

Apart from our arbitrary-m_c calculation, we have confirmed and further extended some of the counterterm contributions in the $m_c = 0$ case to all orders in the Dimensional Regularization (DR) [79] parameter ε. In this way, we have contributed to the analysis of Ref. [2] where the interpolation in m_c is still applied.

The thesis is organized as follows. Sec. 2.1 of Chapter 2 is devoted to a comprehensive analysis of the theoretical framework for B-decays. In Secs. 2.2 and 2.3, the m_c-dependent matrix elements and the branching ratio formula are discussed, respectively. We dedicate

[5] Definitions of the operators and details of the notation will be presented in the following chapters.

Chapter 3 to a presentation of techniques that have been applied for evaluation of our loop integrals: the Feynman and Schwinger parameterizations, Mellin-Barnes techniques, differential equations and the sector decomposition. Explicit results for the MIs we have calculated are also presented there. Our final results for the $\mathcal{O}(\alpha_s^2)$ counterterms are given in Chapter 4, while the (ongoing) bare $\mathcal{O}(\alpha_s^2)$ calculation is discussed in Chapter 5. We conclude in Chapter 6. Finally, several useful formulae are provided in the Appendices.

Chapter 2

Inclusive $\bar{B} \to X_s\,\gamma$ in the Standard Model

In the present chapter, Sec. 2.1 covers the basic and technical aspects of setting up a low energy effective theory that is valid below the electroweak scale. We focus on its elements that are relevant to $\bar{B} \to X_s\,\gamma$. Sec. 2.2 is devoted to discussing the phenomenological role of the matrix elements that constitute the main topic of this thesis. In Sec. 2.3, we present in more detail the current status of the considered process branching ratio calculations.

2.1 Theoretical framework for radiative B-decays

The weak radiative B meson decays are generated by loop diagrams involving the electroweak-scale particles (notably the W boson and the top quark), while the external momenta are of the order of the b-quark mass which is much smaller than the electroweak scale. In consequence, in the perturbatively calculated partonic rate $\Gamma\left(b \to X_s^{\text{partonic}}\gamma\right)$ one encounters QCD corrections that are enhanced by powers of logarithms $\ln(m_W^2/m_b^2)$. In fact, the QCD perturbation series turns out to be a series in powers of $(\alpha_{\rm s}(m_b))^n\ (\alpha_{\rm s}(m_W)\ln(m_W^2/m_b^2))^m$, with $n, m = 0, 1, 2, \ldots$. Given the numerical values of $\alpha_{\rm s}(m_b) \sim 0.22$ and $\alpha_{\rm s}(m_W)\ln(m_W^2/m_b^2) \sim 0.7$, it makes sense to treat these quantities as formally independent, and resum the series in the latter one, still working order-by-order in $\alpha_{\rm s}(m_b)$. It can most conveniently be achieved in the framework of an effective theory where Renormalization Group Equations (RGE) [80] for the Wilson coefficients work as a tool for the large logarithm resummation.[1] In Sec. 2.1.1, the effective Lagrangian is constructed from the SM by decoupling the W boson and all the heavier degrees of freedom, which is closely related to the Operator Product Expansion (OPE) [81, 82]. In perturbation theory, such a procedure can be thought about as an extension of the so-called decoupling theorem by Appelquist and Carazzone [83]. Once the effective Lagrangian is defined, we discuss the three necessary steps for evaluation of the QCD corrections to $\mathcal{B}(\bar{B} \to X_s\,\gamma)$: determining the matching and mixing in Sec. 2.1.2, and calculating the matrix elements in Sec. 2.1.3.

[1] Construction of effective theories and using the RGE is a general method for resummation of all sorts of large logarithms of scales that appear in physical amplitudes in Quantum Field Theory (QFT).

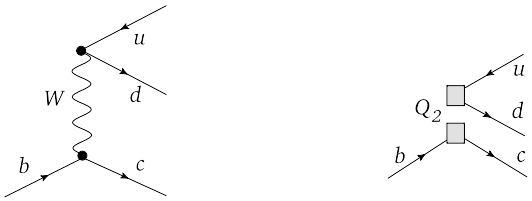

Figure 2.1: The LO $b \to cd\bar{u}$ process in the SM and in the low energy effective theory. Gray boxes show an insertion of one of the effective operators.

2.1.1 The effective Lagrangian and choice of the operators basis

The core idea of OPE [81, 82] is a factorization of long- and short-distance physics. In weak decays, OPE allows to derive an effective low-energy theory for describing the weak interactions of quarks. We shall begin with illustrating this idea using a simpler example than $b \to s\gamma$. Let us consider a tree-level $b \to cd\bar{u}$ transition that is mediated by the W boson, as depicted in Fig. 2.1 (left). There are two reasons why we have chosen this very example for the sake of illustration. First, such a process is sensitive to QCD effects. Second, it involves quarks of four different flavors, so the number of relevant effective operators will be very limited. The amplitude corresponding to the LO Feynman diagram of this process in the SM reads (in the 't Hooft-Feynman gauge):

$$A = \left(\frac{-ig_2}{\sqrt{2}}\right)^2 V_{cb}V_{ud}^* \left(\bar{d}_L\gamma_\mu u_L\right) \frac{ig^{\mu\nu}}{m_W^2 - q^2} \left(\bar{c}_L\gamma_\nu b_L\right) \tag{2.1}$$

where $g_2 = e/\sin\theta_W$, and the maximum momentum transfer squared is $q^2_{max} = (m_b - m_c)^2$. Throughout the thesis, we treat the three lightest (u, d and s) quarks as massless. For brevity, we use identical notation for the quark fields and the corresponding Dirac spinors. Their left- and right- handed projections are denoted in the standard manner, i.e. $\psi_{L,R} = P_{L,R}\,\psi$, where $P_{L,R} = (1 \mp \gamma_5)/2$.

The W-boson mass $m_W \simeq 80$ GeV is over 16 times larger than $\sqrt{q^2} < m_b \sim 5\,\text{GeV}$, i.e. $q^2/m_W^2 < 0.004$. Thus, one can perform a Taylor expansion of the W-propagator into an infinite sum of local terms using $(1-x)^{-1} = \sum_{n=0}^{\infty} x^n$. Then the amplitude takes the form

$$A = -i\,2\sqrt{2}\;G_F\,V_{cb}V_{ud}^* \left(\bar{d}\,u\right)_{V-A} \left(\bar{c}\,b\right)_{V-A} \sum_{n=0}^{\infty} \frac{q^{2n}}{m_W^{2n}} \tag{2.2}$$

where $G_F = g_2^2/(4\sqrt{2}m_W^2)$ is the Fermi constant, and $(2\sqrt{2}G_F)^{-1/2} \simeq 174\,\text{GeV}$. The CKM matrix elements are denoted by V_{ij}, while $\left(\bar{d}\,u\right)_{V-A}$ stands for $\bar{d}_L\gamma_\mu u_L$ (and similarly for other flavors).

It is easy to verify that the r.h.s. of Eq. (2.2) can equivalently be obtained from the following LO effective weak interaction Lagrangian term:

$$\mathcal{L}_{\text{eff}} = -\frac{4G_F}{\sqrt{2}} V_{cb}V_{ud}^* \sum_{n=0}^{\infty} \frac{1}{m_W^{2n}} Q^{(n)}, \tag{2.3}$$

where the operators $Q^{(n)}$ are given (in position space) by

$$\left(\bar{d}\,u\right)_{V-A}\left[(-1)^n\Box^n\right]\left(\bar{c}\,b\right)_{V-A} \tag{2.4}$$

with $\Box \equiv \partial^\alpha\partial_\alpha$ denoting the d'Alembertian. The dimensionality of the operators $Q^{(n)}$ in the units of mass is $6+2n$, i.e. $[Q^{(n)}] = 6+2n$. Due to the suppression of higher-n operators by inverse powers of m_W, the first term is a good approximation. In fact, higher-dimensional operators are practically always negligible from the phenomenological standpoint in the SM analyses of FCNC processes.

Our particular set of operators in Eq. (2.4) is sufficient only at the tree level, before turning on the QCD and QED interactions. Other operators are expected to arise at higher orders in perturbation theory. However, since the number of operators of a given dimension is finite, we can always restrict to a finite basis after fixing the required level of precision for evaluation of physical quantities. Consequently, we never have to deal with explicit renormalization of an infinite tower of operators, and our effective theory is predictive even though it could be called "nonrenormalizable" in the traditional sense.

From now on, we shall restrict to the dimension-six ($n=0$) operators alone, assuming that it is sufficient for the required precision in our example. Taking into account possible generation of other operators at the dimension-six level, we write

$$\mathcal{L}_{\text{eff}} = \frac{4G_F}{\sqrt{2}}V_{cb}V_{ud}^*\sum_m C_m\,Q_m^{(0)} \tag{2.5}$$

where the summation is always finite, and we will drop the superscript (0) below. Eq. (2.5) illustrates that the local operators are weighted by effective couplings C_m called Wilson coefficients.

Let us now figure out explicitly what particular operators can arise from $\left(\bar{d}\,u\right)_{V-A}\left(\bar{c}\,b\right)_{V-A}$ after including effects of the strong interactions. Since these interactions are chirality-conserving, they cannot produce anything but the $(V-A)\times(V-A)$ structures at the dimension-six level. Moreover, the flavor content of all the operators must remain the same. Thus, it is only the color structure (i.e. contraction of the color indices) that may change with respect to our initial operator. We conclude that to all orders in QCD we have the following form of the Lagrangian

$$\mathcal{L}_{\text{eff}} = \frac{4G_F}{\sqrt{2}}V_{cb}V_{ud}^*\left(C_1Q_1^{ducb} + C_2Q_2^{ducb}\right), \tag{2.6}$$

where $Q_1^{ducb} = (\bar{d}_L^i\gamma^\mu u_L^j)(\bar{c}_L^j\gamma_\mu b_L^i)$, $Q_2^{ducb} = (\bar{d}_L^i\gamma^\mu u_L^i)(\bar{c}_L^j\gamma_\mu b_L^j)$, and i, j stand for color indices of the quark fields. Such operators are traditionally called current-current operators. Before turning on the QCD effects, we have $C_1 = 0$ and $C_2 = -1$.

Our operators can easily be rewritten in terms of products of color-singlet and color-octet currents, thanks to the following identity for the $SU(3)$ generators T^a:

$$(T^a)^i{}_j(T^a)^k{}_l = T_F\left(-\frac{1}{N_c}\delta^i_j\delta^k_l + \delta^i_l\delta^k_j\right) \tag{2.7}$$

where $T_F = 1/2$, and $N_c = 3$ stands for the number of quark colors. Moreover, one can show that no other operators arise because there are only two independent singlets in the

tensor product $\bar{\mathbf{3}} \otimes \mathbf{3} \otimes \bar{\mathbf{3}} \otimes \mathbf{3}$ of the fundamental and anti-fundamental representations of $SU(3)$.

The two operators in Eq. (2.6) are chirality conserving. In four spacetime dimensions the Dirac algebra is 16-dimensional, and 8 elements of the standard basis (γ_α, $\gamma_\alpha\gamma_5$) conserve chirality while the remaining 8 ($\mathbb{1}$, γ_5, $\sigma_{\mu\nu}$) do not. In a generic spacetime dimension D that must be considered in DR, we need to take into account the so-called evanescent operators (see Sec. 2.1.2) which vanish in $D = 4$. Some of those operators are shown below in Eq. (2.11) and Eq. (2.12). At higher loops, evanescent operators with longer strings of $\gamma^{\mu 1}\gamma^{\mu 2}\gamma^{\mu 3}\ldots$ appear. Furthermore, the choice of operator basis is not unique, and different bases might be more useful for different physical processes. The only necessary condition is that each basis contains all the possible linearly independent operators that do not vanish by the equations of motion. The full set of operators in each given example can be written without specifying nothing but the particle content and symmetries of a given theory (see, e.g., Ref. [84]).

Now, let us specify the set of operators that are relevant for $\bar{B} \to X_s\gamma$. An example of the LO diagram in the SM has already been shown in Fig. 1.1. For this process, at the leading order in the electroweak interactions,[2] ten operators turn out to be necessary. The relevant effective Lagrangian reads:

$$\mathcal{L}_{\text{eff}} = \mathcal{L}_{QCD\times QED}(u,\, d,\, s,\, c,\, b) + \frac{4G_F}{\sqrt{2}}\left[V_{tb}V_{ts}^*\sum_i^8 C_iQ_i + V_{ub}V_{us}^*\sum_i^2 C_i(Q_i - Q_i^u)\right] \tag{2.8}$$

The first term in the above equation is the QCD and QED Lagrangian for all the quarks except the decoupled top.[3] As far as the second term is concerned, the basis of ten operators can be chosen as follows [86, 87]:

$$\begin{array}{lcllcl}
Q_1^u &=& (\bar{s}_L\gamma_\mu T^a u_L)(\bar{u}_L\gamma^\mu T^a b_L), & Q_4 &=& (\bar{s}_L\gamma_\mu T^a b_L)\sum_q(\bar{q}\gamma^\mu T^a q),\\
Q_2^u &=& (\bar{s}_L\gamma_\mu u_L)(\bar{u}_L\gamma^\mu b_L), & Q_5 &=& (\bar{s}_L\gamma_{\mu 1}\gamma_{\mu 2}\gamma_{\mu 3} b_L)\sum_q(\bar{q}\gamma^{\mu 1}\gamma^{\mu 2}\gamma^{\mu 3} q),\\
Q_1 &=& (\bar{s}_L\gamma_\mu T^a c_L)(\bar{c}_L\gamma^\mu T^a b_L), & Q_6 &=& (\bar{s}_L\gamma_{\mu 1}\gamma_{\mu 2}\gamma_{\mu 3} T^a b_L)\sum_q(\bar{q}\gamma^{\mu 1}\gamma^{\mu 2}\gamma^{\mu 3} T^a q),\\
Q_2 &=& (\bar{s}_L\gamma_\mu c_L)(\bar{c}_L\gamma^\mu b_L), & Q_7 &=& \frac{e}{16\pi^2} m_b\,(\bar{s}_L\sigma_{\mu\nu} b_R)\,F^{\mu\nu},\\
Q_3 &=& (\bar{s}_L\gamma_\mu b_L)\sum_q(\bar{q}\gamma^\mu q), & Q_8 &=& \frac{g}{16\pi^2} m_b\,(\bar{s}_L\sigma_{\mu\nu} T^a b_R)\,G^{a\mu\nu},
\end{array} \tag{2.9}$$

where the sums over q in $Q_{3,\ldots,6}$ run over all the active flavors $q = u,\, d,\, s,\, c,\, b$ in the effective theory. The electromagnetic and gluonic field strength tensors $F^{\mu\nu}$ and $G^{\mu\nu}$ in Q_7 and Q_8, respectively, are contracted with $\sigma_{\mu\nu} = \frac{i}{2}\,[\gamma_\mu, \gamma_\nu]$.

In Fig. 2.2, we show examples of Feynman diagrams that generate some of the ten operators. Fig. 2.2(a) corresponds to the photonic dipole operator Q_7. The gluonic dipole operator Q_8 is generated by analogous diagrams, but with the external photon replaced by an external gluon. Fig. 2.2(b) corresponds to the current-current operators

[2] The extra operators that are relevant for the electroweak corrections only can be found, e.g., in Ref. [85].

[3] We ignore the leptons because they do not matter for our process at the leading order in the electroweak interactions.

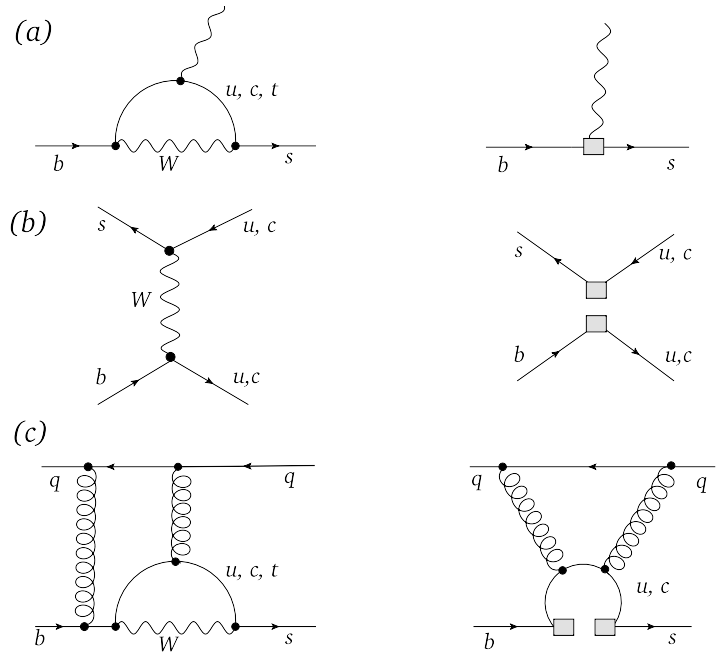

Figure 2.2: Examples of Feynman diagrams that generate the some of the operators in the effective theory for $b \to s\gamma$. One needs to consider both the SM (left side) and the effective theory (right side) diagrams.

(Q_1^u, Q_2^u, Q_1, Q_2). Finally, the QCD penguin operators (Q_3, Q_4, Q_5, Q_6) receive contributions from the diagrams in Fig. 2.2(c).

In Eq. (2.8), unitarity of the CKM matrix has already been used, which explains why $Q_{1,2}^u$ enter in a particular linear combination with $Q_{1,2}$ into the term that gets multiplied by $V_{ub}V_{us}^*$. This term is included in the phenomenological analysis of Refs. [2, 64] but has only a tiny numerical effect on the CP-averaged branching ratio because $(V_{ub}V_{us}^*)/(V_{tb}V_{ts}^*) \simeq -0.008 + 0.018i$ is numerically very small. However, it is the only source of the CP asymmetry in the considered process [88].

The operator basis as it stands in Eq. (2.9) was introduced for the first time in Refs. [86, 87] as a simple modification (in the four-quark operator sector only) of the previously used basis from Ref. [89]. We shall call these bases "CMM" and "GW", respectively, after the article authors' initials. The four-quark operators $Q_1, \ldots, Q_6$ in the GW basis read

$$\begin{aligned}
\mathcal{Q}_1 &= (\bar{s}_L^i \gamma_\mu c_L^j)(\bar{c}_L^j \gamma^\mu b_L^i), & \mathcal{Q}_2 &= (\bar{s}_L^i \gamma_\mu c_L^i)(\bar{c}_L^j \gamma^\mu b_L^j), \\
\mathcal{Q}_3 &= (\bar{s}_L^i \gamma_\mu b_L^i) \textstyle\sum_q (\bar{q}_L^j \gamma^\mu q_L^j), & \mathcal{Q}_4 &= (\bar{s}_L^i \gamma_\mu b_L^j) \textstyle\sum_q (\bar{q}_L^j \gamma^\mu q_L^i), \\
\mathcal{Q}_5 &= (\bar{s}_L^i \gamma_\mu b_L^i) \textstyle\sum_q (\bar{q}_R^j \gamma^\mu q_R^j), & \mathcal{Q}_6 &= (\bar{s}_L^i \gamma_\mu b_L^j) \textstyle\sum_q (\bar{q}_R^j \gamma^\mu q_R^i),
\end{aligned} \tag{2.10}$$

The CMM-basis is more suitable for multiloop calculations because no traces involving γ_5 occur in the Feynman diagrams to all orders in QCD, provided we restrict to the leading order of the expansion in $m_b^2 G_F$, which is a very good approximation. Consequently, we are allowed to use the so-called Naive Dimensional Regularization (NDR) where γ_5 is treated as fully anticommuting, i.e. it anticommutes with all the Dirac matrices γ_μ. This feature makes the Dirac algebra computations rather straightforward and easier to render

completely automatic than in the more general 't Hooft-Veltman (HV) [79] scheme for γ_5 where $\{\gamma_5, \gamma_\mu\} = 0$ for $\mu = 0, 1, 2, 3$ only, and $[\gamma_5, \gamma_\mu] = 0$ otherwise.

In our calculation, we shall use NDR with the (modified) Minimal Subtraction ($\overline{\text{MS}}$) scheme for the Wilson coefficient renormalization. In an effective theory with four-quark operators, such a scheme is not completely specified before defining all the evanescent operators that matter at the considered order in perturbation theory. For the purpose of our considerations in Sec. 2.2, the CMM-basis needs to be supplemented with the following two evanescent operators

$$Q_{11} = (\bar{s}_L\gamma_{\mu1}\gamma_{\mu2}\gamma_{\mu3}T^a c_L)(\bar{c}_L\gamma^{\mu1}\gamma^{\mu2}\gamma^{\mu3}T^a b_L) - 16Q_1, \tag{2.11}$$

$$Q_{12} = (\bar{s}_L\gamma_{\mu1}\gamma_{\mu2}\gamma_{\mu3}c_L)(\bar{c}_L\gamma^{\mu1}\gamma^{\mu2}\gamma^{\mu3}b_L) - 16Q_2. \tag{2.12}$$

Verifying that they indeed vanish in four spacetime dimensions is easily achieved by using the four-dimensional identity

$$\gamma_\mu\gamma_\nu\gamma_\rho = g_{\mu\nu}\gamma_\rho + g_{\nu\rho}\gamma_\mu - g_{\mu\rho}\gamma_\nu + i\epsilon_{\mu\nu\rho\sigma}\gamma^\sigma\gamma_5. \tag{2.13}$$

However, in D dimensions, the above identity does not hold, and the evanescent operators have to be treated on equal footing with the ones in Eq. (2.9).

2.1.2 Determination and renormalization of the Wilson coefficients

The Wilson coefficients C_i in the effective theory Lagrangian (2.8) can be treated as coupling constants that undergo $\overline{\text{MS}}$ renormalization, similarly to the QCD gauge coupling g_s. Once they are fixed at a given renormalization scale μ_0, their values at other scales μ can be calculated using the RGE. However, contrary to the gauge coupling, the initial conditions for the RGE ($C_i(\mu_0)$) do not need to be determined from experiment. Instead, they are fixed by the requirement that the effective theory in its region of validity reproduces the full theory (SM) Green's functions.

Instead of the SM, the role of the full theory could be played by any other model whose beyond-SM degrees of freedom are not much lighter than the W boson. In such a case, the operator basis in Eq. (2.8) might need to be extended. However, for definiteness, we shall restrict to the SM in our discussion here.

Since the effective theory has been obtained from the SM via decoupling of the W boson and heavier particles, its region of validity is restricted to Green's functions in which all the kinematical invariants (products of external momenta) are much smaller than m_W, and all the external particles are light (lighter than W), i.e. they correspond to the effective theory degrees of freedom. The Green's functions of the full and effective theories should be expanded in the ratios

(external momenta and light masses)/(m_W and other heavy masses),

and then compared order-by-order in the above expansion to determine the Wilson coefficients C_i. This procedure is called *matching* because one matches Green's functions of the full and effective theories.

The obtained Wilson coefficients are functions of the heavy masses (m_W, m_t, ...) and the renormalization scale μ_0 at which the matching calculation has been performed.

However, they are independent of the light masses. Thus, one sets μ_0 to be of order of the electroweak scale to avoid appearance of large logarithms in the perturbative expressions for the renormalized Wilson coefficients $C_i(\mu_0)$.

On the other hand, the low-energy amplitudes we want to calculate in the effective theory framework do depend on the light masses like m_b or m_c. They also depend on the renormalization scale μ_b at which they are calculated. In this case, to avoid large logarithms, we set $\mu_b \sim m_b/2$. This scale is chosen to be of the same order as the energy deposit into the hadronic system in the decay $\bar{B} \to X_s\gamma$ where the photon energy spectrum in the decaying meson rest frame is peaked around $E_\gamma \sim m_b/2$ (see the caption of Fig. 1.2).

Thus, one needs to use the RGE to evolve $C_i(\mu)$ from $\mu_0 \sim (m_W, m_t)$ down to $\mu_b \sim m_b/2$. The RGE are governed by the Anomalous Dimension Matrix (ADM) which is derived from the effective theory renormalization constants (see Eq. (2.30) below). Since the Wilson coefficients mix under renormalization, calculating the ADM and solving the RGE goes under the name of determining the *mixing*. Finally, after solving the RGE, we calculate the physical amplitudes which are given by *matrix elements* of the operators Q_i between the final and initial states.

Such a procedure is common for any FCNC process that takes place much below the electroweak scale. It always consists of three steps in which one subsequently determines the *matching*, *mixing* and *matrix elements*. In the remainder of this section, we shall describe a few technical details of the first two steps. A discussion of the matrix elements will follow in Sec. 2.1.3.

Matching

The first thing to note about this step is that the matched Green's functions do not need to correspond to physical external states. We can use perturbative calculations with partonic external states and allow their momenta to acquire any off-shell configurations. However, in the off-shell case, one needs to extend the effective theory Lagrangian by including all the possible operators that vanish by the Equations of Motion (EOM). Their number is always finite once we restrict to operators of a given dimension. An example of such a calculation can be found, e.g., in Sec. 5 of Ref. [90]. The number of encountered operators was quite limited there thanks to using the 't Hooft-Feynman version of the background field gauge [91] for the electroweak interactions and QCD [92], and thus retaining gauge invariance at the level of the SM off-shell Green's functions.

Secondly, in an off-shell matching calculation with arbitrary external momenta, one is allowed to Taylor-expand the Feynman integrands in all the external momenta and light masses prior to integration. Such an expansion is known to generate spurious infrared (IR) divergences which manifest themselves as extra $1/\varepsilon^n$ poles in the DR. However, all such spurious poles cancel out in each of the matching equations for the off-shell amplitudes[4]

$$\mathcal{A}^{\text{full}} = \mathcal{A}^{\text{eff}}. \tag{2.14}$$

The remaining poles are of ultraviolet (UV) origin, and they cancel out after including all the necessary diagrams with UV counterterms on both sides of the matching equa-

[4] i.e. amputated off-shell Green's functions

tion (2.14). In effect, we find relations that are finite in the limit $\varepsilon \to 0$, and we can extract the finite renormalized Wilson coefficients from them. However, one can see that a calculation of the effective theory renormalization constants (a part of the *mixing* step) must be done prior to the matching calculation.

When the above prescription is followed in the DR, an important simplification occurs. The effective theory diagrams contain no massive particles, so expanding the integrands in the external momenta and masses reduces them to scaleless tadpoles (vacuum diagrams with no external momenta and only massless internal lines), so they vanish in the DR. Their vanishing is due to cancellation of the UV and spurious IR divergences, as they are both regulated dimensionally. Thus, the only diagrams to be included on the r.h.s. of the matching equation (2.14) are tree-level diagrams, possibly multiplied by UV-divergent renormalization constants. In effect, the cancellation of $1/\varepsilon^n$ takes place between the UV counterterms on the r.h.s. and spurious IR divergences on the l.h.s. of Eq. (2.14). Explicit examples of such cancellations at the two- and three-loop levels can be found in the matching calculations of Refs. [90] and [93], respectively.

Once such an algorithm is followed, the only Feynman diagrams to be calculated are massive tadpoles with as many different masses as there are massive particles to be decoupled. Usually, when several particles are decoupled together, their masses are of the same order of magnitude. We encounter such a case in the SM when the top quark, the Higgs boson and the weak gauge bosons W and Z are being decoupled together. Keeping all the heavy masses different is not a problem up to two loops, in which case all the necessary integrals are known [94]. However, it may become an issue at three and more loops. Then, Taylor expansions around the point where all the masses are equal leads to a great simplification. One obtains single-scale partly massive tadpoles only, all of which can be calculated up to three loops using the publicly available code MATAD [95]. Such a method has been applied for evaluation of the three-loop (NNLO QCD) matching conditions for the photonic and gluonic dipole operators in Refs. [93, 96].

Let us now quote some explicit matching results for the effective Lagrangian in Eq. (2.8). In general, for the order α_s^n matching computation of $C_i(\mu_0)$, one needs to consider n loops for the four-quark operators ($i = 1, \ldots, 6$) and $n+1$ loops for the dipole operators ($i = 7, 8$), which can be understood after having a look at Fig. 2.2(a) where no internal gluons are present in the one-loop SM diagram.

The only Wilson coefficients $C_i(\mu_0)$ that receive nonvanishing LO contributions are C_2 (tree) together with C_7 and C_8 (one-loop). They read [97]

$$\begin{aligned} C_2 &= 1 + \mathcal{O}(\alpha_s^2) \\ C_7 &= -\frac{x(8x^2+5x-7)}{24(x-1)^3} + \frac{3x-2}{4(x-1)^4}x^2 \ln x + \mathcal{O}(\alpha_s) \\ C_8 &= -\frac{x(8x^2-5x+2)}{8(x-1)^3} - \frac{3}{4(x-1)^4}x^2 \ln x + \mathcal{O}(\alpha_s), \end{aligned} \tag{2.15}$$

where $x = m_t^2/m_W^2$. At the NLO level, two other coefficients become nonvanishing in the

CMM basis. In the $\overline{\rm MS}$ scheme they read [87]

$$C_1 = \frac{15\alpha_{\rm s}}{4\pi} + \mathcal{O}(\alpha_{\rm s}^2)$$
$$C_4 = \frac{\alpha_{\rm s}}{4\pi}[E(x) - \frac{2}{3}] + \mathcal{O}(\alpha_{\rm s}^2) \tag{2.16}$$
$$\tag{2.17}$$

where [97]

$$E(x) = \frac{x(18-11x-x^2)}{12(1-x)^3} + \frac{x^2(15-16x+4x^2)}{6(1-x)^4}\ln x - \frac{2}{3}\ln x \tag{2.18}$$

As far as the two-loop $\mathcal{O}(\alpha_{\rm s})$ (NLO) contributions to $C_{7,8}$ are concerned, we shall not quote them explicitly but only mention that they were first found in Ref. [98], and then confirmed in Refs. [90, 99–101]. At the $\mathcal{O}(\alpha_{\rm s}^2)$ (NNLO) level, all the eight Wilson coefficients receive nonvanishing matching contributions. They were found in Ref. [90] for the four-quark operators, and in Ref. [93] for the dipole operators, which required two- and three-loop calculations, respectively.

Mixing

Let us now discuss the Wilson coefficient renormalization in the effective Lagrangian (2.8). Once we restrict to the leading order in electroweak interactions, such a renormalization is due to the QCD only. In the standard QCD, we have the following relations between the bare and renormalized gauge couplings (g_s), masses (m), quark fields (ψ) and gluon fields (A)

$$g_s^{\rm b} = Z_g\, g_s, \qquad m^{\rm b} = Z_m\, m, \qquad \psi^{\rm b} = Z_\psi^{\frac{1}{2}}\,\psi, \qquad A^{\rm b} = Z_\psi^{\frac{1}{2}}\,A, \tag{2.19}$$

where the superscript b denotes the bare quantities. In the effective theory, analogous relations hold for the Wilson coefficients. However, they do not get renormalized separately but rather mix under renormalization. We have

$$C_i^{\rm b} = \sum_j C_j(\mu)\, Z_{ji}(\alpha_{\rm s}(\mu)) \tag{2.20}$$

i.e. a matrix of renormalization constants has to be considered.

It is worth mentioning that the notion of bare and renormalized Wilson coefficients became popular in the literature only in the 1990's. In the earlier papers, the renormalization constants Z_{ji} were usually absorbed into the operator renormalization, which is only a matter of using a somewhat less practical convention for the derivation of the RGE.

If we follow our convention defined by Eq. (2.20), we can restrict the operator renormalization to the one that is induced by the usual QCD renormalization of fields, masses and couplings contained in each of the operators. Our four-quark operators in Sec. 2.1.1 contain no masses or couplings in their definitions (contrary to the dipole operators), so their renormalization reads $Q_i^{\rm b} = Z_\psi^2\, Q_i$. In the following, we shall restrict our discussion

to the four-quark case, to make our expressions more compact. The renormalized $\mathcal{L}_{\text{eff}}$ then reads

$$\mathcal{L}_{\text{eff}} \sim \sum_{i,\,j} C_j \, Z_{ji} \, Z_\psi^2 Q_i \tag{2.21}$$

Each of the renormalization constants can be written as a sum of n-loop terms with $n = 0, 1, 2, \ldots$. In the case of Z_{ji}, such an expansion reads

$$Z_{ji} = \delta_{ji} + (Z_{ji} - 1)^{(1)} + (Z_{ji} - 1)^{(2)} + \ldots \tag{2.22}$$

Generally, in the MS scheme, the n-loop term has the following form:

$$(Z_{ji} - 1)^{(n)} = \left(\frac{\alpha_{\text{s}}}{4\pi}\right)^n \sum_{k=0}^{n} \frac{1}{\varepsilon^k} Z_{ji}^{nk}, \tag{2.23}$$

where Z_{ji}^{nk} are some rational numbers which depend on no parameters.[5]

One may be surprised that the sum in the above equation goes from $k = 0$ rather than $k = 1$, even though we consider the MS scheme. However, this is a necessary generalization of this scheme in the presence of evanescent operators [102–104]. Nonvanishing Z_{ji}^{n0} are allowed (by the scheme definition) if and only if i corresponds to an evanescent operator, and j corresponds to a physical operator. Moreover, its value is fixed by the renormalization condition, namely that *the renormalized matrix elements of evanescent operators are equal to zero*. Unless such a condition is chosen, an infinite set of evanescent operators would need to be considered already for the LO RGE [102].

In Eqs. (2.11) and (2.12), we have already given two evanescent operators that appear at one loop in the CMM basis. In an NNLO calculation of the ADM, several other evanescent operators become important. They read [86]

$$Q_{15} = (\bar{s}_L\gamma_{\mu1}\gamma_{\mu2}\gamma_{\mu3}\gamma_{\mu4}\gamma_{\mu5}b_L)\sum(\bar{q}\gamma^{\mu1}\gamma^{\mu2}\gamma^{\mu3}\gamma^{\mu4}\gamma^{\mu5}q) + 64Q_3 - 20Q_5 \tag{2.24}$$

$$Q_{16} = (\bar{s}_L\gamma_{\mu1}\gamma_{\mu2}\gamma_{\mu3}\gamma_{\mu4}\gamma_{\mu5}T^a b_L)\sum(\bar{q}\gamma^{\mu1}\gamma^{\mu2}\gamma^{\mu3}\gamma^{\mu4}\gamma^{\mu5}T^a q) + 64Q_4 - 20Q_6 \tag{2.25}$$

$$Q_{21} = (\bar{s}_L\gamma_{\mu1}\gamma_{\mu2}\gamma_{\mu3}\gamma_{\mu4}\gamma_{\mu5}T^a c_L)(\bar{c}_L\gamma^{\mu1}\gamma^{\mu2}\gamma^{\mu3}\gamma^{\mu4}\gamma^{\mu5}T^a b_L) - 256Q_1 - 20Q_{11} \tag{2.26}$$

$$Q_{22} = (\bar{s}_L\gamma_{\mu1}\gamma_{\mu2}\gamma_{\mu3}\gamma_{\mu4}\gamma_{\mu5}c_L)(\bar{c}_L\gamma^{\mu1}\gamma^{\mu2}\gamma^{\mu3}\gamma^{\mu4}\gamma^{\mu5}b_L) - 256Q_2 - 20Q_{12} \tag{2.27}$$

$$\begin{aligned} Q_{25} = {} & (\bar{s}_L\gamma_{\mu1}\gamma_{\mu2}\gamma_{\mu3}\gamma_{\mu4}\gamma_{\mu5}\gamma_{\mu6}\gamma_{\mu7}b_L)\sum(\bar{q}\gamma^{\mu1}\gamma^{\mu2}\gamma^{\mu3}\gamma^{\mu4}\gamma^{\mu5}\gamma^{\mu6}\gamma^{\mu7}q) \\ & + 1280Q_3 - 336Q_5 \end{aligned} \tag{2.28}$$

$$\begin{aligned} Q_{26} = {} & (\bar{s}_L\gamma_{\mu1}\gamma_{\mu2}\gamma_{\mu3}\gamma_{\mu4}\gamma_{\mu5}\gamma_{\mu6}\gamma_{\mu7}T^a b_L)\sum(\bar{q}\gamma^{\mu1}\gamma^{\mu2}\gamma^{\mu3}\gamma^{\mu4}\gamma^{\mu5}\gamma^{\mu6}\gamma^{\mu7}T^a q) \\ & + 1280Q_4 - 336Q_6 \end{aligned} \tag{2.29}$$

The RGE for the Wilson coefficients are derived from the fact that the bare ones in Eq. (2.20) $\left(\vec{C}^{\text{b}} = \hat{Z}^T\vec{C}\right)$ are independent of μ. One finds

$$\frac{\mathrm{d}\vec{C}(\mu)}{\mathrm{d}\ln\mu} = \hat{\gamma}^T(\alpha_{\text{s}}(\mu))\vec{C}(\mu), \quad \text{where} \quad \hat{\gamma} = -\frac{\mathrm{d}\hat{Z}(\mu)}{\mathrm{d}\ln\mu}\,\hat{Z}^{-1} = \hat{Z}\,\frac{\mathrm{d}\hat{Z}^{-1}(\mu)}{\mathrm{d}\ln\mu}. \tag{2.30}$$

[5] We assume that we have 3 colors and 5 flavors, i.e. these quantities are not considered as parameters.

The anomalous dimension matrix $\hat{\gamma}(\alpha_s(\mu))$ in the MS and $\overline{\rm MS}$ schemes has the following block-triangular form

$$\hat{\gamma} = \begin{bmatrix} \hat{\gamma}_{PP} & \hat{\gamma}_{PE} \\ 0 & \hat{\gamma}_{EE} \end{bmatrix} \tag{2.31}$$

where P and E correspond to the physical and evanescent operators. The vanishing entry in the lower-left block is a consequence of defining the MS scheme conventions in such a way that all the matrix elements of evanescent operators vanish after renormalization. The block-triangular form of $\hat{\gamma}(\alpha_s(\mu))$ implies that the Wilson coefficients C_E of the evanescent operators do not affect the RG-evolution of the other Wilson coefficients C_P. Thus, we do not need to solve the RGE for C_E. In the following, we focus on the physical operators only, and we skip the index P, i.e. we set $C_P \equiv C$ and $\hat{\gamma}_{PP} \equiv \hat{\gamma}$.

The RGE in Eq. (2.30) is a first-order differential equation, and it has the following solution

$$\vec{C}(\mu) = \mathrm{T}_{\alpha_s}\, \exp\left[\int_{\alpha_s(\mu_0)}^{\alpha_s(\mu)} d\alpha_s \frac{\hat{\gamma}^T(\alpha_s)}{\beta(\alpha_s)}\right] \vec{C}(\mu_0) \;\equiv\; \hat{\mathcal{U}}(\mu,\mu_0)\,\vec{C}(\mu_0), \tag{2.32}$$

where the T_{α_s}-ordering means that the ADM's with higher α_s stand to the left of those with smaller α_s in each of the monomials obtained after writing the exponent in terms of a series.

In practice, one needs explicit expressions for several terms in the perturbative expansion of our formal solution (2.32) to the RGE. Each of the quantities that occur in this solution has its own expansion in α_s. For the QCD beta function $\beta(\alpha_s(\mu)) \equiv d\alpha_s(\mu)/d\ln\mu$ and for the ADM, such expansions take the form

$$\beta(\alpha_s) = -2\alpha_s \sum_{n=0} \beta^{(n)} \left(\frac{\alpha_s}{4\pi}\right)^{n+1}, \qquad\qquad \hat{\gamma}(\alpha_s) = \sum_{n=0} \hat{\gamma}^{(n)} \left(\frac{\alpha_s}{4\pi}\right)^{n+1}. \tag{2.33}$$

For the Wilson coefficients, we have

$$\vec{C}(\mu) = \sum_{n=0} \vec{C}^{(n)}(\mu) \left(\frac{\alpha_s(\mu)}{4\pi}\right)^n. \tag{2.34}$$

Finally, the evolution matrix $\hat{\mathcal{U}}(\mu,\mu_0)$ defined in Eq. (2.32) can be perturbatively expanded as

$$\hat{\mathcal{U}}(\mu,\mu_0) = \sum_{n=0} \hat{\mathcal{U}}^{(n)}(\mu,\mu_0) \left(\frac{\alpha_s}{4\pi}\right)^n. \tag{2.35}$$

To comment on the explicit form of the above evolution matrix, let us first assume that we have only a single Wilson coefficient, i.e. the anomalous dimension is just a number $\gamma = \gamma^{(0)}\,\frac{\alpha_s}{4\pi} + \ldots$. We can then ignore the T_{α_s}-ordering in Eq. (2.32), and perform the integration in the exponent. Once the ADM and the beta function are restricted to their leading terms, the integration is very simple, and one finds

$$C^{(0)}(\mu) = \left(\frac{\alpha_s(\mu_0)}{\alpha_s(\mu)}\right)^{\gamma^{(0)}/2\beta^{(0)}} C^{(0)}(\mu_0). \tag{2.36}$$

Order	resummation of	γ, β	$C(\mu_0)$
LO	LL: $\left(\alpha_s \ln \frac{\mu_0^2}{\mu^2}\right)^n$	one loop	tree level
NLO	NLL: $\alpha_s \left(\alpha_s \ln \frac{\mu_0^2}{\mu^2}\right)^n$	two loop	one loop
NNLO	NNLL: $\alpha_s^2 \left(\alpha_s \ln \frac{\mu_0^2}{\mu^2}\right)^n$	three loop	two loop

Table 2.1: Order-counting and loop levels for resummation of large logarithms in the four-quark operator case.

In a more general case when we have many Wilson coefficients but the matrix $\hat{\gamma}^{(0)}$ is diagonalizable with real eigenvalues,[6] we can write

$$\left[\hat{V}^{-1}\hat{\gamma}^{(0)T}\hat{V}\right]_{ij} \equiv 2\beta^{(0)}\,\delta_{ij}\,a_{\underline{j}}, \tag{2.37}$$

where a_j are real numbers, and $\hat{V}$ is the diagonalizing matrix. Then the LO solution to the RGE reads

$$C_i(\mu) = V_{ij}\left(\frac{\alpha_s(\mu_0)}{\alpha_s(\mu)}\right)^{a_j}(V^{-1})_{jk}\,C_k(\mu_0). \tag{2.38}$$

It is interesting to observe explicitly that the obtained ratios of α_s at different scales really contain the resummed Leading Logarithms (LL) $\left(\alpha_s \ln \frac{\mu_0^2}{\mu^2}\right)^n$. When the multiplicative factor in Eq. (2.36) is expanded in α_s, one finds

$$\left(\frac{\alpha_s(\mu_0)}{\alpha_s(\mu)}\right)^{\gamma^{(0)}/2\beta^{(0)}} \simeq \left(1 - \beta^{(0)}\frac{\alpha_s(\mu_0)}{4\pi}\ln\frac{\mu_0^2}{\mu^2} + \ldots\right)^{\gamma^{(0)}/2\beta^{(0)}} \tag{2.39}$$

$$= 1 - \frac{\gamma^{(0)}}{2}\frac{\alpha_s(\mu_0)}{4\pi}\ln\frac{\mu_0^2}{\mu^2} + \mathcal{O}\left[\left(\alpha_s \ln\frac{\mu_0^2}{\mu^2}\right)^2\right] \tag{2.40}$$

Similarly, solving the RGE at the NLO is equivalent to resumming the Next-to-Leading Logarithms (NLL), and so forth. This is what is being meant by the RG-improved perturbation theory. Table 2.1 shows the nomenclature for resummation of large logarithms, as well as indicates the necessary numbers of loops in the Feynman diagrams corresponding to various quantities in the case where only the four-quark operators are considered. The loop counting is somewhat different in the dipole operator case, which is due to the fact that they receive no tree-level matching contributions, and that their mixing with operators that do receive such contributions starts at two loops only.

Let us now make a few remarks concerning the practical calculations of the renormalization constants that were needed to determine the necessary ADM's up to the NNLO in the case of $\bar{B} \to X_s\gamma$. Although thousands of Feynman diagrams up to four loops are relevant [105], the calculations were manageable thanks to applying a certain decomposition of the propagator denominators [106]. It goes as follows. For any propagator

[6] We are not aware of examples where the eigenvalues are not real or the matrix is not diagonalizable, neither of a physical argument why it must be the case.

denominator with loop momentum q, external momentum p and mass M, the following identity holds

$$\frac{1}{(q+p)^2-M^2} = \frac{1}{q^2-m^2} + \frac{M^2-p^2-2qp-m^2}{q^2-m^2}\frac{1}{(q+p)^2-M^2} \tag{2.41}$$

for an arbitrary mass parameter m. This mass parameter serves as a regulator of spurious IR divergences. We cannot allow for such divergences in an evaluation of the renormalization constants, contrary to the matching calculations. The very last term on the r.h.s. of the above equation is identical to the initial propagator on the l.h.s. We can thus apply this identity several times, finally obtaining a linear combination of terms that either: *(i)* depend only on loop momenta and the regulator mass m, *(ii)* occur only in Feynman integrals whose superficial degree of divergence is negative.

The terms satisfying the condition *(ii)* can be dropped in a renormalization constant calculation because integrals with a negative superficial degree of divergence are UV-finite after subtraction of subdivergences. Once they are dropped, we are left with only single-scale fully massive tadpole integrals to calculate. Such tadpole integrals can be evaluated according to a recursive algorithm up to three-loops [106], while at the four-loop level they require an IBP reduction to less than 20 MI's, all of which are already known in an analytical manner [107]. Such a method, first applied in Refs [86, 108], is more efficient for renormalization constant calculations than the previously used so-called R^*-operation [109].

In the case of $\bar{B} \to X_s\gamma$, the full 8×8 NLO ADM in the CMM basis was computed in Refs. [86, 108]. Later, in Ref. [87], its two-loop four-quark part was found to agree the earlier calculations in the GW basis. Its three-loop part (corresponding to the mixing of the four-quark operators with the dipole ones) was later confirmed in Ref. [110]. At the NNLO level, the three-loop mixing in the $(Q_1,\ldots,Q_6)$ and $(Q_7,\, Q_8)$ sectors was calculated in Refs. [111] and [112], respectively. Finally, the four-loop mixing between the two sectors was found in Ref. [105].

In many of these cases, the published results for the ADM do not refer to the original Wilson coefficients from Eq. (2.8) but rather to the so-called effective ones [113, 114] that are given by certain linear combinations of them. The explicit form of these linear combinations depends on the regularization scheme. In the NDR scheme, they read

$$\begin{aligned}
C_i^{\text{eff}} &= C_i, \text{ for } i = 1,\ldots,6 \\
C_7^{\text{eff}} &= C_7 - \frac{1}{3}C_3 - \frac{4}{3}C_4 - \frac{20}{3}C_5 - \frac{80}{9}C_6 \\
C_8^{\text{eff}} &= C_8 + C_3 - \frac{1}{6}C_4 + 20C_5 - \frac{10}{3}C_6
\end{aligned} \tag{2.42}$$

These combinations are adjusted in such a way that the LO perturbative decay amplitudes for $b \to s\gamma$ and $b \to sg$ are proportional to the LO terms in $C_7^{\text{eff}}(\mu_b)$ and $C_8^{\text{eff}}(\mu_b)$, respectively. The ADM for the effective coefficients has an analogous expansion as the one in Eq. (2.33)

$$\hat{\gamma}_{\text{eff}}(\alpha_{\text{s}}) = \sum_{n=0} \hat{\gamma}_{\text{eff}}^{(n)} \left(\frac{\alpha_{\text{s}}}{4\pi}\right)^{n+1}. \tag{2.43}$$

The matrix $\hat{\gamma}^{(0)}_{\rm eff}$ is scheme-independent, contrary to the usual $\hat{\gamma}^{(0)}$ that depends, in particular, on the treatment of γ_5 in DR. Both the Wilson coefficients and the matrix elements of the operators depend on the γ_5-scheme. In the NDR scheme, the LO $b \to s\gamma$ amplitude receives contributions from the operators $Q_3, \ldots, Q_7$, whereas in the HV scheme only Q_7 matters. By introducing the effective Wilson coefficients as linear combinations of the original ones, the scheme dependence is avoided. This is possible because the one-loop $b \to s\gamma$ matrix elements of the four quark operators are actually proportional to the tree-level matrix element of the dipole operator. An analogous situation occurs in the $b \to sg$ case and the operator Q_8.

2.1.3 Matrix elements and the role of m_c

After having described the determination and renormalization of the Wilson coefficients, we now pass to the third step of the previously outlined procedure, namely to evaluating the matrix elements of the operators Q_i between the external states of interest. For the $\bar{B} \to X_s\gamma$ decay, one needs to consider the matrix elements $\sum_i \langle X_s\,\gamma \mid Q_i(\mu_b) \mid \bar{B}\rangle$. For example, the LO on-shell decay amplitude is completely governed by the photonic dipole operator matrix element. It reads

$$\frac{4G_F\,V_{tb}V_{ts}^*}{\sqrt{2}}\; C_7^{(0)\rm eff}(\mu_b)\langle X_s\,\gamma \mid Q_7(\mu_b) \mid \bar{B}\rangle. \tag{2.44}$$

Due to the hadronic nature of the external states, nonperturbative QCD effects show up at the stage of the matrix element evaluation. To overcome and/or control this problem, one considers the heavy quark limits, exploiting the fact that the b-quark mass is large compared to the QCD confinement scale Λ. For exclusive decays, the available calculational frameworks are HQET [40], QCD sum rules, light cone sum rules and lattice QCD. For the inclusive decays, HQE allows to express the hadronic matrix elements in terms of the perturbative ones for the underlying quark-level process, e.g., $\sum_i \langle s\,\gamma \mid Q_i(\mu_b) \mid b\rangle$, as already mentioned in Chapter 1. It turns out [54–61] that the considered inclusive decay rate of the B meson can be well approximated by the perturbative b-quark decay rate, as already spelled out in Eq. (1.2). Thus, the matrix elements of the operators $Q_i(\mu)$ in the inclusive case can be effectively evaluated in perturbation theory, in contrast to the exclusive case.

Nonperturbative effects

Let us now make a few additional remarks about the nonperturbative correction $\delta\Gamma_{\rm nonp}$ in Eq. (1.2). It receives contributions from many different sources, a classification of which can be found, e.g., in Ref. [65]. Although that paper was published before the extensive analysis of Ref. [61], the qualitative classification remains valid.

As already mentioned in the Introduction (Chapter 1), the size of nonperturbative effects strongly depends on the cutoff E_0 on the photon energy. The default choice of $E_0 \sim 1.6\,\text{GeV}$ aims at minimizing this problem together with the problem of experimental backgrounds. The photon energy spectrum in $\bar{B} \to X_s\gamma$ has been studied using several different methods. While the most popular one is based on the so-called shape functions (see, e.g., Refs. [115, 116]), other approaches include the Dressed Gluon Exponentiation

Scheme	$E_\gamma < 1.7$	$E_\gamma < 1.8$	$E_\gamma < 1.9$	$E_\gamma < 2.0$	$E_\gamma < 2.242$
Kinetic	0.986 ± 0.001	0.968 ± 0.002	0.939 ± 0.005	0.903 ± 0.009	0.656 ± 0.031
Neubert SF	0.982 ± 0.002	0.962 ± 0.004	0.930 ± 0.008	0.888 ± 0.014	0.665 ± 0.035
Kagan-Neubert	0.988 ± 0.002	0.970 ± 0.005	0.940 ± 0.009	0.892 ± 0.014	0.643 ± 0.033
Average	0.985 ± 0.004	0.967 ± 0.006	0.936 ± 0.010	0.894 ± 0.016	0.655 ± 0.037

Table 2.2: Rescaling factors used by HFAG [51] for an extrapolation of all the available experimental results down to $E_0 = 1.6\,\text{GeV}$ before computing their weighted average.

(DGE) model [117], as well as deriving constraints on the spectrum moments using fixed-order calculations up to $\mathcal{O}(\alpha_s\,\Lambda^2/m_b^2)$ [62]. As far as such fixed-order corrections are concerned, they are relatively straightforward to determine in those contributions to the decay rate that are due to Q_7 alone. In their case, one obtains a well-defined series in powers of Λ/m_b and α_s, similarly to the semileptonic B-meson decays.

Series expansions of the identified nonperturbative contributions begin with with the following suppression factors

$$\begin{aligned} &\alpha_s\,\Lambda/m_b, \\ &\frac{\mu_\pi^2}{m_b^2},\ \frac{\mu_G^2}{m_b^2},\ \frac{\rho_D^3}{m_b^3},\ \frac{\rho_{LS}^3}{m_b^3}, \ldots \\ &\frac{\alpha_s\mu_\pi^2}{(m_b - 2E_0)^2},\ \frac{\alpha_s\mu_G^2}{m_b(m_b - 2E_0)} \end{aligned} \tag{2.45}$$

where μ_π, μ_G, ρ_D, $\rho_{LS} = \mathcal{O}(\Lambda)$ are extracted from the semileptonic $\bar{B} \to X_c e\bar{\nu}$ decay spectra and the B-B^* mass difference. The denominators in the last line of the above list of suppression factors indicate loss of theoretical accuracy when E_0 tends towards its perturbative maximal value of $m_b/2 \sim 2.35\,\text{GeV}$, at which the measured photon energy spectra are peaked (see Fig. 1.2). As we have already mentioned, this is the reason why the experimental results are rescaled by HFAG [51] down to $E_0 = 1.6\,\text{GeV}$ before computing their weighted average. The actual extrapolation factors used by HFAG are listed in the last row of Tab. 2.2. They are obtained by using the measured photon energy spectra for determining parameters of several shape function models, and then averaging over the models. Such a procedure has often been criticized for leading to an underestimation of uncertainties because the considered models do not allow for sufficient freedom in the functional form of the expressions that are being fit to data. Nevertheless, no alternative calculation of the extrapolation factors has so far become available, even though efforts in this direction have been undertaken [118–120].

It has been stressed in Ref. [61] that the dominant nonperturbative uncertainty originates from the interference of the operators Q_7 and $Q_{1,2}$. Previous analyses of this contribution [56–60] were based on an expansion that behaves like

$$\frac{\Lambda^2}{m_c^2} \sum_{n=0} \left(\frac{\Lambda m_b}{m_c^2} \right)^n w_n \tag{2.46}$$

Although the expansion parameter $\Lambda m_b/m_c^2$ is close to unity, it was verified in Ref. [57] that the coefficients w_n of the expansion quickly tend to zero, so the leading $n = 0$

term was claimed to give a reliable approximation. The leading term is parameterized in terms of the nonperturbative quantity μ_G whose numerical value can be extracted from the B-B^* mass difference. The considered nonperturbative correction was found [56] to enhance $\mathcal{B}(\bar{B} \to X_s\gamma)$ by around 3%. However, according to Ref. [61], one needs to worry about nonperturbative effects that are not described by the series (2.46) at all, i.e. which correspond to the values of Λ that are beyond the radius of convergence of this series. The authors of Ref. [61] advocated treating these effects as $\mathcal{O}(\Lambda/m_b)$ ones and estimated them using models of subleading shape functions, finding effects in the range $[-1.7\%, +4.0\%]$ of the $\bar{B} \to X_s\gamma$ branching ratio. Combining them linearly with the other uncertainties, they estimated the overall nonperturbative uncertainty at the $\pm 5\%$ level, which coincides with the previous rough estimate of Refs. [66, 67]. This value has been adopted as it stands in the recent phenomenological update in Refs. [2, 64].

Perturbative contributions

Let us now proceed towards the main topic of the present thesis, namely the perturbative matrix elements that contribute to the partonic rate $\Gamma\left(b \to X_s^{\text{partonic}}\gamma\right)$. We shall very closely follow the notation of the recent article [64], which in turn follows the notation of Ref. [121]. The remainder of this section is devoted to introducing this notation and beginning our discussion of the issue of interpolation in m_c. This issue, further elaborated upon in Sec. 2.3, serves as a main motivation for evaluating our original results to be presented in Chapters 4 and 5.

Since we work at the leading order in the flavor changing electroweak interactions, the partonic decay rate is a quadratic polynomial[7] in the Wilson coefficients C_i^{eff}. It can be written as follows:

$$\Gamma(b \to X_s^{\text{partonic}}\gamma) = \frac{G_F^2 m_b^5 \alpha_{em} |V_{tb}V_{ts}^*|^2}{32\pi^4} \sum_{i,j} C_i^{\text{eff}}(\mu_b) C_j^{\text{eff}}(\mu_b) \widetilde{G}_{ij}(E_0, \mu_b). \tag{2.47}$$

where α_{em} is the on-shell electromagnetic coupling constant. The reason for using the on-shell scheme for the electromagnetic coupling is that the external photon is on shell, and we do not include events where it is being replaced by an electron-positron pair, even if it had the lowest possible invariant mass of $2m_e$. Thus, if the overall factor of α_{em} was renormalized in the $\overline{\text{MS}}$ scheme at the scale m_b (as it was done, e.g., in Ref [86]), large logarithms $\ln m_b^2/m_e^2$ would enhance the $\mathcal{O}(\alpha_{\text{em}})$ QED corrections to around 5% level [122], which would be an unnecessary complication.

The quantities $\widetilde{G}_{ij}$ parameterize interferences between decay amplitudes generated by Q_i and Q_j. They are assumed to be symmetric under $i \leftrightarrow j$. Their perturbative expansions, as well as the corresponding expansions of the effective Wilson coefficients read

$$\widetilde{G}_{ij}(E_0, \mu_b) = \left[\widetilde{G}_{ij}^{(0)}(E_0) + \frac{\alpha_{\text{s}}}{4\pi}\widetilde{G}_{ij}^{(1)}(E_0, \mu_b) + \left(\frac{\alpha_{\text{s}}}{4\pi}\right)^2 \widetilde{G}_{ij}^{(2)}(E_0, \mu_b) + \mathcal{O}(\alpha_{\text{s}}^3)\right] + \dots \tag{2.48}$$

$$C_i^{\text{eff}}(\mu_b) = \left[C_i^{(0)\text{eff}}(\mu_b) + \frac{\alpha_{\text{s}}}{4\pi} C_i^{(1)\text{eff}}(\mu_b) + \left(\frac{\alpha_{\text{s}}}{4\pi}\right)^2 C_i^{(2)\text{eff}}(\mu_b) + \mathcal{O}(\alpha_{\text{s}}^3)\right] + \dots, \tag{2.49}$$

[7] The Wilson coefficients in the SM are real numbers.

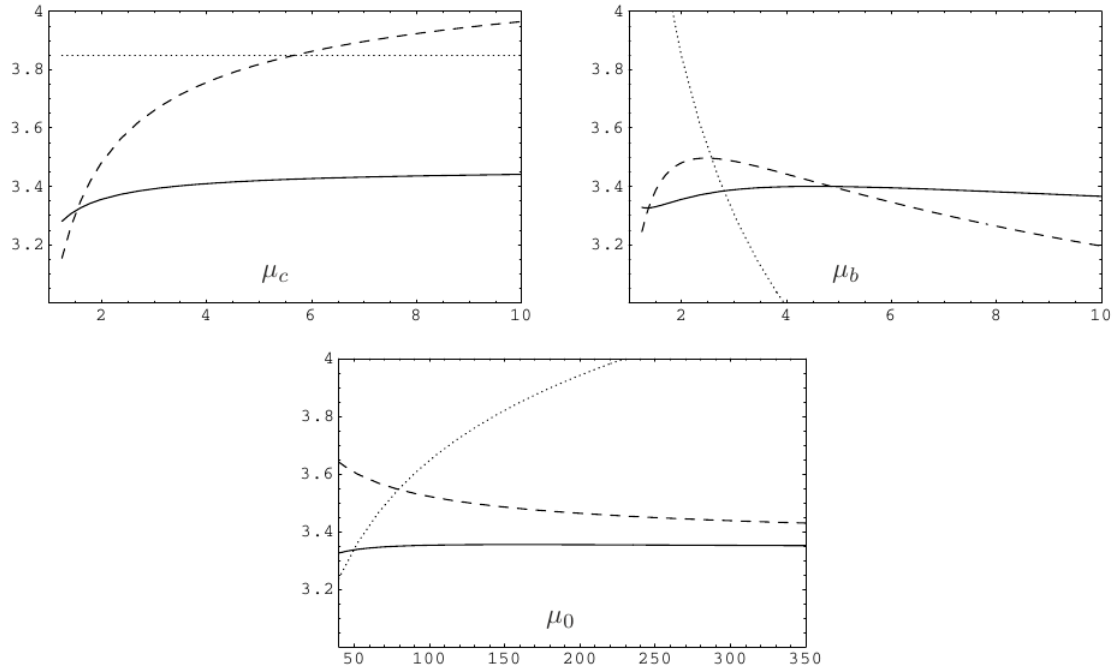

Figure 2.3: Renormalization scale dependence of $\mathcal{B}\left(\bar{B} \to X_s\gamma\right)$ given in units 10^{-4}, as presented in Fig. 6 of Ref. [64]. The LO, NLO and NNLO results are given by the dotted, dashed and solid lines, respectively. The upper-left, upper-right and lower plots describe the dependence on μ_c, μ_b and μ_0 [GeV], respectively. When one of the scales is varied, the remaining ones are set to their default values.

where ellipses stand for higher-order electroweak corrections. The tilde over G indicates the overall normalization to $m^5_{b,\text{pole}}$ in Eq. (2.47). At the LO, the symmetric matrix $\widetilde{G}^{(0)}_{ij}$ takes the form $\widetilde{G}^{(0)}_{ij}(E_0) = \delta_{i7}\delta_{j7} + T^{(0)}_{ij}$, where $T^{(0)}_{ij}$ describe small tree-level contributions to $b \to sq\bar{q}\gamma$ from $Q^u_{1,2}$ and $Q_{3,\ldots,6}$ [123, 124]. Such contributions are small for three reasons: *(i)* kinematical suppression by the four-body phase-space factors in the presence of a relatively high cutoff $E_0 = 1.6\,\text{GeV}$ on the photon energy, *(ii)* smallness of the CKM factor $(V_{ub}V^*_{us})/(V_{tb}V^*_{ts})$, *(iii)* smallness of the Wilson coefficients $C_3(\mu_b), \ldots, C_6(\mu_b)$. The latter two reasons allow for neglecting the penguin and $Q^u_{1,2}$ operators at the NNLO, and keeping them only to a linear approximation in the NLO contributions to $b \to sq\bar{q}\gamma$. Such approximations are present in the recent NNLO analysis of Refs. [2,64], and we shall follow them here. Thus, at the NNLO we shall consider only $\widetilde{G}^{(0)}_{ij}$ with $i, j \in \{1, 2, 7, 8\}$.

The largest contributions to the branching ratio at the NLO ($n = 1$) and NNLO ($n = 2$) originate from $\widetilde{G}^{(n)}_{77}$, $\widetilde{G}^{(n)}_{17}$ and $\widetilde{G}^{(n)}_{27}$. These quantities at the NLO in QCD were evaluated in Refs. [125–129]. The $\mathcal{O}(\alpha_{\text{em}})$ electroweak corrections were calculated in Refs. [85, 122, 130–133]. Their impact on the branching ratio is about 2.5% [85]. Uncertainties stemming from the unknown higher-order ($\mathcal{O}(\alpha^2_{em})$) electroweak terms are thus certainly negligible.

The dependence of $\mathcal{B}\left(\bar{B} \to X_s\gamma\right)$ on m_c enters through the $Q_{1,2}$ matrix elements which start contributing at $\mathcal{O}\left(\alpha_s\right)$. The dominant m_c-dependence comes from two-loop $b \to s\gamma$ amplitudes whose effects are contained in $\widetilde{G}^{(1)}_{17}$ and $\widetilde{G}^{(1)}_{27}$. These NLO contributions depend so strongly on m_c that the induced dependence on the renormalization scale μ_c

at which the charm quark mass is $\overline{\rm MS}$-renormalized causes a serious problem for the precision of the NLO prediction. This is illustrated in Fig. 2.3 (adopted from Ref. [64]) where the NLO results are plotted with the dashed lines. The three plots illustrate the dependence of the branching ratio on μ_c and the previously defined scales μ_b and μ_0 that correspond to the final and initial points of the Wilson coefficient RG-evolution. The dashed lines in the first plot of Fig. 2.3 correspond to a variation of $\mathcal{B}\left(\bar{B}\to X_s\gamma\right)$ at the NLO by around $\pm 8.6\%$ when μ_c is varied in the interval between $m_c(m_c)\simeq 1.27\,\text{GeV}$ and $m_b(m_b)\simeq 4.16\,\text{GeV}$. At the latter scale we have $m_c(4.16\,\text{GeV})\simeq 0.92\,\text{GeV}$. Both values of μ_c are reasonable for the considered process, so the only way to suppress the μ_c-dependence is to evaluate the branching ratio at the NNLO. The NNLO result depends on μ_c not only via $m_c(\mu_c)$ but also contains an explicit logarithm of μ_c that compensates the μ_c-dependence of the NLO contribution. Determining this logarithmic term is very simple, but using it in a phenomenological analysis makes sense only after calculating the full NNLO corrections $\widetilde{G}_{17}^{(2)}$ and $\widetilde{G}_{27}^{(2)}$.

Although this problem was realized already in 2001, and became widely known soon after the publication of Ref. [52], no complete calculation of $\widetilde{G}_{17}^{(2)}$ and $\widetilde{G}_{27}^{(2)}$ for an arbitrary value of m_c is available until now. The reason is an extreme complexity of such a calculation. It requires evaluating a few hundreds of four-loop propagator diagrams with two mass scales. Our current calculation of the counterterm contributions (Chapter 4) is only a first step towards achieving this goal (see Chapter 5).

As we have already mentioned, an interpolation in m_c has been used so far in all the NNLO calculations of $\mathcal{B}\left(\bar{B}\to X_s\gamma\right)$. To describe this point in more detail, we need to introduce the quantities

$$K_{ij}\equiv\frac{\widetilde{G}_{ij}}{G_u^{\rm semi}} \tag{2.50}$$

where $G_u^{\rm semi}$ is related to the partonic $b\to X_u\ell\bar{\nu}$ decay rate as follows

$$\Gamma[b\to X_u\ell\bar{\nu}]=\frac{G_F^2 m_b^5}{192\pi^3}\,|V_{ub}|^2\,G_u^{\rm semi}. \tag{2.51}$$

It was calculated in Ref. [134] up to the NNLO. Here, we only need the explicit NLO expression

$$G_u^{\rm semi}=1+\widetilde{\alpha}_{\rm s}C_F(25/2-2\pi^2)+\mathcal{O}(\widetilde{\alpha}_{\rm s}^2), \tag{2.52}$$

where $\widetilde{\alpha}_{\rm s}=\alpha_{\rm s}/(4\pi)$ and $C_F=4/3$. The relation between $\widetilde{G}_{i7}^{(n)}$ for $i=1,2$ and $K_{i7}=\widetilde{\alpha}_{\rm s}K_{i7}^{(1)}+\widetilde{\alpha}_{\rm s}^2K_{i7}^{(2)}+\mathcal{O}(\widetilde{\alpha}_{\rm s}^3)$ is thus very simple

$$\widetilde{\alpha}_{\rm s}K_{i7}^{(1)}+\widetilde{\alpha}_{\rm s}^2K_{i7}^{(2)}+\mathcal{O}(\widetilde{\alpha}_{\rm s}^3)\;=\;\frac{\widetilde{\alpha}_{\rm s}\,\widetilde{G}_{i7}^{(1)}+\widetilde{\alpha}_{\rm s}^2\,\widetilde{G}_{i7}^{(2)}+\mathcal{O}(\widetilde{\alpha}_{\rm s}^3)}{G_u^{\rm semi}}\,. \tag{2.53}$$

The normalization to $G_u^{\rm semi}$ was introduced in Ref. [52] for the purpose of considering quantities that are insensitive to ambiguities (so-called renormalons) in the perturbative definition of the b-quark pole mass $m_{b,\rm pole}$ whose fifth power comes as a normalization factor in Eqs. (2.47) and (2.51). Both $\widetilde{G}_{ij}$ and $G_u^{\rm semi}$ are sensitive to these ambiguities, but their ratio is not. In consequence, the perturbative series for

$$\sum_{i,j}C_i^{\rm eff}(\mu_b)C_j^{\rm eff}(\mu_b)K_{ij}(E_0,\mu_b)\equiv P(E_0)=P^{(0)}+\widetilde{\alpha}_{\rm s}P^{(1)}+\widetilde{\alpha}_{\rm s}^2P^{(2)}+\mathcal{O}(\widetilde{\alpha}_{\rm s}^3) \tag{2.54}$$

shows much better convergence properties than the analogous expansion for the sum in Eq. (2.47).

In the context of the m_c-interpolation, we are interested in the NNLO correction $P^{(2)}$ on the r.h.s. of Eq. (2.54). When the perturbative expansion of K_{ij} is written in the same way as the one for $\widetilde{G}_{ij}$ in Eq. (2.48), one easily finds that.[8]

$$P^{(2)} = \left(C_i^{(1)} C_j^{(1)} + 2C_i^{(0)} C_j^{(2)}\right) K_{ij}^{(0)} + C_i^{(0)} C_j^{(0)} K_{ij}^{(2)} + 2C_i^{(0)} C_j^{(1)} K_{ij}^{(1)}. \tag{2.55}$$

Following the notation of Ref. [67], let us denote the three terms in the sum on the r.h.s. of the above equation by $P_1^{(2)}$, $P_2^{(2)}$ and $P_3^{(2)}$, respectively. It is only $P_2^{(2)}$ that is not yet fully known for arbitrary m_c, and it needs to be discussed further.

The correction $P_2^{(2)}$ is the only one depending on the NNLO matrix elements $K_{ij}^{(2)}$. Each of them can be split into two parts, in such a way that only the first one depends on the number n_f of the active flavors in our effective theory

$$K_{ij}^{(2)} = n_f A_{ij} + B_{ij}. \tag{2.56}$$

All the contributions A_{ij} for the operators relevant at the NNLO ($i, j \in \{1, 2, 7, 8\}$) are already known for arbitrary m_c [135–138]. They can be used in the Brodsky Lepage Mackenzie (BLM) (or large-$\beta^{(0)}$) approximation [139] which relies on the assumption that the numerically dominant NNLO corrections are proportional to $\beta^{(0)} = (11 - 2n_f)/3$. One writes

$$n_f A_{ij} + B_{ij} = -\frac{3}{2}\beta^{(0)} A_{ij} + B_{ij}^{\text{rem}}, \text{ where } B_{ij}^{\text{rem}} = \left(\frac{33}{2} A_{ij} + B_{ij}\right), \tag{2.57}$$

and then neglects the unknown remainder B_{ij}^{rem}. In Ref. [67], an important step beyond the BLM approximation was made. The correction $P_2^{(2)}$ was split into a sum of the BLM and non-BLM terms

$$P_2^{(2)} = P_2^{(2)\beta^{(0)}} + P_2^{(2)\text{rem}}, \tag{2.58}$$

where

$$P_2^{(2)\beta^{(0)}} = -\frac{3}{2}\beta^{(0)} \sum_{i,j} C_i^{(0)} C_j^{(0)} A_{ij}, \tag{2.59}$$

$$P_2^{(2)\text{rem}} = \sum_{i,j} C_i^{(0)} C_j^{(0)} B_{ij}^{\text{rem}}. \tag{2.60}$$

Next, the non-BLM correction $P_2^{(2)\text{rem}}$ was calculated in the limit $m_c \gg m_b/2$ by performing a formal decoupling of the charm quark in this limit [68]. Finally, $P_2^{(2)\text{rem}}$ was interpolated downwards in m_c using BLM assumptions at $m_c = 0$. The functional form of $P_2^{(2)\text{rem}}$ used for interpolation can be found in Eq. (6.4) of Ref. [67]. In Fig. 2.4 (adopted from Ref. [64]), the (a), (b) and (c) cases of the interpolated $P_2^{(2)\text{rem}}$ correspond to various assumptions for the boundary condition at $m_c = 0$, as given in Eqs. (6.1), (6.2) and (6.3) of the 2006 article [67], respectively. The two vertical dash-dotted lines mark the 1-sigma range for $m_c(m_c)/m_b$. The dashed lines describe the leading terms in the large-m_c expansion. The thin solid lines show the small-m_c expansions (up to $\mathcal{O}\left(m_c^8/m_b^8\right)$) of

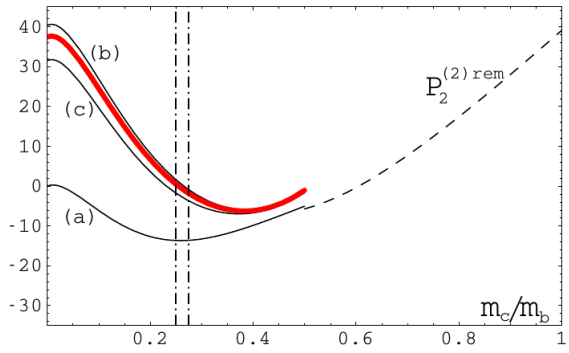

Figure 2.4: Interpolation of $P_2^{(2)\mathrm{rem}}$ in m_c as in Fig. 5 of [64]. It corresponds to Fig. 2b of Ref. [67] but with updated input parameters and with renormalization scales shifted from $(\mu_c, \mu_b) = (1.5, 2.5)$ GeV to $(\mu_c, \mu_b) = (2, 2)$ GeV. In addition, the thick solid (red) line shows the case with the presently known boundary condition at $m_c = 0$ imposed.

the interpolating functions. The shapes of the curves are quite sensitive to the choice of renormalization scales.

The four-loop calculation presented in the 2015 article [64] provided us with the exact form of the boundary conditions at $m_c = 0$. The corresponding interpolation curve is shown as a thick solid (red) line in Fig. 2.4. This line turns out to be very close to the former curve (b), which means that the version (b) of the BLM approximation works very well at $m_c = 0$. It is quite understandable because (b) corresponds to the BLM approximation for the full NNLO correction to the observable branching ratio, while (a) was only the BLM approximation to $P_2^{(2)}$ that is not an observable. Moreover, one concludes that the BLM approximation (b) (the one for the branching ratio) works very well at $m_c = 0$.

Although the red curve in Fig. 2.4 provides a comparison between Refs. [67] and [64], it does not correspond to the final results of the latter paper where the actual interpolation was *not* performed for the whole $P_2^{(2)}$. Instead, it was done only for those parts of the non-BLM contributions to $K_{17}^{(2)}$ and $K_{27}^{(2)}$ whose exact dependence on m_c remains still unknown. A more detailed description of this procedure will be given in Sec. 2.3.

Before closing this section, let us summarize what contributions to the NNLO matrix elements $\widetilde{G}_{ij}^{(2)}$ are already known. As we have already mentioned, we neglect the penguin operators at this level, so we are interested only in $i, j \in \{1, 2, 7, 8\}$. To make the notation more compact, we shall represent the two current-current operators $Q_{1,2}$ by Q_2 alone. Then we are left with only six combinations of indices to consider. Three of them ($\widetilde{G}_{77}^{(2)}$, $\widetilde{G}_{78}^{(2)}$, $\widetilde{G}_{27}^{(2)}$) involve the photonic dipole operator, and the remaining three ($\widetilde{G}_{22}^{(2)}$, $\widetilde{G}_{28}^{(2)}$, $\widetilde{G}_{88}^{(2)}$) do not.

The calculations of $\widetilde{G}_{77}^{(2)}$ [121, 140–143] and $\widetilde{G}_{78}^{(2)}$ [144, 145] have been already completed for an arbitrary value of m_c. Two-body final state contributions to $\widetilde{G}_{22}^{(2)}$, $\widetilde{G}_{28}^{(2)}$ and $\widetilde{G}_{88}^{(2)}$ are also known for arbitrary m_c, as they are products of the formerly calculated NLO corrections. On the other hand, for the remaining (three-body and four-body final state) contributions to these quantities, only results in the BLM approximation are available [135, 137, 138]. This situation is not likely to improve in the near future be-

[8] We shall skip the superscript "eff" at the Wilson coefficients in the remainder of this subsection.

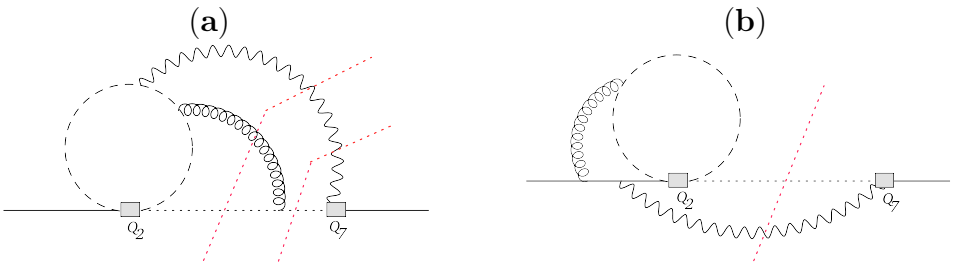

Figure 2.5: Sample Feynman diagrams contributing to the NNLO counterterms with possible 2-particle and 3-particle cuts (red dotted lines). The black solid, dashed and dotted lines denote the b-quark, c-quark and s-quark propagators, respectively.

cause five-loop diagrams (with unitarity cuts) matter for $\widetilde{G}_{22}^{(2)}$. However, the unknown non-BLM terms are not expected to cause a significant uncertainty because the known NLO+(NNLO BLM) terms for the considered quantities affect the branching ratio by less than 4%, which is partly due to phase-space suppression of the $(n > 2)$-body contributions.

It remains to discuss $\widetilde{G}_{27}^{(2)}$ that is numerically important but not yet known in a complete manner. As we have already mentioned, the BLM corrections to this quantity (for arbitrary m_c) are already known [135, 136]. Moreover, effects of massive fermion loops on the gluon lines were computed in Ref. [146]. The remaining non-BLM parts are known in the heavy charm limit [67, 68], and recently also in the $m_c = 0$ case [64], which has served as a basis for the interpolation, the discussion of which will be continued in Sec. 2.3. However, before reaching that point, it is convenient to discuss certain aspects of the NNLO calculations that are very similar in the $m_c = 0$ and $m_c \neq 0$ cases. This is what the next section is devoted to.

2.2 Renormalization of the matrix elements and the NNLO counterterms for arbitrary m_c

Let us now discuss the UV renormalization in the calculation of $\widetilde{G}_{27}^{(2)}$ for an arbitrary value of m_c. The case of $\widetilde{G}_{17}^{(2)}$ is analogous. Examples of four-loop diagrams that need to be calculated for the *bare* contribution $\widetilde{G}_{27}^{(2)\text{bare}}$ are given in Fig. 5.1 in Chapter 5. Apart from them, one needs to calculate the UV counterterm contributions, sample diagrams for which are shown in Fig. 2.5. The latter diagrams represent interferences between the $b \to s\gamma$ and $b \to s\gamma g$ amplitudes generated by the operators Q_2 and Q_7. One needs to consider a particular *unitarity cut* in each diagram (red dotted line) which tells us which particles are the on-shell final-state ones. In the three-body final state cases, their propagators are going to be treated with the *reverse unitarity* approach (see Sec. 3.2.2) before applying the IBP reduction.

The diagrams in Fig. 2.5 are actually the same ones that have already been calculated at the NLO in Refs. [125, 127]. However, one needs to extend these calculations to one more order in ε because the UV-divergent renormalization constants are going to be inserted in the vertices. Moreover, diagrams with squared b-quark propagators need to be considered for the purpose of the b-quark mass renormalization. No such necessity

occurs for the c and s quarks because the latter one is massless, while the renormalization of m_c can be accounted for by differentiation of the NLO results with respect to this mass (see below).

Another set of contributions to be taken into account for the considered UV counterterms are the diagrams with such operators Q_j into which Q_2 mixes at the LO and NLO, i.e. the ones for which the renormalization constants Z_{2j} are nonvanishing at orders $\mathcal{O}(\alpha_{\rm s})$ and $\mathcal{O}(\alpha_{\rm s}^2)$.

Below, we present an explicit expression for obtaining the renormalized $\widetilde{G}_{27}^{(1)}$ and $\widetilde{G}_{27}^{(2)}$ from a set of bare interference terms and the relevant renormalization constants. It is a straightforward generalization of Eq. (2.10) of Ref. [64] to the case of arbitrary m_c. Actually, the only difference is an additive term involving the above-mentioned differentiation with respect to m_c. Moreover, all the necessary ingredients need to be calculated for an arbitrary $z = m_c^2(\mu_c)/m_{b,\rm pole}^2$. The expression reads

$$\begin{aligned}
\widetilde{\alpha}_{\rm s}\widetilde{G}_{27}^{(1)} + \widetilde{\alpha}_{\rm s}^2\widetilde{G}_{27}^{(2)} = Z_b^{OS} Z_m^{OS} \bar{Z}_{77}\Big\{ & \widetilde{\alpha}_{\rm s}^2 s^{3\varepsilon}\widetilde{G}_{27}^{(2)\rm bare} + (Z_m^{OS}-1)s^{\varepsilon}\big[\bar{Z}_{24}\hat{G}_{47}^{(0)m} + \widetilde{\alpha}_{\rm s}s^{\varepsilon}\widetilde{G}_{27}^{(1)m}\big] \\
& + \widetilde{\alpha}_{\rm s}(Z_G^{OS}-1)s^{2\varepsilon}\widetilde{G}_{27}^{(1)3P} + \bar{Z}_{27}Z_m^{OS}\big[\widetilde{G}_{77}^{(0)} + \widetilde{\alpha}_{\rm s}s^{\varepsilon}\widetilde{G}_{77}^{(1)\rm bare}\big] \\
& + \widetilde{\alpha}_{\rm s}\bar{Z}_{28}s^{\varepsilon}\widetilde{G}_{78}^{(1)\rm bare} + \sum_{j=1,\ldots,6,11,12}\bar{Z}_{2j}s^{\varepsilon}\big[\hat{G}_{j7}^{(0)} + \widetilde{\alpha}_{\rm s}s^{\varepsilon}\bar{Z}_g^2\hat{G}_{j7}^{(1)\rm bare}\big]\Big\} \\
& + 2\widetilde{\alpha}_{\rm s}\left(\frac{\mu_b^2}{\mu_c^2}\right)^{\varepsilon} s^{2\varepsilon}(\bar{Z}_m - 1)\, z\frac{d}{dz}\widetilde{G}_{27}^{(1)\rm bare} + \mathcal{O}(\widetilde{\alpha}_{\rm s}^3)
\end{aligned} \tag{2.61}$$

where $s = \frac{4\pi\mu_b^2}{m_b^2}e^{\gamma}$, and $\gamma \simeq 0.5772$ is the Euler-Mascheroni constant.

To explain the meaning of symbols in the above equation, we begin with the renormalization constants. The on-shell [147] renormalization constants of the b-quark field and its mass are denoted by $Z_b^{\rm OS}$ and $Z_m^{\rm OS}$, respectively, while $Z_G^{\rm OS}$ stands for the on-shell renormalization constant of the gluon field. The explicit one-loop expression for $Z_G^{\rm OS}$ depends on the number of massive quarks in the effective theory. In our case, the u, d and s quarks are treated as massless. Moreover, we shall follow the approach of Ref. [64] where the c-quark loops on the gluon lines together with the corresponding UV-counterterms were skipped. Contributions from such loops to $\widetilde{G}_{27}^{(2)}$ have been already evaluated up to the NNLO in Ref. [146], and we shall not re-calculate them. Thus, for our purpose, the one-loop expression for $Z_G^{\rm OS}$ contains only the b-quark loop contributions, which we shall mark by n_b below ($n_b = 1$). In such a case, one finds

$$\begin{aligned}
Z_b^{\rm OS} &= 1 - \frac{4}{3}\,\widetilde{\alpha}_{\rm s}\, s^{\varepsilon}\, e^{\gamma\varepsilon}\,\Gamma(\varepsilon)\,\frac{3-2\varepsilon}{1-2\varepsilon} + \mathcal{O}(\widetilde{\alpha}_{\rm s}^2), \\
Z_G^{\rm OS} &= 1 - \frac{2}{3}\,n_b\,\widetilde{\alpha}_{\rm s}\, s^{\varepsilon}\, e^{\gamma\varepsilon}\,\Gamma(\varepsilon) + \mathcal{O}(\widetilde{\alpha}_{\rm s}^2),
\end{aligned} \tag{2.62}$$

and $Z_m^{\rm OS} = Z_b^{\rm OS} + \mathcal{O}(\widetilde{\alpha}_{\rm s}^2)$. The s-quark field renormalization does not matter for our purpose because $Z_s^{\rm OS} = 1 + \mathcal{O}(\widetilde{\alpha}_{\rm s}^2)$. We use the on-shell scheme for the b-quark mass renormalization to get the final results in terms of the pole mass only, including the overall $m_{b,\rm pole}^5$ in Eq. (2.47).

All the remaining renormalization constants correspond to the $\overline{\rm MS}$ scheme, which is marked in Eq. (2.61) by bars over the corresponding Z's. For compactness, we present

below their MS counterparts.[9] The MS renormalization constants of the quark mass and the gauge coupling are given by $Z_m = 1 - \frac{4\widetilde{\alpha}_s}{\varepsilon} + \mathcal{O}(\widetilde{\alpha}_s^2)$ and $Z_g = 1 + \frac{\widetilde{\alpha}_s}{\varepsilon}\left(-\frac{11}{2} + \frac{f}{3}\right) + \mathcal{O}(\widetilde{\alpha}_s^2)$, respectively, with f denoting the number of active flavors in the effective theory. Since we have skipped the charm quark loops on the gluon lines, we shall substitute $f = n_b + n_l$, where $n_l = 3$ stands for the number of massless flavors.

The relevant MS renormalization constants for the Wilson coefficients have been collected in Eq. (2.9) of Ref. [64]. They read

$$Z_{77} = 1 + \tfrac{16\,\widetilde{\alpha}_s}{3\,\varepsilon} + \mathcal{O}(\widetilde{\alpha}_s^2),$$

$$\begin{aligned}
Z_{11} &= 1 - \tfrac{2\,\widetilde{\alpha}_s}{\varepsilon} + \mathcal{O}(\widetilde{\alpha}_s^2), & Z_{21} &= \tfrac{6\,\widetilde{\alpha}_s}{\varepsilon} + \mathcal{O}(\widetilde{\alpha}_s^2),\\
Z_{12} &= \tfrac{4\,\widetilde{\alpha}_s}{3\,\varepsilon} + \mathcal{O}(\widetilde{\alpha}_s^2), & Z_{22} &= 1 + \mathcal{O}(\widetilde{\alpha}_s^2),\\
Z_{13} &= \widetilde{\alpha}_s^2\left(\tfrac{10}{81\,\varepsilon^2} - \tfrac{353}{243\,\varepsilon}\right) + \mathcal{O}(\widetilde{\alpha}_s^3), & Z_{23} &= \widetilde{\alpha}_s^2\left(-\tfrac{20}{27\,\varepsilon^2} - \tfrac{104}{81\,\varepsilon}\right) + \mathcal{O}(\widetilde{\alpha}_s^3),\\
Z_{14} &= -\tfrac{1}{6}Z_{24} + \widetilde{\alpha}_s^2\left(\tfrac{1}{2\varepsilon^2} - \tfrac{11}{12\,\varepsilon}\right), & Z_{24} &= \tfrac{2\,\widetilde{\alpha}_s}{3\,\varepsilon} + \widetilde{\alpha}_s^2\left(\tfrac{-188+12f}{27\,\varepsilon^2} + \tfrac{338}{81\,\varepsilon}\right) + \mathcal{O}(\widetilde{\alpha}_s^3),\\
Z_{15} &= \widetilde{\alpha}_s^2\left(-\tfrac{1}{81\,\varepsilon^2} + \tfrac{67}{486\,\varepsilon}\right) + \mathcal{O}(\widetilde{\alpha}_s^3), & Z_{25} &= \widetilde{\alpha}_s^2\left(\tfrac{2}{27\,\varepsilon^2} + \tfrac{14}{81\,\varepsilon}\right) + \mathcal{O}(\widetilde{\alpha}_s^3),\\
Z_{16} &= \widetilde{\alpha}_s^2\left(-\tfrac{5}{216\,\varepsilon^2} - \tfrac{35}{648\,\varepsilon}\right) + \mathcal{O}(\widetilde{\alpha}_s^3), & Z_{26} &= \widetilde{\alpha}_s^2\left(\tfrac{5}{36\,\varepsilon^2} + \tfrac{35}{108\,\varepsilon}\right) + \mathcal{O}(\widetilde{\alpha}_s^3),\\
Z_{17} &= -\tfrac{1}{6}Z_{27} + \widetilde{\alpha}_s^2\left(\tfrac{22}{81\,\varepsilon^2} - \tfrac{332}{243\,\varepsilon}\right), & Z_{27} &= \tfrac{116\,\widetilde{\alpha}_s}{81\,\varepsilon} + \widetilde{\alpha}_s^2\left(\tfrac{-3556+744f}{2187\,\varepsilon^2} + \tfrac{13610-44f}{2187\,\varepsilon}\right) + \mathcal{O}(\widetilde{\alpha}_s^3),\\
Z_{18} &= \tfrac{167\,\widetilde{\alpha}_s}{648\,\varepsilon} + \mathcal{O}(\widetilde{\alpha}_s^2), & Z_{28} &= \tfrac{19\,\widetilde{\alpha}_s}{27\,\varepsilon} + \mathcal{O}(\widetilde{\alpha}_s^2),\\
Z_{1(11)} &= \tfrac{5\,\widetilde{\alpha}_s}{12\,\varepsilon} + \mathcal{O}(\widetilde{\alpha}_s^2), & Z_{2(11)} &= \tfrac{\widetilde{\alpha}_s}{\varepsilon} + \mathcal{O}(\widetilde{\alpha}_s^2),\\
Z_{1(12)} &= \tfrac{2\,\widetilde{\alpha}_s}{9\,\varepsilon} + \mathcal{O}(\widetilde{\alpha}_s^2), & Z_{2(12)} &= \mathcal{O}(\widetilde{\alpha}_s^2),
\end{aligned} \tag{2.63}$$

In the last two lines, we encounter renormalization constants corresponding to the evanescent operators Q_{11} and Q_{12} defined in Eqs. (2.11) and (2.12), respectively. Without their contributions, the result on the l.h.s. of Eq. (2.61) would not come out finite.

All the G-symbols on the r.h.s. of Eq. (2.61) stand for interference terms between unrenormalized decay amplitudes. Some of them appear as $\hat{G}_{ij}$ instead of $\widetilde{G}_{ij}$, which indicates that they correspond to Eq. (2.47) written in terms of the original Wilson coefficients (Eq. (2.8)) rather than the effective ones (Eq. (2.42)). Using $\hat{G}_{ij}$'s makes Eq. (2.61) somewhat more compact, and $\hat{G}_{ij} = \widetilde{G}_{ij}$ unless one of the indices belong to the set $\{3, 4, 5, 6\}$, i.e. corresponds to the penguin operators. At present, we keep the same notation for the interference terms in both the $m_c = 0$ and $m_c \neq 0$ cases. However, we will discriminate between them while providing our results in Chapters 4 and 5.

The interference terms marked by "3P" originate from three-particle final states only. Separating such contributions matters for the external gluon field renormalization. All our interference terms are assumed to be calculated without pure-QCD loop corrections on the external lines. This fact determines the way in which the on-shell renormalization constants enter into Eq. (2.61).

The quantities $\hat{G}_{47}^{(0)m}$ and $\widetilde{G}_{27}^{(1)m}$ originate from diagrams with squared b-quark propagators. As we have already mentioned, they matter for the renormalization of m_b. Let us explain in more detail why this is so. For a one-loop renormalization of any mass m, we

[9] The renormalized $\widetilde{G}_{27}^{(n)}$ remain unchanged after replacing the $\overline{\text{MS}}$ constants by the MS ones ($\bar{Z}_g \to Z_g$, $\bar{Z}_m \to Z_m$, $\bar{Z}_{ij} \to Z_{ij}$) simultaneously with replacing $s \to \mu_b^2/m_b^2$ on the r.h.s. of Eq. (2.61) and inside the on-shell constants (2.62).

can calculate diagrams with the bare mass $m^{\rm b}$, and then replace $m^{\rm b} \to m + \delta m$, where m is the renormalized mass. Finally, we Taylor-expand in δm to the first order. Thus, we need a derivative of each diagram with respect to the explicit m (i.e. the one that is explicitly present in the propagators, not the one that arises from the on-shell condition ($p^2 = m_b^2$) in the case of m_b-renormalization). For each fermionic propagator $\frac{i}{\not p - m}$, one has

$$\frac{i}{\not p - m - \delta m} = \frac{i}{\not p - m} + \frac{i\,\delta m}{(\not p - m)^2} + \dots \tag{2.64}$$

Similarly for bosonic propagators,

$$\frac{i}{p^2 - m^2 - \delta m^2} = \frac{i}{p^2 - m^2} + \frac{i\,\delta m^2}{(p^2 - m^2)^2} + \dots . \tag{2.65}$$

For the interferences involving Q_1 and Q_2, we could also consider diagrams with the m_c-propagators squared. However, there is a simpler method which can be applied for the m_c-renormalization, and which was not applicable to the m_b-renormalization. Namely, we can find the relevant counterterm contributions by just differentiating $\widetilde{G}_{27}^{(1)}$ with respect to m_c. It could not have been done for m_b, because m_b in the final results comes both from m_b in the propagators and from the external momentum. Distinguishing the two sources would make the IBP cumbersome, so it is much simpler to just calculate the diagrams with squared propagators in the case of m_b. On the other hand, m_c comes only from the propagators, so we can just differentiate. Now it is easy to understand the last term in Eq. (2.61). We calculate $\widetilde{G}_{27}^{(1)}$ with a bare charm quark mass, as mentioned earlier. Only after getting the analytical result in m_c, we substitute $m_c^{\rm b} = \overline{Z}_m m_c$. Next, we expand in $\alpha_{\rm s}$, and we get the very last term in in Eq. (2.61). Another question is whether the differentiation with respect to z can be easily performed in practice. For this purpose, we shall calculate $\widetilde{G}_{27}^{(1)\rm bare}(z)$ to order $\mathcal{O}(\varepsilon)$ not only numerically but also using a power-logarithmic expansion around $z = 0$ to a sufficient accuracy.

As a final remark in this section, let us note that $\hat{G}_{j7}^{(0)}$ vanish for $j = 1, 2, 11, 12$, which needs to be taken into account when computing the sum in the third line of Eq. (2.61).

2.3 The CP- and isospin-averaged branching ratio

In the present section, we discuss the actual formulae that were used for evaluation of the most recent prediction for the CP- and isospin-averaged branching ratio in Refs. [2, 64]. The main expression used there to express the branching ratio in terms of experimentally measured and theoretically calculated quantities has the following form [52]

$$\mathcal{B}(\bar{B} \to X_s\gamma)_{E_\gamma > E_0} = \mathcal{B}(\bar{B} \to X_c e\bar{\nu})^{\rm exp} \left[\mid V_{tb}V_{ts}^*/V_{cb} \mid^2 \frac{6\alpha_{em}}{\pi\, C}\ [P(E_0) + N(E_0)] \right]. \tag{2.66}$$

Here, the semileptonic phase space factor C [52] is defined as

$$C = |V_{ub}/V_{cb}|^2 \frac{\mathcal{B}(\bar{B} \to X_c e\bar{\nu})}{\mathcal{B}(\bar{B} \to X_u e\bar{\nu})}. \tag{2.67}$$

The reason for using a normalization to the measured semileptonic branching ratio $\mathcal{B}(\bar{B} \to X_c e\bar{\nu})^{\rm exp}$ and employing the factor C is to reduce the uncertainties stemming from the CKM matrix elements and the bottom quark mass in the SM prediction for $\mathcal{B}(\bar{B} \to X_s\gamma)$. The factor C is calculated on the theoretical side using perturbative and nonperturbative parameters determined from fits to the measured semileptonic decay rate and spectra [41].

The other two quantities in Eq. (2.66) to be calculated on the theoretical side are $P(E_0)$ and $N(E_0)$. The former is numerically dominant. It is a perturbative object defined by the equation

$$\frac{\Gamma[b \to X_s^{\rm partonic}\gamma]_{E_\gamma > E_0}}{|V_{cb}/V_{ub}|^2\Gamma[b \to X_u^{\rm partonic} e\bar{\nu}]} \quad = \quad |\, V_{tb}V_{ts}^*/V_{cb}\,|^2\, \frac{6\alpha_{em}}{\pi}\, P(E_0). \tag{2.68}$$

Its relation to the Wilson coefficients and the quantities K_{ij} has been given in Eq. (2.54). The nonperturbative correction $N(E_0)$ contains the contributions that were discussed in Sec. 2.1.3.

Let us focus on the NNLO corrections to the perturbative part $P(E_0)$. Once the penguin operators are neglected at the $\mathcal{O}(\alpha_s^2)$ level, the only NNLO corrections involving Q_7 that are not yet known for arbitrary m_c originate from the functions $F_i(z,\delta)$ in the following expressions for the quantities $K_{17}^{(2)}$ and $K_{27}^{(2)}$ [64]

$$\begin{aligned}
K_{17}^{(2)}(z,\delta) &= -\frac{1}{6}K_{27}^{(2)}(z,\delta) + A_1 + F_1(z,\delta) + \left(\frac{94}{81} - \frac{3}{2}K_{27}^{(1)} - \frac{3}{4}K_{78}^{(1)}\right) L_b - \frac{34}{27}L_b^2, \\
K_{27}^{(2)}(z,\delta) &= A_2 + F_2(z,\delta) - \frac{3}{2}\beta^{(0),\,n_l=3} f_q(z,\delta) + f_b(z) + f_c(z) + \frac{4}{3}\phi_{27}^{(1)}(z,\delta)\ln z \\
&+ \left[(8L_c - 2x_m)\, z\frac{d}{dz} \;+\; (1-\delta)x_m\frac{d}{d\delta}\right] f_{NLO}(z,\delta) + \frac{416}{81}x_m \\
&+ \left(\frac{10}{3}K_{27}^{(1)} - \frac{2}{3}K_{47}^{(1)} - \frac{208}{81}K_{77}^{(1)} - \frac{35}{27}K_{78}^{(1)} - \frac{254}{81}\right) L_b - \frac{5948}{729}L_b^2.
\end{aligned} \tag{2.69}$$

Here, $\delta = 1 - 2E_0/m_b$, $\beta^{(0),\,n_l=3} = 9$, $L_b = \ln(\mu_b^2/m_b^2)$ and $L_c = \ln(\mu_c^2/m_c^2)$. The function $\phi_{27}^{(1)}(z,\delta)$ is given in Appendix B here. The relevant NLO quantities $K_{ij}^{(1)}$ are collected in Appendix C of Ref. [64].

There are several quantities on the r.h.s. of Eq. (2.69) which require to be specified and discussed. We do it item-by-item below.

- The functions $F_i(z,\delta)$ are defined in such a manner that $F_i(0,1) = 0$. Apart from that, the only thing we know about them at present are the leading terms of their

large-z asymptotic expansions. From the results of Refs. [67, 68], one finds

$$\begin{aligned} F_1(z,\delta) &= \frac{70}{27}\ln^2 z + \left(\frac{119}{27} - \frac{2}{9}\pi^2 + \frac{3}{2}\phi_{78}^{(1)}(\delta)\right)\ln z - \frac{493}{2916} - \frac{5}{54}\pi^2 + \frac{232}{27}\zeta(3) \\ &+ \frac{5}{8}\phi_{78}^{(1)}(\delta) - A_1 + \mathcal{O}\left(\frac{1}{z}\right), \\ F_2(z,\delta) &= -\frac{4736}{729}\ln^2 z + \left\{-\frac{165385}{2187} + \frac{1186}{729}\pi^2 - \frac{2\pi}{9\sqrt{3}} + \frac{2}{3}Y_1 + \frac{4}{3}\phi_{47}^{(1)}(\delta) + \frac{832}{81}\phi_{77}^{(1)}(\delta)\right. \\ &+ \left.\frac{70}{27}\phi_{78}^{(1)}(\delta)\right\}(\ln z + 1) - \frac{956435}{19683} - \frac{2662}{2187}\pi^2 + \frac{20060}{243}\zeta(3) - \frac{1624}{243}\phi_{77}^{(1)}(\delta) \\ &- \frac{293}{162}\phi_{78}^{(1)}(\delta) - A_2 + \mathcal{O}\left(\frac{1}{z}\right). \end{aligned} \tag{2.70}$$

The necessary $\phi_{ij}^{(1)}$ functions are given in Appendix B here. The constant Y_1 can be found in Appendix B of Ref. [64].

- The remaining (known) m_c-dependent quantities on the r.h.s. of Eq. (2.69) read

$$\begin{aligned} f_{NLO}(z,\delta) &= \mathrm{Re}\, r_2^{(1)}(z) + 2\phi_{27}^{(1)}(z,\delta), \\ f_q(z,\delta) &= \mathrm{Re}\, r_2^{(2)}(z) - \tfrac{4}{3}h_{27}^{(2)}(z,\delta), \\ f_b(z) &\simeq -1.836 + 2.608\, z + 0.8271\, z^2 - 2.441\, z\ln z, \\ f_c(z) &\simeq 9.099 + 13.20\, z - 19.68\, z^2 + 25.71\, z\ln z. \end{aligned} \tag{2.71}$$

The function $f_q(z)$ describes the NNLO BLM terms. Explicit formulae for $r_2^{(1)}(z)$ and $\mathrm{Re}\, r_2^{(2)}(z)$ can be found, e.g., in Refs. [67, 129].

- The constants A_1 and A_2 are known only numerically. They read

$$A_1 \simeq 22.605, \qquad A_2 \simeq 75.603. \tag{2.72}$$

These values are recovered from the $m_c = 0$ calculation of Ref. [64], and from the condition $F_i(0,1) = 0$.

- In the evaluation of the analytical results for K_{ij}, the pole mass of the b quark is used first. Next, one shifts to any renormalon-free scheme using the one-loop relation

$$\frac{m_{b,\mathrm{pole}}}{m_{b,\mathrm{X}}} = 1 + \widetilde{\alpha}_{\mathrm{s}} x_m + \mathcal{O}(\widetilde{\alpha}_{\mathrm{s}}^2). \tag{2.73}$$

where $m_{b,\mathrm{X}}$ denotes the renormalized mass in the new scheme. Only after such a shift, a numerical value of $m_{b,\mathrm{X}}$ is substituted. This explains the appearance of x_m in Eq. (2.69). For the so-called kinetic and 1S schemes, we have

$$x_m = \frac{64\mu_{\mathrm{kin}}}{9m_b}\left(1 + \frac{3\mu_{\mathrm{kin}}}{8m_b}\right), \text{ in the kinetic scheme,} \tag{2.74}$$

$$x_m = \tfrac{8}{9}\pi\alpha_\Upsilon, \qquad \text{in the 1S scheme.} \tag{2.75}$$

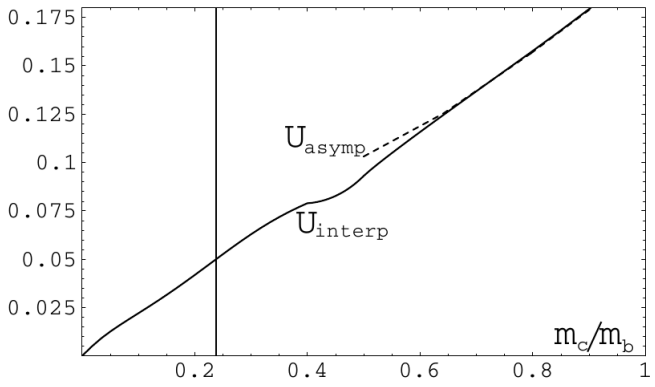

Figure 2.6: The function $U_{\rm interp}(z,1)$ (solid line) and asymptotic behavior of the true function $U(z,1)$ for $m_c \gg m_b/2$ (dashed line), as presented in Fig. 4 of Ref. [64]. The vertical line corresponds to the measured value of m_c/m_b.

In the analysis of Refs [2, 64], the kinetic scheme was used. For the central value of the SM prediction, the renormalization scales were set to $\mu_0 = 160\,\text{GeV}$ and $\mu_b = \mu_c = 2\,\text{GeV}$.

- In the 2015 version of the phenomenological analysis [2, 64], the m_c-interpolation is applied only to the functions $F_i(z,\delta)$. One takes $K_{17}^{(2)}$ and $K_{27}^{(2)}$ as they stand in Eq. (2.69), and replaces the unknown $F_i(z,\delta)$ by $F_i^{\rm interp}(z,1)$ which are assumed to be linear combinations of $f_q(z,1)$, $f_{NLO}(z,1)$, $z\frac{d}{dz}f_{NLO}(z,1)$ and a constant term. The coefficients in these linear combinations are fixed in a unique manner once we require that the interpolated functions satisfy the condition $F_i^{\rm interp}(0,1) = 0$ and match the known large-z asymptotic behavior of $F_i(z,1)$ that follows from Eq. (2.70). Explicitly, one finds

$$\begin{aligned} F_1^{\rm interp}(z,1) &= -23.75 + \frac{35}{12}\,f_q(z,1) + \left(\frac{2129}{936} - \frac{9}{52}\pi^2 - 0.84\,z\frac{d}{dz}\right) f_{NLO}(z,1), \\ F_2^{\rm interp}(z,1) &= -3.01 - \frac{592}{81}\,f_q(z,1) + \left(-10.34 - 9.55\,z\frac{d}{dz}\right) f_{NLO}(z,1). \end{aligned} \quad (2.76)$$

We note that the interpolation is performed for $\delta = 1$, while all the known contributions are evaluated at $\delta = 1 - 2E_0/m_b \simeq 0.3$ for $E_0 = 1.6\,\text{GeV}$. Such an approximation is enforced by the fact that the $m_c = 0$ calculation of the full NNLO corrections $\widetilde{G}_{17}$ and $\widetilde{G}_{27}$ in Ref. [64] was done only at $\delta = 1$, for technical reasons. However, the δ-dependence of the known parts of $\widetilde{G}_{17}$ and $\widetilde{G}_{27}$ is very weak, and the same is expected for $F_i(z,\delta)$. In any case, the uncertainty due to interpolation (see the next section) will also include the effect of setting δ to unity in the interpolated functions.

Let $\Delta\mathcal{B}(\bar{B} \to X_s\gamma)$ denote the contribution from the interpolated $F_{1,2}(z,\delta)$ to $\mathcal{B}(\bar{B} \to$

$X_s\gamma$). We define the function $U(z,\delta)$ as follows

$$\frac{\Delta\mathcal{B}(\bar{B}\to X_s\gamma)}{\mathcal{B}(\bar{B}\to X_s\gamma)} \;\simeq\; U(z,\delta) \;\equiv\; \frac{\alpha_{\rm s}^2(\mu_b)}{8\pi^2}\;\frac{C_1^{(0)}(\mu_b)F_1(z,\delta)+\left(C_2^{(0)}(\mu_b)-\frac{1}{6}C_1^{(0)}(\mu_b)\right)F_2(z,\delta)}{C_7^{(0)\rm eff}(\mu_b)}. \tag{2.77}$$

This function quantifies the relative effect of the interpolated corrections on the branching ratio. For $\mu_b = 2.0\,\text{GeV}$, we have $\alpha_{\rm s}(\mu_b) \simeq 0.293$, $C_1^{(0)}(\mu_b) \simeq -0.902$, $C_2^{(0)}(\mu_b) \simeq 1.073$, and $C_7^{(0)\rm eff}(\mu_b) \simeq -0.385$. With these inputs, one finds the following interpolated expression for $U(z,1)$

$$U_{\rm interp}(z,1) \;=\; x_1 \,+\, x_2\, f_q(z,1) \,+\, \left(x_3 \,+\, x_4\, z\frac{d}{dz}\right) f_{NLO}(z,1), \tag{2.78}$$

where $x_i \simeq (-0.0502,\ 0.0328,\ 0.0373,\ 0.0309)$. It is plotted by the solid line in Fig. 2.6. The dashed line shows the known asymptotic behavior for $m_c \gg m_b/2$. The boundary at $(0,0)$ is fixed by the condition $F_i(0,1) = 0$. One can read out that the interpolated correction grows from 0 to around $+5\%$ when m_c grows from zero to the measured value (marked by the vertical line).

Before closing this section, let us comment on the relation of decay rates to the CP- and isospin-averaged branching ratio in an untagged measurement at $\Upsilon(4S)$. The CP-averaged decay rates are

$$\Gamma_0 = \frac{\Gamma(\bar{B}^0\to X_s\gamma)+\Gamma(B^0\to X_{\bar{s}}\gamma)}{2}, \qquad \Gamma_\pm = \frac{\Gamma(B^-\to X_s\gamma)+\Gamma(B^+\to X_{\bar{s}}\gamma)}{2}, \tag{2.79}$$

with their isospin average $\Gamma = (\Gamma_0+\Gamma_\pm)/2$ and asymmetry $\Delta_{0\pm} = (\Gamma_0-\Gamma_\pm)/(\Gamma_0+\Gamma_\pm)$. In the above equation, we have specified the final state strangeness (-1 for X_s and $+1$ for $X_{\bar{s}}$) and the neutral B-meson flavors by ignoring the effects of the $K^0\bar{K}^0$ and $B^0\bar{B}^0$ mixing. Taking the $K^0\bar{K}^0$ mixing into account is equivalent to replacing X_s and $X_{\bar{s}}$ by $X_{|s|}$ with an unspecified strangeness sign. It leaves Γ_0 and $\Gamma_\pm$ invariant. Next, to take the $B^0\bar{B}^0$ mixing into account, one should use in Γ_0 the time-integrated decay rates of mesons whose flavor is fixed at the production time. Such a change has almost no effect on Γ_0 because mass eigenstates in the $B^0\bar{B}^0$ system are very close to being orthogonal ($|p/q| = 1$) and having the same decay width [22]. Thus the neutral meson mixing effects can be ignored in our case.

The CP- and isospin-averaged width Γ (defined above) is related to the CP- and isospin-averaged branching ratio of $\mathcal{B}(\bar{B}\to X_s\gamma)$ as follows

$$\mathcal{B}(\bar{B}\to X_s\gamma) = \tau_{B^0}\Gamma\left(\frac{1+r_f r_\tau}{1+r_f}+\Delta_{0\pm}\frac{1-r_f r_\tau}{1+r_f}\right). \tag{2.80}$$

where $r_f = f^{+-}/f^{00} = 1.059\pm0.027$ [51] and $r_\tau = \tau_{B^+}/\tau_{B^0} = 1.076\pm0.004$ [51] are the production rate ratios and the measured lifetime ratios of the charged and neutral B mesons at $\Upsilon(4S)$. Since the measured value of $\Delta_{0\pm} = -0.01\pm0.06$ (for $E_\gamma > 1.9\,\text{GeV}$) [22, 49, 50] is small, the last term in Eq. (2.80) is practically negligible.

$\mathcal{B}(\bar{B} \to X_c e \bar{\nu})$	1.50%	$m_b^{\rm kin}$	0.27%
$\alpha_{\rm s}(M_Z)$	0.75%	$m_c(\mu_c)$	0.57%
$m_{t,\rm pole}$	0.19%	m_b/m_q	0.37%
$\lambda = s_{12}$	0.02%	μ_G^2	0.69%
$A = s_{23}/s_{12}^2$	0.01%	μ_π^2	0.03%
$\bar{\rho}$	0.12%	ρ_D^3	0.74%
$\bar{\eta}$	0.01%	ρ_{LS}^3	0.05%

Table 2.3: A breakdown of parametric uncertainties in the SM prediction [2, 64] for $\mathcal{B}(\bar{B} \to X_s\gamma)$.

2.3.1 Theoretical uncertainties in the SM prediction for $\mathcal{B}(\bar{B} \to X_s\gamma)$

The calculations described in the previous section give us the SM prediction for the branching ratio. In Eq. (1.4) and below, as well as in Table 1.1, we quoted its central value together with the estimated uncertainties of four different types. The nonperturbative one has already been discussed in Sec. 2.1.3. Here, we shall comment on the remaining three types.

Parametric uncertainties

A list of all the input parameters used for the branching ratio evaluation can be found in Appendix D of Ref. [64]. Individual errors in their determination and the corresponding correlation matrix lead to an overall parametric uncertainty in $\mathcal{B}(\bar{B} \to X_s\gamma)$ of $\pm 2.0\%$ (more precisely, $\pm 2.04\%$). Contributions to this uncertainty from particular parameters (before taking correlations into account) are summarized in Tab. 2.3.

The main parametric uncertainty ($\pm 1.5\%$) originates from the semileptonic branching ratio $\mathcal{B}(\bar{B} \to X_c e \bar{\nu})$, while the next one ($\pm 0.75\%$) comes from $\alpha_{\rm s}(M_Z)$. Similarly to $\mathcal{B}(\bar{B} \to X_s\gamma)$, the semileptonic branching ratio $\mathcal{B}(\bar{B} \to X_c e \bar{\nu})$ is CP- and isospin-averaged, and its isospin asymmetry is negligible. When Eq. (2.68) is used for evaluating the SM prediction for the radiative decay, neither lifetimes nor production rates enter the calculation, despite their presence in Eq. (2.80).

The influence of the b-quark mass m_b^{kin} on the final parametric uncertainty is below 0.3%, i.e. it is subdominant with respect to that of $\mathcal{B}(\bar{B} \to X_c e \bar{\nu})$ or $\alpha_{\rm s}(M_Z)$. The nonperturbative parameters μ_G^2, μ_π^2, ρ_D^3 and ρ_{LS}^3 affect only $N(E_0)$ in Eq. (2.68). As far as the CKM matrix is concerned, the Wolfenstein parameters (λ, A, $\bar{\rho}$, $\bar{\eta}$) are being used (see, for example, Eq. (12.4) of Ref. [22] for their definitions). Their numerical values are adopted from the most recent fit of the CKMfitter [148] collaboration. The ones of the UTfit [149] collaboration are in agreement with them within the quoted errors.

The parameter m_b/m_q for $q = u, d, s$ requires an extended discussion. It regulates collinear divergences that would appear in the tree-level LO contributions, as well as in some of the NLO terms (e.g., $K_{88}^{(1)}$) if the light quark masses were set to zero. Actually, these masses *are* set to zero everywhere in the calculation except for the collinear logarithms $\ln(m_b/m_q)$. The presence of such logarithms in some of the interference terms indicates that the perturbative expressions do not give good approximations for these

terms. In fact, one should use nonperturbative fragmentation functions (extracted from experiment) to estimate the collinear effects. Such estimates have been worked out in Refs. [137, 150, 151]. The overall conclusions are as follows: *(i)* The collinear logarithms arise only in such contributions to $\mathcal{B}(\bar{B} \to X_s\gamma)$ that receive strong suppression by either small Wilson coefficients, small CKM angles and/or other factors like $Q_d^2 = 1/9$. *(ii)* Those suppressed contributions are by themselves very uncertain because the fragmentation functions are not known precisely enough. *(iii)* The allowed (wide) ranges for these contributions are quite well reproduced by the perturbative expressions when m_b/m_q is varied in the range $[10, 50]$ which roughly corresponds to the range $[m_B/m_K, m_B/m_\pi]$, where $m_K \simeq 0.5\,\text{GeV}$ and $m_\pi \simeq 0.1\,\text{GeV}$ are the kaon and pion masses, respectively. Indeed, the latter masses serve as collinear regulators in the physical case. In the calculation of Refs. [2, 64], the perturbative expressions with $m_b/m_q \in [10, 50]$ were used, and the corresponding uncertainty was treated as parametric. However, it could also be treated as a nonperturbative one.

A reduction of the overall parametric uncertainty from $\pm 3\%$ in Refs. [66, 67] to $\pm 2\%$ in Refs. [2, 64] was possible mainly thanks to the recent semileptonic fits [41], as well as to a more precise value of $\alpha_s(M_Z)$ [22]. In the future, a lower parametric uncertainty can be achieved by using

$$R_\gamma = \frac{\mathcal{B}(\bar{B} \to X_s\gamma) \;+\; \mathcal{B}(\bar{B} \to X_d\gamma)}{\mathcal{B}(\bar{B} \to X_c e\bar{\nu})} \tag{2.81}$$

instead of $\mathcal{B}(\bar{B} \to X_s\gamma)$ itself as an observable that provides constraints on new physics. On the theory side, such a choice removes the dominant parametric uncertainty ($\pm 1.5\%$ from the semileptonic ratio) but at the same time increases sensitivity to m_b/m_q. However, the net effect is a noticeable decrease of the parametric uncertainty (from $\pm 2.0\%$ to $\binom{+1.2}{-1.7}\,\%$). On the experimental side, the division by $\mathcal{B}(\bar{B} \to X_c e\bar{\nu})$ has almost no effect on the uncertainty, while including $\mathcal{B}(\bar{B} \to X_d\gamma)$ has a positive effect because the final-state flavor is not identified in the fully inclusive measurements. A prediction for R_γ in the SM has been provided in Ref. [2]. It reads

$$R_\gamma = (3.31 \pm 0.22) \times 10^{-3}. \tag{2.82}$$

Uncertainties due to the interpolation in m_c

The particular choice of the functions for the interpolation in Eq. (2.76) has been motivated by the fact that these very functions multiply explicit logarithms of renormalization scales in Eq. (2.69) and/or are relevant in the BLM approximation that is correlated with the renormalization of α_s. If the dominant effects among the unknown NNLO corrections are due to renormalization (which often happens in perturbation theory) then the interpolating functions should reproduce the z-dependence of $F_i(z, 1)$ quite well.

On the other hand, given that we know very little about the true functions $F_i(z, \delta)$, the corresponding uncertainty estimate is extremely arbitrary. It is set to $\pm 3\%$ after observing in Fig. 2.6 that the interpolated contribution follows roughly a straight line, and it grows from 0 to 5% when m_c grows from zero to the measured value (marked by a vertical line). None of the functions of z that we know in this problem ($f_{NLO}(z)$, $z\,\frac{d}{dz} f_{NLO}(z)$, $f_q(z), f_c(z), f_b(z)$) depends on z in a particularly strong manner. They are all monotonous, without particularly steep slopes anywhere, which can be seen in the

plots of Refs. [67, 146]. There is no reason to expect that the unknown NNLO function $U(z,\delta)$ is going to be qualitatively different. Most probably, it starts somewhere around 0.1 at $m_c \simeq m_b/2$ and goes monotonically towards zero, crossing the vertical line at the physical value of m_c somewhere half-way. The $\pm 3\%$ uncertainty should be considered as a "theoretical 1σ" error around the $+5\%$ central value, which means that the "2σ" range is $[-1\%, +11\%]$ and covers everything we might get from monotonous functions. Taking "3σ" gives $[-4\%, +14\%]$, which seems to be sufficiently conservative.

Uncertainties due to the higher-order $\mathcal{O}(\alpha_s^3)$ corrections

At the time when only the LO results for $\mathcal{B}(\bar{B} \to X_s\gamma)$ were known, perturbative uncertainties due to the then-unknown $\mathcal{O}(\alpha_s)$ corrections were estimated at the $\pm 25\%$ level [114]. Presently, uncertainties due to the unknown $\mathcal{O}(\alpha_s^3)$ corrections are estimated at the $\pm 3\%$ level. This estimate is based on studying the branching ratio dependence on the renormalization scales. It is shown in Fig. 2.3. Since accidental cancellations in the scale dependences might occur, one also takes into account that the $\mathcal{O}(\alpha_s^n)$ corrections should be given by $(\alpha_s(\mu_b)/\pi)^n$ times a factor of order unity. For $\mu_b = 2\,\text{GeV}$ one has

$$\frac{\alpha_s(\mu_b)}{\pi} \simeq 0.093, \qquad \left(\frac{\alpha_s(\mu_b)}{\pi}\right)^2 \simeq 0.0087, \qquad \left(\frac{\alpha_s(\mu_b)}{\pi}\right)^3 \simeq 0.00081, \tag{2.83}$$

which means that the $\pm 3\%$ estimate for the $\mathcal{O}(\alpha_s^3)$ correction corresponds to the order-unity number equal to around 37 for a "theoretical 1σ". This number is actually significantly larger than unity. Thus, both the scale-dependence in Fig. 2.3 and verifying the size of $(\alpha_s(\mu_b)/\pi)^3$ point towards a conclusion that $\pm 3\%$ is an acceptable uncertainty estimate, despite the fact that we deal with renormalization scales which are only a few times larger than the confinement scale Λ.

Chapter 3

A description of the calculational methods

In the present chapter, we describe the calculational methods that have been used in our evaluation of the interference terms $\widetilde{G}_{27}^{(1)\mathrm{bare}}$, $\widetilde{G}_{27}^{(1)3P}$, $\widetilde{G}_{7(12)}^{(1)\mathrm{bare}}$ and $\widetilde{G}_{27}^{(1)m}$ defined in Sec. 2.2. They constitute a complete[1] set of m_c-dependent objects that determine the UV counterterms on the r.h.s. of Eq. (2.61). Apart from finding them for arbitrary $z = m_c^2/m_b^2$, we have also performed their and $\hat{G}_{47}^{(1)\mathrm{bare}}$ calculation in the $z = 0$ case from the outset, i.e. performing a separate IBP reduction and calculation of the MIs. In this way, we have cross-checked and confirmed the published results for these quantities in Ref. [64]. Moreover, the $z = 0$ results provide tests for our arbitrary-z ones, except for one object which diverges as $\ln z$ when $z \to 0$, but contains an extra $1/\varepsilon$ divergence when calculated at $z = 0$ from the outset.

As far as the arbitrary-z results are concerned, we will compare them with those of Ref. [152] in the cases of $\widetilde{G}_{27}^{(1)\mathrm{bare}}$ and $\widetilde{G}_{27}^{(1)3P}$. The remaining two cases ($\widetilde{G}_{7(12)}^{(1)\mathrm{bare}}$ and $\widetilde{G}_{27}^{(1)m}$) are entirely new.

In the present chapter, apart from describing the methods, we shall present explicit results for all the relevant master integrals. The final results for the interference terms will be given in Chapter 4.

We have extensively used both the symbolic and numerical tools of `Mathematica` under which most of our own codes have been written. Apart from them, numerical routines in `Fortran` and `C++` have been used.

Our introduction to multi-loop techniques is going to be brief and concentrated on our particular needs. For more details on these techniques, we refer the reader to Ref. [153] and references therein.

[1] As in Sec. 2.2, we assume that bare diagrams with the charm loops on the gluon lines and all the related UV counterterms are not included in our calculation, as they are already known from Ref. [146].

3.1 Feynman integrals and methods of their evaluation

When evaluating higher-order corrections in perturbation theory, one has to deal with Feynman integrals contributing to the S-matrix[2]. In the momentum space, the generic structure of a Feynman integral having L loops and N internal lines (propagators), in the spacetime dimension D, with loop momenta k_i and external momenta p_i (all assumed to be independent) can be cast into the following form:

$$\mathcal{F}_L = \int \prod_{i=1}^{L} d^D k_i \, \frac{[\text{Polynomials in } (k_i \cdot k_j) \text{ and } (k_i \cdot p_j)]}{[Q_1^2 - m_1^2 + i0]^{n_1} \, \ldots \, [Q_N^2 - m_N^2 + i0]^{n_N}} \tag{3.1}$$

where $n_1, \ldots, n_N \in \mathbb{Z}$. The products $(k_i \cdot k_j)$ and $(k_i \cdot p_j)$ contain both reducible and irreducible numerators. The number of such independent products is $\mathcal{N} = L(L+1)/2 + L\,E$, where E is the number of external momenta. The momenta Q_i are linear combinations of loop momenta and external momenta. They can be written as

$$Q_i = \sum_{j=1}^{L} \alpha_{ij} k_j + \sum_{j=1}^{E} \beta_{ij} p_j, \tag{3.2}$$

where α_{ij}, $\beta_{ij} \in \{-1, 0, 1\}$. We shall use the following convention: when the powers of propagators are integers, we write them either as $+k^2 + i0$ or $-k^2 - i0$, but when they are non-integer, we always use $-k^2 - i0$. The latter choice is more natural if we wish to obtain a Euclidean $(-k^2)$ form of the integrand. In the following, for brevity, we shall drop indicating the Feynman "$i0$" prescription. Typically, divergences in the Feynman integrals can be attributed to a specific semi-physical reason: in the UV (large loop momenta) and in the IR (for massless particles, small loop momenta or collinear configurations $k_i \sim p_j$ or $k_i \sim k_j$). Because of this fact, one needs to give more precise meaning to these integrals by means of regularization. An observation that the Feynman integrals become finite if the dimension of spacetime D becomes non-integer leads to the technique of Dimensional Regularization (DR) [79]. In DR, the basic defining property is that the Feynman integrals F are *analytic* in the complex D-plane.

Due to the dimensionality shifting in the DR, one performs slight modifications in the QCD Lagrangian $\mathcal{L}$ density which is polynomial in the fields, their derivatives and masses. Since the action $\int d^D x \, \mathcal{L}$ is a dimensionless quantity, it is straightforward to extract the mass dimensionalities of the quark fields ($[\psi_{f,i}] = (D-1)/2$), and gluon fields ($[A_\mu^\alpha] = D/2 - 1$) from their respective kinetic energy terms (quadratic part of the Lagrangian). The coupling constant dimensionality is then deduced from the interaction terms (non-quadratic part of the Lagrangian). One finds $[g] = 2 - D/2$, which means that in $D = 4$ the coupling constant g dimensionless. The following simple integral is sufficient to illustrate the underlying concept of DR explicitly

$$I(n) = \int d^D k \frac{1}{(-k^2 + M^2)^n} \;=\; i\pi^{D/2} \, \frac{\Gamma(n - D/2)}{\Gamma(n)} \, M^{D-2n} \tag{3.3}$$

where n is an integer. The above integrand has dimension $[mass]^{-2n}$ and the integration volume $d^D k$ has dimension $[mass]^D$. To keep the dimensionality in units of mass the

[2]Sample diagrams to be evaluated are given in Fig. 2.5.

same as in the $D = 4$ case, one usually introduces the so-called renormalization scale parameter μ. It comes as μ^{4-D} in front of each integral measure.

There are important advantages of DR:

- The Feynman rules and all the symmetries (Lorentz invariance, gauge invariance, unitarity, etc) of the theory do not depend on D. Thus, these symmetries remain manifest at all stages of the calculation.

- The scaleless integrals vanish in DR.

- Integrals that diverge for $D = 4$ turn out to be well-behaved when D is not an integer. Setting $D = 4 - 2\varepsilon$, where ε serves as regularization parameter, we find them as *meromorphic* functions in ε. This means that only $1/\varepsilon^j$ poles and no branch cuts in ε occur. Multiple $1/\varepsilon^j$ poles remain also after proper subtraction of *subdivergences* by means of renormalization. However, an important theorem of QFT (see the book by J.C Collins in Ref. [19]) states: *An overall singularity at $D = 4$ of a dimensionally regularized Feynman amplitude is a polynomial in its external momenta after a subtraction of subdivergences corresponding to all its genuine one-particle-irreducible subgraphs has been performed.* There are additional poles in the S-matrix elements if the IR divergencies are regularized dimensionally. The Laurent expansion of Eq. (3.1) in DR reads

$$\mathcal{F}_L(\varepsilon) = \sum_{j=-2L}^{\infty} f_{j,L}\, \varepsilon^j \tag{3.4}$$

  where $f_{j,L}$ is function of kinematical invariants (constructed from the external momenta, masses of the external particles and of the particles running in the loops). It is well known that Feynman integrals may have *discontinuities* [154]. In general, $f_{j,L}$ as a function of the products $p_i \cdot p_j$ is analytic everywhere besides its branch cuts. Appendix A contains examples of functions that we have encountered in the present project. A detailed discussion of analytic properties of Feynman integrals can be found in Ref. [155].

  In the case of putting massless propagators on-shell, the branch cuts may extend between points where some of the kinematical invariants are zero or infinity. For massive propagators we have *thresholds*, and the branch cut structure may not be simple. For example, the $b \to s\,\gamma$ amplitude has a real threshold at $m_b^2 = 4\,m_c^2$ which corresponds to opening of the $b \to c\bar{c}s$ channel. To predict what classes of functions may appear in a given calculation, it is important to think about the asymptotic behavior of the integrals in (potentially) singular limits. In the Feynman parameterization (to be discussed below), thresholds may be parameterized at the integrand level, as a combination of kinematical invariants and Feynman parameters. The full set of thresholds can be determined solving the Landau equations of an integrand [156].

There are also some limitations of DR:

- Noncommutativity and nonuniqueness of limits in ε and kinematical invariants for *nonphysical* quantities in massless theories[3]. For instance, the limits $\varepsilon \to 0$ and $M \to 0$ do not commute for $n = 2$ in the integral (3.3). Moreover, to regularize IR divergences, one may introduce a small cut-off mass for the massless particles, except for nonabelian gauge bosons.[4] The cut-off mass is sent to zero only after evaluating the physical quantities which are IR-safe (either by themselves or thanks to experimental IR cutoffs). Alternatively, one can use DR to regularize both the IR and the UV divergences, but in that case the limit $\varepsilon \to 0$ can *only* be taken for the above-mentioned physical quantities.

- Inclusion of chiral fermions generates the so-called γ_5 problem that requires special care in D dimensions. The γ_5 matrix appears in our calculations due to weak operator insertions. We encounter a single γ_5 in the $Q_{7,8}$ and $Q_{3,\ldots,6}$ vertices, and two γ_5's $Q_{1,2}$. Here, we apply the Naive Dimensional Regularization (NDR) scheme where γ_5 is treated as a completely anticommuting object, i.e. $\{\gamma^\mu, \gamma_5\} = 0$ for all the Dirac matrices γ^μ. Despite the fact that such a scheme is algebraically inconsistent in the general case [79], it is acceptable for our calculation because in the CMM basis we avoid traces $Tr(\gamma^\mu\gamma^\nu\gamma^\rho\gamma^\sigma\gamma_5) \sim \varepsilon^{\mu\nu\rho\sigma}$ in the physical amplitudes.

- Due to our use of DR, we have to consider nonphysical terms, called evanescent operators [102–104], that algebraically vanish in $D = 4$. Examples of such terms have already been given in Eqs. (2.11), (2.12) and (2.24)-(2.29).

At the end of this section, let us briefly mention a few more general facts about Feynman integrals. The relation $L = I - V + 1$ holds for any L-loop integral (planar or nonplanar) having I internal lines and V vertices. Its superficial degree of divergence R in 4 dimensions is $R = 4\,L + P$, where P is an integer evaluated using *power counting*. The counting goes as follows. Let all the loop momenta *simultaneously* become large $k_i \to \Omega\, k_i$ with $\Omega \to \infty$ in the integrand J of Eq. (3.1). Then J scales according to $J \to \Omega^P J$, and we can read out P. The Weinberg theorem [157] states the following: *Suppose the degree of divergence of a given diagram is R, and for each of its subdiagrams the degree of divergence is R_s. The considered diagram is absolutely convergent if all the R_s together with R are negative.* It is worth to mention that in some cases the divergence may become weaker due to some symmetries. An example is the electron one-loop self-energy diagram for which we have $R = 1$, but from explicit calculation it has only $R = 0$, i.e. a logarithmic divergence.

3.2 Integration by parts, reverse unitarity and reduction to master integrals

In perturbation theory, as the number of loops, legs and scales increases, the number of integrals grows very fast with increasing orders in the coupling constant. Thus, one needs to deal with hundreds of multi-dimensional integrals. Such calculations are usually performed with the help of symbolic computer algebra codes, according to algorithms

[3] This issue has lead us to evaluate $m_c = 0$ contributions in Sec. 4.2 from the outset.

[4] For abelian ones it is acceptable but destroys the gauge invariance until the massless limit is taken.

that can be rendered fully automatic, at least for particular steps of the procedure. The algorithm we have followed is described in the present section.

3.2.1 Integration by parts

We have used `FeynArts` [158] for automatic generation of the necessary Feynman diagrams. The diagrams we deal with correspond to interference terms in the decay width, and summing or averaging over polarizations is understood. Thus, performing the Dirac algebra calculations amounts to evaluation of traces. It has been done with the help of a self-written `Mathematica` code. As a result, the considered interference terms were expressed as linear combinations of scalar integrals of the form (3.1).

Some of the momentum products in the numerator of Eq. (3.1) can be written as linear combinations of denominators, and then simplified, which is called Passarino-Veltman reduction [159]. Once it is performed, we are left only with numerators that are called irreducible, and will be denoted by S_i below. The integrals to be evaluated take then the following form:

$$F(a_1,\ldots,a_M,-r_1,\ldots,-r_s)=\sum\int\prod_{i=1}^{L}d^Dk_i\;\frac{\mathcal{S}_1^{r_1}\;\ldots\;\mathcal{S}_s^{r_s}}{D_1^{a_1}\;\ldots\;D_M^{a_M}} \tag{3.5}$$

with a_i being any integers, and r_i being non-negative integers. These powers are often called *indices* of an integral. For instance, in the case of the Feynman diagram of Fig. 2.5(a) with a two-body unitarity cut, we have obtained the following denominators D_i and irreducible numerators S_i:

$$\begin{aligned}
D_1 &= -(k_1+p_2)^2, & D_2 &= -k_1^2,\\
D_3 &= -k_2^2+m_c^2, & D_4 &= -(k_2+p_1)^2+m_c^2,\\
D_5 &= -(k_1+k_2)^2+m_c^2,\\
\mathcal{S}_1 &= k_1\cdot p_1, & \mathcal{S}_2 &= k_2\cdot p_2,
\end{aligned} \tag{3.6}$$

with $\mathcal{O}(10^2)$ different sets of indices. Here, p_1 and p_2 stand for the final-state photon and s-quark momenta, respectively. A sample integral reads

$$F(0,1,1,1,1,0,-2)=\int\int d^Dk_1d^Dk_2\;\frac{(k_2\cdot p_2)^2}{D_2D_3D_4D_5}. \tag{3.7}$$

After these preliminary steps, the main breakthrough in reducing the number of integrals is achieved via integration by parts. The IBP reduction method [69, 70, 160] is based on the fact that the *dimensionally regularized* integral of a total derivative is equal to zero. For example, denoting the integrand in Eq. (3.5) by J, and choosing any of its loop momenta k_i, we can write

$$\int d^Dk_i\,\frac{\partial}{\partial k_i^\mu}(v^\mu J)=0, \tag{3.8}$$

where v^μ stands for either k_j^μ or p_j^μ. Each such identity gives us a linear relation between several integrals.

Let us illustrate the above statement by considering only a single loop momentum k^μ, and choosing $v^\mu = k^\mu$. By the chain rule, we have

$$\int d^D k \frac{\partial}{\partial k^\mu}(k^\mu J) = \int d^D k\, k^\mu \left(\frac{\partial}{\partial k^\mu} J\right) + D \int d^D k\, J \tag{3.9}$$

where we have used $\frac{\partial}{\partial k^\mu}\, k^\mu = D$. The D-dimensional volume integral on the l.h.s. of Eq. (3.9) can be converted by the Gauss theorem to a surface integral that may be dropped out whenever J vanishes sufficiently fast at infinity. Even if this is not the case, the IBP reduction for *dimensionally regularized* integrals can be implemented with ignoring the surface terms irrespective of the asymptotic behavior of the integrand. Thus, in our example, we have

$$D \int d^D k\; J \;=\; -\int d^D k\, k_\mu \left(\frac{\partial}{\partial k_\mu} J\right) \tag{3.10}$$

Once Eq. (3.8) is used for a particular integral, we find linear relations involving many different integrals. We can then apply Eq. (3.8) to them, bringing even more integrals into the game, and so on. However, it turns out that the number of new integrals grows slower than the number of generated identities, and at some point the system of generated equations closes, allowing us to express all our initial integrals (as well as many other ones) in terms of a few Master Integrals (MIs). While there exists a proof that the number of MIs is finite [161], we never know before performing the actual IBP reduction how many of them will be found for a particular topology that is defined by the denominators D_i.

3.2.2 Reverse unitarity

Before continuing our discussion of the IBP, let us describe the so-called "reverse unitarity" trick [162]. Our original Feynman diagrams contain unitarity cuts, which means they involve $(D-1)$-dimensional phase-space integrals that are inconvenient for the IBP method in the $(n > 2)$-body final state cases. To avoid this problem, one first converts them to D-dimensional ones using the well-known identity that holds for a particle with mass m, and for any function $J(k)$:

$$\int \frac{\mathrm{d}^{D-1}\vec{k}}{2\sqrt{\vec{k}^2 + m^2}\,(2\pi)^{D-1}} J(k) = \int \frac{\mathrm{d}^D k}{(2\pi)^D} \theta(k^0)\delta(k^2 - m^2) J(k). \tag{3.11}$$

Next, one uses the relation

$$2\pi i\, \delta(k^2 - m^2) = \frac{1}{k^2 - m^2 - i0} - \frac{1}{k^2 - m^2 + i0}. \tag{3.12}$$

Once the above expressions are substituted, we obtain integrals that look as originating from diagrams with no unitarity cuts at all (no phase-space integrals), except for the factors $\theta(k^0)$ and possibly different signs of the "$i0$" terms in some of the propagators. However, neither the signs of the "$i0$" terms nor the factors of $\theta(k^0)$ have any influence on the linear relations between integrals that one obtains using the IBP. The integral on the l.h.s. of Eq. (3.9) still vanishes even if the integrand is multiplied by $\theta(k^0)$, while the algebraic effect of differentiation with respect to momenta (raising or lowering the

indices) is insensitive to the "$i0$" terms. Thus, the IBP can be performed as for the loop integrals. Once the MIs are found, the above two identities are applied "backwards", and the phase-space integrals are re-introduced for the actual evaluation of the MIs.

In fact, there is an important simplification in the IBP when some of the propagators are cut (i.e. they originate from using the reverse unitarity method). If we encounter integrals where any of the cut propagators has a non-positive index, we can immediately set them to zero. It follows from the fact that the difference on the r.h.s. of Eq. (3.12) would give a null distribution if the propagators were raised to non-positive powers.

The code `REDUZE` [75] has a built-in option for using the reverse unitarity. It automatically takes care of neglecting integrals with negative indices of the cut propagators. Moreover, it avoids producing MIs with dots on the cut propagators, i.e. with their indices larger than 1. Such integrals have no other meaning but being linear combinations of the integrals that contain no such dots.

On the other hand, the code `FIRE` [73, 74] (which we have extensively used) allows to neglect cut propagators with negative indices, but has no automatic protection against MIs with dots on the cut propagators. One needs to solve the problem "by hand" by introducing explicit preferences for the MIs of various topologies. We shall return to this issue below.

Let us stress that we have applied the reverse unitarity method only in the three-body final state case. In the two-body case, the phase-space integrals are trivial due to Dirac δ-functions. What they give for massless final state particles is a multiplication by a fixed ε-independent number (the same as in $D = 4$) and, in addition, by

$$P_2 = \frac{\Gamma(1-\varepsilon)}{\Gamma(2-2\varepsilon)} e^{\gamma\varepsilon}. \tag{3.13}$$

In the following, the quantity P_2 will be called a "two-body phase-space factor."

3.2.3 Reduction to master integrals

Let us illustrate the action of the IBP using the one-loop integrals $I(n)$ from Eq. (3.3). If we did not know the result for arbitrary n, we could still find relations between those integrals proceeding as follows:

$$\int d^D k \frac{\partial}{\partial k^\mu} \left(k^\mu \frac{1}{(-k^2+M^2)^n} \right) = 0 \qquad \Rightarrow \qquad (D-2n)\, I(n) + 2nM^2\, I(n+1) = 0$$

$$\Rightarrow \qquad I(n+1) = \frac{n - D/2}{M^2 n} I(n). \tag{3.14}$$

Moreover, $I(n) = 0$ for $n \leq 0$. Thus, any $I(n)$ for $n > 1$ is given by a recurrence relation which allows to express it in terms of $I(1)$ that serves as a master integral.

In more general cases, the IBP does not give us recurrences that are easy to solve. Instead, one applies the so-called Laporta algorithm [71] which amounts to postulating an order relation among the integrals. It specifies which integrals should be eliminated first from the system of linear equations, and which ones should be retained and treated as simpler. We shall not quote the postulated rules in full length but only mention that integrals with lower numbers of denominators and lower absolute values of the indices in Eq. (3.5) are treated as simpler. Since the IBP relations are linear, one can think about

the reduction as expressing vectors of a linear space in terms of some basis that is given by the MIs. The choice of the basis involves some arbitrariness that is limited by the above-mentioned order relation but not totally eliminated.

Apart from the IBP relations, other sorts of identities have been considered in the literature, in particular the Lorentz Invariance (LI) [163] Gram [164] or quasi-Shouten [165] ones. However, in our calculation, only the IBP relations and the Laporta algorithm have been used, as implemented in the (already mentioned) code `FIRE` [73, 74]. The other IBP codes quoted in Chapter 1 have served us for certain cross-checks only.

The name `FIRE` stands for "Feynman Integral REduction". It uses a special version of the Gauss elimination method to solve the system of linear equations that is generated by the application of the IBP relations. We have extensively used both the `Mathematica` and `C++` versions of the program. Its operation in the `C++` case is divided into three steps:

1. In the first step, the input for the second step (reduction) is prepared within `Mathematica`. This includes construction of all the generic IBP relations from which the explicit IBP identities are derived by simple substitutions of indices. Moreover, certain symmetry relations, as well as the co-called boundary conditions (sectors of indices where the integrals vanish) are identified, too. Finally, configuration files and lists of indices of the integrals to be reduced are prepared in a format that is readable for the `C++` part of the code.

2. The second step is the only one where the `C++` code is being used. It is the main part of the reduction, for which computing efficiency is an issue, as the number of generated identities and redundant integrals is very large. In our case, the `C++` code does the job in a short time (a few minutes), but its `Mathematica` counterpart requires several hours.

3. In the third step, the output of the `C++` code is read by `Mathematica` and converted to a user-friendly format. It contains a table of the MIs, as well as coefficients with which they come into expressions for the initial integrals.

After the reduction, each of the integrals (Eq. (3.5)) becomes a linear combination of the master integrals $\mathcal{M}_i$ that is parameterized by known coefficients $\mathcal{C}_i$

$$F = \sum \mathcal{C}_i \, \mathcal{M}_i. \tag{3.15}$$

In our case, it is convenient to normalize all the integrals with appropriate powers of m_b to make them dimensionless. Moreover, in our evaluation of the dimensionless bare interference terms ($\widetilde{G}_{ij}^{(n)\mathrm{bare}}$, etc.), we set $\mu^2 = e^\gamma m_b^2/(4\pi)$ for the renormalization scale.[5] Under such conventions, the bare interference terms, the MIs and the IBP coefficients $\mathcal{C}_i$ are functions of only two variables: ε and $z = m_c^2/m_b^2$. For instance, Eq. (3.7) after reduction becomes

$$\begin{aligned} F(0,1,1,1,1,0,-2) = {} & \mathcal{C}_1 \, F(0,0,0,1,1,0,0) + \mathcal{C}_2 \, F(0,1,0,1,1,0,0) \\ & + \mathcal{C}_3 \, F(0,1,0,1,2,0,0) + \mathcal{C}_4 \, F(0,1,1,1,1,0,0) \end{aligned} \tag{3.16}$$

[5] This fact has already been taken into account in Eq. (2.61) where an arbitrary scale μ_b is considered. It enters only via the factors s^ε there.

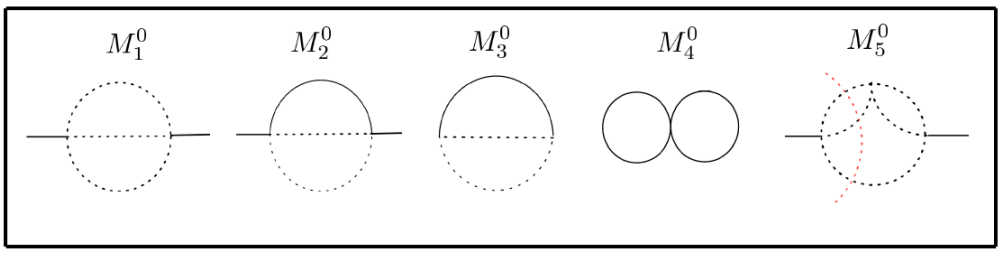

Figure 3.1: Master integrals for $\widetilde{G}_{27}^{(1)\text{bare}}$ in the massless charm quark case (see the text). These MIs together with the ones given in Fig. 4.1 form a compete MI set for our $m_c = 0$ calculation.

where the F's on the r.h.s. are the master integrals. As far as the IBP coefficients are concerned, we shall quote them explicitly for the complete interference terms in the next chapter. At present, let us only give one simple example, namely Fig. 2.5(b) in the case of a massless charm quark. Then we have

$$\text{Fig. } 2.5(b) \overset{z=0}{=\!=} Q_d \left[\frac{8(1-\varepsilon)^2(9-\varepsilon-12\varepsilon^2)}{9(3-2\varepsilon)} M_2^0 - \frac{2(1-\varepsilon)^2(9-4\varepsilon-4\varepsilon^2)}{3(3-2\varepsilon)} M_3^0 \right], \quad (3.17)$$

where the MIs denoted by M_2^0 and M_3^0 are drawn in Fig. 3.1.

In our drawing conventions for the MIs, the internal lines are shown as solid, dashed or dotted ones when the corresponding masses in the propagators are equal to m_b, m_c or zero, respectively. The external lines are solid or dotted when the corresponding external momentum p satisfies $p^2 = m_b^2$ or $p^2 = 0$, respectively. Raising a propagator to a power n is indicated by drawing n big dots on the corresponding line. A propagator with a single dot can be seen, e.g., in $\mathcal{M}_{10}$ in Fig. 3.2. Such propagators are called "dotted propagators", which should not be confused with dotted lines that indicate massless propagators. Let us recall that only in the three-body $b \to s\gamma g$ case we use the reverse unitarity and draw the integrals as three-loop ones with unitarity cuts. In the two-body case, we perform the IBP reduction for the $b \to s\gamma$ amplitudes. In such a case, the master integrals are two-loop only, and they are not necessarily three-particle vertex ones. Actually, in Fig. 3.1, we encounter only propagator-type or tadpole diagrams.

The coefficients in Eq. (3.17) are regular in the $\varepsilon \to 0$ limit. However, in a general case, one often finds coefficients that are singular in this limit.[6] The corresponding MIs must then be calculated up to higher orders in ε to compensate the spurious $1/\varepsilon^n$ poles in the IBP coefficients, which might lead to considerable difficulties in some cases. However, since the choice of the MIs is not unique, one can take advantage of this fact, and search for a basis in which all the $\mathcal{C}_i$ are finite in the $\varepsilon \to 0$ limit. Such bases are called ε-finite, and their existence has been shown in Ref. [166]. The price to pay for using an ε-finite basis is frequent appearance of MIs having either non-trivial irreducible numerators or a few propagators raised to powers larger than unity (i.e. dotted propagators). We will further comment on the ε-finite bases and pseudo-thresholds in Sec. 3.3.3.

The MIs we have obtained in the arbitrary m_c case are shown in Fig. 3.2. An irreducible numerator occurs only in one of them ($\mathcal{M}_3$), and it corresponds to a product of

[6] Apart from that, singularities in the $\mathcal{C}_i$ might occur at particular values of z, e.g., at the *pseudo-threshold* $z = 1$.

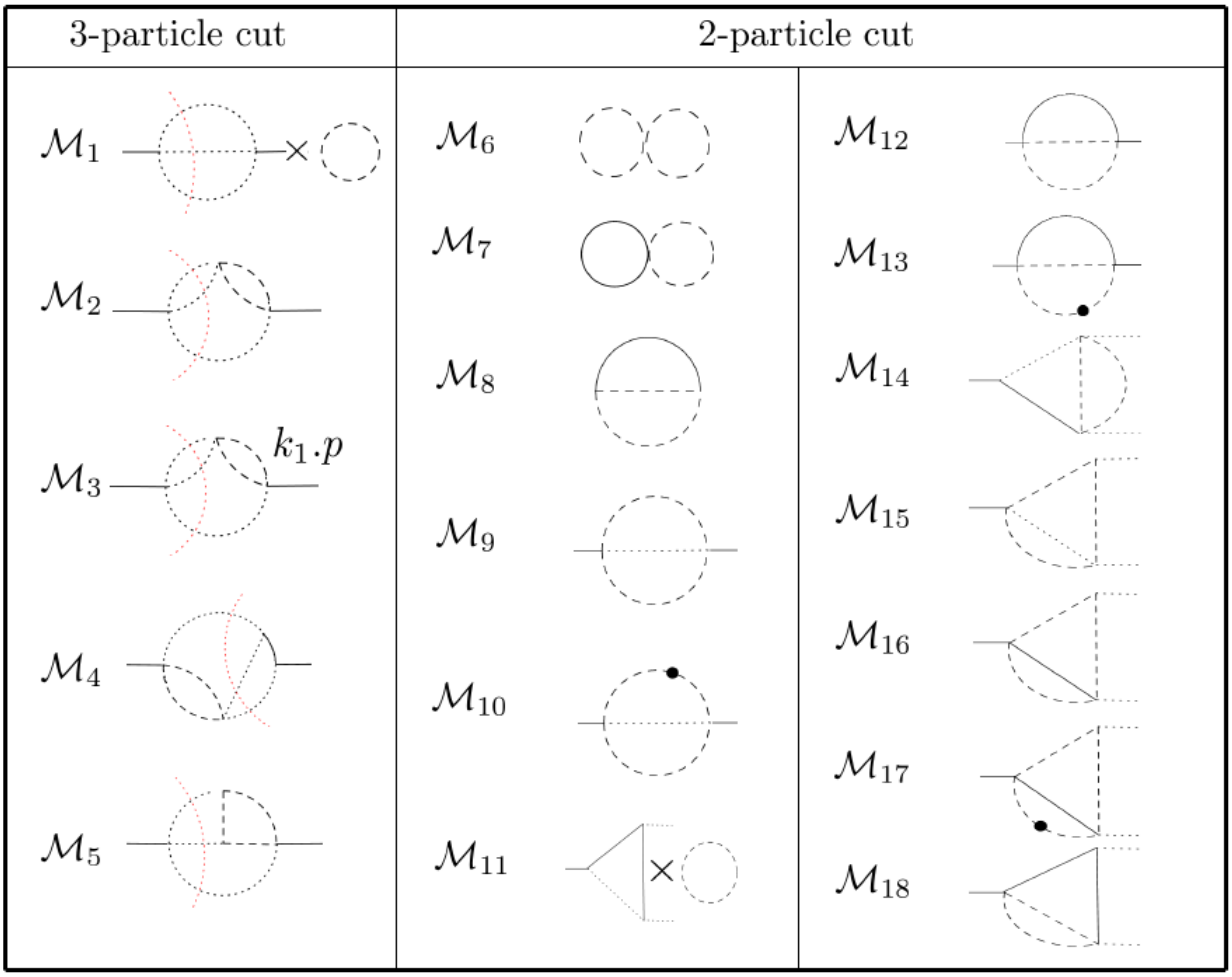

Figure 3.2: Master integrals for $\widetilde{G}^{(1)\text{bare}}_{27}$, $\widetilde{G}^{(1)\text{bare}}_{7(12)}$ and $\widetilde{G}^{(1)m}_{27}$ in the arbitrary m_c case.

the b- and s-quark momenta that affects the phase-space integration.

The MIs in Fig. 3.2 are not exactly the ones that `FIRE` provided in an automatic manner. First, the automatic reduction is performed topology-by-topology. However, since many of the MIs have several vanishing indices, it very often happens that MIs originating from different topologies are actually identical. Determining the set of truly independent MIs was done "by hand" in our case. It was manageable because the number of the original MIs was quite limited. Another problem is that `FIRE` sometimes fails to figure out that some integrals are actually related and/or produces unwanted MIs with dots on the cut lines. A set of several redundant integrals that we had to deal with is displayed in Fig. 3.3. Expressions for them in terms of the true MIs read (skipping the trivial $\mathcal{R}_{23}$):

$$\mathcal{R}_{19} = -\frac{2(3-4\varepsilon)(2-2z-\varepsilon(5-8z))}{\varepsilon(1-4z)^2}\mathcal{M}_3 - \frac{4(1-3\varepsilon+2\varepsilon^2)(2-5z)}{\varepsilon(1-4z)^2}\mathcal{M}_1 + \frac{2(-3+6z-6z^2+3\varepsilon(4-11z+12z^2)+\varepsilon^2(-11+38z-48z^2))}{\varepsilon(1-4z)^2}\mathcal{M}_2, \qquad (3.18)$$

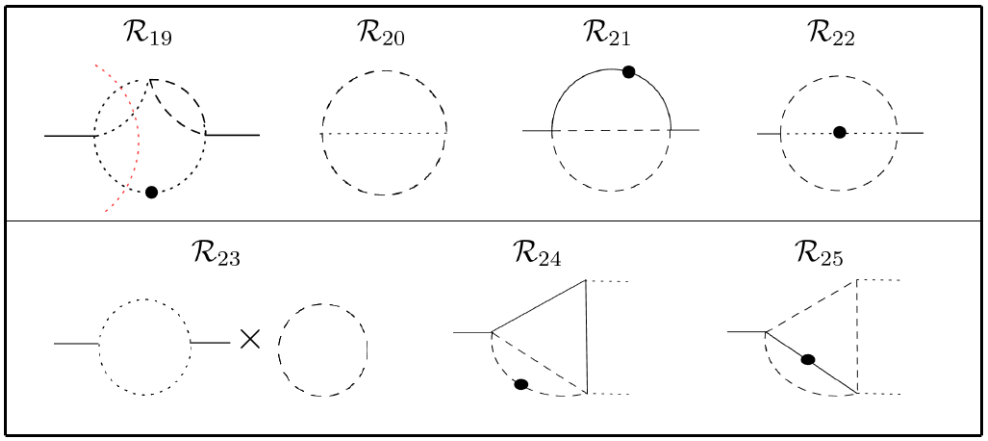

Figure 3.3: Redundant (reducible) integrals that required non-automatic treatment in the arbitrary m_c case.

$$\mathcal{R}_{20} = -\frac{1-\varepsilon}{z\,(1-2\varepsilon)}\mathcal{M}_6 \tag{3.19}$$

$$\mathcal{R}_{21} = -\frac{(2-3\varepsilon)}{2}\mathcal{M}_{12} - z\,\mathcal{M}_{13} - \frac{(1-\varepsilon)^2}{2\,z\,(1-2\varepsilon)}\mathcal{M}_6 \tag{3.20}$$

$$\mathcal{R}_{22} = \frac{2(1-\varepsilon)^2}{\varepsilon(1-4z)}\mathcal{M}_6 + \frac{(2-7\varepsilon+6\varepsilon^2)(1-2z)}{\varepsilon(1-4z)}\mathcal{M}_9 + \frac{4(1-2\varepsilon)(1-z)z}{\varepsilon(1-4z)}\mathcal{M}_{10} \tag{3.21}$$

$$\mathcal{R}_{24} = -\frac{1}{2}\left(\frac{(1-\varepsilon)}{z}\,(\mathcal{M}_{18}-\mathcal{M}_8) + \frac{(2-3\varepsilon)}{z}\mathcal{M}_{12} + 2\mathcal{M}_{13}\right) \tag{3.22}$$

$$\mathcal{R}_{25} = -\frac{(1-\varepsilon)^2(1-z)}{2\,z^2\,(1-2\varepsilon)}\mathcal{M}_6 + (1-\varepsilon)\mathcal{M}_8 - \frac{(2-3\varepsilon)(1+z)}{2\,z}\mathcal{M}_{12} - \\ - \frac{(1+z^2)}{z}\mathcal{M}_{13} - (1-\varepsilon)\mathcal{M}_{16} - z\,\mathcal{M}_{17} \tag{3.23}$$

We have determined the above expressions either by launching separate runs of `FIRE` in a slightly different setup for particular integrals only, or by noticing that certain linear relations follow from the differential equations (to be discussed below).

It is interesting to note that our MI basis in the 3-body case is actually an ε-finite basis, and one of the integrals does contain an irreducible numerator. The basis would not be ε-finite if $\mathcal{R}_{19}$ had not been eliminated. However, getting rid of this integral was a must because its appearance was due to the previously-mentioned incapability of `FIRE` to automatically avoid integrals with dots on the cut propagators. Obviously, such integrals cannot serve as MIs because they are meaningless (or, more precisely, their only meaning is given by their IBP relations to integrals without such dots).

3.3 Evaluation of the master integrals

Among possible methods to evaluate master integrals, one should mention using the Feynman and Schwinger parameterizations, Mellin-Barnes representation [167–169], differential equations [76–78], sector decomposition [170], nested sums [171] and difference equations [172]. In this section, we discuss evaluation of the MIs by the methods that

we have used in our particular calculation. In order to cross-check the results, we have always applied at least two independent methods to compute all the MIs.

3.3.1 The Feynman and Schwinger parameterizations

The Feynman parameterization is closely related to the Schwinger (alpha) parameterization.[7] This is why we discuss them simultaneously in the present subsection. Using the Feynman parameters is by far the most standard "handbook" method. Unfortunately, it is not sufficient for most of the MIs we had to deal with in our present calculation. However, the simplest MIs could have been determined this way. We briefly describe these methods for a few sample MIs, and present the final expressions for them.

The Feynman parameterization is based on the following formula

$$\frac{1}{A_1^{n_1}\dots A_N^{n_N}} = \frac{\Gamma(N)}{\Gamma(n_1)\dots\Gamma(n_N)} \int_0^1 \left(\prod_{i=1}^N dx_i\right) \delta\left(1-\sum_{i=1}^N x_i\right) \times \frac{x_1^{n_1-1}\dots x_N^{n_N-1}}{(x_1A_1+\dots+x_NA_N)^N} \tag{3.24}$$

where $N=\sum_{i=1}^N n_i$, and n_i do not need to be integers. The numbers A_j are going to be substituted below by $[-Q_j^2+m_j^2]$. In the case when all the A_j are equal to unity, Eq. (3.24) reduces to

$$\int_0^1 \left(\prod_i^N dx_i\, x_i^{n_i-1}\right) \delta\left(1-\sum_{i=1}^N x_i\right) = \frac{\Gamma(n_1)\dots\Gamma(n_N)}{\Gamma(N)}. \tag{3.25}$$

The Schwinger parametric representation is based on

$$\frac{1}{A^n} = \frac{e^{in\pi/2}}{\Gamma(n)} \int_0^\infty d\alpha\, \alpha^{n-1} e^{-iA\alpha}. \tag{3.26}$$

Using the above equation for each of the denominators in

$$F^{scalar} = \int \prod_{i=1}^L d^Dk_i\, \frac{1}{[-Q_1^2+m_1^2]^{n_1}\,\dots\,[-Q_N^2+m_N^2]^{n_N}}, \tag{3.27}$$

performing the integration over loop momenta, introducing an extra integrand over η via

$$1 = \int_0^\infty d\eta\, \delta\left(\eta-\sum_{i=1}^N \alpha_i\right), \tag{3.28}$$

replacing α_i by ηx_i, and integrating[8] over η, one finds [153, 173] that F^{scalar} takes the following form

$$F^{scalar} = \left(i\pi^{D/2}\right)^L \frac{\Gamma(N-\frac{D}{2}L)}{\Gamma(n_1)\dots\Gamma(n_N)} \int_0^1 \left(\prod_i^N dx_i\, x_i^{n_i-1}\right) \delta\left(1-\sum_{i=1}^N x_i\right) \frac{U(x)^{N-\frac{D}{2}(L+1)}}{F(x)^{N-\frac{D}{2}L}}. \tag{3.29}$$

[7] In fact, any choice of the Feynman parameters can be achieved by starting from the Schwinger representation and making certain changes of variables.

[8] see, e.g., Eq. (6-90) in the book by Itzykson & Zuber in Ref. [19].

The functions $U(x)$ and $F(x)$ are polynomials in x_i that are homogeneous of degree L and $L+1$, respectively. We can also map $x_i \in [0,1]$ to $y_i \in [0,\infty]$ by $y_i = \frac{x_i}{1-x_i}$ i.e., by $x_i = \frac{y_i}{y_i+1}$ in Eq. (3.29).

The fact that $U(x)$ and $F(x)$ are polynomials in x_i is important to obtain the Mellin-Barnes (MB) representation and sector decomposition of Feynman integrals that we are going to discuss in the next sections. From Eq. (3.29) it is clear that the integrand is bounded in its limits by powers of x_i with certain exponents, which means these integrals have only non-essential singularities in the kinematical variables. The singularities can be of removable type, poles or branch points.

All the MIs in Fig. 3.1 are simple enough to be evaluated using the Feynman parameter method. Our results read

$$P_2\mathcal{M}_1^0 = -e^{3\gamma\varepsilon}\cos(2\pi\varepsilon)\frac{\Gamma(-1+2\varepsilon)\Gamma^4(1-\varepsilon)}{\Gamma(3-3\varepsilon)\Gamma(2-2\varepsilon)} \tag{3.30}$$

$$P_2\mathcal{M}_2^0 = e^{3\gamma\varepsilon}\frac{\Gamma(-1+2\varepsilon)\Gamma^3(1-\varepsilon)\Gamma(\varepsilon)\Gamma(3-4\varepsilon)}{\Gamma^2(2-2\varepsilon)\Gamma(3-3\varepsilon)} \tag{3.31}$$

$$P_2\mathcal{M}_3^0 = e^{3\gamma\varepsilon}\frac{\Gamma(-1+2\varepsilon)\Gamma^2(1-\varepsilon)\Gamma(\varepsilon)}{(1-\varepsilon)\Gamma(2-2\varepsilon)} \tag{3.32}$$

$$P_2\mathcal{M}_4^0 = -\frac{e^{3\gamma\varepsilon}\Gamma^2(-1+\varepsilon)\Gamma(1-\varepsilon)}{\Gamma(2-2\varepsilon)} \tag{3.33}$$

$$\mathcal{M}_5^0 = -e^{3\gamma\varepsilon}\cos(\pi\varepsilon)\frac{\Gamma(\varepsilon)\Gamma^4(1-\varepsilon)\Gamma(1-2\varepsilon)}{\Gamma^2(2-2\varepsilon)\Gamma(3-4\varepsilon)}, \tag{3.34}$$

where the two-body phase-space factor P_2 has been defined in Eq. (3.13). We give the explicit MIs (above and in the following) after removing the global normalization factor of $1/(16\pi^2)$ for each loop integration, while the integration measure d^Dk is assumed to be normalized to $1/(2\pi)^D$. Let us recall, that we use $\mu^2 = e^\gamma m_b^2/(4\pi)$ for the renormalization scale, and include a factor of $\mu^{2\varepsilon}$ for each loop together with an appropriate integer power of m_b to make each integral dimensionless. The imaginary parts of the MIs are skipped because they are irrelevant for evaluating the considered correction to the CP-averaged branching ratio.

In the case of $\mathcal{M}_2^0$, the Feynman-parameter integral reads

$$\mathcal{M}_2^0 = -e^{2\gamma\varepsilon}\,\Gamma(-1+2\varepsilon)\int_0^1 dx\int_0^1 dy\frac{x^{-\varepsilon}(1-x)^{-\varepsilon}y^{-1+\varepsilon}}{(1-y)^{-2+4\varepsilon}}, \tag{3.35}$$

after using Eq. (3.24) with $N=3$ and $n_1=n_2=n_3=1$ and a simple change of variables. Next, we take into account that

$$\int_0^1 dt\, t^{-1+a}(1-t)^{-1+b} = \frac{\Gamma(a)\Gamma(b)}{\Gamma(a+b)}, \tag{3.36}$$

which immediately gives us the final result (3.31).

In the case of $\mathcal{M}_5^0$, we encounter an integral over the three-body phase space

$$\mathcal{M}_5^0 = -e^{\gamma\varepsilon}\cos(\pi\varepsilon)\frac{\Gamma(\varepsilon)\Gamma^2(1-\varepsilon)}{\Gamma(2-2\varepsilon)}\,\frac{128\pi^3\mu^{4\varepsilon}}{m_b^2}\int y_{23}^{-\varepsilon}\,dPS_3 \tag{3.37}$$

where $y_{ij} = \frac{2p_ip_j}{m_b^2}$. This integration can be performed as follows:

$$\begin{aligned}\frac{128\pi^3\mu^{4\varepsilon}}{m_b^2}\int y_{23}^{-\varepsilon}\,dPS_3 &= \frac{e^{2\gamma\varepsilon}}{\Gamma(2-2\varepsilon)}\int_0^1 dy_{12}\int_0^{1-y_{12}} dy_{23}\,(1-y_{12}-y_{23})^{-\varepsilon}y_{12}^{-\varepsilon}y_{23}^{-2\varepsilon}\\ &= e^{2\gamma\varepsilon}\,\frac{\Gamma^2(1-\varepsilon)\Gamma(1-2\varepsilon)}{\Gamma(2-2\varepsilon)\Gamma(3-4\varepsilon)},\end{aligned} \tag{3.38}$$

where we have mapped a generic region $x \in [a,b]$ to $y \in [0,1]$ by $x = a + (b-a)y$ using

$$\int_a^b f(x)\,dx = \int_0^1 f(a+(b-a)y)\,(b-a)\,dy \tag{3.39}$$

The main obstacle of the Feynman parameter method is due to presence of divergencies that arise in the Feynman parameter integrations when the expansion in ε is performed prior to integration. On the other hand, without such an expansion, numerical methods are not applicable, while the analytical results are often difficult or impossible to determine in terms of known special functions. Overcoming this problem requires performing a proper separation of poles by adding and subtracting suitable (analytically calculable) terms before expansion in ε. After such a subtraction, an expansion of the remainder can be performed prior to integration. In the resulting expressions (if evaluated analytically), one often needs to integrate polylogarithms multiplied by rational functions, which frequently result in Harmonic PolyLogarithms (HPL) [174]. The integrals with kernels involving polylogarithms have been studied, e.g., in Refs. [175] and [176].

Let us now confirm the relation (3.19) using the Feynman parameters. We begin with

$$\frac{1}{256\pi^4}\mathcal{M}_6 = \frac{\mu^{4\varepsilon}}{m_b^4}\int\frac{d^Dq_1}{(2\pi)^D}\frac{d^Dq_2}{(2\pi)^D}\frac{1}{(m_c^2-q_1^2)(m_c^2-q_2^2)}. \tag{3.40}$$

We know that

$$\mu^{2\varepsilon}\int\frac{d^Dk}{(2\pi)^D}\frac{1}{(m^2-k^2)^\alpha} = \frac{i}{16\pi^2}\left(\frac{4\pi\mu^2}{m^2}\right)^\varepsilon(m^2)^{2-\alpha}\frac{\Gamma(\alpha-2+\varepsilon)}{\Gamma(\alpha)} \tag{3.41}$$

Thus,

$$\mathcal{M}_6 = -\left(\frac{4\pi\mu^2}{m_b^2}\right)^\varepsilon\left(\frac{m_b^2}{m_c^2}\right)^{2\varepsilon}\frac{(m_c^2)^2}{m_b^4}\Gamma^2(-1+\varepsilon) \tag{3.42}$$

using, $\frac{1}{\Gamma^2(1+\varepsilon)} = \big[\frac{1}{\varepsilon(-1+\varepsilon)\Gamma(-1+\varepsilon)}\big]^2$ and $\frac{m_c^2}{m_b^2}\equiv z$, we get,

$$\mathcal{M}_6(z,\varepsilon) = e^{2\gamma\varepsilon}\,\Gamma^2(1+\varepsilon)\big[\frac{-z^{2-2\varepsilon}}{\varepsilon^2(1-\varepsilon)^2}\big] \tag{3.43}$$

Now, let us consider $\mathcal{R}_{20}$. Using Eqs. (3.41) and (3.24), we find

$$\begin{aligned}
\frac{1}{256\pi^4}\mathcal{R}_{20} &= \frac{1}{m_b^2}\mu^{4\varepsilon}\int\frac{d^Dq_1}{(2\pi)^D}\frac{d^Dq_2}{(2\pi)^D}\frac{1}{(m_c^2-q_1^2)(m_c^2-(q_1-q_2)^2)}\frac{1}{(-q_2^2)}\\
&= \frac{1}{m_b^2}\mu^{4\varepsilon}\int\frac{d^Dq_2}{(2\pi)^D}\int_0^1 dx\int\frac{d^Dq_1}{(2\pi)^D}\frac{1}{[m_c^2-x(1-x)q_2^2-q_1^2]^2}\frac{1}{(-q_2^2)}\\
&= \frac{1}{m_b^2}\mu^{4\varepsilon}\int\frac{d^Dq_2}{(2\pi)^D}\int_0^1 dx\frac{1}{(-q_2^2)}\frac{i}{16\pi^2}\left(\frac{4\pi\mu^2}{m_c^2-x(1-x)q_2^2}\right)^{\varepsilon}\times\frac{\Gamma(\varepsilon)}{\Gamma(2)}\\
&= \int_0^1 dx\frac{i}{16\pi^2}\frac{(4\pi\mu^2)^{\varepsilon}}{m_b^2}\frac{\Gamma(\varepsilon)}{[x(1-x)]^{\varepsilon}}\mu^{2\varepsilon}\int\frac{d^Dq_2}{(2\pi)^D}\frac{1}{(-q_2^2)}\frac{1}{[\frac{m_c^2}{x(1-x)}-q_2^2]^{\varepsilon}},
\end{aligned}$$

where,

$$\frac{1}{(-q_2^2)}\frac{1}{[\frac{m_c^2}{x(1-x)}-q_2^2]^{\varepsilon}} = \int_0^1 dy\frac{y^{-1+\varepsilon}}{[(1-y)(y\frac{m_c^2}{x(1-x)}-q_2^2)]^{1+\varepsilon}}\frac{\Gamma(1+\varepsilon)}{\Gamma(1)\Gamma(\varepsilon)}.$$

Thus,

$$\begin{aligned}
\mathcal{R}_{20} = e^{2\gamma\varepsilon}\Gamma^2(1+\varepsilon)\frac{1}{\Gamma^2(1+\varepsilon)}(m_b^2)^{-1+2\varepsilon}(-1)\frac{\Gamma(\varepsilon)\Gamma(1+\varepsilon)}{\Gamma(\varepsilon)}\frac{\Gamma(-1+2\varepsilon)}{\Gamma(1+\varepsilon)}\times\\
\int_0^1 dx\int_0^1 dy\; y^{-1+\varepsilon}\frac{1}{x^{\varepsilon}(1-x)^{\varepsilon}}\left[y\frac{m_c^2}{x(1-x)}\right]^{1-2\varepsilon}.
\end{aligned}\tag{3.44}$$

Simplifying the above expression, we get

$$\begin{aligned}
\mathcal{R}_{20}(z,\varepsilon) &= e^{2\gamma\varepsilon}\Gamma^2(1+\varepsilon)z^{1-2\varepsilon}\Gamma(-1+2\varepsilon)\int_0^1 dx x^{-1+\varepsilon}(1-x)^{-1+\varepsilon}\int_0^1 dy y^{-\varepsilon}\\
&= e^{2\gamma\varepsilon}\Gamma^2(1+\varepsilon)\left[\frac{z^{1-2\varepsilon}}{\varepsilon^2(1-\varepsilon)(1-2\varepsilon)}\right]\\
&= -\frac{1}{z}\frac{1-\varepsilon}{1-2\varepsilon}\,\mathcal{M}_6(z,\varepsilon).
\end{aligned}$$

Hence, we have verified Eq. (3.19) using the Feynman parameters,

Next, we turn our attention to $\mathcal{M}_8$ and evaluate this integral using the Feynman parameters for $m_c = 0$. The final result reads

$$\begin{aligned}
\mathcal{M}_8(0,\varepsilon) &= e^{2\gamma\varepsilon}\frac{\Gamma(\varepsilon)\Gamma(2\varepsilon)\Gamma(1-\varepsilon)}{(1-2\varepsilon)(1-\varepsilon)}\\
&= e^{2\gamma\varepsilon}\left[\frac{1}{2\varepsilon^2}+\frac{3}{2\varepsilon}+\frac{\pi^2}{4}+\frac{7}{2}+\varepsilon\left(-\frac{4\zeta(3)}{3}+\frac{3\pi^2}{4}+\frac{15}{2}\right)+O(\varepsilon)\right].
\end{aligned}\tag{3.45}$$

We will see later in Sec. 3.3.3 that this result is important to get a full result for $\mathcal{M}_8$ at large and small z.

The master integral $\mathcal{M}_{11}$ is a product of one-loop massive tadpole and vertex diagrams. It is easy to evaluate it exactly in ε using the Feynman parameters. The complete result is given by

$$\mathcal{M}_{11} = \frac{e^{2\gamma\varepsilon}z^{1-\varepsilon}\Gamma(-1+\varepsilon)\Gamma(\varepsilon+1)(\psi(1-2\varepsilon)-\psi(1-\varepsilon))}{\varepsilon},\tag{3.46}$$

where the ψ function definition is recalled in Eq. (A.15) in Appendix A. The above result can alternatively be written as

$$\mathcal{M}_{11} = e^{2\gamma\varepsilon}\frac{z^{1-\varepsilon}\Gamma(1+\varepsilon)\Gamma(-1+\varepsilon)}{(1-\varepsilon)}{}_3F_2\left(1,1,1+\varepsilon;2-\varepsilon,2;1\right). \tag{3.47}$$

The definition of the hypergeometric functions ${}_nF_m$ and their relevant properties are also recalled in Appendix A.

3.3.2 The Mellin-Barnes method

The Mellin-Barnes method [167–169] is based on transforming sums in the propagator denominators (or in the denominators of the Feynman parameter integrals) into products of simpler terms, at the cost of introducing extra Mellin integrations that involve Γ-functions.[9] The basic formula reads

$$\frac{1}{(X+Y)^N} = \frac{1}{2\pi i}\int_{-i\infty}^{+i\infty} d\xi X^\xi Y^{-N-\xi}\frac{\Gamma(N+\xi)\Gamma(-\xi)}{\Gamma(N)} \tag{3.48}$$

where $N > 1$, while X and Y are complex numbers satisfying $|\arg(X) - \arg(Y)| < \pi$. One can see that the integrand in the above expression has poles at $\xi = m$ due to $\Gamma(-\xi)$, and at $\xi = -N-m$ due to $\Gamma(N+\xi)$. They are called right (or infrared) and left (or ultraviolet) poles (using the nomenclature of Smirnov [153]), where $m = 0, 1, 2, \ldots\infty$. One closes the integration contour to one side, and takes residues inside the contour at the poles of all the Γ-functions. In the following, we are going to close the contour of integration to the right, and sum the series of residues following the Cauchy residue theorem

$$\oint f(z)\,dz = 2\pi i\sum_i \mathrm{Res}\{f(z_i)\}. \tag{3.49}$$

The Γ-function is holomorphic everywhere in the whole complex plane except at the points $-m = 0, -1, -2, \ldots$ at which simple poles arise. The corresponding residues are

$$\begin{aligned}\mathrm{Res}\{\Gamma(x)\}_{x=-m} &= \mathrm{Res}\{\Gamma(z-m)\}_{z=0} = \mathrm{Res}\{\frac{\Gamma(1+z)}{z(z-1)\ldots(z-m)}\}_{z=0}\\ &= \lim_{z\to 0}\frac{\Gamma(1+z)}{(z-1)\ldots(z-m)} = \frac{(-1)^m}{m!}.\end{aligned} \tag{3.50}$$

Summing up all the residues in Eq. (3.48), one reproduces the usual Taylor expansion

$$\frac{1}{(X+Y)^N} = \sum_{m=0}^{\infty} X^m Y^{-N-m}\frac{\Gamma(N+m)}{\Gamma(N)}\frac{(-1)^m}{m!} = Y^{-N}\sum_{m=0}^{\infty}\frac{\Gamma(N+m)}{\Gamma(N)}\frac{(-X/Y)^m}{m!}. \tag{3.51}$$

A similar result is obtained by summing up the left residues. By iteration, the formula (3.48) gets generalized to

$$\begin{aligned}\frac{1}{(X_1+\ldots+X_n)^N} = \frac{1}{(2\pi i)^{n-1}}\int_{-i\infty}^{+i\infty} d\xi_1\ldots d\xi_{n-1}X_1^{\xi_1}\ldots X_{n-1}^{\xi_{n-1}}X_n^{-N-\xi-\ldots-\xi_{n-1}}\\ \times\frac{\Gamma(-\xi_1)\ldots\Gamma(-\xi_{n-1})\Gamma(N+\xi_1+\ldots\xi_{n-1})}{\Gamma(N)}.\end{aligned} \tag{3.52}$$

[9] An early application of the MB technique to the Feynman parameter integrals dates back to Ref. [127] where virtual $\mathcal{O}(\alpha_s)$ corrections to the inclusive $b\to s\gamma$ decay were calculated.

So long as we sum up the residues, the MB technique alone gives us only a series which may either serve as an iterative approximation to the full Feynman integral (as in Ref. [127]) or needs to be resummed. One can also make use of Eq. (3.36) whenever it helps.

The sum on the l.h.s. of Eq. (3.52) can come from the function $F(x)$ in Eq. (3.29). For instance, in the case of the master integral $\mathcal{M}_{15}$, we find

$$U(x) = x_1 + x_2 + x_3, \tag{3.53}$$
$$F(x) = z\, U(x)^2 - \ x_1 x_3. \tag{3.54}$$

By counting the terms in $F(x)$, one expects a four-dimensional MB-representation. However, after application of the first Barnes lemma

$$\frac{1}{2\pi i}\int_{-i\infty}^{+i\infty} ds\ \Gamma(a+s)\Gamma(b+s)\Gamma(c-s)\Gamma(d-s) = \frac{\Gamma(a+c)\Gamma(a+d)\Gamma(b+c)\Gamma(b+d)}{\Gamma(a+b+c+d)}. \tag{3.55}$$

we are left with a one-dimensional MB-representation only

$$\mathcal{M}_{15} = \frac{e^{2\gamma\varepsilon}\Gamma(1-\varepsilon)}{2\pi i}\int_{-i\infty}^{+i\infty} d\xi \frac{(-1)^{(-\xi)} z^\xi\, \Gamma^2(1-2\varepsilon-\xi)\Gamma(-\varepsilon-\xi)\Gamma(1-\varepsilon-\xi)\Gamma(-\xi)\Gamma(2\varepsilon+\xi)}{\Gamma(1-2\varepsilon-2\xi)\Gamma(2-3\varepsilon-\xi)\Gamma(2-2\varepsilon-\xi)}. \tag{3.56}$$

In the case of constructing an MB-representation of the Feynman integral (3.27) with an arbitrary number of propagators and arbitrary indices, a publicly available `Mathematica` code `AMBRE` [177] provides the desired representation in the following form:

$$\frac{1}{(2\pi i)^N}\int_{-i\infty}^{+i\infty}\cdots\int_{-i\infty}^{+i\infty}\prod_l^N d\xi_l \prod_k z_k^{d_k}\ \frac{\prod_i \Gamma(a_i + b_i\varepsilon + \sum_j c_{ij}\xi_j)}{\prod_i \Gamma(a'_i + b'_i\varepsilon + \sum_j c'_{ij}\xi_j)}. \tag{3.57}$$

where $a_i, \ldots, c'_{ij}$ are rational numbers. Typically, $c_{ij} = \pm 1$. Here, z_k are kinematical variables, and d_k are linear combinations of ε and ξ_l.

If our master integrals have phase-space cuts, extra integrals enter the calculation. We may then have a mixture of Γ-functions involving MB-parameters in the arguments and/or simple Euler-type integrals like the one in Eq. (3.36) that are easy to calculate.

For the evaluation of our present MIs in the three-body case, we have proceeded as in the above description. For example, in the case of $\mathcal{M}_5$, the phase-space integration gives

$$\frac{e^{3\gamma\varepsilon}\Gamma^2(1-\varepsilon)\Gamma(-2\varepsilon-\xi)}{\Gamma(2-2\varepsilon)\Gamma(-4\varepsilon-\xi+2)}, \tag{3.58}$$

and a full MB-representation of this integral reads

$$\mathcal{M}_5 = \frac{e^{3\gamma\varepsilon}\Gamma^2(1-\varepsilon)}{2\pi i}\int_{-i\infty}^{+i\infty} d\xi \frac{(-1)^{-\varepsilon-\xi} z^\xi \Gamma(-\xi)\Gamma(-2\varepsilon-\xi)\Gamma^2(-\varepsilon-\xi)\Gamma(\varepsilon+\xi+1)}{\Gamma(2-2\varepsilon)\Gamma(-2\varepsilon-2\xi+1)\Gamma(-4\varepsilon-\xi+2)}. \tag{3.59}$$

It may happen that one encounters mixtures of MB integrals and Euler-type integrals involving hypergeometric functions with MB parameters in their arguments, as often happens when four-body phase space integrals are considered. In such cases, it is useful

not to apply the Euler representation (A.36) for hypergeometric functions but rather use the following MB representation:

$$ {}_pF_q\left(a_1,\ldots,a_p;b_1,\ldots,b_p;z\right) = \frac{1}{2\pi i}\int_{\alpha-i\infty}^{\alpha+i\infty} d\xi\ (-z)^{-\xi}\ \Gamma(\xi)\left[\prod_{i=1}^{p}\frac{\Gamma(a_i-\xi)}{\Gamma(a_i)}\right]\left[\prod_{i=1}^{q}\frac{\Gamma(b_i)}{\Gamma(b_i-\xi)}\right]. \tag{3.60}$$

Once we increase the number of Γ-functions by using the above formula, we have more possibilities of applying the Barnes lemmas, Gauss's identity (implemented in the code `barnesroutines.m` [178]), and hypergeometric functions, to get a closed and compact form of the result we are after.[10]. If obtaining a closed form in ε and z is not possible, public packages MB.m [179] and/or MBresolve [180] can be used to resolve ε-singularities and Laurent-expand the resulting integrals in ε. For example, for the case $\mathcal{M}_4$, we have expanded up to $\mathcal{O}(1)$ in ε, and got $1/\varepsilon + 7 - \ln(z)$ plus

$$\frac{1}{2\pi i}\int_{-i\infty-1/4}^{+i\infty-1/4} d\xi \frac{e^{-i\pi\xi}z^{\xi}\Gamma^4(1-\xi)\Gamma(-\xi)\Gamma(\xi)}{\Gamma(2-2\xi)\Gamma^2(2-\xi)}, \tag{3.61}$$

which corresponds to expressing $\mathcal{M}_4$ in terms of an MB integral regularized at $\xi = -1/4$.

Similarly, for $\mathcal{M}_{15}$ expanded up to $\mathcal{O}(1)$ in ε, we have obtained the following MB integral

$$\mathcal{P}_{15} = \frac{1}{2\pi i}\int_{-i\infty+\xi_1}^{+i\infty+\xi_1} d\xi \frac{e^{-i\pi\xi}z^{\xi}\Gamma^3(1-\xi)\Gamma^2(-\xi)\Gamma(\xi)}{\Gamma(1-2\xi)\Gamma^2(2-\xi)} \tag{3.62}$$

which gets regularized at, for instance, $\xi_1 \simeq -0.895075$. Once the ε singularities are resolved, the above description can be repeated to obtain ε-expanded MB integrals in a closed form with respect to z.

We have encountered cases where casting a closed form with respect to z is not straightforward. Then the code `MB.m` [179] was used to get asymptotic expansions. For example, the MB integral in Eq. (3.62) has the following expansion up to $\mathcal{O}(z^5)$

$$\begin{aligned}\mathcal{P}_{15} = &-\frac{L^2}{2} - 2L + i\pi L + \frac{\pi^2}{2} + 2i\pi - 3 + \frac{1}{3}\Big(- L^3 + 3i\pi L^2 + 3\left(2+\pi^2\right)L \\ &- 6(2-2\zeta(3)) - i\pi^3 - 6i\pi\Big)z + (-3L + 3i\pi + 4)z^2 + \frac{1}{6}(-10L + 10i\pi + 1)z^3 \\ &- \frac{1}{54}(105L - 105i\pi + 37)z^4 - \frac{1}{80}(252L - 252i\pi + 149)z^5 + \mathcal{O}(z^6),\end{aligned} \tag{3.63}$$

where $L \equiv \ln z$.

3.3.3 Differential equations

The Differential Equation (DE) method has been worked out in Refs. [76–78]. Its nice feature is that it can be applied to multiloop integrals with arbitrary scales, and it is suitable to both analytical and numerical calculations. In the latter case, results for large numbers of MIs can be obtained in an automated manner, and in the whole parameter

[10] For useful MB identities and corollaries, see the books in Ref [153].

space. As far as the analytical solutions are concerned, they may be given in terms of elliptic integrals, as it is the case for a fully massive two-loop propagator-type topology with different masses. In such cases, obtaining fully analytical solutions might be difficult or impossible. Nevertheless, integrals of such kind can easily be treated numerically for arbitrary kinematics, and in a fully automated manner. In our case, some of the integrals, e.g., $\mathcal{M}_5$ and $\mathcal{M}_{17}$, are hard to access analytically with the help of the previously described methods. However, we have managed to obtain an analytical result (in terms of an expansion in z) for $\mathcal{M}_{17}$ using the DE method.

The DE method is based on the fact that the IBP identities (and possibly other identities) allow to write a closed system of first-order DEs (homogeneous and/or inhomogeneous) for the MIs in the kinematical invariants. In our case, we are interested in the DEs in the variable z. A derivative of any MI with respect to z is given as a linear combination of some Feynman integrals. They can be reduced to the MIs using the IBP, and, in effect, we obtain a system of DEs of the following form

$$\frac{\mathrm{d}}{\mathrm{d}z}\mathcal{M}_n(z,\varepsilon) = \sum_m R_{nm}(z,\varepsilon)\mathcal{M}_m(z,\varepsilon). \tag{3.64}$$

The coefficients $R_{nm}(z,\varepsilon)$ are rational functions of z and ε. The above system of coupled DEs is solved exactly whenever possible for a generic value of ε. In our case the method of Euler's variation of constants for an inhomogeneous linear equation has often been sufficient. If an analytical solution for a generic ε is not feasible, the DEs and MIs are Laurent-expanded around $\varepsilon = 0$, starting from the highest pole, up to the required order, e.g.,

$$\mathcal{M}_n(z,\varepsilon) = \frac{1}{\varepsilon^2}\mathcal{M}_{n,-2}(z) + \frac{1}{\varepsilon}\mathcal{M}_{n,-1}(z) + \mathcal{M}_{n,0}(z) + \varepsilon\mathcal{M}_{n,1}(z) + \ldots \tag{3.65}$$

In this way, a system of coupled DEs for the coefficients of the ε-expansions is obtained

$$\frac{\mathrm{d}}{\mathrm{d}z}\mathcal{M}_{n,k}(z) = \sum_{m,j} R_{nkmj}(z)\mathcal{M}_{m,j}(z). \tag{3.66}$$

The boundary conditions for the above DEs should be chosen at some value of z_0 where the calculation is simpler than at a general z. In our case, we have considered either z_0 large enough for the asymptotic expansion in $1/z$ to be convergent, or z_0 small enough for the asymptotic expansion in z to be convergent. The corresponding series expansion coefficients satisfy recurrence relations that follow from the DEs themselves. Thus, only a few constants (z-independent numbers) in a given expansion need to be fixed using an "external" method like the MB method or the expansion by regions implemented in the code `exp` [181].[11] In some cases, regularity conditions in certain limits supply additional restrictions on the constants.

The DEs in Eq. (3.66) form a system of linear equations in which the coefficients are rational functions of z only. The final results obtained with the DE method are insensitive to z-independent but ε-dependent common global normalization factors. Such factors can

[11] This code is not public. We have obtained the corresponding large-z expansions from M. Steinhauser. We were able to verify them using other methods for all but one MI, namely $\mathcal{M}_{16}$.

be included either before or after solving the DEs. In our expressions below, we have skipped the z-independent two-body phase-space factor P_2 from Eq. (3.13). Thus, our normalization of the two-body MIs in this subsection is consistent with the one of the previous subsections.

The denominators of the functions $R_{nkmj}(z)$ in Eq (3.66) have the following form

$$\begin{aligned} &\text{in the 3-body case: } z^p(1-4z)^q, \\ &\text{in the 2-body case: } z^p(1-4z)^q(1-z)^r, \end{aligned} \tag{3.67}$$

where p, q, r are some nonnegative integer powers. This means that the points $z = 0$, $z = 1/4$ (and also $z = 1$ for the 2-body case) are singular points of our system of equations. The point $z = 1/4$ is a physical threshold for $c\bar{c}$ production, the point $z = 0$ is IR-singular (as we include no $c\bar{c}$ production), while $z = 1$ is a pseudo-threshold. Choosing an optimal basis for the MIs may considerably simplify the form of the systems of DEs, and hence their solution. The guidance for the pursuit of suitable basis of MIs lies in the qualitative properties of the solution, such as ε-finite basis and uniform weight (homogeneous transcendentality). There is no general criteria for determining such an optimal basis. However, recently, it has been proposed in Ref. [182] to solve the systems of DEs for MIs with *algebraic* methods (transformation matrix, integral representations manipulations, etc.) where the dependence on ε is factorized from the kinematics. This issue was further explored in Ref. [183] where an iterative integration of the DEs was proposed. With the such a "canonical" basis of the MIs, the formalism of Harmonic Polylogarithms (HPLs) [174] turns out to be very useful.

Let us now discuss the evaluation of our master integrals using the DE method. One can easily verify the relation 3.19 using this technique. The differential equations derived from the IBP for $\mathcal{M}_6$ and $\mathcal{R}_{20}$ read

$$\mathcal{M}_6'(z,\varepsilon) = \frac{2-2\varepsilon}{z}\mathcal{M}_6(z,\varepsilon), \tag{3.68}$$

$$\mathcal{R}_{20}'(z,\varepsilon) = -\frac{1}{z^2}(1-\varepsilon)\mathcal{M}_6(z,\varepsilon), \tag{3.69}$$

where prime denotes a derivative with respect to z. Differentiating Eq. (3.19) with respect to z, and then substituting (3.68) and (3.69) there, we indeed verify that Eq. (3.19) is correct up to an additive z-independent number. The fact that this number equals to zero follows from the fact that both $\mathcal{M}_6$ and $\mathcal{R}_{20}$ vanish for $z = 0$, as they become scaleless in this limit.

Next, let us consider the master integral $\mathcal{M}_8$. It satisfies the following DE:

$$\mathcal{M}_8' + \frac{2-4\varepsilon}{1-4z}\mathcal{M}_8 = \frac{2-2\varepsilon}{z(1-4z)}(\mathcal{M}_6 - \mathcal{M}_7). \tag{3.70}$$

The solutions of the DEs for $\mathcal{M}_7$ and $\mathcal{M}_6$ are

$$\mathcal{M}_6(z,\varepsilon) = -e^{2\gamma\varepsilon}\frac{\Gamma^2(1+\varepsilon)z^{2(1-\varepsilon)}}{\varepsilon^2(1-\varepsilon)^2} \quad \text{and} \quad \mathcal{M}_7(z,\varepsilon) \quad = -e^{2\gamma\varepsilon}\frac{\Gamma^2(1+\varepsilon)z^{1-\varepsilon}}{\varepsilon^2(1-\varepsilon)^2}. \tag{3.71}$$

Solving the DE in Eq. (3.70) with the boundary condition at $z = 0$, we find

$$\mathcal{M}_8(z,\varepsilon) = (1-4z)^{(\frac{1}{2}-\varepsilon)}\big[\mathcal{M}_8(0,\varepsilon) + \Phi_8\big], \tag{3.72}$$

where

$$\Phi_8(z,\varepsilon) = e^{2\gamma\varepsilon}\frac{\Gamma^2(1+\varepsilon)}{\varepsilon^2(1-\varepsilon)^2}\left[z^{1-2\varepsilon}\Big(- z\,{}_2F_1(2-2\varepsilon,\frac{3}{2}-\varepsilon,3-2\varepsilon,4z) + 2z^{\varepsilon}\,{}_2F_1(1-\varepsilon,\frac{3}{2}-\varepsilon,2-\varepsilon,4z)\Big)\right]. \tag{3.73}$$

and $\mathcal{M}_8(0,\varepsilon)$ is given in Eq. (3.45).

The above expression is convenient for expansions in z, but inconvenient for expansions in $1/z$. To derive an alternative expression for $\mathcal{M}_8$, we use the Euler transformation identity

$${}_2F_1(a,b,c,x) = (1-x)^{c-a-b}\,{}_2F_1(c-a,c-b,c,x), \tag{3.74}$$

and afterwards an analytic continuation[12] to express all the hypergeometric functions in terms of $1/z$. After some manipulations, we get

$$\begin{aligned}\mathcal{M}_8(z,\varepsilon) = {} & e^{2\gamma\varepsilon}\,z^{1-2\varepsilon}\left(\frac{\Gamma^2(\varepsilon)}{(1-\varepsilon)(1-2\varepsilon)}\,{}_2F_1(1,-1+2\varepsilon,\frac{1}{2}+\varepsilon,\frac{1}{4z}) + \frac{\Gamma^2(\varepsilon)}{1-\varepsilon}z^{-1+\varepsilon}\,{}_2F_1(1,\varepsilon,\frac{3}{2},\frac{1}{4z})\right)\\ & + (-1+4z)^{\frac{1}{2}-\varepsilon}\mathcal{M}_8(0,\varepsilon)\\ & + e^{2\gamma\varepsilon}(-1+4z)^{\frac{1}{2}-\varepsilon}\frac{\Gamma^2(\varepsilon)}{(1-\varepsilon)^2\Gamma(\frac{3}{2}-\varepsilon)}e^{-i\pi(-1+\varepsilon)}(4)^{-1+\varepsilon}\left(2\Gamma(\frac{1}{2})\Gamma(2-\varepsilon)\right.\\ & \left. - \Gamma(3-2\varepsilon)\Gamma(-\frac{1}{2}+\varepsilon)e^{-i\pi(-1+\varepsilon)}(4)^{-1+\varepsilon}\right).\end{aligned} \tag{3.75}$$

To show that the above result agrees with Ref. [94], it is sufficient to check that the last three lines give zero, i.e. that

$$\mathcal{M}_8(0,\varepsilon) = e^{2\gamma\varepsilon}\frac{\Gamma^2(\varepsilon)}{(1-\varepsilon)^2\Gamma(\frac{3}{2}-\varepsilon)}\frac{1}{2}\left(\sqrt{\pi}\Gamma(2-\varepsilon)4^{\varepsilon}e^{-i\pi\varepsilon} - \frac{1}{4}\frac{\Gamma(3-2\varepsilon)\Gamma(\frac{1}{2}+\varepsilon)}{1-2\varepsilon}4^{2\varepsilon}e^{-2i\pi\varepsilon}\right). \tag{3.76}$$

The above relation implies, of course, vanishing of the imaginary part on the r.h.s.

$$-\sqrt{\pi}\Gamma(2-\varepsilon)4^{\varepsilon}\sin\pi\varepsilon + \frac{1}{4}\frac{\Gamma(3-2\varepsilon)\Gamma(\frac{1}{2}+\varepsilon)}{1-2\varepsilon}4^{2\varepsilon}\sin 2\pi\varepsilon = 0. \tag{3.77}$$

Indeed, Eq. (3.76) holds due to the following two identities

$$\begin{aligned}\Gamma\left(\frac{n}{2}+\varepsilon\right) &= \frac{\Gamma(n-1+2\varepsilon)}{\Gamma(\frac{n-1}{2}+\varepsilon)}\sqrt{\pi}2^{1-2(\frac{n}{2}+\varepsilon-\frac{1}{2})} \quad \text{when } n \text{ is an integer,}\\ \sin(\pi\varepsilon) &= \frac{\pi\varepsilon}{\Gamma(1+\varepsilon)\Gamma(1-\varepsilon)},\end{aligned} \tag{3.78}$$

from which one derives that

$$\begin{aligned}\Gamma\left(\frac{1}{2}\pm\varepsilon\right) &= \frac{\Gamma(1\pm 2\varepsilon)}{\Gamma(1\pm\varepsilon)}\sqrt{\pi}4^{\mp\varepsilon},\\ \cos(\pi\varepsilon) &= \frac{\Gamma(1+\varepsilon)\Gamma(1-\varepsilon)}{\Gamma(1+2\varepsilon)\Gamma(1-2\varepsilon)} = \frac{\pi}{\Gamma\left(\frac{1}{2}+\varepsilon\right)\Gamma\left(\frac{1}{2}-\varepsilon\right)}.\end{aligned} \tag{3.79}$$

[12] See Appendix A. At this point, the Feynman "i0" prescription becomes important for the branch choice, and one must treat z as $z - i0$.

Finally, our result for $\mathcal{M}_8$ that is convenient for expansions in $1/z$ reads

$$\mathcal{M}_8(z,\varepsilon) = e^{2\gamma\varepsilon} z^{1-2\varepsilon}\left(\frac{\Gamma^2(\varepsilon)}{(1-\varepsilon)(1-2\varepsilon)}{}_2F_1(1,-1+2\varepsilon,\frac{1}{2}+\varepsilon,\frac{1}{4z}) + \frac{\Gamma^2(\varepsilon)}{1-\varepsilon}z^{-1+\varepsilon}{}_2F_1(1,\varepsilon,\frac{3}{2},\frac{1}{4z})\right). \tag{3.80}$$

In the following, expressions like Eqs. (3.72) & (3.73) will be called "small-z" solutions for a given MI, while expressions like Eq. (3.80) will be called "large-z" solutions. However, one should remember that they are just different ways of writing an exact expression for the same function of z. They are valid for any z up to branch choice ambiguities in the analytic continuation.

The master integrals $\mathcal{M}_{12}$ and $\mathcal{M}_{13}$:

The coupled differential equations for these MI's are given by

$$\mathcal{M}'_{12} = -2\mathcal{M}_{13}, \tag{3.81}$$

$$\mathcal{M}'_{13} + \frac{-1+4\varepsilon+3\varepsilon-8\varepsilon z}{2z(1-z)}\mathcal{M}_{13} = -\frac{2-7\varepsilon+6\varepsilon^2}{4z(1-z)}\mathcal{M}_{12} + \frac{(1-\varepsilon)^2}{4z^2(1-z)}(\mathcal{M}_6 - 2\mathcal{M}_7). \tag{3.82}$$

From them, it is easy to derive the following inhomogeneous hypergeometric differential equation for the sunset integral $\mathcal{M}_{12}$:

$$z(1-z)\mathcal{M}''_{12} - \left[\frac{1-4\varepsilon}{2} - \left(\frac{3}{2}-4\varepsilon\right)z\right]\mathcal{M}'_{12} - \left(\frac{1-2\varepsilon}{2}\right)(2-3\varepsilon)\,\mathcal{M}_{12} = \frac{1}{2}e^{2\gamma\varepsilon}\,\Gamma^2(\varepsilon)(z^{1-2\varepsilon}-2z^{-\varepsilon}). \tag{3.83}$$

The large-z result for $\mathcal{M}_{12}$ reads

$$\begin{aligned}\mathcal{M}_{12} = e^{2\gamma\varepsilon}\,\Gamma^2(\varepsilon)\Bigg[&\frac{z^{1-2\varepsilon}}{(1-\varepsilon)(1-2\varepsilon)}\;{}_3F_2\left(\frac{1}{2},1,-1+2\varepsilon;2-\varepsilon,\frac{1}{2}+\varepsilon;\frac{1}{z}\right)\\ &+\frac{z^{-\varepsilon}}{1-\varepsilon}\;{}_3F_2\left(1,\frac{3}{2}-\varepsilon,\varepsilon;\frac{3}{2},3-2\varepsilon;\frac{1}{z}\right)\Bigg].\end{aligned} \tag{3.84}$$

Eq. (3.84) is in agreement with the Appendix of Ref. [184]. Our explicit result for small z is

$$\begin{aligned}\mathcal{M}_{12} = e^{2\gamma\varepsilon}\Bigg[&\frac{\pi^2 2^{4-8\varepsilon} z^{\frac{3}{2}-2\varepsilon}\Gamma(1+4\varepsilon)\,{}_2F_1\left(1-\varepsilon,\varepsilon-\frac{1}{2};\frac{5}{2}-2\varepsilon;z\right)}{\varepsilon(1-2\varepsilon)(3-4\varepsilon)(1-4\varepsilon)\Gamma^2(\varepsilon)}\\ &+\frac{z^{1-\varepsilon}\Gamma^2(\varepsilon)}{2(1-\varepsilon)}\left(z^{1-\varepsilon}{}_3F_2\left(1,3/2-\varepsilon,\varepsilon;3/2,3-2\varepsilon;z\right) + \frac{4\,{}_3F_2\left(\frac{1}{2},1,2\varepsilon-1;2-\varepsilon,\varepsilon+\frac{1}{2};z\right)}{(1-2\varepsilon)}\right)\\ &-\frac{2\pi^3\csc(\pi\varepsilon)\csc(2\pi\varepsilon)\csc(4\pi\varepsilon)(1-4\varepsilon)\Gamma(-\varepsilon)\,{}_2F_1\left(\varepsilon-\frac{1}{2},3\varepsilon-2;2\varepsilon-\frac{1}{2};z\right)}{(1-2\varepsilon)\Gamma^2(-2\varepsilon)\Gamma(3-3\varepsilon)\Gamma(1+4\varepsilon)}\Bigg].\end{aligned} \tag{3.85}$$

In the derivation of the above equation, we have used the second identity from Eq. (3.79).

As far as $\mathcal{M}_{13}$ is concerned, our large-z result reads

$$\mathcal{M}_{13} = e^{2\gamma\varepsilon}\Bigg[- \frac{z^{-2\varepsilon}\Gamma^2(1+\varepsilon)}{4\varepsilon^2(1-\varepsilon)}\Bigg(2\,{}_3F_2\left(\frac{1}{2},1,2\varepsilon-1;2-\varepsilon,\varepsilon+\frac{1}{2};\frac{1}{z}\right) + \frac{z^{-1}}{(2-\varepsilon)\left(\frac{1}{2}+\varepsilon\right)}$$
$$\times\ {}_3F_2\left(\frac{3}{2},2,2\varepsilon;3-\varepsilon,\varepsilon+\frac{3}{2};\frac{1}{z}\right)\Bigg) + \frac{z^{-\varepsilon-1}\Gamma^2(1+\varepsilon)}{6\varepsilon(1-\varepsilon)}\Bigg(3\,{}_3F_2\left(1,\frac{3}{2}-\varepsilon,\varepsilon;\frac{3}{2},3-2\varepsilon;\frac{1}{z}\right)$$
$$+ z^{-1}\,{}_3F_2\left(2,\frac{5}{2}-\varepsilon,\varepsilon+1;\frac{5}{2},4-2\varepsilon;\frac{1}{z}\right)\Bigg)\Bigg], \tag{3.86}$$

while the explicit small-z result is

$$\mathcal{M}_{13} = e^{2\gamma\varepsilon}\Bigg[- \frac{z^{(1/2-2\varepsilon)\varepsilon}\,\pi^2 4^{1-4\varepsilon}\Gamma(1+4\varepsilon)}{(3-4\varepsilon)(1-4\varepsilon)\Gamma^2(1+\varepsilon)}\Bigg(\frac{2(1-\varepsilon)\,{}_2F_1\left(2-\varepsilon,\varepsilon-\frac{1}{2};\frac{5}{2}-2\varepsilon;z\right)}{(1-2\varepsilon)}$$
$$+\ {}_2F_1\left(1-\varepsilon,\varepsilon-1/2;5/2-2\varepsilon;z\right)\Bigg) - \frac{z^{-\varepsilon}\Gamma^2(\varepsilon)}{(1-\varepsilon)(1-2\varepsilon)}\Bigg({}_3F_2\left(\frac{1}{2},2,2\varepsilon-1;2-\varepsilon,\varepsilon+\frac{1}{2};z\right)$$
$$-\varepsilon\ {}_3F_2\left(\frac{1}{2},1,2\varepsilon-1;2-\varepsilon,\varepsilon+\frac{1}{2};z\right)\Bigg) - \frac{z^{(1-2\varepsilon)}\Gamma^2(\varepsilon)}{4(1-\varepsilon)}$$
$$\times\left((1-2\varepsilon)\,{}_3F_2\left(1,\frac{3}{2}-\varepsilon,\varepsilon;\frac{3}{2},3-2\varepsilon;z\right) + {}_3F_2\left(2,\frac{3}{2}-\varepsilon,\varepsilon;\frac{3}{2},3-2\varepsilon;z\right)\right)$$
$$+ \frac{\pi^3 2^{1-2\varepsilon}\csc(\pi\varepsilon)\csc(4\pi\varepsilon)\,{}_2F_1\left(\varepsilon+\frac{1}{2},3\varepsilon-1;2\varepsilon+\frac{1}{2};z\right)}{\Gamma(2-3\varepsilon)\Gamma\left(\frac{1}{2}-\varepsilon\right)\Gamma\left(2\varepsilon+\frac{1}{2}\right)}\Bigg]. \tag{3.87}$$

The master integral $\mathcal{M}_{14}$:

Our differential equation for $\mathcal{M}_{14}$ is

$$\mathcal{M}'_{14} + \frac{3\varepsilon-1}{z}\mathcal{M}_{14} = \frac{(1-\varepsilon)^2}{z^2(1-2\varepsilon)}\mathcal{M}_6 + \frac{1-\varepsilon}{z}\mathcal{M}_8. \tag{3.88}$$

Its solution for large z is given by

$$\mathcal{M}_{14} = e^{2\gamma\varepsilon}\frac{\Gamma(\varepsilon)^2}{\varepsilon(1-2\varepsilon)}\Bigg(z^{1-2\varepsilon}\left[{}_3F_2\left(1,-\varepsilon,2\varepsilon-1;1-\varepsilon,\varepsilon+\frac{1}{2};\frac{1}{4z}\right)-1\right]$$
$$-\,z^{-\varepsilon}\,\varepsilon\,{}_3F_2\left(1,1-2\varepsilon,\varepsilon;\frac{3}{2},2-2\varepsilon;\frac{1}{4z}\right)\Bigg), \tag{3.89}$$

and an analytic continuation of $\mathcal{M}_{14}$ to small z reads

$$\mathcal{M}_{14} = e^{2\gamma\varepsilon}\Bigg[\frac{z^{1-\varepsilon}\Gamma^2(\varepsilon)}{\varepsilon(1-\varepsilon)}\Big({}_3F_2\left(1/2,1,2\varepsilon;2-\varepsilon,1+2\varepsilon;4z\right) - \frac{z^{1-\varepsilon}\,\varepsilon\,{}_3F_2\left(1,\frac{3}{2}-\varepsilon,\varepsilon+1;3-2\varepsilon,2+\varepsilon;4z\right)}{(1+\varepsilon)}\Big)$$
$$-\frac{z^{1-2\varepsilon}\Gamma^2(\varepsilon)}{\varepsilon(1-2\varepsilon)} - \frac{z^{1-3\varepsilon}\pi\csc(2\pi\varepsilon)\Gamma(\varepsilon)\Gamma(2\varepsilon)\Gamma(3\varepsilon-1)}{\Gamma(4\varepsilon)} - \frac{\pi^2\csc(\pi\varepsilon)\csc(2\pi\varepsilon)\,{}_2F_1\left(\varepsilon-\frac{1}{2},3\varepsilon-1;3\varepsilon;4z\right)}{(1-3\varepsilon)\Gamma(2-2\varepsilon)}\Bigg]. \tag{3.90}$$

The master integrals $\mathcal{M}_9$ and $\mathcal{M}_{10}$:

The coupled differential equations for this set of sunset integrals are

$$\begin{aligned}\mathcal{M}_9' &= -2\mathcal{M}_{10},\\ \mathcal{M}_{10}' + \frac{\varepsilon + 6\varepsilon - 16\varepsilon z}{z(1-4z)}\mathcal{M}_{10} &= -\frac{2-7\varepsilon+6\varepsilon^2}{z(1-4z)}\mathcal{M}_9 + \frac{(1-\varepsilon)^2}{z^2(1-4z)}\mathcal{M}_6.\end{aligned} \tag{3.91}$$

For $\mathcal{M}_9$, the inhomogeneous hypergeometric differential equation is

$$x(1-x)\mathcal{M}_9'' + \left[\left(\varepsilon + \left(\frac{3}{2} - 4\varepsilon\right)x\right]\mathcal{M}_9' - \left(\frac{1-2\varepsilon}{2}\right)(2-3\varepsilon)\,\mathcal{M}_9 - 2e^{2\gamma\varepsilon}\,\Gamma^2(\varepsilon)\left(\frac{1}{4}\right)^{2-2\varepsilon} x^{1-2\varepsilon} = 0, \tag{3.92}$$

where $x = 4\ z$. The large-z result for $\mathcal{M}_9$ takes the form

$$\mathcal{M}_9 = e^{2\gamma\varepsilon}\,\Gamma^2(\varepsilon)\frac{z^{1-2\varepsilon}}{(1-\varepsilon)(1-2\varepsilon)}{}_3F_2\left(1, \varepsilon, -1+2\varepsilon; 2-\varepsilon, \frac{1}{2}+\varepsilon; \frac{1}{4z}\right). \tag{3.93}$$

Eq. (3.93) is in agreement with Eq.(4.26) of Ref. [185]. Our explicit small-z solution for $\mathcal{M}_9$ reads

$$\begin{aligned}\mathcal{M}_9 = e^{2\gamma\varepsilon}\Big[\ &\frac{z^{2-2\varepsilon}\Gamma(\varepsilon)^2{}_3F_2\left(1, \frac{3}{2}-\varepsilon, \varepsilon; 3-2\varepsilon, 2-\varepsilon; 4z\right)}{(1-\varepsilon)^2} + \frac{2\,z^{1-\varepsilon}e^{i\pi\varepsilon}\Gamma^2(\varepsilon)\Gamma^2(1-\varepsilon){}_2F_1\left(\frac{1}{2}, 2\varepsilon-1; 2-\varepsilon; 4z\right)}{(1-\varepsilon)(1-2\varepsilon)\Gamma(1-2\varepsilon)}\\ -\ &\frac{e^{2i\pi\varepsilon}\Gamma^3(1-\varepsilon)\Gamma(1+2\varepsilon){}_2F_1\left(\varepsilon-\frac{1}{2}, 3\varepsilon-2; \varepsilon; 4z\right)}{2\varepsilon(2-3\varepsilon)(1-2\varepsilon)(1-3\varepsilon)\Gamma(1-3\varepsilon)}.\Big]\end{aligned} \tag{3.94}$$

Now, from $\mathcal{M}_9$ we can easily derive the result for $\mathcal{M}_{10}$, using the first equation in Eq. (3.91). The large-z solution for $\mathcal{M}_{10}$ reads

$$\begin{aligned}\mathcal{M}_{10} = -e^{2\gamma\varepsilon}\,z^{-2\varepsilon}\Gamma^2(1+\varepsilon)\Bigg[&\frac{{}_3F_2\left(1, \varepsilon, 2\varepsilon-1; 2-\varepsilon, \varepsilon+\frac{1}{2}; \frac{1}{4z}\right)}{2\varepsilon^2(1-2\varepsilon)}\\ &+ \frac{z^{-1}\,{}_3F_2\left(2, 2\varepsilon, \varepsilon+1; 3-\varepsilon, \varepsilon+\frac{3}{2}; \frac{1}{4z}\right)}{8\varepsilon(1-\varepsilon)(2-\varepsilon)\left(\varepsilon+\frac{1}{2}\right)}\Bigg],\end{aligned} \tag{3.95}$$

and the small-z solution is given by

$$\begin{aligned}
\mathcal{M}_{10} = e^{2\gamma\varepsilon}\Bigg[& - \frac{i\pi\varepsilon z^{-\varepsilon}\Gamma(1-\varepsilon)\Gamma(\varepsilon)\,{}_3F_2\left(\frac{1}{2},\varepsilon+1,2\varepsilon-1;2-\varepsilon,\varepsilon;4z\right)}{(2\varepsilon^2-3\varepsilon+1)\,\Gamma(1-2\varepsilon)} \\
& - \frac{\varepsilon^2 z^{-\varepsilon}\Gamma(1-\varepsilon)^3\Gamma(\varepsilon)^3\,{}_3F_2\left(\frac{1}{2},\varepsilon+1,2\varepsilon-1;2-\varepsilon,\varepsilon;4z\right)}{(2\varepsilon^2-3\varepsilon+1)\,\Gamma(1-2\varepsilon)^2\Gamma(2\varepsilon+1)} \\
& + \frac{i\pi\Gamma(1-\varepsilon)^3\,{}_2F_1\left(\varepsilon-\frac{1}{2},3\varepsilon-2;\varepsilon;4z\right)}{2\,(9\varepsilon^2-9\varepsilon+2)\,z\Gamma(1-3\varepsilon)\Gamma(1-2\varepsilon)} \\
& + \frac{\Gamma(1-2\varepsilon)\Gamma(1-\varepsilon)^3\Gamma(2\varepsilon+1)^2\,{}_2F_1\left(\varepsilon-\frac{1}{2},3\varepsilon-2;\varepsilon;4z\right)}{4\varepsilon\,(9\varepsilon^2-9\varepsilon+2)\,z\Gamma(1-4\varepsilon)\Gamma(1-3\varepsilon)\Gamma(4\varepsilon+1)} \\
& - \frac{i\pi\Gamma(1-\varepsilon)^3\,{}_3F_2\left(\varepsilon-\frac{1}{2},2\varepsilon,3\varepsilon-2;\varepsilon,2\varepsilon-1;4z\right)}{2\,(9\varepsilon^2-9\varepsilon+2)\,z\Gamma(1-3\varepsilon)\Gamma(1-2\varepsilon)} \\
& - \frac{\Gamma(1-2\varepsilon)\Gamma(1-\varepsilon)^3\Gamma(2\varepsilon+1)^2\,{}_3F_2\left(\varepsilon-\frac{1}{2},2\varepsilon,3\varepsilon-2;\varepsilon,2\varepsilon-1;4z\right)}{4\varepsilon\,(9\varepsilon^2-9\varepsilon+2)\,z\Gamma(1-4\varepsilon)\Gamma(1-3\varepsilon)\Gamma(4\varepsilon+1)} \\
& + \frac{i\pi z^{-\varepsilon}\Gamma(1-\varepsilon)\Gamma(\varepsilon)\,{}_2F_1\left(\frac{1}{2},2\varepsilon-1;2-\varepsilon;4z\right)}{(\varepsilon-1)\Gamma(1-2\varepsilon)} \\
& + \frac{\varepsilon z^{-\varepsilon}\Gamma(1-\varepsilon)^3\Gamma(\varepsilon)^3\,{}_2F_1\left(\frac{1}{2},2\varepsilon-1;2-\varepsilon;4z\right)}{(\varepsilon-1)\Gamma(1-2\varepsilon)^2\Gamma(2\varepsilon+1)} \\
& + \frac{\varepsilon z^{1-2\varepsilon}\Gamma(\varepsilon)^2\,{}_3F_2\left(1,\frac{3}{2}-\varepsilon,\varepsilon;3-2\varepsilon,2-\varepsilon;4z\right)}{(\varepsilon-1)}\Bigg]
\end{aligned} \tag{3.96}$$

The master integral $\mathcal{M}_{15}$:

The differential equation for $\mathcal{M}_{15}$ is

$$\mathcal{M}_{15}' - \frac{1-2\varepsilon}{z}\mathcal{M}_{15} = -\frac{1}{z}\mathcal{M}_{10}. \tag{3.97}$$

The large z solution reads

$$\begin{aligned}
\mathcal{M}_{15} = e^{2\gamma\varepsilon}\frac{\Gamma^2(1+\varepsilon)\,z^{-2\varepsilon}}{2\varepsilon^2(1-\varepsilon)(1-2\varepsilon)}\Bigg[& {}_3F_2\left(1,\varepsilon,2\varepsilon-1;2-\varepsilon,\varepsilon+\frac{1}{2};\frac{1}{4z}\right) \\
& - 2(1-\varepsilon){}_4F_3\left(1,1,\varepsilon,2\varepsilon-1;2,2-\varepsilon,\varepsilon+\frac{1}{2};\frac{1}{4z}\right)\Bigg].
\end{aligned} \tag{3.98}$$

In order to get a small-z solution for $\mathcal{M}_{15}$, an analytic continuation of

$${}_4F_3\left(1,1,\varepsilon,2\varepsilon-1;2,2-\varepsilon,\varepsilon+\frac{1}{2};\frac{1}{4z}\right) \tag{3.99}$$

is required. However, the above hypergeometric function does not fulfill the requirements given in the text below Eq. (A.32) in Appendix A. Fortunately, we have been able to obtain the small-z solution of this MI using the MB method. Our explicit expression for the expansion of $\mathcal{M}_{15}$ around $z = 0$ will be given below, in Eq. (3.106).

The master integral $\mathcal{M}_{18}$:

The large z result is

$$\begin{aligned}\mathcal{M}_{18} = e^{2\gamma\varepsilon}\Bigg[&- \frac{2^{-2\varepsilon}\sqrt{\pi}\Gamma(\varepsilon)^2\Gamma(2\varepsilon+1)\,{}_3\tilde{F}_2\left(1,2\varepsilon-1,\varepsilon;\varepsilon+\frac{1}{2},\varepsilon+1;\frac{1}{4z}\right)z^{1-2\varepsilon}}{\varepsilon(2\varepsilon-1)} \\ &+ \frac{2^{-2\varepsilon}\sqrt{\pi}\Gamma(2-\varepsilon)\Gamma(\varepsilon+1)^2\Gamma(2\varepsilon+1)\,{}_4\tilde{F}_3\left(\frac{1}{2},1,2\varepsilon-1,\varepsilon;2-\varepsilon,\varepsilon+\frac{1}{2},\varepsilon+1;\frac{1}{z}\right)z^{1-2\varepsilon}}{\varepsilon^3(2\varepsilon-1)} \\ &+ \frac{2^{-2\varepsilon}\sqrt{\pi}\Gamma(1-\varepsilon)\Gamma(\varepsilon+1)^2\Gamma(2\varepsilon+1)\,{}_4\tilde{F}_3\left(\frac{3}{2},2,2\varepsilon,\varepsilon+1;3-\varepsilon,\varepsilon+\frac{3}{2},\varepsilon+2;\frac{1}{z}\right)z^{-2\varepsilon}}{2\varepsilon^2} \\ &+ z^{-\varepsilon}\Gamma(\varepsilon)^2\Bigg({}_3F_2(1,1,\varepsilon;\frac{3}{2},2;\frac{1}{4z}) + \frac{{}_3F_2\left(1,\frac{3}{2}-\varepsilon,\varepsilon;\frac{3}{2},3-2\varepsilon;\frac{1}{z}\right)}{\varepsilon-1} \\ &+ \frac{(1-2\varepsilon)\,{}_4F_3\left(1,1,\frac{3}{2}-\varepsilon,\varepsilon;\frac{3}{2},2,3-2\varepsilon;\frac{1}{z}\right)}{\varepsilon-1}\Bigg)\Bigg]. \end{aligned} \tag{3.100}$$

Again, due to two troublesome hypergeometric functions, one of which is ${}_2F_1\left(1,1,\varepsilon;\frac{3}{2},2;\frac{1}{4z}\right)$, we are not able to analytically continue to small z. Instead, an expansion around $z=0$ obtained using the MB method will be given in Eq. (3.109).

The master integrals $\mathcal{M}_{16}$ and $\mathcal{M}_{17}$:

These are the most complicated MIs in our problem. The corresponding system of DEs is given by

$$\begin{aligned}\frac{\mathrm{d}}{\mathrm{d}z}\mathcal{M}_{16} + \frac{\varepsilon}{z}\mathcal{M}_{16} &= \frac{(1-\varepsilon)^2}{2z^2(1-2\varepsilon)}\mathcal{M}_6 + \frac{1-\varepsilon}{z}\mathcal{M}_8 - \frac{2-3\varepsilon}{2z}\mathcal{M}_{12} - \mathcal{M}_{13} - \mathcal{M}_{17}, \\ \frac{\mathrm{d}}{\mathrm{d}z}\mathcal{M}_{17} + \frac{2\varepsilon}{z}\mathcal{M}_{17} &= \frac{(1-\varepsilon)^2}{2z^2(1-z)(1-4z)}\left[2\mathcal{M}_7 - \frac{2-3z+4z^2}{2z}\mathcal{M}_6\right] + \frac{2-6\varepsilon+4\varepsilon^2}{z(1-4z)}\mathcal{M}_8 \\ &\quad - \frac{2-7\varepsilon+6\varepsilon^2}{4z(1-z)}\mathcal{M}_{12} - \frac{(1-2\varepsilon)(1+z)}{2z(1-z)}\mathcal{M}_{13}. \end{aligned} \tag{3.101}$$

All the MIs in the above DEs except for $\mathcal{M}_{16}$ and $\mathcal{M}_{17}$ are already known from our previous calculations. Nevertheless, we are not able to solve this system exactly in ε. Thus, we need to expand in this parameter, and consider a system of sub-DEs, as in Eq. (3.66). For $\mathcal{M}_{16}$ they read

$$\begin{aligned}
\tfrac{\mathrm{d}}{\mathrm{d}z}\mathcal{M}_{16,-2} &= \frac{\mathcal{M}_{6,-2}}{2z^2} + \frac{\mathcal{M}_{8,-2}}{z} - \frac{\mathcal{M}_{12,-2}}{z} - \mathcal{M}_{13,-2} - \mathcal{M}_{17,-2} \\
\tfrac{\mathrm{d}}{\mathrm{d}z}\mathcal{M}_{16,-1} &= -\frac{\mathcal{M}_{8,-2}}{z} + \frac{3}{2z}\mathcal{M}_{12,-2} - \frac{\mathcal{M}_{16,-2}}{z} + \frac{\mathcal{M}_{6,-1}}{2z^2} + \frac{\mathcal{M}_{8,-1}}{z} - \frac{\mathcal{M}_{12,-1}}{z} - \mathcal{M}_{13,-1} - \mathcal{M}_{17,-1}, \\
\tfrac{\mathrm{d}}{\mathrm{d}z}\mathcal{M}_{16,\ 0} &= \frac{\mathcal{M}_{6,-2}}{2z^2} - \frac{\mathcal{M}_{8,-1}}{z} + \frac{3}{2z}\mathcal{M}_{12,-1} - \frac{\mathcal{M}_{16,-1}}{z} + \frac{\mathcal{M}_{6,0}}{2z^2} + \frac{\mathcal{M}_{8,0}}{z} - \frac{\mathcal{M}_{12,0}}{z} - \mathcal{M}_{13,0} - \mathcal{M}_{17,0}, \\
\tfrac{\mathrm{d}}{\mathrm{d}z}\mathcal{M}_{16,+1} &= \frac{\mathcal{M}_{6,-2}}{z^2} + \frac{\mathcal{M}_{6,-1}}{2z^2} - \frac{\mathcal{M}_{8,0}}{z} + \frac{3}{2z}\mathcal{M}_{12,0} + \frac{\mathcal{M}_{6,+1}}{2z^2} + \frac{\mathcal{M}_{8,+1}}{z} - \frac{\mathcal{M}_{12,+1}}{z} - \mathcal{M}_{13,+1} - \mathcal{M}_{17,+1}.
\end{aligned} \tag{3.102}$$

In our first approach, we have solved the system of sub-DEs numerically using the routine `ZVODE` [186] based on the `ODEPACK` package [187] and upgraded [146] to quad-double precision with the help of the `QD` library [188]. In these codes, the rational functions $R_{nkmj}(z)$ are treated using the Horner form to speed up the calculation, and the DEs are

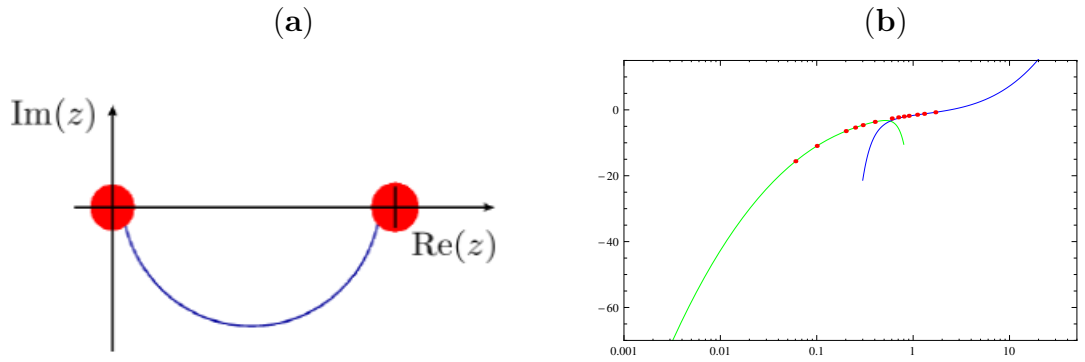

Figure 3.4: (a) An illustration of our method for solving the DE numerically. The solid (blue) line shows the path in the complex plane along which the numerical solution was carried out. The initial point at $z \gg 1$ and the final point at $z \ll 1$ are inside the red blobs where power-logarithmic expansions can be used (see the text). (b) The $\mathcal{O}(\varepsilon)$ part of $\mathcal{M}_{16}$ (i.e. $\mathcal{M}_{16,+1}$) as a function of z obtained from small-z expansions (solid green line), large-z expansions (solid blue line) and the numerical solutions of the DEs (red dots).

solved using a double-exponential integration method. Since the DEs in Eq. (3.101) have singularities on the real axis, at $z \in \{0, \frac{1}{4}, 1\}$, we have solved the sub-DEs along various ellipses in the complex plane, whose shapes depended on the initial and final values of z. This is illustrated in Fig. 3.4(a).

As an example, let us quote the numerical value of $\mathcal{M}_{16}$ at $z = 1$ that we have obtained using the initial conditions for our DEs at $z = 20$. Despite the fact that $z = 1$ is a singular point of our DEs (3.101), `ZVODE` was able to give us a value of $\mathcal{M}_{16}$ at this point quite precisely, namely

$$\mathcal{M}_{16}(1,\varepsilon) \simeq -\frac{0.499999943 + 0.000000001\,i}{\varepsilon^2} - \frac{0.500000340 - 0.000000018\,i}{\varepsilon} - (0.235586819 - 0.000000013\,i)\,\varepsilon^0 - (1.634399507 + 0.000000122\,i)\,\varepsilon^1 + \mathcal{O}(\varepsilon^2). \tag{3.103}$$

The above result should be compared to what we have obtained by calculating $\mathcal{M}_{16}$ directly at $z = 1$ using the Feynman parameters

$$\mathcal{M}_{16}(1,\varepsilon) \simeq -\frac{1}{2\varepsilon^2} - \frac{1}{2\varepsilon} - 0.235585368 - 1.634395361\,\varepsilon + \mathcal{O}(\varepsilon^2). \tag{3.104}$$

One concludes that the accuracy in both cases is better than 10^{-5}, and most probably limited by the accuracy of the numerical integration in the latter case. Obviously, the non-vanishing imaginary parts in Eq. (3.103) arise only due to the numerical inaccuracy of `ZVODE` in the process of solving the DEs along an ellipse in the complex plane.

Let us now comment on our determination of the boundary conditions for the DEs at some large value of z (e.g., $z = 20$). In this case, a large-mass asymptotic expansions [181] have been applied first to get a few leading terms of the expansion in $w = 1/z$ of each $\mathcal{M}_{n,k}$ that is relevant for our sub-DEs (3.66). The expansions have the following power-logarithmic form

$$\mathcal{M}_i(w,\varepsilon) = \sum_{n,m,k} c_{inmk}\varepsilon^n w^m \ln^k(w). \tag{3.105}$$

For each n, there exists a maximal power $k_{\max}$ of the logarithm in the above expression. It is related to the maximal power of $1/\varepsilon$ in a given integral (see Eq. (3.4)). Once Eq. (3.105) is substituted to the DEs, one obtains recurrence relations among the coefficients c_{inmk}. Thus, even if we did not know our leading terms, we could use the DEs to parameterize the expansions (up to a fixed order in ε) in terms of a finite number of unknown constants. Since we knew the leading terms, we could determine the expansions in a complete manner to as many terms as we wanted. We have chosen to expand all our MIs up to w^{15} and w^{30} in the two- and three-body cases, respectively.[13] This is more than sufficient for the numerical accuracy we need. Of course, for most (but not all) the MIs, we were able to cross-check these expansions against the exact results that have already been presented in the preceeding parts of this section.

A similar method has been applied for the small-z power-logarithmic expansions. We began with using the DE (and the known exact results) to express the expansions in terms of as small number of unknown constants as possible. Next, we used a combination of various methods (asymptotic expansions, Feynman parameterization and MB techniques) to determine these constants either analytically or numerically. We have managed to obtain exact results for all but two constants whose numerical determination follows from the DE method with boundary conditions at $z = 20$.

As an independent check, we have evaluated our MIs numerically using the method of sector decomposition implemented in the codes FIESTA [173], SecDec [189], as well as several others. FIESTA stands for Feynman Integral Evaluation by a Sector decomposiTion Approach. It is a `Mathematica` code for numerical evaluation of the MIs, based on Eq. (3.29) and using the `CUBA` library [190].

Let us now present our final results for the small-z expansions of $\mathcal{M}_{15}$-$\mathcal{M}_{18}$. Although we need these MIs up to $\mathcal{O}(\varepsilon^2)$, our explicit expressions below terminate at $\mathcal{O}(\varepsilon)$ for brevity reasons. This is why all the presented expansion coefficients are exact. The two above-mentioned constants that we have determined only numerically will show up in our final results in the next chapter. Our expansions read (with $L \equiv \ln z$):

$$\begin{aligned}
\mathcal{M}_{15} = &-\frac{1}{2\varepsilon^2} - \frac{1-2L}{2\varepsilon} - \frac{L^2}{2} + 3L - \frac{7\pi^2}{12} + \frac{5}{2} + \left(\frac{L^3}{3} + \left(-2-\pi^2\right)L - 4\zeta(3) + 4\right) z \\
&+ (3L-4)z^2 + \left(\frac{5L}{3} - \frac{1}{6}\right) z^3 + \left(\frac{35L}{18} + \frac{37}{54}\right) z^4 + \left(\frac{63L}{20} + \frac{149}{80}\right) z^5 \\
&+ \Bigg[\frac{L^3}{6} - \frac{3L^2}{2} + 7L - \frac{\pi^2 L}{2} - \frac{8\zeta(3)}{3} - \frac{47\pi^2}{12} + \frac{35}{2} \\
&+ \left(-\frac{5L^4}{12} + \frac{L^3}{3} + \frac{1}{3}\left(6+\pi^2\right)L^2 + 2L(\zeta(3)-4) - \pi^2 L - 4\zeta(3) + \frac{83\pi^4}{180} + \frac{7\pi^2}{3} + 10\right) z \\
&+ \left(-\frac{5L}{2} - \frac{13\pi^2}{2} - \frac{1}{4}\right) z^2 + \left(\frac{97L}{18} - \frac{65\pi^2}{18} - \frac{91}{9}\right) z^3 + \left(\frac{2143L}{216} - \frac{455\pi^2}{108} - \frac{8387}{864}\right) z^4 \\
&+ \left(\frac{7927L}{400} - \frac{273\pi^2}{40} - \frac{132691}{12000}\right) z^5\Bigg]\varepsilon + \mathcal{O}(z^6, \varepsilon^2),
\end{aligned} \tag{3.106}$$

[13] Actually, the three-body case is simple enough to get all the expansions from the Feynman-parameter method only.

$$
\begin{aligned}
\mathcal{M}_{16} = &-\frac{1}{2\varepsilon^2} - \frac{1-2L}{2\varepsilon} + -\frac{L^2}{2} + 3L - \frac{\pi^2 L}{6} - 2\zeta(3) + \frac{\pi^2}{12} + \frac{5}{2} + \left(-\frac{L^3}{6} + L + 4\zeta(3) - 2\right) z \\
&+ \left(-\frac{3L^2}{2} + \frac{7L}{4} - \frac{\pi^2}{2} + 1\right) z^2 + \left(-\frac{5L^2}{3} - \frac{43L}{36} - \frac{5\pi^2}{9} + \frac{157}{36}\right) z^3 \\
&+ \left(-\frac{35L^2}{12} - \frac{569L}{144} - \frac{35\pi^2}{36} + \frac{3281}{432}\right) z^4 + \left(-\frac{63L^2}{10} - \frac{4231L}{400} - \frac{21\pi^2}{10} + \frac{37183}{2400}\right) z^5 \\
&+ \Bigg[\frac{L^3}{6} - \frac{3L^2}{2} + \frac{\pi^2 L^2}{12} - 3L\zeta(3) + 7L - \frac{8\zeta(3)}{3} - \frac{41\pi^4}{180} + \frac{13\pi^2}{12} + \frac{35}{2} \\
&+ \left(\frac{63L^3}{10} - \frac{221L^2}{100} - \frac{271179L}{14000} + \frac{63\zeta(3)}{5} - \frac{7217\pi^2}{1200} + \frac{124002463}{3920000}\right) z^5 \\
&+ \left(\frac{35L^3}{12} - \frac{53L^2}{48} - \frac{59983L}{8640} + \frac{35\zeta(3)}{6} - \frac{167\pi^2}{72} + \frac{6210137}{518400}\right) z^4 \\
&+ \left(\frac{5L^3}{3} - \frac{8L^2}{9} - \frac{97L}{36} + \frac{10\zeta(3)}{3} - \frac{89\pi^2}{108} + \frac{2879}{648}\right) z^3 \\
&+ \left(\frac{3L^3}{2} - \frac{7L^2}{4} - \frac{35L}{8} + 3\zeta(3) + \frac{2\pi^2}{3} + \frac{189}{16}\right) z^2 \\
&+ \left(\frac{5L^4}{24} - \frac{L^3}{6} - L^2 - 2L\zeta(3) + 4L + 4\zeta(3) + \frac{17\pi^4}{180} - 5\right) z \\
&- \frac{128\pi^2 z^{9/2}}{3969} - \frac{96\pi^2 z^{7/2}}{1225} - \frac{64}{225}\pi^2 z^{5/2} - \frac{32}{9}\pi^2 z^{3/2}\Bigg]\varepsilon \\
&+ \mathcal{O}(z^6, \varepsilon^2),
\end{aligned}
\tag{3.107}
$$

$$
\begin{aligned}
\mathcal{M}_{17} = &\frac{L^3}{6} - 4\zeta(3) + \left(2L^2 - L + \frac{2}{3}\left(\pi^2 - 3\right)\right) z + \left(3L^2 + \frac{15L}{4} + \pi^2 - \frac{29}{4}\right) z^2 \\
&+ \left(\frac{20L^2}{3} + \frac{107L}{9} + \frac{4}{27}\left(15\pi^2 - 104\right)\right) z^3 + \left(\frac{35L^2}{2} + \frac{1709L}{48} + \frac{35}{288}\left(48\pi^2 - 311\right)\right) z^4 \\
&+ \left(\frac{252L^2}{5} + \frac{2749L}{25} + \frac{84\pi^2}{5} - \frac{77137}{750}\right) z^5 \\
&+ \Bigg[-\frac{5L^4}{24} + 2L\zeta(3) - \frac{17\pi^4}{180} + \left(-2L^3 + 8L - 4\zeta(3) - \pi^2 - 14\right) z \\
&+ \left(-\frac{252L^3}{5} - 5L^2 + \frac{5935891L}{31500} - \frac{504\zeta(3)}{5} + \frac{3997\pi^2}{75} - \frac{10008906931}{39690000}\right) z^5 \\
&+ \left(-\frac{35L^3}{2} - \frac{43L^2}{12} + \frac{139793L}{2520} - 35\zeta(3) + \frac{2387\pi^2}{144} - \frac{326907481}{4233600}\right) z^4 \\
&+ \left(-\frac{20L^3}{3} - 2L^2 + \frac{4517L}{270} - \frac{40\zeta(3)}{3} + \frac{47\pi^2}{9} - \frac{188609}{8100}\right) z^3 \\
&+ \left(-3L^3 - L^2 + \frac{17L}{3} - 6\zeta(3) + \frac{17\pi^2}{12} - \frac{443}{72}\right) z^2 \\
&+ \frac{4}{81}\pi^2 z^{9/2} + \frac{4}{49}\pi^2 z^{7/2} + \frac{4}{25}\pi^2 z^{5/2} + \frac{4}{9}\pi^2 z^{3/2} + 4\pi^2\sqrt{z}\Bigg]\varepsilon \\
&+ \mathcal{O}(z^6, \varepsilon^2),
\end{aligned}
\tag{3.108}
$$

$$
\begin{aligned}
\mathcal{M}_{18} = &-\frac{1}{2\varepsilon^2} - \frac{1}{2\varepsilon} + \frac{1}{72}\Big(\left(180 - 42\pi^2\right) + \left(-24\pi^2 L - 288\zeta(3) + 24\pi^2\right) z \\
&+ \left(72L^2 - 144L + 24\pi^2 + 72\right) z^2 + \left(72L^2 + 36L + 24\pi^2 - 180\right) z^3 \\
&+ \left(120L^2 + 152L + 40\pi^2 - 314\right) z^4 + \left(252L^2 + 411L + 84\pi^2 - 626\right) z^5 \Big) \\
&+ \left[\frac{35}{2} - \frac{26\zeta(3)}{3} - \frac{11\pi^2}{12} + \left(\frac{\pi^2 L^2}{6} - 6L\zeta(3) - \frac{\pi^2 L}{3} + 6\zeta(3) - \frac{41\pi^4}{90} + \frac{\pi^2}{3} \right) z \right. \\
&+ \left(-\frac{7L^3}{2} + \frac{271L^2}{120} + \frac{580121L}{50400} - 7\zeta(3) + \frac{647\pi^2}{180} - \frac{422670601}{21168000} \right) z^5 \\
&+ \left(-\frac{5L^3}{3} + \frac{47L^2}{36} + \frac{1483L}{360} - \frac{10\zeta(3)}{3} + \frac{79\pi^2}{54} - \frac{540971}{64800} \right) z^4 \\
&+ \left(-L^3 + \frac{7L^2}{6} + \frac{5L}{4} - 2\zeta(3) + \frac{5\pi^2}{9} - \frac{841}{216} \right) z^3 \\
&+ \left(-L^3 + \frac{5L^2}{2} + \frac{L}{2} - 2\zeta(3) - \frac{2\pi^2}{3} - \frac{45}{4} \right) z^2 \\
&\left. + \frac{16}{441}\pi^2 z^{9/2} + \frac{16}{175}\pi^2 z^{7/2} + \frac{16}{45}\pi^2 z^{5/2} + \frac{16}{3}\pi^2 z^{3/2} \right] \varepsilon \\
&+ \mathcal{O}(z^6, \varepsilon^2),
\end{aligned} \tag{3.109}
$$

To summarize, the presented collection of our results for all the two-body MIs ($\mathcal{M}_6$-$\mathcal{M}_{18}$) for arbitrary z includes closed small-z and large-z forms for $\mathcal{M}_6$-$\mathcal{M}_{14}$, and small-z expansions for $\mathcal{M}_{15}$-$\mathcal{M}_{18}$. In addition, closed forms at large z were given for $\mathcal{M}_{15}$ and $\mathcal{M}_{18}$.

Let us now summarize our results for the three-body MIs $\mathcal{M}_1$-$\mathcal{M}_5$. The differential equations for them read

$$
\begin{aligned}
\mathcal{M}_1' &= \frac{(1-\varepsilon)}{z}\mathcal{M}_1, \\
\mathcal{M}_2' - \frac{2(-1+\varepsilon-z+2\varepsilon z)}{z(1-4z)}\mathcal{M}_2 &= 2\frac{(\varepsilon-1)\mathcal{M}_1 - (3-4\varepsilon)\mathcal{M}_3}{z(1-4z)}, \\
\mathcal{M}_3' - \frac{(3-4\varepsilon)}{z}\mathcal{M}_3 &= \frac{(1-\varepsilon)}{z}\mathcal{M}_2, \\
\mathcal{M}_4' - \frac{(1-3\varepsilon-4z+12\varepsilon z)}{z(1-4z)}\mathcal{M}_4 &= \frac{2(\varepsilon-1)\mathcal{M}_1 + (-4+6\varepsilon+6z-12\varepsilon z)\mathcal{M}_2 - (6-8\varepsilon)\mathcal{M}_3}{z(1-4z)}, \\
\mathcal{M}_5' + \frac{\varepsilon}{z}\mathcal{M}_5 &= -\frac{(1-\varepsilon)\mathcal{M}_1 + (1-\varepsilon+z-2\varepsilon z)\mathcal{M}_2 + (3-4\varepsilon)\mathcal{M}_3}{z^2(1-4z)}.
\end{aligned} \tag{3.110}
$$

Below, we present a closed form for $\mathcal{M}_1$ and small-z expansions for $\mathcal{M}_2$-$\mathcal{M}_5$. They read

$$
\mathcal{M}_1 = -\frac{e^{3\gamma\varepsilon} z^{1-\varepsilon}\Gamma^3(1-\varepsilon)\Gamma(\varepsilon-1)}{\Gamma(3-3\varepsilon)\Gamma(2-2\varepsilon)}, \tag{3.111}
$$

$$
\begin{aligned}
\mathcal{M}_2 = &\frac{1}{2\varepsilon} - 5 + \left(-L^2 + \pi^2 - 2\right) z + \left(L^2 - L + \frac{1}{2}\left(-3 - 2\pi^2\right) \right) z^2 + \left(2L - \frac{4}{3} \right) z^3 \\
&+ \left(\frac{5L}{3} + \frac{1}{4} \right) z^4 + \left(\frac{7L}{3} + \frac{17}{15} \right) z^5 + \Big[-32 + \frac{7\pi^2}{8} + \left(L^3 - 6L^2 - 2L + 6\zeta(3) + 6\pi^2 - 20\right) z
\end{aligned}
$$

$$
\begin{aligned}
&+\left(-L^3+\frac{7L^2}{2}-\frac{3L}{2}-6\zeta(3)-2\pi^2-\frac{13}{4}\right)z^2+\left(L^2+2L-4\pi^2-\frac{15}{2}\right)z^3\\
&+\left(\frac{5L^2}{6}+\frac{37L}{4}-\frac{10\pi^2}{3}-\frac{1553}{144}\right)z^4+\left(\frac{7L^2}{6}+\frac{179L}{10}-\frac{14\pi^2}{3}-\frac{39943}{3600}\right)z^5\Bigg]\varepsilon\\
&+\Bigg[\left(-\frac{35L^3}{18}+\frac{111L^2}{20}-\frac{7\pi^2L}{4}+\frac{184843L}{3600}-42\zeta(3)-\frac{2063\pi^2}{60}-\frac{2500861}{36000}\right)z^5\\
&+\left(-\frac{25L^3}{18}+\frac{31L^2}{8}-\frac{5\pi^2L}{4}+\frac{2621L}{144}-30\zeta(3)-\frac{291\pi^2}{16}-\frac{6319}{192}\right)z^4\\
&+\left(-\frac{5L^3}{3}+5L^2-\frac{3\pi^2L}{2}+\frac{49L}{6}-36\zeta(3)-\frac{17\pi^2}{3}-\frac{307}{18}\right)z^3\\
&+\left(\frac{7L^4}{12}-\frac{19L^3}{6}-\frac{3\pi^2L^2}{4}+\frac{31L^2}{4}-12L\zeta(3)+\frac{3\pi^2L}{4}-\frac{15L}{4}-6\zeta(3)+\frac{47\pi^4}{60}-\frac{23\pi^2}{8}-\frac{65}{8}\right)z^2\\
&+\left(-\frac{7L^4}{12}+6L^3+\frac{3\pi^2L^2}{4}-23L^2+12L\zeta(3)-20L+36\zeta(3)-\frac{47\pi^4}{60}+\frac{59\pi^2}{2}-134\right)z\\
&+\frac{23\zeta(3)}{2}+\frac{35\pi^2}{4}-168\Bigg]\varepsilon^2+\mathcal{O}(z^6,\varepsilon^3),
\end{aligned}
\tag{3.112}
$$

$$
\begin{aligned}
\mathcal{M}_3=&\frac{1}{6\varepsilon}+\frac{31}{18}+\frac{1}{180}\left(90L^2+90L-90\pi^2+225\right)z+\frac{1}{180}\left(-180L^2-180L+180\pi^2+90\right)z^2\\
&+\frac{1}{180}\left(180L^2-240L-180\pi^2-250\right)z^3+\frac{1}{180}(300L-255)z^4+\frac{1}{180}(210L-3)z^5\\
&+\Bigg[\frac{305}{27}-\frac{7\pi^2}{24}+\left(-\frac{L^3}{2}+\frac{11L^2}{4}+\frac{19L}{4}-3\zeta(3)-\frac{7\pi^2}{2}+\frac{111}{8}\right)z\\
&+\left(L^3-\frac{7L^2}{2}-\frac{21L}{2}+6\zeta(3)+5\pi^2-\frac{27}{4}\right)z^2+\left(-L^3+\frac{8L^2}{3}-\frac{11L}{18}-6\zeta(3)-\frac{2\pi^2}{3}-\frac{44}{27}\right)z^3\\
&+\left(\frac{5L^2}{6}-\frac{3L}{4}-\frac{10\pi^2}{3}-\frac{665}{144}\right)z^4+\left(\frac{7L^2}{12}+\frac{73L}{15}-\frac{7\pi^2}{3}-\frac{61303}{7200}\right)z^5\Bigg]\varepsilon\\
&+\frac{1}{648000}\Bigg[\left(-630000L^3+1609200L^2-567000\pi^2L+2919870L-13608000\zeta(3)-6320700\pi^2-9338274\right)z^5\\
&+\left(-900000L^3+2511000L^2-810000\pi^2L+2722500L-19440000\zeta(3)-175500\pi^2-5090625\right)z^4\\
&+\Big(378000L^4-1440000L^3-486000\pi^2L^2+2790000L^2-7776000L\zeta(3)+648000\pi^2L-1968000L\\
&+2592000\zeta(3)+507600\pi^4-621000\pi^2-2989000\Big)z^3\\
&+\Big(-378000L^4+2484000L^3+486000\pi^2L^2-4374000L^2+7776000L\zeta(3)+486000\pi^2L-34506000L\\
&+23328000\zeta(3)-507600\pi^4+14013000\pi^2-48843000\Big)z^2\\
&+\Big(189000L^4-1890000L^3-243000\pi^2L^2+6237000L^2-3888000L\zeta(3)-243000\pi^2L+18225000L\\
&-15552000\zeta(3)+253800\pi^4-12271500\pi^2+64030500\Big)z\\
&+-2484000\zeta(3)+39136000-1953000\pi^2\Bigg]\varepsilon^2+\mathcal{O}(z^6,\varepsilon^3),
\end{aligned}
\tag{3.113}
$$

$$
\begin{aligned}
\mathcal{M}_4 = &-\frac{1}{\varepsilon} - 11 + \left(\frac{1}{3}(L-3)L^2 - \pi^2 L + 2L - 4\zeta(3) + \pi^2 - 2\right) z + (2L-3)z^2 + \left(L - \frac{1}{6}\right) z^3 \\
&+ \left(\frac{10L}{9} + \frac{19}{54}\right) z^4 + \left(\frac{7L}{4} + \frac{239}{240}\right) z^5 + \Bigg[-77 + \frac{7\pi^2}{4} \\
&+ \left(\frac{1}{6}(16-3L)L^3 + \frac{3\pi^2 L^2}{2} - 8L^2 + 2(3L-7)\zeta(3) - 5\pi^2 L + 16L + \frac{2\pi^4}{5} + 5\pi^2 - 16\right) z \\
&+ \left(L^2 - 5L - 4\pi^2 + \frac{13}{2}\right) z^2 + \left(\frac{L^2}{2} + 4L - 2\pi^2 - \frac{43}{6}\right) z^3 \\
&+ \left(\frac{5L^2}{9} + \frac{403L}{54} - \frac{20\pi^2}{9} - \frac{4285}{648}\right) z^4 + \left(\frac{7L^2}{8} + \frac{1751L}{120} - \frac{7\pi^2}{2} - \frac{17059}{2400}\right) z^5 \Bigg] \varepsilon \\
&+ \Bigg[+ 23\zeta(3) + \frac{77\pi^2}{4} - 439 + \left(\frac{1}{12}(5L-37)L^4 - \frac{7\pi^2 L^3}{4} + \frac{41L^3}{3} + \frac{33\pi^2 L^2}{4} - 41L^2 \right. \\
&+ 3(14-5L)L\zeta(3) - \frac{5\pi^4 L}{12} - \frac{41\pi^2 L}{2} + 82L - 76\zeta(5) + 13\pi^2\zeta(3) - 58\zeta(3) + \frac{73\pi^4}{60} \\
&\left. + \frac{41\pi^2}{2} - 82\right) z + \left(-\frac{5L^3}{3} + \frac{13L^2}{2} - \frac{3\pi^2 L}{2} + \frac{23L}{2} - 36\zeta(3) + \frac{25\pi^2}{4} - \frac{191}{4}\right) z^2 \\
&+ \left(-\frac{5L^3}{6} + \frac{5L^2}{2} - \frac{3\pi^2 L}{4} + \frac{55L}{12} - 18\zeta(3) - \frac{197\pi^2}{24} - \frac{791}{72}\right) z^3 \\
&+ \left(-\frac{25L^3}{27} + \frac{289L^2}{108} - \frac{5\pi^2 L}{6} + \frac{11537L}{648} - 20\zeta(3) - \frac{1043\pi^2}{72} - \frac{229979}{7776}\right) z^4 \\
&+ \left(-\frac{35L^3}{24} + \frac{517L^2}{120} - \frac{21\pi^2 L}{16} + \frac{221213L}{4800} - \frac{63\zeta(3)}{2} - \frac{26821\pi^2}{960} - \frac{5428877}{96000}\right) z^5 \Bigg] \varepsilon^2 \\
&+ \mathcal{O}(z^6, \varepsilon^3),
\end{aligned} \tag{3.114}
$$

$$
\begin{aligned}
\mathcal{M}_5 = &-1 + 2\zeta(3) + \frac{\pi^2}{2} - L + \frac{\pi^2 L}{2} - \frac{L^2}{2} - \frac{L^3}{6} + \left(L^2 - 2L - \pi^2\right) z + \left(\frac{3L}{2} - \frac{5}{4}\right) z^2 \\
&+ \left(\frac{10L}{9} + \frac{2}{27}\right) z^3 + \left(\frac{35L}{24} + \frac{61}{96}\right) z^4 + \left(\frac{63L}{25} + \frac{202}{125}\right) z^5 \\
&+ \Bigg[\frac{L^4}{6} - \frac{L^3}{3} - 3L^2 - \frac{\pi^2 L^2}{4} + L\zeta(3) - 10L + \frac{5\pi^2 L}{2} + 13\zeta(3) - \frac{13\pi^4}{60} + \frac{9\pi^2}{2} - 14 \\
&+ \left(-L^3 + 4L^2 - 4L - 6\zeta(3) - \pi^2\right) z + \left(\frac{3L^2}{4} + \frac{L}{2} - 3\pi^2 - \frac{19}{4}\right) z^2 \\
&+ \left(\frac{5L^2}{9} + \frac{154L}{27} - \frac{20\pi^2}{9} - \frac{409}{54}\right) z^3 + \left(\frac{35L^2}{48} + \frac{43L}{4} - \frac{35\pi^2}{12} - \frac{4345}{576}\right) z^4 \\
&+ \left(\frac{63L^2}{50} + \frac{5533L}{250} - \frac{126\pi^2}{25} - \frac{16889}{2000}\right) z^5 \Bigg] \varepsilon \\
&+ \Bigg[- \frac{11L^5}{120} + \frac{13L^4}{24} + \frac{5\pi^2 L^3}{24} + \frac{L^3}{6} + \frac{5L^2\zeta(3)}{2} - \frac{7\pi^2 L^2}{8} - \frac{23L^2}{2} + 11L\zeta(3) \\
&- \frac{7\pi^4 L}{40} + \frac{41\pi^2 L}{4} - 63L + 20\zeta(5) - \frac{15\pi^2\zeta(3)}{2} + 71\zeta(3) - \frac{59\pi^4}{40} + \frac{113\pi^2}{4} - 119 \\
&+ \left(\frac{7L^4}{12} - \frac{10L^3}{3} - \frac{3\pi^2 L^2}{4} + 9L^2 - 2L(6\zeta(3)+5) + \frac{3\pi^2 L}{2} + 6\zeta(3) + \frac{47\pi^4}{60} - 3\pi^2\right) z \\
&+ \left(-\frac{5L^3}{4} + 4L^2 - \frac{9\pi^2 L}{8} + \frac{35L}{8} - 27\zeta(3) + \frac{1}{16}\left(-169 - 41\pi^2\right)\right) z^2 \\
&+ \left(-\frac{25L^3}{27} + \frac{71L^2}{27} - \frac{5\pi^2 L}{6} + \frac{1583L}{162} - 20\zeta(3) + \frac{1}{486}\left(-9545 - 5499\pi^2\right)\right) z^3
\end{aligned} \tag{3.115}
$$

$$+\left(-\frac{175L^3}{144}+\frac{111L^2}{32}-\frac{35\pi^2L}{32}+\frac{33473L}{1152}-\frac{105\zeta(3)}{4}+\frac{-195277-95412\pi^2}{4608}\right)z^4$$
$$+\left(-\frac{21L^3}{10}+\frac{3109L^2}{500}-\frac{189\pi^2L}{100}+\frac{2240339L}{30000}-\frac{1134\zeta(3)}{25}\right.$$
$$\left.-\frac{179\left(46109+23600\pi^2\right)}{100000}\right)z^5\Bigg]\varepsilon^2+\mathcal{O}(z^6,\varepsilon^3). \tag{3.116}$$

Chapter 4

Results for the NNLO QCD counterterm contributions

In this chapter, we present our final results for the considered interference terms $\widetilde{G}_{27}^{(1)\text{bare}}$, $\widetilde{G}_{7(12)}^{(1)\text{bare}}$ and $\widetilde{G}_{27}^{(1)m}$. We write them as

$$\begin{aligned}
\widetilde{G}_{27}^{(1)\text{bare}} &= \widetilde{G}_{27}^{(1)2P} + \widetilde{G}_{27}^{(1)3P}, \\
\widetilde{G}_{7(12)}^{(1)\text{bare}} &= \widetilde{G}_{7(12)}^{(1)2P} + \widetilde{G}_{7(12)}^{(1)3P}, \\
\widetilde{G}_{27}^{(1)m} &= \widetilde{G}_{27}^{(1)m,2P} + \widetilde{G}_{27}^{(1)m,3P},
\end{aligned} \tag{4.1}$$

where the superscripts $2P$ and $3P$ indicate the two- and three-body final state contributions, respectively. These quantities enter the renormalization formula (2.61) for the Q_2-Q_7 interference where the n_c-terms (the charm-quark loops on the gluon lines together with the corresponding UV-counterterms) were skipped, as they are already known [146]. Of course, an analogous formula for the Q_1-Q_7 interference will also be necessary. In both expressions, we also encounter $\widetilde{G}_{17}^{(1)\text{bare}} = -\frac{1}{6}\widetilde{G}_{27}^{(1)\text{bare}}$, $\widetilde{G}_{7(11)}^{(1)\text{bare}} = -\frac{1}{6}\widetilde{G}_{7(12)}^{(1)\text{bare}}$, and $\widetilde{G}_{17}^{(1)m} = -\frac{1}{6}\widetilde{G}_{27}^{(1)m}$, where the color factor of $-\frac{1}{6}$ comes from the relation $T^a T^b T^a = -\frac{1}{6}T^b$ for the $SU(3)$ generators. After taking this color factor into account, it is sufficient to restrict our considerations to the quantities from Eq. (4.1). They give us a complete set of z-dependent counterterms for the renormalization of $\widetilde{G}_{17}^{(2)}$ and $\widetilde{G}_{27}^{(2)}$. Apart from them, we shall present our results for $\hat{G}_{47}^{(1)\text{bare}}$ with skipped n_c-terms, which is z-independent.

Below, in Sec. 4.1, our z-dependent results will be given in terms of expansions. Next, in Sec. 4.2, all the considered NNLO QCD counterterms for $z = 0$ are summarized. Sec. 4.3 is devoted to presenting plots of the involved functions of z, and their interpretation. Finally, in Sec. 4.4, we write our results as linear combinations of the MIs where the coefficients are given exactly in z and ε. This may become convenient if an extension of our calculation to higher orders in ε becomes necessary in the future. All our results in the present chapter contain the necessary D-dimensional phase-space factors, and are given for the renormalization scale $\mu^2 = e^\gamma m_b^2/(4\pi)$.

4.1 Final results for an arbitrary charm quark mass

We have evaluated the small-z expansions of all the three-body and two-body contributions up to $\mathcal{O}(z^{30})$ and $\mathcal{O}(z^{15})$, respectively. Similarly, the large-z expansions were calculated up to $\mathcal{O}(1/z^{30})$ and $\mathcal{O}(1/z^{15})$ in the three- and two-body cases, respectively. All these terms are included in the plots of Sec. 4.3. However, the analytical expressions will be given only up to $\mathcal{O}(z^5)$ and $\mathcal{O}(1/z^5)$, as it is perfectly sufficient for phenomenological purposes. The abbreviation L stands for $\ln z$.

Three-body contributions

Our three-body results are evaluated for $\delta = 1$, i.e. for $E_0 = 0$, which means that no cut on the photon energy is imposed in the considered NNLO corrections.[1] We need to know the first two terms in their ε-expansion, which we denote as follows

$$\widetilde{G}_{27}^{(1)3P}(z,\varepsilon) = g_0(z) + \varepsilon\, g_1(z) + \mathcal{O}(\varepsilon^2), \tag{4.2}$$

$$\widetilde{G}_{7(12)}^{(1)3P}(z,\varepsilon) = 0 + \varepsilon\, h_1(z) + \mathcal{O}(\varepsilon^2), \tag{4.3}$$

$$\widetilde{G}_{27}^{(1)m,3P}(z,\varepsilon) = j_0(z) + \varepsilon\, j_1(z) + \mathcal{O}(\varepsilon^2). \tag{4.4}$$

Our exact expression for the function $g_0(z)$ is

$$\begin{aligned} g_0(z) &\overset{z\le\frac{1}{4}}{=\!=} -\frac{4}{27} - \frac{14}{9}z + \frac{8}{3}z^2 + \frac{8}{3}z(1-2z)\,s\,L + \frac{16}{9}z(6z^2-4z+1)(\pi^2/4 - L^2), \\ g_0(z) &\overset{z>\frac{1}{4}}{=\!=} -\frac{4}{27} - \frac{14}{9}z + \frac{8}{3}z^2 + \frac{8}{3}z(1-2z)\,t\,A + \frac{16}{9}z(6z^2-4z+1)A^2, \end{aligned} \tag{4.5}$$

where $s = \sqrt{1-4z}$, $L = \ln(1+s) - \frac{1}{2}\ln 4z$, $t = \sqrt{4z-1}$ and $A = \arctan(1/t)$. From among the functions occurring on the r.h.s. of Eqs. (4.2)-(4.4), the function $g_0(z)$ is the only one for which we have a result in a closed form. For the remaining functions, we shall present only their small- and large-z expansions. For $g_1(z)$ they read

$$\begin{aligned} g_1(z) = &-\frac{106}{81} + \frac{2}{27}\left(4L^3 - 30L^2 + 6\left(\pi^2 - 27\right)L + 60\zeta(3) + 57\pi^2 - 291\right) z \\ &+ \frac{4}{27}\left(-16L^3 + 18L^2 + 6\left(25 + 2\pi^2\right)L - 24\zeta(3) - 54\pi^2 + 93\right) z^2 \\ &- \frac{4}{81}\left(-54L^3 + 27L^2 + 174L - 324\zeta(3) + 27\pi^2 - 97\right) z^3 \\ &+ \frac{2}{243}\left(-360L^2 + 804L + 1440\pi^2 + 1625\right) z^4 \\ &+ \frac{1}{2430}\left(-6300L^2 - 43950L + 25200\pi^2 + 83401\right) z^5 + \mathcal{O}(z^6), \end{aligned} \tag{4.6}$$

$$\begin{aligned} g_1(z) = &\left(-\frac{L}{162} + \frac{61}{1944}\right)\frac{1}{z} + \left(-\frac{L}{2025} + \frac{94}{30375}\right)\frac{1}{z^2} + \left(-\frac{L}{18900} + \frac{209}{567000}\right)\frac{1}{z^3} \\ &+ \left(-\frac{2L}{297675} + \frac{1574}{31255875}\right)\frac{1}{z^4} + \left(-\frac{L}{1047816} + \frac{6661}{880165440}\right)\frac{1}{z^5} + \mathcal{O}\left(\frac{1}{z^6}\right). \end{aligned} \tag{4.7}$$

[1] This does not lead to any IR divergence thanks to the fact that the photon interaction in Q_7 is via the electromagnetic field strength tensor $F_{\mu\nu}$.

Our exact expression for $g_0(z)$ agrees with the results of Refs. [125, 152] where only expansions and/or unintegrated expressions were given. As far as $g_1(z)$ is concerned, a calculation of the corresponding diagrams up to $\mathcal{O}(\varepsilon)$ was done in Ref. [152]. However, the three-body phase space integration there was performed in $D = 4$, so our $g_1(z)$ cannot be derived from their results. Performing the phase-space integration for arbitrary D is essential when the reverse unitarity trick is applied, which is hard to avoid in the future bare NNLO calculation (see the next chapter).

All the other three-body results in this section are new, i.e. they have not been considered in the literature before (apart from the $z = 0$ case in Ref. [64]). As far as $h_1(z)$ is concerned, we have found a simple relation

$$h_1(z) = -20\, g_0(z), \tag{4.8}$$

which can be determined without calculation of any MIs but only by comparing the coefficients at them in the three-body contributions to $\widetilde{G}_{27}^{(1)3P}(z,\varepsilon)$ and $\widetilde{G}_{7(12)}^{(1)3P}(z,\varepsilon)$ interference terms. All the coefficients get rescaled by the factor

$$-4\varepsilon(5+\varepsilon) = -20\varepsilon + \mathcal{O}(\varepsilon^2), \tag{4.9}$$

which implies that the relation (4.8) holds.

Our results for the small- and large-z expansions of the functions $j_0(z)$ and $j_1(z)$ read

$$\begin{aligned} j_0(z) = {} & \frac{302}{81} + \frac{20L}{27} + \frac{1}{135}\big(10L^4 - 20L^3 - 30\left(2\pi^2 - 5\right)L^2 \\ & - 30\left(16\zeta(3) + 3 - 2\pi^2\right)L + 240\zeta(3) + 2\pi^4 - 150\pi^2 + 315\big)\, z \\ & + \frac{4}{9}\left(-2L^2 + 6L + 2\pi^2 - 11\right) z^2 - \frac{4}{81}\left(-9L^2 + 12L + 9\pi^2 + 8\right) z^3 \\ & + \frac{10}{729}(60L - 43)\, z^4 + \frac{1}{54}(35L + 3)\, z^5 + \mathcal{O}(z^6), \end{aligned} \tag{4.10}$$

$$j_0(z) = \frac{5}{324}\frac{1}{z} + \frac{17}{36450}\frac{1}{z^2} + \frac{13}{453600}\frac{1}{z^3} + \frac{37}{14883750}\frac{1}{z^4} + \frac{5}{18860688}\frac{1}{z^5} + \mathcal{O}\left(\frac{1}{z^6}\right), \tag{4.11}$$

$$\begin{aligned} j_1(z) = {} & \frac{11225}{243} - \frac{20\pi^2}{27} + \frac{52L}{9} - \frac{10L^2}{27} + \frac{1}{135}\Big(- 14L^5 + 90L^4 + 40\left(2\pi^2 - 9\right)L^3 \\ & + \left(600\zeta(3) + 660 - 450\pi^2\right)L^2 + \left(-120(27\zeta(3) + 26) + 630\pi^2 + 46\pi^4\right)L \\ & + 3\big(5\pi^2(8\zeta(3) - 35) + 90(6\zeta(3) + 8\zeta(5) + 1) - 4\pi^4\big)\Big)\, z \\ & + \frac{4}{9}\left(-4L^3 - 6L^2 + 6\left(1 + 3\pi^2\right)L + 84\zeta(3) - 3\pi^2 - 71\right) z^2 \\ & - \frac{2}{243}\left(54L^3 - 603L^2 + 2292L + 324\zeta(3) + 495\pi^2 - 2132\right) z^3 \\ & + \frac{1}{1458}\left(600L^2 + 1260L - 2400\pi^2 - 8371\right) z^4 \\ & + \frac{1}{3240}\left(1050L^2 + 7920L - 4200\pi^2 - 16771\right) z^5 + \mathcal{O}(z^6), \end{aligned} \tag{4.12}$$

$$j_1(z) = \left(-\frac{5L}{324} + \frac{119}{1296}\right)\frac{1}{z} + \left(-\frac{17L}{36450} + \frac{3271}{1093500}\right)\frac{1}{z^2} + \left(-\frac{13L}{453600} + \frac{5269}{27216000}\right)\frac{1}{z^3} + \left(-\frac{37L}{14883750} + \frac{611}{34728750}\right)\frac{1}{z^4} + \left(-\frac{5L}{18860688} + \frac{31001}{15842977920}\right)\frac{1}{z^5} + \mathcal{O}\left(\frac{1}{z^6}\right). \tag{4.13}$$

Two-body contributions

By analogy to Eqs. (4.2)-(4.4), the two-body contributions can be written as

$$\widetilde{G}_{27}^{(1)2P}(z,\varepsilon) = -\frac{92}{81\varepsilon} + f_0(z) + \varepsilon\, f_1(z) + \mathcal{O}(\varepsilon^2), \tag{4.14}$$

$$\widetilde{G}_{7(12)}^{(1)2P}(z,\varepsilon) = \frac{2096}{81} + \varepsilon\, e_1(z) + \mathcal{O}(\varepsilon^2), \tag{4.15}$$

$$\widetilde{G}_{27}^{(1)m,2P}(z,\varepsilon) = -\frac{1}{3\varepsilon^2} + \frac{1}{\varepsilon} r_{-1}(z) + r_0(z) + \varepsilon\, r_1(z) + \mathcal{O}(\varepsilon^2). \tag{4.16}$$

Our results for $f_0(z)$ and $f_1(z)$ read

$$\begin{aligned} f_0(z) = &-\frac{1942}{243} - \frac{8}{27}\left(-L^3 - 3L^2 + 9\left(\pi^2 - 4\right)L + 36\zeta(3) + 5\pi^2 - 48\right) z + \frac{32}{27}\pi^2 z^{3/2} \\ &+ \frac{8}{27}\left(L^3 - 6\left(\pi^2 - 2\right)L + 2\left(9 + \pi^2\right)\right) z^2 - \frac{4}{81}\left(126L^2 - 182L + 14\pi^2 + 9\right) z^3 \\ &- \frac{4}{6075}\left(9900L^2 + 12405L + 3300\pi^2 - 27937\right) z^4 \\ &- \frac{1}{23814}\left(335160L^2 + 555828L + 111720\pi^2 - 816731\right) z^5 \\ &- \frac{1}{546750}\left(19731600L^2 + 37900890L + 6577200\pi^2 - 44551813\right) z^6 \\ &- \left(\frac{4592L^2}{45} + \frac{316568L}{1485} + \frac{4592\pi^2}{135} - \frac{5577659732}{25727625}\right) z^7 \\ &- \left(\frac{19360L^2}{63} + \frac{11650480L}{17199} + \frac{19360\pi^2}{189} - \frac{218830877266}{352149525}\right) z^8 + \mathcal{O}(z^9), \end{aligned} \tag{4.17}$$

$$f_0(z) = -\frac{58}{243} + \frac{208L}{81} + \left(\frac{2069}{6075} + \frac{38L}{135}\right)\frac{1}{z} + \left(\frac{2029}{23814} + \frac{86L}{945}\right)\frac{1}{z^2} + \left(\frac{3080267}{107163000} + \frac{673L}{17010}\right)\frac{1}{z^3} + \left(\frac{39148379}{3241680750} + \frac{9626L}{467775}\right)\frac{1}{z^4} + \left(\frac{1813338739}{306792666180} + \frac{2927L}{243243}\right)\frac{1}{z^5} + \mathcal{O}\left(\frac{1}{z^6}\right), \tag{4.18}$$

$$\begin{aligned} f_1(z) = &-\frac{26231}{729} + \frac{259\pi^2}{243} + \frac{2}{405}\Big(-75L^4 + 60L^3 + 30\left(7\pi^2 - 18\right)L^2 \\ &- 60\left(54\zeta(3) - 168 + 37\pi^2\right)L - 2\left(90(62\zeta(3) - 117) + 1770\pi^2 + 23\pi^4\right)\Big) z \\ &- \frac{64}{81}\pi^2(3L - 26 + 12\ln(2))\, z^{3/2} + \frac{2}{81}\Big(-15L^4 + 60L^3 + 24\left(\pi^2 - 3\right)L^2 \\ &- 24\left(8\pi^2 - 3\right)L + 432\zeta(3) + 40\pi^4 + 60\pi^2 + 1332\Big) z^2 - \frac{1120}{81}\pi^2 z^{5/2} \\ &+ \frac{1}{729}\left(4536L^3 - 7020L^2 + 6\left(192\pi^2 - 691\right)L + 8208\zeta(3) - 6540\pi^2 + 22381\right) z^3 \end{aligned}$$

$$+\frac{1232\pi^2 z^{7/2}}{2025}+\frac{2}{91125}\Big(297000L^3-202500L^2-235530L+594000\zeta(3)$$
$$-279150\pi^2+813599\Big)z^4-\frac{544\pi^2}{99225}z^{9/2}+\Big(\frac{380L^3}{27}-\frac{191L^2}{27}-\frac{975313L}{26460}$$
$$+\frac{760\zeta(3)}{27}-\frac{29447\pi^2}{1701}+\frac{7328120063}{100018800}\Big)z^5+\mathcal{O}(z^6), \tag{4.19}$$

$$f_1(z)=-\frac{901}{243}+\frac{23\pi^2}{243}+\frac{116L}{243}-\frac{220L^2}{81}+\left(-\frac{19L^2}{45}+\frac{962L}{6075}+\frac{62797}{182250}\right)\frac{1}{z}+\Big(-\frac{43L^2}{315}$$
$$+\frac{11842L}{59535}+\frac{55026787}{250047000}\Big)\frac{1}{z^2}+\left(-\frac{673L^2}{11340}+\frac{1739092L}{13395375}+\frac{13428353551}{135025380000}\right)\frac{1}{z^3}$$
$$+\left(-\frac{4813L^2}{155925}+\frac{271244357L}{3241680750}+\frac{1108455907039}{22464847597500}\right)\frac{1}{z^4}$$
$$+\left(-\frac{2927L^2}{162162}+\frac{17211154537L}{306792666180}+\frac{186599590161437}{6909737824039050}\right)\frac{1}{z^5}+\mathcal{O}\left(\frac{1}{z^6}\right). \tag{4.20}$$

The function $f_0(z)$ is related to $a(z)$ and $b(z)$ that parameterize the z-dependence of the NLO interference term $\widetilde{G}_{27}^{(1)}$, namely

$$f_0(z)=-\frac{1942}{243}+2\,\mathrm{Re}\left[a(z)+b(z)\right]. \tag{4.21}$$

This interference term was first determined in Ref. [127] in terms of an expansion around $z=0$ up to $\mathcal{O}(z^3)$. In Ref. [128], this result was confirmed using a different method and extended up to $\mathcal{O}(z^6)$. The actual functions $a(z)$ and $b(z)$ were defined in Ref. [129] where they were given not only as power-logarithmic expansions but also in terms of relatively simple ε-independent two- and three-fold Feynman parameter integrals. Their explicit large-z expansions up to $\mathcal{O}(1/z^2)$ were given in Ref. [67]. Here, we have confirmed $f_0(z)$ both for small and large z, and provided expansions up to $\mathcal{O}(z^8)$ and $\mathcal{O}(1/z^5)$, respectively.

As far as $f_1(z)$ is concerned, we now confirm the findings of Ref. [152], and extend their small-z expansion up to $\mathcal{O}(z^5)$. All the other two-body results in this section are entirely new.

For the function $e_1(z)$, we have found the following relation

$$e_1(z)=\frac{39112}{243}-8\,\mathrm{Re}\left[5\,a(z)+b(z)\right]. \tag{4.22}$$

Similarly to the three-body case, one can derive it without calculating any MI but just observing common rescaling factors in the coefficients that multiply the MIs in the expressions for $\widetilde{G}_{7(12)}^{(1)\mathrm{bare}}$ and $\widetilde{G}_{27}^{(1)\mathrm{bare}}$. More precisely, the rescaling factors are different in the contributions that are proportional to Q_u and Q_d, i.e. the up-type and down-type quark charges. The functions $a(z)$ and $b(z)$ correspond to the Q_u- and Q_d-parts of $\widetilde{G}_{27}^{(1)}$, respectively.

As far as the functions $r_i(z)$ are concerned, our results read

$$r_{-1}(z)=-1-\frac{4\pi^2}{81}-2z+\mathcal{O}(z^8), \tag{4.23}$$

$$r_{-1}(z)=-1-\frac{4\pi^2}{81}-2z+\mathcal{O}\left(\frac{1}{z^{14}}\right), \tag{4.24}$$

$$
\begin{aligned}
r_0(z) = {} & \frac{35}{9} - \frac{161\pi^2}{972} - \frac{40\zeta(3)}{27} - \frac{64\pi^2}{9} z^{1/2} + \frac{1}{135}\Big(5L^4 - 160L^3 + 20\left(18+\pi^2\right)L^2 \\
& - 40\left(63+10\pi^2\right)L + 8\left(-120\zeta(3) + 285 + 20\pi^2 + \pi^4\right)\Big) z + \frac{208\pi^2}{81} z^{3/2} \\
& + \frac{2}{81}\left(288L^2 - 93L + 117\pi^2 - 151\right) z^2 + \frac{1}{36450}\Big(428400L^2 + 802770L + 142800\pi^2 \\
& - 968803\Big) z^3 + \left(\frac{884L^2}{27} + \frac{1219637L}{17010} + \frac{884\pi^2}{81} - \frac{6421768}{99225}\right) z^4 \\
& + \left(\frac{4616L^2}{45} + \frac{27419831L}{113400} + \frac{4616\pi^2}{135} - \frac{1077816623}{5715360}\right) z^5 + \mathcal{O}(z^6), \qquad (4.25)
\end{aligned}
$$

$$
\begin{aligned}
r_0(z) = {} & \frac{L^2}{3} + \left(\frac{4\pi^2}{81} + \frac{20}{9}\right) L + \frac{10}{9} + \frac{\pi^2}{324} - \frac{8\zeta(3)}{9} + \left(4L - \frac{4}{3}\right) z + \left(\frac{101L}{135} + \frac{1937}{4050}\right) \frac{1}{z} \\
& + \left(\frac{181L}{486} + \frac{8437}{34020}\right) \frac{1}{z^2} + \left(\frac{41803L}{204120} + \frac{28038091}{257191200}\right) \frac{1}{z^3} \\
& + \left(\frac{28309L}{222750} + \frac{335697253}{6174630000}\right) \frac{1}{z^4} + \left(\frac{174632L}{2027025} + \frac{33421938911}{1095688093500}\right) \frac{1}{z^5} \\
& + \mathcal{O}\left(\frac{1}{z^6}\right), \qquad (4.26)
\end{aligned}
$$

$$
\begin{aligned}
r_1(z) = {} & \frac{2521}{54} + \frac{2135\pi^2}{2916} - \frac{7\pi^4}{81} - \frac{65\zeta(3)}{81} + \frac{64\pi^2}{9}\left(2L - 7 + 8\ln(2)\right) z^{1/2} \\
& + \frac{1}{2835}\Bigg[420(-6N_1 + 6N_2 + 156\zeta(5) + 164\zeta(3) + 81) - 168L^5 \\
& + 4935L^4 - 560\left(42+\pi^2\right)L^3 + 420L^2\left(24\zeta(3) + 195 + 17\pi^2\right) + 14L\Big(-180(76\zeta(3) + 69) \\
& - 1980\pi^2 + 29\pi^4\Big) + \pi^2\left(2520\zeta(3) + \frac{434141881077795151618433}{100785118005794722500}\right) - 7694\pi^4\Bigg] z \\
& - \frac{32\pi^2}{81}\left(13L - 122 + 52\ln(2)\right) z^{3/2} + \Bigg[-8L^3 + \frac{163L^2}{9} - \frac{1273L}{81} + \pi^2\left(\frac{74}{27} - \frac{8L}{9}\right) \\
& + 12\zeta(3) - \frac{4535}{243}\Bigg] z^2 - \frac{10672\pi^2}{6075} z^{5/2} + \frac{1}{546750}\Big(-6426000L^3 + 2434500L^2 \\
& + 21040935L - 12852000\zeta(3) + 6877050\pi^2 - 29395538\Big) z^3 + \frac{12232\pi^2}{165375} z^{7/2} \\
& + \left(-\frac{884L^3}{27} + \frac{2039L^2}{243} + \frac{339179431L}{2381400} - \frac{1768\zeta(3)}{27} + \frac{984643\pi^2}{25515} - \frac{559021904543}{3000564000}\right) z^4 \\
& + \frac{415936\pi^2}{3750705} z^{9/2} + \Bigg[-\frac{4616L^3}{45} + \frac{67127L^2}{2700} + \frac{72559774859L}{142884000} - \frac{9232\zeta(3)}{45} \\
& + \frac{1627121\pi^2}{12600} - \frac{54916240328153}{90016920000}\Bigg] z^5 + \mathcal{O}(z^6), \qquad (4.27)
\end{aligned}
$$

$$
\begin{aligned}
r_1(z) = &-\frac{L^3}{3} - \left(\frac{2\pi^2}{81} + \frac{7}{3}\right) L^2 + \left(\frac{8\zeta(3)}{9} + \frac{2\pi^2}{81} - \frac{76}{27}\right) L + \frac{5\zeta(3)}{9} - \frac{23\pi^4}{1215} + \frac{\pi^2}{108} - \frac{194}{81} \\
&+ \left(-4L^2 + \frac{8L}{3} + \frac{\pi^2}{6} - \frac{104}{9}\right) z - \left(\frac{101L^2}{90} - \frac{1678L}{2025} + \frac{601}{13500}\right) \frac{1}{z} \\
&- \left(\frac{181L^2}{324} - \frac{4273L}{5103} - \frac{18757763}{42865200}\right) \frac{1}{z^2} \\
&- \left(\frac{41803L^2}{136080} - \frac{86836613L}{128595600} - \frac{96323169497}{324060912000}\right) \frac{1}{z^3} \\
&- \left(\frac{28309L^2}{148500} - \frac{802815799L}{1543657500} - \frac{15945714976267}{85580371800000}\right) \frac{1}{z^4} \\
&- \left(\frac{87316L^2}{675675} - \frac{443812747943L}{1095688093500} - \frac{11960939601604831}{98710540343415000}\right) \frac{1}{z^5} + \mathcal{O}\left(\frac{1}{z^6}\right). \qquad (4.28)
\end{aligned}
$$

A careful reader has noticed that the expression for the small-z expansion of $r_1(z)$ is not free of yet-undefined constants. These are the very two constants which, as mentioned in the previous chapter, we were able to determine only numerically. Their values are $N_1 \simeq 16.6256$ and $N_2 \simeq -116.775$.

Let us note that the $\mathcal{O}(z^8)$ and $\mathcal{O}\left(\frac{1}{z^{14}}\right)$ remainders in $r_{-1}(z)$ do not vanish. Astonishingly, it is precisely at these orders when some nonvanishing terms begin to appear.

4.2 Results for $m_c = 0$

In this section, we present results of our calculation performed at $z = 0$ from the outset, i.e. with a separate IBP reduction and calculation of the MIs. We confirm the results of Ref. [64] for $\widetilde{G}_{27}^{(1)\text{bare}}(0,\varepsilon)$, $\widetilde{G}_{27}^{(1)3P}(0,\varepsilon)$, $\widetilde{G}_{7(12)}^{(1)\text{bare}}(0,\varepsilon)$, $\widetilde{G}_{27}^{(1)m}(0,\varepsilon)$, and $\hat{G}_{47}^{(1)\text{bare}}(\varepsilon)$. We also extend them to all orders in ε, except for the latter case. As before, all the three-body results are calculated for $\delta = 1$.

The $z = 0$ calculation from the outset provides cross-checks for most of our arbitrary-z results because, as we verify, for $n = 2, 3$

$$
\begin{aligned}
\lim_{z\to 0} \widetilde{G}_{27}^{(1)nP}(z,\varepsilon) &= \widetilde{G}_{27}^{(1)nP}(0,\varepsilon), \\
\lim_{z\to 0} \widetilde{G}_{7(12)}^{(1)nP}(z,\varepsilon) &= \widetilde{G}_{7(12)}^{(1)nP}(0,\varepsilon), \\
\lim_{z\to 0} \widetilde{G}_{27}^{(1)m,2P}(z,\varepsilon) &= \widetilde{G}_{27}^{(1)m,2P}(0,\varepsilon). \qquad (4.29)
\end{aligned}
$$

However,

$$
\lim_{z\to 0} \widetilde{G}_{27}^{(1)m,3P}(z,\varepsilon) \neq \widetilde{G}_{27}^{(1)m,3P}(0,\varepsilon), \qquad (4.30)
$$

due to the logarithmic divergence at $z \to 0$ of the functions $j_0(z)$ and $j_1(z)$ in Eqs. (4.10) and (4.12). These divergences manifest themselves as an extra $1/\varepsilon$ pole in $\widetilde{G}_{27}^{(1)m,3P}(0,\varepsilon)$, as it often happens in the dimensional regularization for IR-limits of quantities that are not IR-safe. Since the contributions to $\widetilde{G}_{27}^{(1)m}$ alone do not form physical quantities by themselves, it is hard to find an argument why it is only in the three-body case that such a phenomenon occurs.

Extensions to all orders in ε

Let us now list all the contributions that we have calculated to all orders in ε. The three-body ones read

$$\widetilde{G}_{27}^{(1)3P}(0,\varepsilon) = -Q_u e^{3\gamma\varepsilon}\cos(\pi\varepsilon)\frac{8\,(1-\varepsilon^2)\,\Gamma(1+\varepsilon)\Gamma^4(1-\varepsilon)}{3(2-3\varepsilon)\Gamma(4-4\varepsilon)\Gamma(1-2\varepsilon)}, \tag{4.31}$$

$$\widetilde{G}_{7(12)}^{(1)3P}(0,\varepsilon) = -4\varepsilon\,(5+\varepsilon)\,\widetilde{G}_{27}^{(1)3P}(0,\varepsilon), \tag{4.32}$$

$$\begin{aligned}\widetilde{G}_{27}^{(1)m,3P}(0,\varepsilon) &= -Q_u e^{3\gamma\varepsilon}\cos(\pi\varepsilon)\\ &\times \frac{4\,(20\varepsilon^6-36\varepsilon^5+17\varepsilon^4+6\varepsilon^3-27\varepsilon^2+30\varepsilon-10)\,\Gamma(\varepsilon)\Gamma^4(1-\varepsilon)}{3(2-3\varepsilon)(1-3\varepsilon)\Gamma(4-4\varepsilon)\Gamma^3(1-2\varepsilon)}.\end{aligned} \tag{4.33}$$

As far as the two-body contributions are concerned, our results can be written as

$$\widetilde{G}_{27}^{(1)2P}(0,\varepsilon) = \widetilde{G}_{27}^{(1)2P}(0,\varepsilon)_u + \widetilde{G}_{27}^{(1)2P}(0,\varepsilon)_d, \tag{4.34}$$

$$\widetilde{G}_{7(12)}^{(1)2P}(0,\varepsilon) = -4\varepsilon\left[(5+\varepsilon)\,\widetilde{G}_{27}^{(1)2P}(0,\varepsilon)_u + (1+\varepsilon)\widetilde{G}_{27}^{(1)2P}(0,\varepsilon)_d\right], \tag{4.35}$$

$$\widetilde{G}_{27}^{(1)m,2P}(0,\varepsilon) = \widetilde{G}_{27}^{(1)m,2P}(0,\varepsilon)_u + \widetilde{G}_{27}^{(1)m,2P}(0,\varepsilon)_d, \tag{4.36}$$

where

$$\widetilde{G}_{27}^{(1)2P}(0,\varepsilon)_u = Q_u\frac{4e^{3\gamma\varepsilon}(1+\varepsilon)\Gamma^3(1-\varepsilon)\Gamma(2\varepsilon-1)}{3(1-2\varepsilon)(2-3\varepsilon)\Gamma(3-3\varepsilon)\Gamma^2(2-2\varepsilon)\Gamma(2-\varepsilon)}T_\varepsilon^1,$$

$$\widetilde{G}_{27}^{(1)2P}(0,\varepsilon)_d = Q_d\frac{8e^{3\gamma\varepsilon}(1-\varepsilon)^2\Gamma^3(1-\varepsilon)\Gamma(2\varepsilon-1)}{9(3-2\varepsilon)\Gamma(3-3\varepsilon)\Gamma^2(2-2\varepsilon)\Gamma(2-\varepsilon)}T_\varepsilon^2,$$

$$\widetilde{G}_{27}^{(1)m,2P}(0,\varepsilon) = Q_u\frac{-2e^{3\gamma\varepsilon}\Gamma^3(1-\varepsilon)\Gamma(2+\varepsilon)\Gamma(2\varepsilon-1)}{3(1-2\varepsilon)(2-3\varepsilon)(1-3\varepsilon)(1-4\varepsilon)\Gamma(3-3\varepsilon)\Gamma^2(2-2\varepsilon)\Gamma(2-\varepsilon)}T_\varepsilon^3,$$

$$\widetilde{G}_{27}^{(1)m,2P}(0,\varepsilon)_d = Q_d\frac{2e^{3\gamma\varepsilon}(\varepsilon-1)^2\Gamma(1-\varepsilon)^3}{3\varepsilon(2\varepsilon-3)\Gamma(3-3\varepsilon)\Gamma(2-2\varepsilon)^2\Gamma(2-\varepsilon)}T_\varepsilon^4, \tag{4.37}$$

and

$$\begin{aligned}T_\varepsilon^1 &= \left(-24\varepsilon^3+37\varepsilon^2-17\varepsilon+2\right)\Gamma(3-4\varepsilon)\Gamma(2-\varepsilon)\Gamma(1+\varepsilon) - 2(1-\varepsilon)\Gamma(2-2\varepsilon)\\ &\times\Big(\left(2\varepsilon^2-1\right)\Gamma(3-3\varepsilon)\Gamma(1+\varepsilon) + \cos(2\pi\varepsilon)\left(6\varepsilon^3-10\varepsilon^2+7\varepsilon-2\right)\Gamma(1-\varepsilon)\Gamma(2-\varepsilon)\Big),\\ T_\varepsilon^2 &= (11-16\varepsilon)\varepsilon\Gamma(3-4\varepsilon)\Gamma(2-\varepsilon)\Gamma(\varepsilon) - 2(1-\varepsilon)\Gamma(2-2\varepsilon)\Big(3\Gamma(3-3\varepsilon)\Gamma(1+\varepsilon)\\ &+\cos(2\pi\varepsilon)(1+\varepsilon)\Gamma(1-\varepsilon)\Gamma(2-\varepsilon)\Big),\\ T_\varepsilon^3 &= 2\left(192\varepsilon^6-512\varepsilon^5+356\varepsilon^4+140\varepsilon^3-270\varepsilon^2+107\varepsilon-13\right)\Gamma(3-3\varepsilon)\Gamma(2-2\varepsilon)\\ &+\left(-1728\varepsilon^6+5256\varepsilon^5-6036\varepsilon^4+3124\varepsilon^3-607\varepsilon^2-33\varepsilon+18\right)\Gamma(3-4\varepsilon)\Gamma(2-\varepsilon),\\ T_\varepsilon^4 &= \left(32\varepsilon^4-52\varepsilon^3+8\varepsilon^2+17\varepsilon-4\right)\Gamma(3-3\varepsilon)\Gamma(2-2\varepsilon)\Gamma(\varepsilon)\Gamma(2\varepsilon-1)\\ &-2\left(32\varepsilon^4-46\varepsilon^3+15\varepsilon^2+3\varepsilon-2\right)\Gamma(3-4\varepsilon)\Gamma(2-\varepsilon)\Gamma(\varepsilon)\Gamma(2\varepsilon-1).\end{aligned} \tag{4.38}$$

It remains to discuss $\hat{G}_{47}^{(1)}(\varepsilon)$. We can write it as a sum of several contributions as follows:[2]

$$\begin{aligned}\hat{G}_{47}^{(1)\text{bare}}(\varepsilon) &= X_{3s} + \kappa n_l X_\kappa + n_l X_l + n_b X_b + X_4 + X_5 + X_T \\ &- \frac{1}{6}\left[\widetilde{G}_{27}^{(1)\text{bare}}(0,\varepsilon) + \widetilde{G}_{27}^{(1)\text{bare}}(1,\varepsilon) + \widetilde{G}_{27}^{(1)\text{bare}}(1,\varepsilon)_{L\to R}\right]_{Q_u\to Q_d}, \quad (4.39)\end{aligned}$$

where $n_l = 3$, $n_b = 1$ and $\kappa = 1$. The four-body final state contributions are given by X_{3s} and X_κ, while the remaining terms multiplied by n_l or n_b originate from two-body contributions with closed (involving Dirac traces) massless or b-quark loops, respectively. Such loops give no three-body contributions due to the Furry theorem.

All the nonvanishing three-body contributions are contained inside $\widetilde{G}_{27}^{(1)\text{bare}}(0,\varepsilon)$, $\widetilde{G}_{27}^{(1)\text{bare}}(1,\varepsilon)$, $\widetilde{G}_{27}^{(1)\text{bare}}(1,\varepsilon)_{L\to R}$, and X_4 which originate from diagrams where the s-quark and b-quark loops are open (involve no Dirac traces). The notation for the first two of these symbols are self-explanatory, while the third one corresponds to the Q_2 operator where the $(\bar{c}b)_{V-A}$ current was replaced by the $(\bar{c}b)_{V+A}$ one. Finally, X_4 originates from the two- and three-body diagrams with open b-quark loops where $\hat{G}_{47}^{(0)}$ comes as a multiplicative factor.

The last two terms in the first line of Eq. (4.39) (X_5 and X_T) originate only from two-body contributions involving the open b-quark loops. The first one corresponds to the diagrams denoted by G_5 in Fig. 1 of Ref. [129]. The second one originates from the diagrams involving tadpole loops of the b quark.

Among all the terms on the r.h.s. of Eq. (4.39), there are only three which we have evaluated exactly in ε. They include $\left[\widetilde{G}_{27}^{(1)}(0,\varepsilon)\right]_{Q_u\to Q_d}$ (cf. Eqs. (4.31) and (4.34)), as well as

$$\begin{aligned}X_5 &= -e^{3\gamma\varepsilon}\pi\csc(\pi\varepsilon)\frac{32(1-\varepsilon)^2\Gamma(1+\varepsilon)}{27(2-\varepsilon)\Gamma(1-2\varepsilon)}, \\ X_l &= -\frac{4e^{3\gamma\varepsilon}(1-\varepsilon)\Gamma^3(1-\varepsilon)}{27\varepsilon(3-2\varepsilon)\Gamma(3-3\varepsilon)\Gamma^2(2-2\varepsilon)\Gamma(2-\varepsilon)}T_\varepsilon^5, \quad (4.40)\end{aligned}$$

where

$$\begin{aligned}T_\varepsilon^5 &= 2\cos(2\pi\varepsilon)\varepsilon\Gamma(2-\varepsilon)\Gamma(2\varepsilon-1)\Big(2\left(\varepsilon^2-1\right)\Gamma(2-2\varepsilon)\Gamma(1-\varepsilon) + (11-16\varepsilon)\varepsilon\Gamma(3-4\varepsilon)\Gamma(\varepsilon)\Big) \\ &+ \Gamma(3-3\varepsilon)\Gamma(2-2\varepsilon)\Gamma(\varepsilon)\Big(\left(12\varepsilon^3-16\varepsilon^2+8\varepsilon-3\right)\Gamma(2\varepsilon-1) + (2\varepsilon-3)\Gamma(2\varepsilon)\Big). \quad (4.41)\end{aligned}$$

Before discussing the remaining terms in Eq. (4.39), let us quote all the LO quantities from Eq. (2.4) of Ref. [64] which we have re-evaluated exactly in ε

$$\widetilde{G}_{77}^{(0)} = \frac{\Gamma(2-\varepsilon)}{\Gamma(2-2\varepsilon)}e^{\gamma\varepsilon}, \quad (4.42)$$

$$\hat{G}_{47}^{(0)\text{bare}} = -\frac{4}{9}\Gamma(1+\varepsilon)e^{\gamma\varepsilon}\widetilde{G}_{77}^{(0)}, \quad (4.43)$$

$$\hat{G}_{37}^{(0)} = \frac{3}{4}\hat{G}_{47}^{(0)}, \quad (4.44)$$

[2] Let us recall that the n_c-terms have been skipped.

$$\hat{G}_{67}^{(0)} = 4(5 - 3\varepsilon - \varepsilon^2)\hat{G}_{47}^{(0)}, \tag{4.45}$$

$$\hat{G}_{57}^{(0)} = \frac{3}{4}\hat{G}_{67}^{(0)}. \tag{4.46}$$

Results calculated only to a finite order in ε

The final ε-expanded expression for $\hat{G}_{47}^{(1)\mathrm{bare}}(\varepsilon)$ in Eq. (2.4) of Ref. [64] reads

$$\begin{aligned}\hat{G}_{47}^{(1)\mathrm{bare}}(\varepsilon) = {} & \frac{16}{3\varepsilon^2} + \frac{3674}{243\varepsilon} + 43.76456245573869 + 94.9884724116\,\varepsilon \\ & + \kappa n_l \left(-\frac{16}{243\varepsilon} + \frac{44\pi^2 - 612}{243}\varepsilon\right) + n_l \left(\frac{16}{81\varepsilon} - \frac{4}{243} + \frac{264\pi^2 - 2186}{729}\varepsilon\right) \\ & + n_b \left(\frac{16}{81\varepsilon} + 0.04680853247986 + 0.3194493123\,\varepsilon\right) + \mathcal{O}(\varepsilon^2)\end{aligned} \tag{4.47}$$

We have verified all the contributions to this expression (cf. Eq. (4.39)), except for

$$X_T = \frac{16}{3\varepsilon^2} + \frac{152}{9\varepsilon} + \frac{1288}{27} - \frac{4\pi^2}{9} + 90.432090762728134858947\,\varepsilon + \mathcal{O}(\varepsilon^2), \tag{4.48}$$

the four-body ones which were cross-checked by M. Poradziński [191]

$$\begin{aligned} X_{3s} &= -\frac{10}{729} + \varepsilon\left(\frac{157}{729} - \frac{31\pi^2}{729}\right) + \mathcal{O}(\varepsilon^2), \\ X_{\kappa} &= -\frac{16}{243} + \varepsilon\left(\frac{44}{243}\pi^2 - \frac{68}{27}\right) + \mathcal{O}(\varepsilon^2), \end{aligned} \tag{4.49}$$

and except for [121, 144]

$$\begin{aligned} \widetilde{G}_{77}^{(1)} &= \frac{4}{3\varepsilon} + \frac{124}{9} - \frac{16}{9}\pi^2 + \varepsilon\left(\frac{212}{3} - \frac{58}{9}\pi^2 - \frac{64}{3}\zeta(3)\right) + \mathcal{O}(\varepsilon^2), \\ \widetilde{G}_{78}^{(1)3P} &= \frac{100}{27} - \frac{8\pi^2}{27} + \varepsilon\left(-\frac{112\zeta(3)}{9} + \frac{70}{3} - \frac{4\pi^2}{9}\right) + \mathcal{O}(\varepsilon^2) \end{aligned} \tag{4.50}$$

which enter into the formula

$$X_4 \;=\; \hat{G}_{47}^{(0)}\,\frac{\widetilde{G}_{77}^{(1)} + \frac{3}{8}\widetilde{G}_{78}^{(1)3P}}{\widetilde{G}_{77}^{(0)}}. \tag{4.51}$$

The latter expression includes the two-body contribution from the diagram G_6 of Ref. [129], as well as the corresponding three-body contribution. One determines the sum of these terms by using $\widetilde{G}_{77}^{(1)}$ (both two- and three-body) together with $\widetilde{y}_4 = \hat{G}_{47}^{(0)}/\widetilde{G}_{77}^{(0)}$ which is a generalization of $\widetilde{y}_4$ from Eq. (6.8) of Ref. [129] to all orders in ε. There is also another contribution for which we need $\widetilde{z}_4$, which is an analogue of $\widetilde{y}_4$ but coming for a one-loop diagram with an external gluon. The diagram with the gluon differs from the one with the photon only by some charge and color factors, namely $\widetilde{z}_4 = \frac{3}{8}\widetilde{y}_4$.

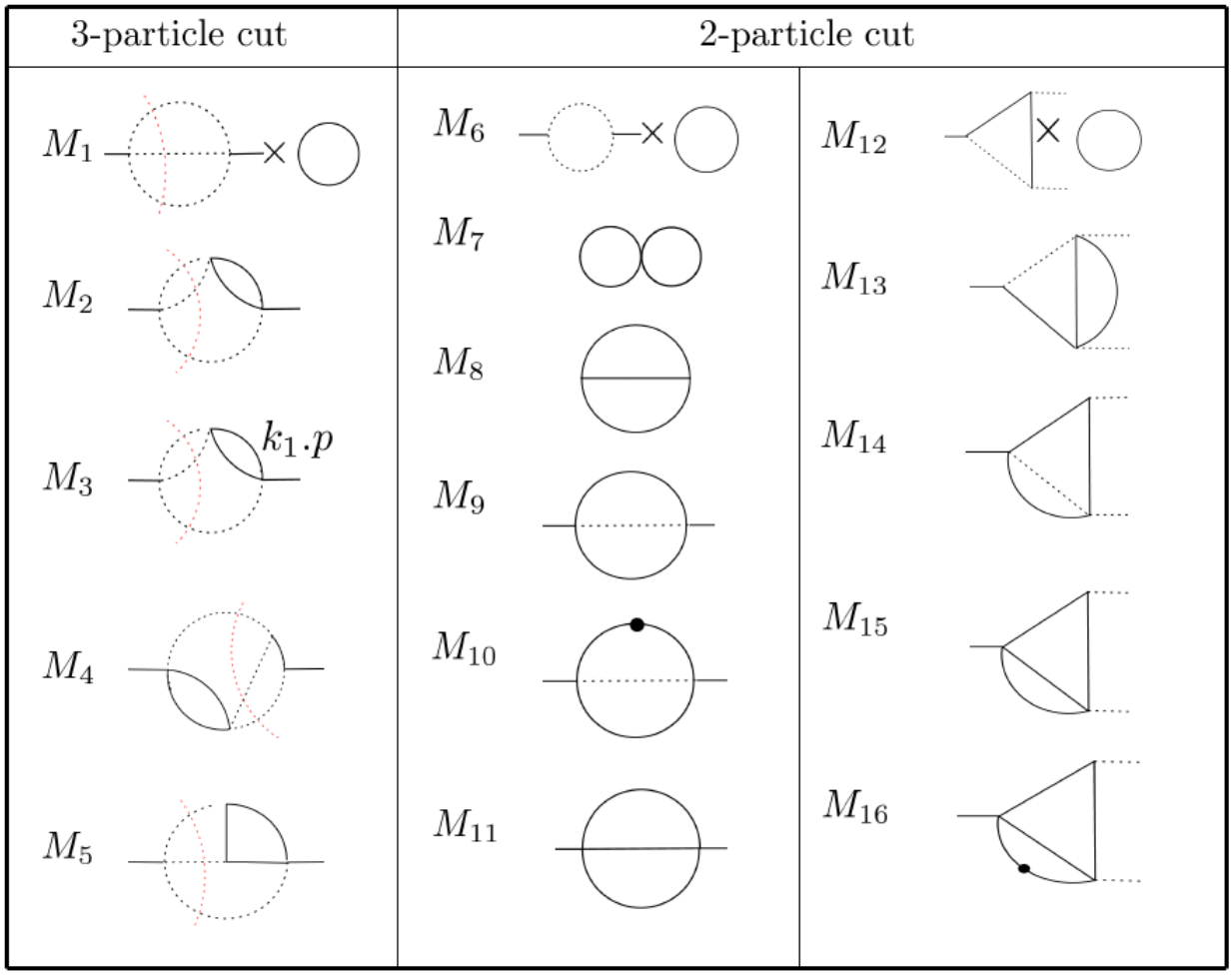

Figure 4.1: Master integrals for the b-quark loop contributions to $\hat{G}_{47}^{(1)}$.

To complete listing the explicit expressions for the r.h.s. of Eq. (4.39), it remains to quote our own results for X_b, $\widetilde{G}_{27}^{(1)\mathrm{bare}}(1,\varepsilon)$ and $\widetilde{G}_{27}^{(1)\mathrm{bare}}(1,\varepsilon)_{L\to R}$, all of which originate from diagrams with the b-quark loops. They read

$$\begin{aligned} X_b &= \frac{16}{81\varepsilon} + 0.04680856 + 0.31944943\,\varepsilon + \mathcal{O}(\varepsilon^2), \\ \widetilde{G}_{27}^{(1)\mathrm{bare}}(1,\varepsilon) &= \widetilde{G}_{27}^{(1)2P}(1,\varepsilon) + \widetilde{G}_{27}^{(1)3P}(1,\varepsilon), \\ \widetilde{G}_{27}^{(1)\mathrm{bare}}(1,\varepsilon)_{L\to R} &= \widetilde{G}_{27}^{(1)2P}(1,\varepsilon)_{L\to R} + \widetilde{G}_{27}^{(1)3P}(1,\varepsilon)_{L\to R}, \end{aligned} \tag{4.52}$$

where

$$\begin{aligned} \left[\widetilde{G}_{27}^{(1)2P}(1,\varepsilon) + \widetilde{G}_{27}^{(1)2P}(1,\varepsilon)_{L\to R}\right]_{Q_u\to Q_d} &= -\frac{214}{81\varepsilon} + 8.07696 + 1.84113\,\varepsilon + \mathcal{O}(\varepsilon^2), \\ \left[\widetilde{G}_{27}^{(1)3P}(1,\varepsilon) + \widetilde{G}_{27}^{(1)3P}(1,\varepsilon)_{L\to R}\right]_{Q_u\to Q_d} &= \frac{13 + 2\pi^2 - 6\pi\sqrt{3}}{9} - 0.0056863\,\varepsilon + \mathcal{O}(\varepsilon^2). \end{aligned} \tag{4.53}$$

Their evaluation involved the MIs depicted in Fig. 4.1. Apart from one trivial case (M_6),

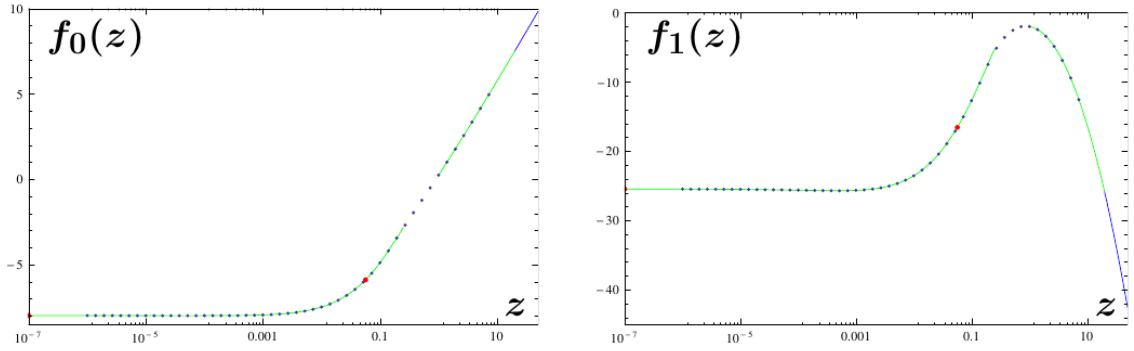

Figure 4.2: The functions $f_i(z)$ defined in Eq. (4.14).

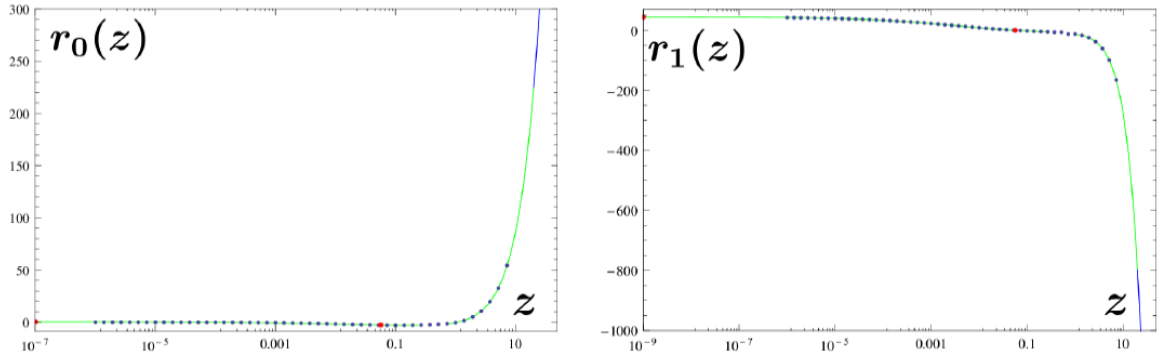

Figure 4.3: The functions $r_i(z)$ defined in Eq. (4.16).

all of them can be obtained from Fig. 3.2 by setting $m_c = m_b$. Thus, no new evaluation of the MIs was necessary. Moreover, in the $z = 1$ case, the Feynman parameter integration (analytical or numerical) was sufficient to determine all the MIs that were not yet available from the literature.

4.3 Plots and their interpretation

In this section, we present plots of the functions $f_i(z)$, $r_i(z)$, $g_i(z)$ and $j_i(z)$ that have been defined in Eqs. (4.2)-(4.4) and (4.14)-(4.16). They are displayed in Figs. 4.2–4.5.

In each of these plots, our results obtained with the help of a numerical solution to the DE are shown by (blue) dots. Some of these dots are slightly bigger and red, which indicates either the $z = 0$ limit or the physical point used as a central value in the phenomenological analysis of Refs. [2, 64], namely $z \simeq 0.05672$. The numerical solutions of the DE were obtained using an initial condition at $z = 20$ evaluated using our large-z expansions. The curves describing these expansions for $z \geq 20$ are displayed by the solid (blue) lines. The remaining solid (green) lines show either the large-z expansions for $\frac{1}{4} < z < 20$ or the small-z expansions for $0 < z < \frac{1}{4}$. The physical $c\bar{c}$ production threshold at $z = \frac{1}{4}$ defines the convergence radii of both expansions. In the two-body cases ($f_0(z)$, $f_1(z)$, $r_0(z)$ and $r_1(z)$), there are visible regions around $z = \frac{1}{4}$ where the expansions are not plotted, as they would become very inaccurate there. Only the dots from the numerical solutions are present in these regions. In the three-body cases ($g_0(z)$,

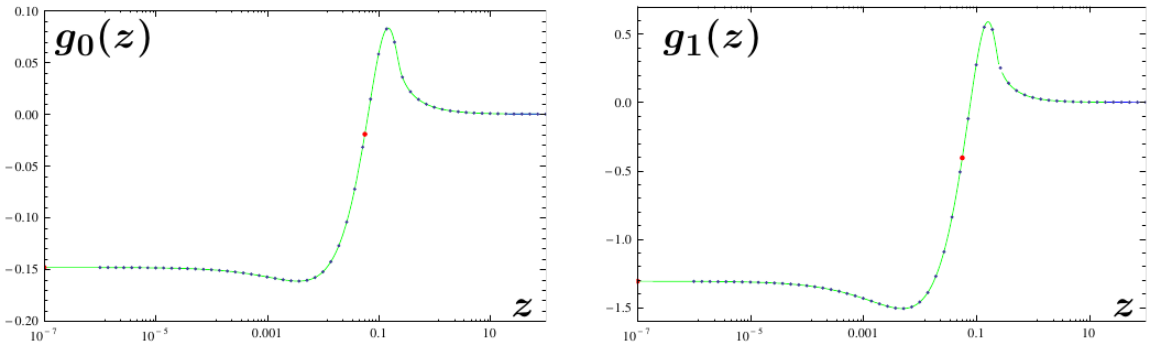

Figure 4.4: The functions $g_i(z)$ defined in Eq. (4.2).

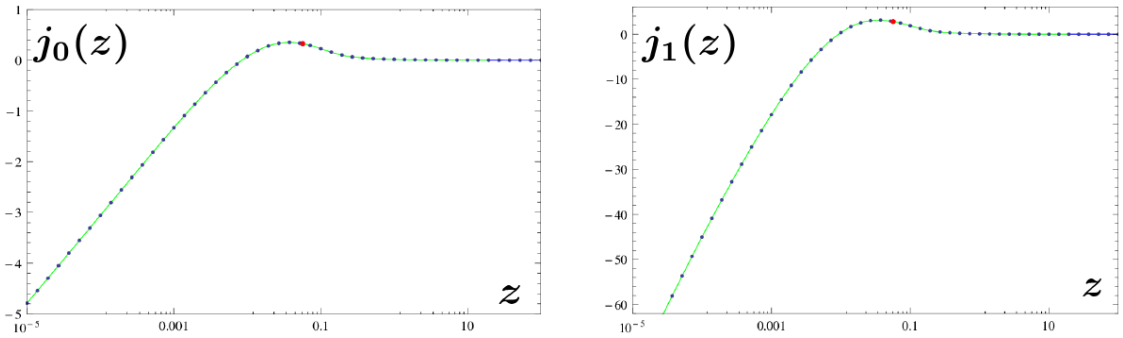

Figure 4.5: The functions $j_i(z)$ defined in Eq. (4.4).

$g_1(z)$, $j_0(z)$ and $j_1(z)$), our expansions are sufficiently deep that the inaccuracies near $z = \frac{1}{4}$ are invisible in the plots.

The points $z = \frac{1}{4}$ and $z = 0$ are singular points of our differential equations for the MIs. We may expect that the decay amplitudes at these points in the complex plane of the variable z are not meromorphic functions but rather have branch-point singularities. The decay rate is finite and continuous at $z = \frac{1}{4}$, but its n-th derivative with respect to z along the real axis is likely to diverge for some n. We cannot prove that this is the case in our particular example because only certain parts of our results are known in a closed form. However, we can see that the exact expression for the function $g_0(z)$ in Eq. (4.5) involves $\sqrt{|1-4z|}$, which signals non-analyticity at $z = 1/4$. A similar property is observed in the two-body contribution from the diagram denoted by G_1 in Fig.1 of Ref. [129], in which case an analytical result in a closed form is known. As an another example, one might mention the dilepton invariant mass spectrum in $b \to s\, e^+ e^-$ where a visible kink at the $c\bar{c}$ production threshold arises (see, e.g., Figs. 8-10 in Ref. [192]).

Our plots are presented in a logarithmic scale for z, for the purpose of illustrating nice convergence to the (independently calculated) values at $z = 0$ for all the functions except $j_0(z)$ and $j_1(z)$. As we have already mentioned, the latter two functions exhibit logarithmic divergences when z tends to 0. This fact manifests itself as an extra $1/\varepsilon$ pole when the corresponding interference term $\widetilde{G}_{27}^{(1)m,3P}$ is calculated at $z = 0$ from the outset. One can see this by comparing Eq. (4.4) which is finite when $\varepsilon \to 0$, and Eq. (4.33) that contains a $1/\varepsilon$ pole.

4.4 Exact coefficients at the master integrals

In the current section, we give our results for various interference terms as linear combinations of the master integrals that are retained as symbols. The coefficients in these linear combinations are presented exactly in z and ε. Such a presentation is aimed at possible future extension of the calculation to even higher orders in ε, which would certainly become necessary beyond the NNLO.

4.4.1 Coefficients for an arbitrary charm quark mass

Let us begin with our three-body results for arbitrary z, and for $\delta = 1$. They can be cast as follows:

$$\widetilde{G}_{27}^{(1)3P}(z,\varepsilon) = \sum_{i=1}^{5} \mathcal{A}_i^{3P} \mathcal{M}_i, \tag{4.54}$$

$$\widetilde{G}_{7(12)}^{(1)3P}(z,\varepsilon) = -4\varepsilon(5+\varepsilon)\, \widetilde{G}_{27}^{(1)3P}(z,\varepsilon), \tag{4.55}$$

$$\widetilde{G}_{27}^{(1)m,3P}(z,\varepsilon) = \mathcal{A}_6^{3P}\mathcal{M}_1 + \mathcal{A}_7^{3P}\mathcal{M}_2 + \mathcal{A}_8^{3P}\mathcal{M}_3 + \mathcal{A}_9^{3P}\mathcal{M}_4 + \mathcal{A}_{10}^{3P}\mathcal{M}_5, \tag{4.56}$$

where the coefficients in the above linear combinations are given by

$$\begin{aligned}
\mathcal{A}_1^{3P} &= \tfrac{32\varepsilon(1-\varepsilon^2)(1-\varepsilon)^2}{D_\varepsilon}, & \mathcal{A}_2^{3P} &= -\tfrac{16\left(1-\varepsilon^2\right)\left(2\varepsilon^2(6z+1)-2\varepsilon(3z+1)+1\right)}{E_\varepsilon}, \\
\mathcal{A}_3^{3P} &= \tfrac{16}{E_\varepsilon}\left(4\varepsilon^4-6\varepsilon^3-\varepsilon^2+6\varepsilon-3\right), & \mathcal{A}_4^{3P} &= -\tfrac{32\varepsilon}{E_\varepsilon}\left(4\varepsilon^3-\varepsilon^2-4\varepsilon+1\right)z, \\
\mathcal{A}_5^{3P} &= \tfrac{16\varepsilon\left(1-\varepsilon^2\right)z}{E_\varepsilon},
\end{aligned}$$

$$\mathcal{A}_6^{3P} = \frac{4\left(1-\varepsilon^2\right)}{3E_\varepsilon(1-2\varepsilon)^2 z}\Big(96\varepsilon^5 z - 36\varepsilon^4(12z+1) + 48\varepsilon^3(14z+3) - \varepsilon^2(444z+191) + 4\varepsilon(27z+26) - 20\Big),$$

$$\mathcal{A}_7^{3P} = \frac{8(1+\varepsilon)}{D_\varepsilon}\Big(16\varepsilon^6(6z+1) - 4\varepsilon^5(96z+7) + \varepsilon^4(504z-4) - 3\varepsilon^3(92z-9) + \varepsilon^2(54z-7) - 6\varepsilon + 2\Big),$$

$$\mathcal{A}_8^{3P} = -\frac{8\varepsilon}{D_\varepsilon}\left(64\varepsilon^6 - 184\varepsilon^5 + 96\varepsilon^4 + 134\varepsilon^3 - 160\varepsilon^2 + 49\varepsilon - 1\right),$$

$$\mathcal{A}_9^{3P} = -\frac{4(\varepsilon+1)}{D_\varepsilon}\Big(16\varepsilon^6(8z+3) - 32\varepsilon^5(15z+4) + 112\varepsilon^4(5z+1) - 32\varepsilon^3(8z+1) + \varepsilon^2(36z+3) - 5\varepsilon + 2\Big),$$

$$\mathcal{A}_{10}^{3P} = \frac{8}{D_\varepsilon}\left(8\varepsilon^5 - 4\varepsilon^4 - 13\varepsilon^3 + 6\varepsilon^2 + 5\varepsilon - 2\right)z, \tag{4.57}$$

with the following short-hand notation: $D_\varepsilon = 9\varepsilon\left(6\varepsilon^2 - 7\varepsilon + 2\right)$, and $E_\varepsilon = 9(2-3\varepsilon)$.

As far as our two-body results are concerned, we write them as

$$\widetilde{G}_{27}^{(1)2P}(z,\varepsilon) = \widetilde{G}_{27}^{(1)2P}(z,\varepsilon)_u + \widetilde{G}_{27}^{(1)2P}(z,\varepsilon)_d, \tag{4.58}$$

$$\widetilde{G}_{27}^{(1)2P}(z,\varepsilon) = -4\varepsilon\left[(5+\varepsilon)\,\widetilde{G}_{27}^{(1)2P}(z,\varepsilon)_u + (1+\varepsilon)\widetilde{G}_{27}^{(1)2P}(z,\varepsilon)_d\right], \tag{4.59}$$

$$\widetilde{G}_{27}^{(1)m,2P}(z,\varepsilon) = \widetilde{G}_{27}^{(1)m,2P}(z,\varepsilon)_u + \widetilde{G}_{27}^{(1)m,2P}(z,\varepsilon)_d. \tag{4.60}$$

The quantities on the r.h.s. of the above expressions are given by the following linear combinations of the MIs:

$$\widetilde{G}_{27}^{(1)2P}(z,\varepsilon)_d = \mathcal{A}_1\mathcal{M}_7 + \mathcal{A}_2\mathcal{M}_6 + \mathcal{A}_3\mathcal{M}_8 + \mathcal{A}_4\mathcal{M}_{12} + \mathcal{A}_5\mathcal{M}_{13} + \mathcal{A}_6\mathcal{M}_{10} + \mathcal{A}_7\mathcal{M}_9, \quad (4.61)$$

$$\widetilde{G}_{27}^{(1)2P}(z,\varepsilon)_u = \mathcal{A}_8\mathcal{M}_7 + \mathcal{A}_9\mathcal{M}_6 + \mathcal{A}_{10}\mathcal{M}_8 + \mathcal{A}_{11}\mathcal{M}_{14} + \mathcal{A}_{12}\mathcal{M}_{12} + \mathcal{A}_{13}\mathcal{M}_{13} + \mathcal{A}_{14}\mathcal{M}_{15} + \mathcal{A}_{15}\mathcal{M}_{10} + \mathcal{A}_{16}\mathcal{M}_9 + \mathcal{A}_{17}\mathcal{M}_{16} + \mathcal{A}_{18}\mathcal{M}_{17}, \quad (4.62)$$

$$\widetilde{G}_{27}^{(1)m,2P}(z,\varepsilon)_d = \mathcal{A}_{19}\mathcal{M}_7 + \mathcal{A}_{20}\mathcal{M}_6 + \mathcal{A}_{21}\mathcal{M}_8 + \mathcal{A}_{22}\mathcal{M}_{12} + \mathcal{A}_{23}\mathcal{M}_{13} + \mathcal{A}_{24}\mathcal{M}_{18} + \mathcal{A}_{25}\mathcal{M}_{11}, \quad (4.63)$$

$$\widetilde{G}_{27}^{(1)m,2P}(z,\varepsilon)_u = \mathcal{A}_{26}\mathcal{M}_7 + \mathcal{A}_{27}\mathcal{M}_6 + \mathcal{A}_{28}\mathcal{M}_8 + \mathcal{A}_{29}\mathcal{M}_{14} + \mathcal{A}_{30}\mathcal{M}_{12} + \mathcal{A}_{31}\mathcal{M}_{13} + \mathcal{A}_{32}\mathcal{M}_{16} + \mathcal{A}_{33}\mathcal{M}_{17}. \quad (4.64)$$

The coefficients $\mathcal{A}_i$ in the above equations read

$$\begin{aligned}
\mathcal{A}_1 &= \tfrac{2(1-\varepsilon)\left(4\varepsilon^2+\varepsilon-3\right)}{3\varepsilon(3-2\varepsilon)}, & \mathcal{A}_2 &= \tfrac{(1-\varepsilon)\left(16\varepsilon^4 z+\varepsilon^3(12-56z)+\varepsilon^2(38z-18)+29\varepsilon z-3z\right)}{3\varepsilon(3-2\varepsilon)(1-2\varepsilon)(2\varepsilon+1)z},\\
\mathcal{A}_3 &= -\tfrac{4(1-\varepsilon)^3(\varepsilon(2z-1)+3z)}{3-2\varepsilon}, & \mathcal{A}_4 &= -\tfrac{(1-\varepsilon)^2\left(8\varepsilon^3(5z-4)+2\varepsilon^2(4z+11)-41\varepsilon z+6z\right)}{3\varepsilon(3-2\varepsilon)},\\
\mathcal{A}_5 &= \tfrac{2(1-\varepsilon)^2\left(16\varepsilon^2+4\varepsilon-3\right)(z-1)z}{3\varepsilon(3-2\varepsilon)}, & \mathcal{A}_6 &= -\tfrac{4(1-\varepsilon)^2\left(\varepsilon^2(10z-1)+11\varepsilon z-14z+1\right)}{9-6\varepsilon},\\
\mathcal{A}_7 &= \tfrac{8(1-\varepsilon)^2(\varepsilon+1)z(4z-1)}{9-6\varepsilon}, & & \\
\mathcal{A}_8 &= -\tfrac{4(1-\varepsilon)^3\varepsilon(\varepsilon+1)}{6\varepsilon^2-7\varepsilon+2}, & \mathcal{A}_9 &= -\tfrac{(1-\varepsilon)^2(1+\varepsilon)\left(16\varepsilon^3 z+\varepsilon^2(3-12z)-6\varepsilon z+\varepsilon+4z-2\right)}{(1-2\varepsilon)^2(2-3\varepsilon)z},\\
\mathcal{A}_{10} &= -\tfrac{2\left(1-\varepsilon^2\right)\left(\varepsilon^3(8z-2)-10\varepsilon z+\varepsilon+4z\right)}{6\varepsilon^2-7\varepsilon+2}, & \mathcal{A}_{11} &= -\tfrac{4\varepsilon\left(4\varepsilon^3-\varepsilon^2-4\varepsilon+1\right)z}{2-3\varepsilon},\\
\mathcal{A}_{12} &= -\tfrac{(1+\varepsilon)\left(8\varepsilon^3-\varepsilon^2(12z+7)+14\varepsilon z+\varepsilon-4z\right)}{1-2\varepsilon}, & \mathcal{A}_{13} &= -\tfrac{2(1+\varepsilon)z(\varepsilon(4z-7)-2z+3)}{1-2\varepsilon},\\
\mathcal{A}_{14} &= -\tfrac{2\left(1-\varepsilon^2\right)(2\varepsilon z+\varepsilon-z-1)}{1-2\varepsilon}, & \mathcal{A}_{15} &= -\tfrac{2\left(1-\varepsilon^2\right)(1-4z)}{1-2\varepsilon},\\
\mathcal{A}_{16} &= -\tfrac{2(1-\varepsilon)^2\left(2\varepsilon^2-\varepsilon-3\right)}{1-2\varepsilon}, & \mathcal{A}_{17} &= 6\left(1-\varepsilon^2\right)z,\\
\mathcal{A}_{18} &= -\tfrac{2(1+\varepsilon)(\varepsilon(4z-1)-2z+1)z}{1-2\varepsilon}, & &
\end{aligned}$$

$$\mathcal{A}_{19} = -\frac{(1-\varepsilon)^2}{3}\left(\frac{12(1-\varepsilon)^2}{1-4z} - \frac{(2-\varepsilon)(1-\varepsilon)}{z(1-2\varepsilon)} + \frac{13-\varepsilon(\varepsilon(24\varepsilon^2+10\varepsilon-107)+89)}{\varepsilon(3-2\varepsilon)}\right),$$

$$\mathcal{A}_{20} = \frac{(1-\varepsilon)^2}{6}\left(\frac{13-\varepsilon\left(\varepsilon\left(48\varepsilon^3-102\varepsilon-5\right)+78\right)}{\varepsilon(4\varepsilon(2-\varepsilon)+3)} + \frac{\varepsilon\left(8\varepsilon^2-22\varepsilon+19\right)+2}{z(1-4\varepsilon^2)} + \frac{24(1-\varepsilon)^2}{1-4z}\right),$$

$$\begin{aligned}
\mathcal{A}_{21} = &-\frac{(1-\varepsilon)}{6(3-2\varepsilon)z(1-4z)}\\
&\times\Big(96\varepsilon^4(1-2z)^2z + \varepsilon^3\left(-192z^3+704z^2-268z+2\right) - \varepsilon^2\left(896z^3+104z^2-256z+9\right)\\
&+\varepsilon\left(816z^3-368z^2-95z+13\right) - 88z^3+146z^2+11z-6\Big),
\end{aligned}$$

$$\begin{aligned}
\mathcal{A}_{22} = &-\frac{(1-\varepsilon)}{6\varepsilon(3-2\varepsilon)z}\\
&\times\Big(48\varepsilon^5z(3z-4) - 6\varepsilon^4\left(16z^2-80z+1\right) + \varepsilon^3\left(-366z^2-422z+25\right) + \varepsilon^2\left(505z^2+161z-32\right)\\
&+\varepsilon\left(-213z^2-26z+12\right) + 26z^2\Big),
\end{aligned}$$

$$
\begin{aligned}
\mathcal{A}_{23} &= \frac{(1-\varepsilon)}{3\varepsilon(3-2\varepsilon)} \\
&\quad \times \Big(48\varepsilon^4(z-2)z + 4\varepsilon^3(40z-1) - 2\varepsilon^2\left(61z^2+27z-7\right) + 3\varepsilon\left(29z^2-7z-4\right) - 13(z-1)z\Big), \\
\mathcal{A}_{24} &= -\frac{(2-\varepsilon)(1-\varepsilon)^2}{6z}, \\
\mathcal{A}_{25} &= \frac{(2-\varepsilon)(1-\varepsilon)^2}{3z} = -2\mathcal{A}_{24}, \\
\mathcal{A}_{26} &= 4\,\mathcal{F}_\varepsilon\Big(\varepsilon^4(4z-6) + \varepsilon^3(19-6z) + \varepsilon^2(3z-22) + 11\varepsilon - 2\Big), \\
\mathcal{A}_{27} &= -\mathcal{F}_\varepsilon\Big(4\varepsilon^5(26z-9) + \varepsilon^4(114-320z) + \varepsilon^3(374z-141) + \varepsilon^2(81-197z) \\
&\quad + \varepsilon(41z-21) - 2z + 2\Big), \\
\mathcal{A}_{28} &= -\mathcal{G}_\varepsilon\,(1-\varepsilon)\left(48\varepsilon^5 - 8\varepsilon^4(22z+9) + 8\varepsilon^3(48z+1) - 4\varepsilon^2(73z-5) + \varepsilon(78z-1) - 4z - 2\right), \\
\mathcal{A}_{29} &= \mathcal{G}_\varepsilon\Big(48\varepsilon^6 - 64\varepsilon^5(z+2) + 112\varepsilon^4(z+1) - 8\varepsilon^3(9z+4) + 3\varepsilon^2(4z+1) - 5\varepsilon + 2\Big), \\
\mathcal{A}_{30} &= \mathcal{H}_\varepsilon\Big(48\varepsilon^5 - 4\varepsilon^4(18z+23) + 2\varepsilon^3(84z+29) - \varepsilon^2(134z+23) + \varepsilon(39z+14) - 2(z+2)\Big), \\
\mathcal{A}_{31} &= -2\,\mathcal{H}_\varepsilon\Big(16\varepsilon^4 z + 4\varepsilon^3\left(-6z^2+z+1\right) + 2\varepsilon^2\left(20z^2-18z-5\right) + \varepsilon\left(-18z^2+16z+8\right) \\
&\quad + z^2 + z - 2\Big), \\
\mathcal{A}_{32} &= -\frac{\left(24\varepsilon^5 - 40\varepsilon^4 - 6\varepsilon^3 + 39\varepsilon^2 - 18\varepsilon + 1\right)z}{\varepsilon(1-2\varepsilon)}, \\
\mathcal{A}_{33} &= 2z\,\mathcal{H}_\varepsilon\Big(4\varepsilon^3(6z-1) + \varepsilon^2(8-40z) + 6\varepsilon(3z-1) - z + 1\Big),
\end{aligned}
\tag{4.65}
$$

where the following short-hand notation has been used

$$
\mathcal{F}_\varepsilon \;=\; \tfrac{\left(1-\varepsilon^2\right)}{2\varepsilon(1-2\varepsilon)^2(2-3\varepsilon)z}, \qquad \mathcal{G}_\varepsilon \;=\; \tfrac{(1+\varepsilon)}{2\varepsilon(6\varepsilon^2-7\varepsilon+2)}, \qquad \mathcal{H}_\varepsilon \;=\; \tfrac{(1+\varepsilon)}{2\varepsilon(1-2\varepsilon)}. \tag{4.66}
$$

4.4.2 Coefficients for the case of a vanishing charm quark mass

Our expressions become much more compact in the $z = 0$ case, which the current subsection is devoted to. The corresponding MIs are given in Figs. 3.1 and 4.1. Here, we split our results into the terms that are proportional to the quark charges Q_u and Q_d. Starting from the quantities defined in in Eqs. (4.34)– (4.36), we write

$$
\begin{aligned}
\widetilde{G}_{27}^{(1)2P}(0,\varepsilon)_d &= Q_d\left(A_1\,\mathcal{M}_1^0 + A_2\,\mathcal{M}_2^0 + A_3\,\mathcal{M}_3^0\right), \\
\widetilde{G}_{27}^{(1)2P}(0,\varepsilon)_u &= Q_u\left(A_4\,\mathcal{M}_1^0 + A_5\,\mathcal{M}_2^0 + A_6\,\mathcal{M}_3^0\right), \\
\widetilde{G}_{27}^{(1)3P}(0,\varepsilon) &= Q_u\,A_7\,\mathcal{M}_5^0, \\
\widetilde{G}_{27}^{(1)m,2P}(0,\varepsilon)_d &= Q_d\left(A_8\,\mathcal{M}_2^0 + A_9\,\mathcal{M}_3^0\right), \\
\widetilde{G}_{27}^{(1)m,2P}(0,\varepsilon)_u &= Q_u\left(A_{10}\,\mathcal{M}_2^0 + A_{11}\,\mathcal{M}_3^0\right), \\
\widetilde{G}_{27}^{m(1)3P}(0,\varepsilon) &= Q_u\,A_{12}\,\mathcal{M}_5^0,
\end{aligned}
\tag{4.67}
$$

where the coefficients A_i are given by

$$
\begin{aligned}
A_1 &= \tfrac{16(1+\varepsilon)(1-\varepsilon)^3}{9(3-2\varepsilon)}, & A_2 &= \tfrac{8\varepsilon(11-6\varepsilon)(1-\varepsilon)^2}{9(3-2\varepsilon)},\\
A_3 &= -\tfrac{16\varepsilon(1-\varepsilon)^3}{3(3-2\varepsilon)}, & A_4 &= -\tfrac{8(1-2\varepsilon+\varepsilon^2+2\varepsilon^3-2\varepsilon^4)}{3-6\varepsilon},\\
A_5 &= \tfrac{4(1-6\varepsilon+\varepsilon^2+8\varepsilon^3)}{3-6\varepsilon}, & A_6 &= \tfrac{8\varepsilon(1-3\varepsilon^2+2\varepsilon^4)}{3(2-7\varepsilon+6\varepsilon^2)},\\
A_7 &= \tfrac{96\varepsilon(1-\varepsilon)^2(1-2\varepsilon)^2}{(2-3\varepsilon)(3-4\varepsilon)}, & & \\
A_8 &= -\tfrac{4(1-\varepsilon)^2(2-3\varepsilon-15\varepsilon^2+46\varepsilon^3-32\varepsilon^4)}{3\varepsilon(3-2\varepsilon)}, & A_9 &= \tfrac{2(1-\varepsilon)^2(4-17\varepsilon-8\varepsilon^2+52\varepsilon^3-32\varepsilon^4)}{3\varepsilon(3-2\varepsilon)},\\
A_{10} &= -\tfrac{2\varepsilon(9+33\varepsilon-212\varepsilon^2+156\varepsilon^3+200\varepsilon^4-192\varepsilon^5)}{3(1-6\varepsilon+8\varepsilon^2)}, & A_{11} &= \tfrac{4\varepsilon(13-42\varepsilon-5\varepsilon^2+110\varepsilon^3-56\varepsilon^4-68\varepsilon^5+48\varepsilon^6)}{3(1-2\varepsilon)(2-3\varepsilon)(1-3\varepsilon)},\\
A_{12} &= \tfrac{48(1-\varepsilon^2)(10-30\varepsilon+37\varepsilon^2-36\varepsilon^3+20\varepsilon^4)}{(2-3\varepsilon)(1-3\varepsilon)(3-4\varepsilon)}, & & \qquad (4.68)
\end{aligned}
$$

In addition, we give the IBP coefficients for three quantities that matter for $\hat{G}^{(1)}_{47}$, namely

$$
\begin{aligned}
\left[\widetilde{G}^{(1)3P}_{27}(1,\varepsilon)_{L\to R}\right]_{Q_u\to Q_d} &= A_{13}M_1 + A_{14}M_2 + A_{15}M_3 + A_{16}M_4 + A_{17}M_5,\\
\left[\widetilde{G}^{(1)2P}_{27}(1,\varepsilon)_{L\to R}\right]_{Qu\to Q_d} &= A_{18}M_6 + A_{19}M_7 + A_{20}M_9 + A_{21}M_{10} + A_{22}M_8 + A_{23}M_{11}\\
&\quad + A_{24}M_{12} + A_{25}M_{15} + A_{26}M_{16} + A_{27}M_{14} + A_{28}M_{13},\\
X_b &= A_{29}M_7 + A_{30}M_9 + A_{31}M_{10} + A_{32}M_8 + A_{33}M_{11}\\
&\quad + A_{34}M_{15} + A_{35}M_{16} + A_{36}M_{17} + A_{37}M_{18}, \qquad (4.69)
\end{aligned}
$$

where M_i denote the master integrals from Fig. 4.1. The coefficients A_i read

$$
\begin{aligned}
A_{13} &= -\frac{\varepsilon\left(-180\varepsilon^5+60\varepsilon^4+623\varepsilon^3-624\varepsilon^2+30\varepsilon+92\right)}{243(1-2\varepsilon)^2(2-3\varepsilon)},\\
A_{14} &= -\frac{2\left(222\varepsilon^6+23\varepsilon^5-487\varepsilon^4+88\varepsilon^3+322\varepsilon^2-174\varepsilon+24\right)}{81\left(6\varepsilon^3-13\varepsilon^2+9\varepsilon-2\right)},\\
A_{15} &= \frac{2\left(216\varepsilon^6-278\varepsilon^5-473\varepsilon^4+1207\varepsilon^3-1002\varepsilon^2+404\varepsilon-72\right)}{81\left(6\varepsilon^3-13\varepsilon^2+9\varepsilon-2\right)},\\
A_{16} &= -\frac{4\varepsilon\left(32\varepsilon^5-70\varepsilon^3+41\varepsilon^2+2\varepsilon-2\right)}{27(1-\varepsilon)(1-2\varepsilon)(2-3\varepsilon)},\\
A_{17} &= \frac{2\varepsilon\left(6\varepsilon^4+\varepsilon^3-22\varepsilon^2+40\varepsilon-24\right)}{81\left(6\varepsilon^2-7\varepsilon+2\right)},
\end{aligned}
$$

$$
\begin{aligned}
A_{18} &= \tfrac{2}{27}\varepsilon\left(\varepsilon^3+\varepsilon^2-4\varepsilon+2\right), & A_{19} &= \tfrac{-36\varepsilon^7-180\varepsilon^6+455\varepsilon^5-301\varepsilon^4+178\varepsilon^3-186\varepsilon^2+52\varepsilon+16}{54(1-2\varepsilon)^2(3\varepsilon-2)},\\
A_{20} &= \tfrac{2\left(6\varepsilon^5+\varepsilon^4-38\varepsilon^3+48\varepsilon^2-22\varepsilon+4\right)}{27(1-\varepsilon)}, & A_{22} &= \tfrac{4\left(12\varepsilon^6-23\varepsilon^5-58\varepsilon^4+122\varepsilon^3-69\varepsilon^2+17\varepsilon-4\right)}{27(6\varepsilon^2-7\varepsilon+2)},\\
A_{21} &= -\tfrac{2\varepsilon\left(\varepsilon^3-6\varepsilon+4\right)}{9(1-\varepsilon)}, & A_{23} &= \tfrac{\varepsilon\left(-36\varepsilon^5+24\varepsilon^4+147\varepsilon^3-230\varepsilon^2+122\varepsilon-24\right)}{54(1-\varepsilon)(1-2\varepsilon)},\\
A_{24} &= -\tfrac{4}{27}\varepsilon\left(\varepsilon^3-3\varepsilon+2\right), & A_{25} &= \tfrac{2\varepsilon^2\left(6\varepsilon^2+2\varepsilon-5\right)}{54\varepsilon-27},\\
A_{26} &= \tfrac{2\left(4\varepsilon^5-11\varepsilon^3+2\varepsilon^2-6\varepsilon+8\right)}{27(2\varepsilon^2-3\varepsilon+1)}, & A_{27} &= \tfrac{4}{27}\varepsilon\left(2\varepsilon^2+2\varepsilon-3\right),\\
A_{28} &= \tfrac{4\varepsilon\left(32\varepsilon^5-70\varepsilon^3+41\varepsilon^2+2\varepsilon-2\right)}{27(1-\varepsilon)(1-2\varepsilon)(2-3\varepsilon)}, & &
\end{aligned}
$$

$$
\begin{aligned}
A_{29} &= \tfrac{-80\varepsilon^7-176\varepsilon^6+1200\varepsilon^5-1556\varepsilon^4+411\varepsilon^3+457\varepsilon^2-292\varepsilon+36}{27(1-2\varepsilon)^2\varepsilon(2\varepsilon-3)(2\varepsilon+1)}, & A_{30} &= \tfrac{16(\varepsilon-1)\left(9\varepsilon^2+11\varepsilon-13\right)}{81-54\varepsilon},\\
A_{31} &= \tfrac{32(\varepsilon-1)(\varepsilon+1)}{9(2\varepsilon-3)}, & A_{32} &= -\tfrac{2\left(72\varepsilon^4-364\varepsilon^3+570\varepsilon^2-339\varepsilon+63\right)}{9(4\varepsilon^2-8\varepsilon+3)},\\
A_{33} &= \tfrac{-136\varepsilon^6+4\varepsilon^5+902\varepsilon^4-1445\varepsilon^3+872\varepsilon^2-224\varepsilon+24}{27\varepsilon(4\varepsilon^3-12\varepsilon^2+11\varepsilon-3)}, & A_{34} &= -\tfrac{2\left(8\varepsilon^4-4\varepsilon^3-14\varepsilon^2+5\varepsilon+6\right)}{9(4\varepsilon^2-8\varepsilon+3)},\\
A_{35} &= \tfrac{4\left(8\varepsilon^4-4\varepsilon^3-14\varepsilon^2+5\varepsilon+6\right)}{9(\varepsilon-1)(2\varepsilon-3)(2\varepsilon-1)}, & A_{36} &= 8\varepsilon-10,\\
A_{37} &= \tfrac{2}{27}(1-\varepsilon). & &
\end{aligned}
\tag{4.70}
$$

Chapter 5

Outlook: bare NNLO QCD contributions for arbitrary m_c

Our counterterm calculation at $z = 0$ has served for cross-checking the inputs for the phenomenological analysis in Refs. [2,64]. However, its extension to arbitrary z, which is the main topic of this thesis, cannot be used for any phenomenological purpose until the corresponding bare NNLO interference terms $\widetilde{G}_{17}^{(2)\text{bare}}$ and $\widetilde{G}_{27}^{(2)\text{bare}}$ are also determined for arbitrary z, or at least in the vicinity of its physical value $z \simeq 0.057$. Such a calculation involves diagrams like the ones shown in Fig. 5.1. Their computation at $z = 0$ in

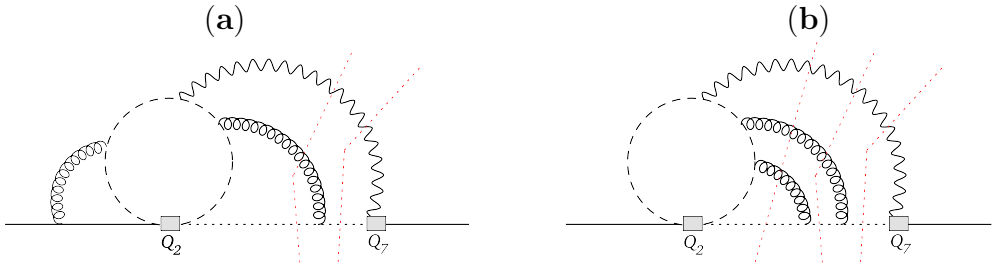

Figure 5.1: Sample Feynman diagrams contributing to the bare NNLO interference term $\widetilde{G}_{27}^{(2)\text{bare}}$ with possible two-, three- and four-particle cuts (red dotted lines). The black solid, dashed and dotted lines denote the b-quark, c-quark and s-quark propagators, respectively.

Refs. [64] is already considered an achievement due to the large number of difficult MIs that had to be determined. An extension to arbitrary z is thus an ambitious task which, unfortunately, has not come close to being completed in the time scale of the current PhD work.

Although the author of the present thesis has not been involved himself in the bare NNLO calculations, the issue deserves a brief description which the current chapter is devoted to. The calculation was first attempted by the authors of Ref. [146] (R. Boughezal, M. Czakon and T. Schutzmeier) who began with considering the two-particle cut contributions. They generated the relevant diagrams, preformed the Dirac algebra calculation that produced 19469 scalar integrals to compute, and identified the relevant 473 master integrals. However, their IBP routine [193] was unable to determine coefficients at these MIs because the database it used had a 20 GB size restriction. Shifting to the use of another database would require a total reconstruction of the code, which has not been

attempted due to involvement of the authors in other, LHC-oriented physics projects. In the end, their calculation was restricted to the n_c-terms alone [146] and to the $z = 0$ case, both of which were accessible with their IBP codes. The $z = 0$ calculation was completed only recently [64], with participation of several other researchers.

Another attempt to perform the IBP reduction for arbitrary z was undertaken by M. Misiak, A.V. Smirnov, V.A. Smirnov and M. Steinhauser in 2011 when the `C++` version of the code `FIRE` [73,74] became available. Even though the code was not yet public at the time, the involvement of its author and the hospitality of the CERN IT team allowed to complete the IBP reduction of the two-particle-cut diagrams in around two months. The most difficult diagrams required over 74 GB RAM for intermediate results, and the cluster nodes had to be protected against jobs submitted by other users. That IBP reduction was considered to be just a test of whether completing the project was feasible at all with the scalar integral set generated previously by the authors of Ref. [146]. The result of the test was positive, but too little attention was paid to notational details, namely to making the outputs automatically accessible to the code `exp` [181] that needs to be used for evaluating the large-z expansions of the MIs.

In 2012, M. Steinhauser alone performed another calculation of the two-body contributions from the outset, namely generation of the diagrams, performing the Dirac algebra and reduction of the scalar integrals to the MIs using `FIRE`. His final results are now `exp`-compatible. However, proceeding with the calculation was postponed due to involvement of the team members in other projects, including completing the $z = 0$ calculation and the phenomenological analysis of $\bar{B} \to X_{s,d}\gamma$ that could not wait any longer for getting updated.

Once the arbitrary-z bare NNLO calculations are re-started in the near future, the first step will be to perform the IBP reduction also for the three- and four-body final state contributions. Next, all the MIs need to be treated using the same method as in Ref [146]. This method has been followed in the present thesis for the numerical solution of the DEs. It amounts to using asymptotic expansions at large z and extending them with the help of DEs to obtain high-accuracy approximations to the MIs at some finite value of z (e.g., $z = 20$). Next, the sub-DEs (see Eq. (3.66)) are solved numerically along an ellipse in the complex plane to reach the desired value on the real axis below the $c\bar{c}$ threshold $z = \frac{1}{4}$. Let us note that our current numerical solution of the sub-DEs involved a set of $\mathcal{O}(10^2)$ functions. Enlarging the number of functions by one or two orders of magnitude for the bare NNLO case should not lead to technical problems given the experience gained in the $z = 0$ case [64].

The boundary conditions for the MIs at large z will be given in terms of single-scale MIs. The latter MIs are going to be much simpler than the original ones, which is the purpose of using the DEs at all. However, even those simpler MIs may not be completely trivial and the number of them may be sizeable. In such a case, they are going to be treated in the same manner as the single-scale propagator MIs were treated in the $z = 0$ calculation [64]. The external momentum was assumed to be arbitrary rather than given by $p^2 = m_b^2$, and another set of DEs was formed and numerically solved. The new boundary conditions were given in terms of a manageable (smaller) set of much simpler integrals, namely tadpoles and massless propagator integrals. A similar method is expected to work in the case of arbitrary z, and it should actually lead to a simpler set of propagator integrals, i.e. three-loop rather than four-loop ones.

Once the bare NNLO calculations are completed, the counterterms evaluated in the present thesis will become useful for a phenomenological analysis. Such a new analysis is going to be free of the m_c-interpolation issue, which will definitely improve the accuracy of the SM prediction for the branching ratio of $\bar{B} \to X_s\gamma$. However, there will still remain some uncertainty stemming from the fact that the calculations of $\widetilde{G}_{17}^{(2)}$ and $\widetilde{G}_{27}^{(2)}$ are preformed at $\delta = 1$. An extension to the default value of $\delta = 1 - 2E_0/m_b \simeq 0.3$ will require repeating the three- and four-body calculations of the bare NNLO terms and the counterterms with an explicit cut on the photon energy. Such a calculation is feasible using the method of Ref. [140]. However, the $\delta = 1$ calculation must be completed first, as it is a necessary step for including the two-body contributions.

Given the complexity of the project and the fate of the previous attempts, it is hard to predict the time scale of the bare NNLO calculation. However, one can realistically hope for its completion before Belle-II starts collecting data in 2017. Improving the theory accuracy in $\bar{B} \to X_s\gamma$ will become an urgent issue then.

Chapter 6

Conclusions

In the present thesis, we evaluated [1] the exact dependence on the charm-quark mass of all the necessary ultraviolet-counterterm diagrams that contribute to the yet-unknown parts of the NNLO QCD corrections $K_{17}^{(2)}$ and $K_{27}^{(2)}$ to the weak radiative B-meson decay branching ratio. These corrections originate from interferences of the four-quark and photonic dipole operators. At present, they are estimated using an interpolation in m_c, which generates one of the the main uncertainties in the perturbative contribution to $\mathcal{B}(\bar{B} \to X_s\gamma)^{\rm SM}$. Our calculation is a step towards removing this uncertainty. However, a phenomenological use of our results will be possible only after future determination of the bare NNLO contributions to the considered interference terms.

Apart from our calculation for arbitrary m_c, we evaluated many of the necessary counterterm contributions at $m_c = 0$, and presented them to all orders in ε wherever possible. Our results contributed to the evaluation of the $m_c = 0$ boundary for the interpolation, and thus to the recently published updated phenomenological analysis of $\mathcal{B}(\bar{B} \to X_s\gamma)^{\rm SM}$ [2].

The thesis contains many technical details that have not been presented elsewhere, namely explicit expressions for all the relevant quantities in terms of the master integrals, as well as results for these integrals obtained using several different methods, involving Mellin-Barnes techniques and differential equations.

At present, the experimental determination of $\mathcal{B}(\bar{B} \to X_s\gamma)$ agrees with the SM prediction within uncertainties that are similar on the experimental and theoretical sides, and amount to around 7% each. A factor-of-two reduction of each of them is feasible in the near future. On the experimental side, it is likely to come from high-statistics measurement using the hadronic tag for the recoiling B-meson, which essentially eliminates the so-called continuum background. Such measurements have been statistics-limited so far. On the theory side, the two main issues are re-considering the estimates of non-perturbative effects, and eliminating the m_c-interpolation in the perturbative NNLO contributions. Our calculation has contributed to a future resolution of the latter issue.

Acknowledgments

My special thanks to my advisor, Professor Mikołaj Misiak, for many fruitful discussions we had, and his permanent encouragement during my work. It was always a great pleasure to work with him. My thanks to Aqeel Ahmed, Michał Poradziński, Mateusz Iskrzyński and others for their support at the University of Warsaw. During my stay at the RWTH Aachen University, numerous stimulating discussions with Professor Michał Czakon, Paul Fiedler and David Heymes were extremely helpful on my path to complete this work. I am grateful to Professor Matthias Steinhauser, Thomas Hermann, Otto Eberhardt, Wolfgang Gregor Hollik and Martin Wiebusch from Karlsruhe Institute of Technology to make my stay there pleasant and fruitful. I am indebted to Tobias Huber for discussions related to the calculation of loop integrals with the Mellin-Barnes method at the conference *Loops and Legs 2014*. I thank Alexander Smirnov for his help on the `C++` version of his reduction code `FIRE` that has made my work much more efficient. Finally, I would like to thank my parents for their unconditional support. Last, but not least, I thank my wife Maryam and son M. Ali for their patience and permanent encouragement.

This work has been supported in part by the Foundation for Polish Science International PhD Projects Programme co-financed by the EU European Regional Development Fund, by the National Science Centre (Poland) research project, decision DEC-2014/13/B/ST2/03969, by the National Centre for Physics (Pakistan), and by the Karlsruhe Institute of Technology.

Appendices

Appendix A: Dirac algebra, Feynman rules and special functions

Dirac traces in D dimensions

A convenient recursive formula for evaluating traces of even numbers of γ matrices reads

$$tr(\gamma^{\nu_1}\gamma^{\nu_2}\dots\gamma^{\nu_n}) = \sum_{k=2}^{n}(-1)^k \;\; g^{\nu_1\nu_k} \times tr(\gamma^{\nu_2}\dots\widehat{\gamma^{\nu_k}}\dots\gamma^{\nu_n}), \tag{A.1}$$

$$tr(\gamma^{\nu_1}\gamma^{\nu_2}) = 4g^{\nu_1\nu_2}, \tag{A.2}$$

$$g^{\nu}{}_{\nu} = D, \tag{A.3}$$

where $\widehat{\gamma^{\nu_k}}$ in Eq. (A.1) means that one has to omit γ^{ν_k} in the product under the trace.

Effective theory Feynman rule for the Q_7-operator insertion

The operator Q_7 defined in Eq. (2.9) contains the product $\sigma^{\mu\nu}F_{\mu\nu}$, where

$$\sigma^{\mu\nu} = \frac{i}{2}[\gamma^\mu, \gamma^\nu], \tag{A.4}$$

$$F_{\mu\nu} = \partial_\mu A_\nu - \partial_\nu A_\mu. \tag{A.5}$$

The corresponding Feynman rule can be obtained by a mnemotechnic replacement $\partial_\mu \to +iq_\mu$, where q_μ is the outgoing photon momentum. Thus, one gets

$$\sigma^{\mu\nu}F_{\mu\nu} \to +2[\not\varepsilon, \not q], \tag{A.6}$$

where ε^μ is the photon polarization vector.

Logarithm

We follow the conventions in which the default Riemann sheet for the logarithm is defined with a branch cut on the negative real axis. This means that for a real positive x, we have

$$\ln(-x \pm i0) = \ln x \pm i\pi.$$

Gamma and Beta functions

The Γ and B functions are defined by

$$\Gamma(x) = \int_0^\infty t^{x-1} e^{-t} dt, \qquad B(x,y) = \frac{\Gamma(x)\Gamma(y)}{\Gamma(x+y)} = \int_0^1 t^{x-1}(1-t)^{y-1} dt. \tag{A.7}$$

The function $\Gamma(z)$ is meromorphic and different from 0 in the whole complex plane. It has simple poles at $z = -n$, where $n \in \mathbb{N} \cup \{0\}$.

The Feynman integrals in $D = 4 - 2\varepsilon$ dimensions typically contain Γ functions with arguments $(n + m\varepsilon)$, where n is an integer. For an expansion in ε of such Γ functions, one first reduces them to $\Gamma(1 + m\varepsilon)$ using the identity $\Gamma(1 + z) = z\Gamma(z)$, from which it follows that

$$\Gamma(n+x) = \Gamma(1+x) \times \begin{cases} (1+x)_{n-1}, & \text{when } n \geq 1, \\ 1/(n+x)_{1-n}, & \text{when } n \leq 0, \end{cases} \tag{A.8}$$

where $(z)_k$ denotes the Pochhammer symbol

$$(z)_k \equiv \frac{\Gamma(z+k)}{\Gamma(z)} = z(z+1)\dots(z+k-1), \quad \text{for} \quad k \in \mathbb{N}. \tag{A.9}$$

Next, one uses the following formula:

$$\Gamma(1+\varepsilon) = \exp\Big[-\gamma\varepsilon + \sum_{n=2}^{\infty} \frac{(-1)^n \zeta(n)}{n} \varepsilon^n \Big], \tag{A.10}$$

where $\gamma \simeq 0.5772$ is the Euler-Mascheroni constant, and $\zeta(x) = \sum_{l=1}^{\infty} \frac{1}{l^x}$ is the Riemann ζ-function. A useful identity reads

$$\Gamma(1-z)\Gamma(z) = \frac{\pi}{\sin(\pi z)}, \tag{A.11}$$

from which it follows that

$$\frac{\Gamma(z)}{\Gamma(z-n)} = (-1)^n \frac{\Gamma(n+1-z)}{\Gamma(1-z)} \tag{A.12}$$

for any integer n. The following relation that holds for a positive integer n is also useful:

$$\Gamma(nz) = (2\pi)^{\frac{1-n}{2}} n^{nz-\frac{1}{2}} \prod_{k=0}^{n-1} \Gamma\left(z + \frac{k}{n}\right). \tag{A.13}$$

For $n = 2$, it gives

$$\Gamma(2z) = \frac{2^{2z-1}}{\sqrt{\pi}} \Gamma(z) \Gamma\left(z + \frac{1}{2}\right). \tag{A.14}$$

The ψ function

The function $\psi(z)$ (denoted by `PolyGamma[z]` under `Mathematica`) can be defined by

$$\psi(z) = \frac{d}{dz}\ln\Gamma(z) \qquad \text{or} \qquad \psi(z) = \int_0^1 d\xi \left(\frac{\xi^{z-1}}{\xi-1} - \frac{1}{\ln\xi}\right). \tag{A.15}$$

It satisfies the following identities:

$$\psi(z+n) = \psi(z) + \sum_{i=0}^{n-1} \frac{1}{z+i} \qquad \text{and} \qquad \psi(1-z) - \psi(z) = \pi\cot(\pi z). \tag{A.16}$$

The n-th derivative of the ψ function, namely

$$\psi^{(n)}(z) = \frac{d^n}{dz^n}\psi(z) \tag{A.17}$$

is denoted by `PolyGamma[n,z]` under `Mathematica`. It satisfies an identity which becomes useful when applying the MB method

$$\psi^{(n)}(z) = \frac{(-1)^{n+1}n!}{2\pi i}\int_{\alpha-i\infty}^{\alpha+i\infty} ds\, \frac{\Gamma(s)\Gamma(1-s)\Gamma(z-s)^{n+1}(-1)^{-s}}{\Gamma(1+z-s)^{n+1}}, \quad \text{for } 0<\alpha<1 \wedge n\in\mathbb{N}. \tag{A.18}$$

In Sec. 3.3.2, we mentioned transforming the MB integral into a multiple series and then subsequently summing up the series. For instance, for a sum of the form

$$S_i(n) = \sum_{j=1}^{n} \frac{1}{j^i} \tag{A.19}$$

we can use (cf. Eqs. (A.10) and (A.16))

$$\psi(n) = S_1(n-1) - \gamma, \tag{A.20}$$

$$\psi^{(k)}(n) = (-1)^k k!(S_{k+1}(n-1) - \zeta(k+1)), \;\; k = 1,2,\ldots \tag{A.21}$$

Polylogarithms

The classical polylogarithms are recursively defined by

$$Li_1(z) = -\ln(1-z) \qquad \text{and} \qquad Li_{n+1}(z) = \int_0^z \frac{d\xi}{\xi} Li_n(\xi), \text{ for } n\in\mathbb{N}. \tag{A.22}$$

They are generalized by the Euler polylogarithms defined (for $a\in\mathbb{C}$, $\mathrm{Re}\, a > 1$ and $|z|<1$) as

$$Li_a(z) = \sum_{n=1}^{\infty}\frac{z^n}{n^a}, \tag{A.23}$$

which satisfy the following identities:

$$Li_a(z) = -\frac{1}{\Gamma(a)}\int_0^1 d\xi\, \frac{\ln^{a-1}(1/\xi)}{\xi - \frac{1}{z}} \qquad \text{and} \qquad Li_{a+1}(z) = \int_0^z \frac{d\xi}{\xi} Li_a(\xi). \tag{A.24}$$

A useful MB formula for $Li_2(z)$ reads

$$Li_2(z) = -\frac{1}{2\pi i}\int_{\mathcal{L}} ds\,(-z)^{-s}\frac{\Gamma(1+s)\Gamma^3(-s)}{\Gamma^2(1-s)}, \quad \text{when} \quad |\arg(-z)| < \pi. \tag{A.25}$$

The Nielsen (generalized) polylogarithms are defined as

$$S_{a,b}(z) = \frac{(-1)^{a+b-1}}{(a-1)!\,b!}\int_0^1 d\xi \frac{ln^{a-1}(\xi)\,ln^b(1-z\xi)}{\xi}, \tag{A.26}$$

where a and b are positive integers. For some additional integrals that are not yet implemented in default `Mathematica`, see Appendix A.2 of Ref. [194] devoted to the package `HypExp`.

Hypergeometric differential equation and functions

The hypergeometric functions [195] frequently appear in the Feynman integral calculations. In our case, several of the relevant DE systems were reducible to a single second-order inhomogeneous hypergeometric DE

$$\underbrace{z(1-z)f''(z) + [c-(a+b+1)z]f'(z) - abf(z)}_{\text{homogeneous part}} + \underbrace{\sum_{k=1}^{k_{\max}} d_k z^{p_k}}_{\text{inhomogeneous part}} = 0, \tag{A.27}$$

where a, b, c, d_k and p_k are some parameters which may in general be complex, but we have encountered only real ones.

A general solution to Eq. (A.27) is a sum of any specific solution to this equation and an arbitrary linear combination of two independent solutions to the homogeneous hypergeometric equation. From among many possible ways of writing such a general solution, we choose the following two ones:

$$\begin{aligned}
f(z) &= N\ {}_2F_1(a,b;c;z) \ +\ Mz^{1-c}\ {}_2F_1(1+a-c,1+b-c;2-c;z) \\
&\quad -\ \sum_{k=1}^{k_{\max}} \frac{d_k z^{p_k+1}}{(p_k+1)(p_k+c)}\ {}_3F_2\left(1,p_k+a+1,p_k+b+1;p_k+c+1,p_k+2;z\right), \\
f(z) &= Az^{-a}\ {}_2F_1\left(a,1+a-c;1+a-b;\frac{1}{z}\right) \ +\ Bz^{-b}\ {}_2F_1\left(b,1+b-c;1+b-a;\frac{1}{z}\right) \\
&\quad +\ \sum_{k=1}^{k_{\max}} \frac{d_k z^{p_k}}{(p_k+a)(p_k+b)}\ {}_3F_2\left(1,-p_k,1-p_k-c;1-p_k-a,1-p_k-b;\frac{1}{z}\right),
\end{aligned} \tag{A.28}$$

where N, M, A and B are arbitrary complex constants. The first (second) form is more convenient for small-z (large-z) expansions that are performed according to

$${}_pF_q\left(a_1,\ldots,a_p;b_1,\ldots,b_q;y\right) = \sum_{n=0}^{\infty}\frac{(a_1)_n\ldots(a_p)_n}{(b_1)_n\ldots(b_q)_n}\,\frac{y^n}{n!}, \tag{A.29}$$

where we take either $y = z$ or $y = 1/z$. The first solution is valid provided $c \notin \mathbb{Z}$ and $-p_k, -p_k+c \notin \mathbb{N}$. The second solution is valid provided $a-b \notin \mathbb{Z}$ and $p_k+a, p_k+b \notin \mathbb{N}\cup\{0\}$.

We demand that $f(z)$ is analytic in the fourth quadrant where $\mathrm{Re}\, z > 0$ and $\mathrm{Im}\, z \leq 0$. It is motivated by the fact that our DEs in the variable $z = m_c^2/m_b^2$ could equivalently be written as DEs in the variable m_c^2, i.e. m_b^2 serves only as a real rescaling factor that makes our variables dimensionless. The variable m_c^2, when extended to the complex plane, must be treated according to the Feynman "$i0$" prescription for the propagator, which means taking "$m_c^2 - i0$". This defines the quadrant in which our function must be analytic.

Once the region of analyticity is specified, the relations between the constants (N, M) and (A, B) become unique. We find

$$A = N \ \frac{\Gamma(b-a)\Gamma(c)}{\Gamma(b)\Gamma(c-a)} e^{-i\pi a} - M \ \frac{\Gamma(b-a)\Gamma(2-c)}{\Gamma(1-a)\Gamma(1+b-c)} e^{i\pi(c-a)} + \frac{\Gamma(b-a)}{\Gamma(1-a)\Gamma(c-a)} \sum_{k=1}^{k_{\max}} d_k \frac{\Gamma(-p_k-a)\Gamma(p_k+c)\Gamma(p_k+1)}{\Gamma(p_k+b+1)} e^{-i\pi(p_k+a)}, \tag{A.30}$$

$$B = A(a \leftrightarrow b), \tag{A.31}$$

after substituting $(-z)^\kappa = e^{+i\pi\kappa}|z|^\kappa$ into the handbook expression for an analytic continuation of the hypergeometric function [195, 196]

$${}_{p+1}F_p\left(\begin{matrix} a_1, a_2, \ldots, a_{p+1} \\ b_1, b_2, \ldots, b_p \end{matrix}; z\right) = \frac{\prod_{l=1}^{p}\Gamma(b_l)}{\prod_{l=1}^{p+1}\Gamma(a_l)} \sum_{m=1}^{p+1} \frac{\Gamma(a_m)\prod_{l=1,l\neq m}^{p+1}\Gamma(a_l - a_m)}{\prod_{l=1}^{p}\Gamma(b_l - a_m)} \ (-z)^{-a_m} \times {}_{p+1}F_p\left(\begin{matrix} a_m, 1+a_m-b_1, 1+a_m-b_2, \ldots, 1+a_m-b_p \\ 1+a_m-a_1, \ldots, \widehat{1}, \ldots, 1+a_m-a_{p+1} \end{matrix}; \frac{1}{z}\right). \tag{A.32}$$

In the above equation, $\widehat{1}$ indicates that $(1 + a_m - a_m)$ should not be included among the arguments.

Eq. (A.32) holds provided *none* of the differences $(a_l - a_m)$ for $l \neq m$ is an integer. If some of these differences is an integer, some arguments of the Γ functions as well as the parameters of the hypergeometric functions may contain nonpositive integers, which may give rise to divergences. To get rid of them (i.e., to regularize our expression) one can introduce new auxiliary parameters. However, other than hypergeometric special functions usually enter the calculation when the regulator is released, and the problem of analytic continuation becomes nontrivial.

Another useful formula for the analytic continuation is

$${}_2F_1\left(a_1, a_2; b_1; z\right) = (1-z)^{-a_1} \, {}_2F_1\left(a_1, b_1 - a_2; b_1; \frac{z}{z-1}\right). \tag{A.33}$$

From Eq. (A.29), one easily derives identities for derivatives and integrals of the hypergeometric functions

$$\begin{aligned} \frac{\partial}{\partial z} \ {}_pF_q\left(\{a_i\}; \{b_j\}; z\right) &= \frac{\prod_{i=1}^{p} a_i}{\prod_{j=1}^{q} b_j} \ {}_pF_q\left(\{a_i+1\}; \{b_j+1\}; z\right) \\ \int dz \ {}_pF_q\left(\{a_i\}; \{b_j\}; z\right) &= \frac{\prod_{j=1}^{q}(b_j-1)}{\prod_{i=1}^{p}(a_i-1)} \ {}_pF_q\left(\{a_i-1\}; \{b_j-1\}; z\right), \\ \int dz \, z^{\alpha-1} \, {}_pF_q\left(\{a_i\}; \{b_j\}; z\right) &= \frac{z^\alpha}{\alpha} \ {}_{p+1}F_{q+1}\left(\alpha, \{a_i\}; \alpha+1, \{b_j\}; z\right). \end{aligned} \tag{A.34}$$

In the evaluation of phase-space integrals and in the Feynman parameter method, one encounters an integral representation of ${}_2F_1$ function of the form [195]

$$ {}_2F_1\left(a_1,a_2;b_1;z\right)=\frac{\Gamma(b_1)}{\Gamma(a_2)\Gamma(b_1-a_2)}\int_0^1 d\xi\ \frac{\xi^{a_2-1}(1-\xi)^{b_1-a_2-1}}{(1-z\xi)^{a_1}}, \tag{A.35}$$

where $\mathrm{Re}\, a_2>0$ and $\mathrm{Re}(b_1-a_2)>0$.

Let us also note a recursive integral relation between the hypergeometric functions

$$ \begin{aligned} {}_pF_q\left(a_1,\dots a_p;b_1,\dots b_q;z\right)=\frac{\Gamma(b_q)}{\Gamma(a_p)\Gamma(b_q-a_p)}\int_0^1 d\xi\ \xi^{a_p-1}(1-\xi)^{b_q-a_p-1} \\ \times\ {}_{p-1}F_{q-1}\left(a_1,\dots a_{p-1};b_1,\dots b_{q-1};z\xi\right). \end{aligned} \tag{A.36}$$

The MB representation for a hypergeometric function reads

$$ {}_pF_q\left(a_1,\dots,a_p;b_1,\dots,b_p;z\right)=\frac{1}{2\pi i}\int_{\alpha-i\infty}^{\alpha+i\infty} d\xi\ (-z)^{-\xi}\ \Gamma(\xi)\left[\prod_{i=1}^{p}\frac{\Gamma(a_i-\xi)}{\Gamma(a_i)}\right]\left[\prod_{i=1}^{q}\frac{\Gamma(b_i)}{\Gamma(b_i-\xi)}\right]. \tag{A.37}$$

Appendix B: The ϕ_{ij} functions

In this Appendix, we list explicit expressions for the ϕ_{ij} functions that have appeared in Eqs. (2.69) and (2.70).

When $z<(1-\delta)/4$ (which is the phenomenologically relevant region), we have [64]

$$ \begin{aligned} \phi_{27}^{(1)}(z,\delta)=&-\frac{2}{27}\delta(3-3\delta+\delta^2)+\frac{4}{3}z\delta s_\delta L_\delta+\frac{12-8\pi^2}{9}z^2\delta+\frac{4}{3}z(1-2z)(s_0L_0-s_\delta L_\delta)\\ &+\frac{2\pi^2-7}{9}z\delta(2-\delta)-\frac{8}{9}z(6z^2-4z+1)(L_0^2-L_\delta^2)-\frac{8}{9}z\delta(2-\delta-4z)L_\delta^2, \end{aligned} \tag{B.1}$$

with $s_\delta=\sqrt{(1-\delta)(1-\delta-4z)}$, $s_0=\sqrt{1-4z}$, $L_\delta=\ln\frac{\sqrt{1-\delta}+\sqrt{1-\delta-4z}}{2\sqrt{z}}$ and $L_0=\ln\frac{1+\sqrt{1-4z}}{2\sqrt{z}}$.

The other relevant ϕ_{ij} functions describe the NLO three-body contributions that are independent of z. They read

$$ \phi_{77}^{(1)}(\delta)=-\frac{2}{3}\ln^2\delta-\frac{7}{3}\ln\delta-\frac{31}{9}+\frac{10}{3}\delta+\frac{1}{3}\delta^2-\frac{2}{9}\delta^3+\frac{1}{3}\delta(\delta-4)\ln\delta, \tag{B.2}$$

$$ \phi_{78}^{(1)}(\delta)=\frac{8}{9}\big[\mathrm{Li}_2(1-\delta)-\frac{1}{6}\pi^2-\delta\ln\delta+\frac{9}{4}\delta-\frac{1}{4}\delta^2+\frac{1}{12}\delta^3\big], \tag{B.3}$$

and

$$ \phi_{47}^{(1)}(\delta)=\phi_{47}^{(1)\mathrm{A}}(\delta)+\phi_{47}^{(1)\mathrm{B}}(\delta), \tag{B.4}$$

where

$$ \begin{aligned} \phi_{47}^{(1)\mathrm{A}}(\delta)=&\frac{1}{54}\pi\left(3\sqrt{3}-\pi\right)+\frac{1}{81}\delta^3-\frac{25}{108}\delta^2+\frac{5}{54}\delta+\frac{2}{9}\left(\delta^2+2\delta+3\right)\arctan^2\sqrt{\frac{1-\delta}{3+\delta}}\\ &-\frac{1}{3}\left(\delta^2+4\delta+3\right)\sqrt{\frac{1-\delta}{3+\delta}}\arctan\sqrt{\frac{1-\delta}{3+\delta}}, \end{aligned} \tag{B.5}$$

$$ \phi_{47}^{(1)\mathrm{B}}(\delta)=\frac{34\delta^2+59\delta-18}{486}\frac{\delta^2\ln\delta}{1-\delta}+\frac{433\delta^3+429\delta^2-720}{2916}. \tag{B.6}$$

Bibliography

[1] M. Misiak, A. Rehman and M. Steinhauser, to be published.

[2] M. Misiak, H. Asatrian, R. Boughezal, M. Czakon, T. Ewerth, A. Ferroglia, P. Fiedler, P. Gambino, C. Greub, U. Haisch, T. Huber, M. Kamiński, G. Ossola, M. Poradziński, A. Rehman, T. Schutzmeier, M. Steinhauser and J. Virto, *Updated NNLO QCD predictions for the weak radiative B-meson decays*, Phys. Rev. Lett. **114** (2015) 22, 221801 [arXiv:1503.01789].

[3] S. L. Glashow, *Partial Symmetries Of Weak Interactions*, Nucl. Phys. **22** (1961) 579.

[4] S. Weinberg, *A Model Of Leptons*, Phys. Rev. Lett. **19** (1967) 1264.

[5] A. Salam, *Weak And Electromagnetic Interactions*, Originally printed in 'Svartholm: Elementary Particle Theory, Proceedings Of The Nobel Symposium Held 1968 At Lerum, Sweden', Stockholm 1968, 367-377.

[6] M. Gell-Mann, *A Schematic Model Of Baryons And Mesons*, Phys. Lett. **8** (1964) 214.

[7] M. Y. Han and Y. Nambu, *Three-triplet model with double SU(3) symmetry*, Phys. Rev. B **139** (1965) 1006.

[8] D. J. Gross and F. Wilczek, *Ultraviolet Behavior of Non-abelian Gauge Theories*, Phys. Rev. Lett. **30** (1973) 1343.

[9] H. D. Politzer, *Reliable Perturbative Results for Strong Interactions?*, Phys. Rev. Lett. **30** (1973) 1346.

[10] S. Weinberg, *Nonabelian Gauge Theories Of The Strong Interactions*, Phys. Rev. Lett. **31** (1973) 494.

[11] H. Fritzsch, M. Gell-Mann and H. Leutwyler, *Advantages Of The Color Octet Gluon Picture*, Phys. Lett. B **47** (1973) 365.

[12] P.W. Higgs, *Broken symmetries and the masses of gauge bosons*, Phys. Rev. Lett. **13** (1964) 508.

[13] G. S. Guralnik, C. R. Hagen, and T. W. B. Kibble, *Global conservation laws and massless particles*, Phys. Rev. Lett. **13** (1964) 585.

[14] F. Englert and R. Brout, *Broken symmetry and the mass of gauge vector mesons*, Phys. Rev. Lett. **13** (1964) 321.

[15] P. W. Higgs, *Spontaneous Symmetry Breakdown without Massless Bosons*, Phys. Rev. **145** (1966) 1156.

[16] T. W. B. Kibble, *Symmetry breaking in non-Abelian gauge theories*, Phys. Rev. **155** (1967) 1554.

[17] G. 't Hooft, *Renormalization of Massless Yang-Mills Fields*, Nucl. Phys. B **33** (1971) 173.

[18] G. 't Hooft, *Renormalizable Lagrangians for massive yang-mills fields*, Nucl. Phys. B **35** (1971) 167.

[19] J.C. Collins, *Renormalization*, Cambridge University Press (1984);
C. Itzykson and J.-B. Zuber, *Quantum Field Theory*, McGraw Hill Inc. (1980);
T. Muta, *Foundations of Chromodynamics*, World Scientific, 1987;
M.E. Peskin and D.V. Schroeder, *An Introduction to Quantum Field Theory*, Addison-Wesley Publishing Company (1996);
F. Mandl and G. Shaw, *Quantum Field Theory*, John Wiley and Sons (1993);
T.-P. Cheng and L.-F. Li, *Gauge Theory of Elementary Particle Physics*, Clarendon Press, Oxford (1984);
L.H. Ryder, *Quantum Field Theory*, Cambridge University Press (1985);
J.F. Donoghue, E. Golowich and B.R. Holstein, *Dynamics of the Standard Model*, Cambridge Monographs (1992);
S. Pokorski, *Gauge Field Theory*, Cambridge Monographs (2000);
S. Weinberg, *The Quantum Theory of Fields*, Cambridge University Press (2005).

[20] ATLAS Collaboration, G. Aad *et al.*, *Combined search for the Standard Model Higgs boson using up to* 4.9 fb^{-1} *of pp collision data at* $\sqrt{s} = 7$ *TeV with the ATLAS detector at the LHC*, Phys. Lett. B **710** (2012) 49 [arXiv:1202.1408].

[21] CMS Collaboration, S. Chatrchyan *et al.*, *Combined results of searches for the standard model Higgs boson in pp collisions at* $\sqrt{s} = 7$ *TeV*, Phys. Lett. B **710** (2012) 26 [arXiv:1202.1488].

[22] K. A. Olive *et al.* (Particle Data Group Collaboration), *Review of Particle Physics*, Chin. Phys. C **38** (2014) 090001.

[23] The LEP Collaborations (ALEPH DELPHI L3 OPAL), LEP Electroweak Working Group, and SLD Heavy Flavor Group. A combination of preliminary Electroweak measurements and constraints on the Standard Model, http://lepewwg.web.cern.ch/LEPEWWG.

[24] J. van der Bij and M. J. G. Veltman, *Two Loop Large Higgs Mass Correction to the rho Parameter*. Nucl. Phys. B **231** (1984) 205.

[25] J. J. van der Bij, K. G. Chetyrkin, M. Faisst, G. Jikia, and T. Seidensticker, *Three-loop leading top mass contributions to the rho parameter*, Phys. Lett. B **498** (2001) 156 [hep-ph/0011373].

[26] Giuseppe Degrassi and Paolo Gambino, *Two-loop heavy top corrections to the Z^0 boson partial widths*, Nucl. Phys. B **567** (2000) 3 [hep-ph/9905472].

[27] M. Faisst, Johann H. Kuhn, T. Seidensticker and O. Veretin, *Three loop top quark contributions to the rho parameter*, Nucl. Phys. B **665** (2003) 649 [hep-ph/0302275].

[28] R. Boughezal, J. B. Tausk, and J. J. van der Bij, *Three-loop electroweak correction to the rho parameter in the large Higgs mass limit*, Nucl. Phys. B **713** (2005) 278 [hep-ph/0410216].

[29] A. Czarnecki, *Muon g-2: A theoretical review*, Nucl. Phys. Proc. Suppl. **144** (2005) 201.

[30] A. Ferroglia, C. Greub, A. Sirlin and Z. Zhang, *Contributions of the W-boson propagator to μ and τ leptonic decay rates*, Phys.Rev. D **88** (2013) 3 [arXiv:1307.6900].

[31] M. Awramik, M. Czakon, A. Freitas, and G. Weiglein, *Complete two-loop electroweak fermionic corrections to $sin^2\theta^{lept}_{eff}$ and indirect determination of the Higgs boson mass*, Phys. Rev. Lett. **93** (2004) 201805 [hep-ph/0407317];
L. Basso, O. Fischer, J. J. van der Bij, *Precision tests of unitarity in leptonic mixing* Europhys.Lett. **105** (2014) 11001 [arXiv:1310.2057].

[32] T. Kinoshita, *Tenth-order QED contribution to the electron g-2 and high precision test of quantum electrodynamics*, Int. J. Mod. Phys. A **29** (2014) 1430003;
Tatsumi Aoyama, Masashi Hayakawa, Toichiro Kinoshita and Makiko Nio, *Tenth-Order Electron Anomalous Magnetic Moment — Contribution of Diagrams without Closed Lepton Loops*, Phys. Rev. D **91** (2015) 3, 033006 [arXiv:1412.8284].

[33] M. Baker, P. Marquard, A. Penin, J. Piclum and M. Steinhauser, *Hyperfine splitting in positronium to $\mathcal{O}(\alpha^7 m_e)$: one-photon annihilation contribution*, Phys. Rev. Lett. **112** (2014) 120407 [arXiv:1402.0876].

[34] N. Cabibbo, *Unitary symmetry and leptonic decays*, Phys. Rev. Lett. **10** (1963) 531.

[35] M. Kobayashi and T. Maskawa, *CP Violation In The Renormalizable Theory Of Weak Interaction*, Prog. Theor. Phys. **49** (1973) 652.

[36] A. J. Buras, *Climbing NLO and NNLO Summits of Weak Decays*, [arXiv:1102.5650];
A. J. Buras, *Weak Hamiltonian, CP violation and rare decays* , [hep-ph/9806471];
G. Buchalla, A. J. Buras and M. E. Lautenbacher, *Weak Decays Beyond Leading logarithms*, Rev. Mod. Phys. (1996) **68** 1125 [hep-ph/9512380].

[37] M. Artuso, E. Barberio and S. Stone, *B Meson Decays*, PMC Phys. A **3** (2009) 3 [arXiv:0902.3743]

[38] A. J. Buras, L. Merlo and E. Stamou, *The Impact of Flavor Changing Neutral Gauge Bosons on* $\bar{B} \to X_s\gamma$, JHEP **1108** (2011) 124 [arXiv:1105.5146];
U. Haisch, $B \to X_s\gamma$: *Standard Model and Beyond*, [arXiv:0805.2141].

[39] S. Bertolini, F. Borzumati, A. Masiero and G. Ridolfi, *Effects of supergravity induced electroweak breaking on rare B decays and mixings*, Nucl. Phys. B **353** (1991) 591;
P. L. Cho and M. Misiak, $b \to s\gamma$ *Decay in* $SU(2)_L \times SU(2)_R \times U(1)$ *Extensions of the Standard Model*, Phys. Rev. D **49** (1994) 5894 [hep-ph/9310332];
K. Fujikawa and A. Yamada, *Test of the chiral structure of the top-bottom charged current by the process* $b \to s\gamma$, Phys. Rev. D **49** (1994) 5890.

[40] N. Isgur and M. B. Wise, *Weak Decays of Heavy Mesons in the Static Quark Approximation*, Phys. Lett. B **232** (1989) 113; *Weak Transition Form-factors Between Heavy Mesons*, Phys. Lett. B **237** (1990) 527.

[41] P. Gambino and C. Schwanda, *Inclusive semileptonic fits, heavy quark masses, and* V_{cb}, Phys. Rev. D **89** (2014) 014022 [arXiv:1307.4551];
A. Alberti, P. Gambino, K.J. Healey and S. Nandi, *Precision determination of the Cabibbo-Kobayashi-Maskawa element* V_{cb}, Phys. Rev. Lett. **114** (2015) 061802 [arXiv:1411.6560].

[42] CLEO, R. Ammar *et al.*, *Evidence for penguin-diagram decays: First observation of* $B \to K^*(892)\gamma$, Phys. Rev. Lett. **71** (1993) 674.

[43] S. Chen *et al.* (CLEO Collaboration), *Branching Fraction and Photon Energy Spectrum* $b \to s\,\gamma$, Phys. Rev. Lett. **87** (2001) 251807 [hep-ex/0108032].

[44] A. Limosani *et al.* (BELLE Collaboration), *Measurement of Inclusive Radiative B-meson Decays with a Photon Energy Threshold of* 1.7 *GeV*, Phys. Rev. Lett. **103** (2009) 241801 [arXiv:0907.1384].

[45] K. Abe *et al.* (BELLE Collaboration), *A Measurement of the Branching Fraction for the Inclusive* $B \to X(s)\,\gamma$ *Decays with the Belle Detector* , Phys. Lett. B **511** (2001) 151 [hep-ex/0103042].

[46] J. P. Lees *et al.* (BABAR Collaboration), *Precision Measurement of the* $B \to X_s\gamma$ *Photon Energy Spectrum, Branching Fraction, and Direct CP Asymmetry* $A_{CP}(B \to X_{s+d}\,\gamma$, Phys. Rev. Lett. **109** (2012) 191801 [arXiv:1207.2690].

[47] J. P. Lees *et al.* (BABAR Collaboration), *Measurement of* $\mathcal{B}(B \to X_s\gamma)$*, the* $B \to X_s\gamma$ *photon energy spectrum, and the direct CP asymmetry in* $B \to X_{s+d}\,\gamma$ *decays*, Phys. Rev. D **86** (2012) 112008 [arXiv:1207.5772].

[48] J. P. Lees *et al.* (BABAR Collaboration), *Exclusive Measurements of* $b \to s\gamma$ *Transition Rate and Photon Energy Spectrum*, Phys. Rev. D **86** (2012) 052012 [arXiv:1207.2520].

[49] B. Aubert *et al.* (BABAR Collaboration), *Measurement of the* $B \to X_s\gamma$ *Branching Fraction and Photon Energy Spectrum using the Recoil Method*, Phys. Rev. D **77** (2008) 051103 [arXiv:0711.4889].

[50] B. Aubert *et al.* (BaBar Collaboration), *Measurements of the $B \to X_s\gamma$ branching fraction and photon spectrum from a sum of exclusive final states*, Phys. Rev. D **72** (2005) 052004 [hep-ex/0508004].

[51] Y. Amhis *et al.* (Heavy Flavor Averaging Group), *Averages of b-hadron, c-hadron, and τ-lepton properties as of summer 2014*, [arXiv:1412.7515]; Additional information and updates: `http://www.slac.stanford.edu/xorg/hfag/` .

[52] P. Gambino and M. Misiak, *Quark mass effects in $\bar{B} \to X_s\gamma$*, Nucl.Phys. B **611** (2001) 338 [hep-ph/0104034].

[53] T. Aushev *et al.*, *Physics at Super B Factory*, [arXiv:1002.5012]; T. Abe (BELLE II Collaboration), *Belle II Technical Design Report*, [arXiv:1011.0352].

[54] I.I. Bigi *et al.*, *A QCD 'manifesto' on inclusive decays of beauty and charm*, DPF92 Proceedings (Batavia, November 1992) [hep-ph/9212227].

[55] A.F. Falk, M.E. Luke and M.J. Savage, *Nonperturbative contributions to the inclusive rare decays $B \to X_s\gamma$ and $B \to X_s l^+ l^-$*, Phys. Rev. D **49**, 3367 (1994) [hep-ph/9308288].

[56] G. Buchalla, G. Isidori and S.J. Rey, *Corrections of order Λ^2_{QCD}/m_c^2 to inclusive rare B decays* , Nucl. Phys. B **511**, 594 (1998) [hep-ph/9705253].

[57] Z. Ligeti, L. Randall and M.B. Wise, *Comment on nonperturbative effects in $\bar{B} \to X_s\gamma$*, Phys. Lett. B **402**, 178 (1997) [hep-ph/9702322].

[58] A.K. Grant, A.G. Morgan, S. Nussinov and R.D. Peccei, *Comment on nonperturbative $\mathcal{O}(1/m_c^2)$ corrections to $\Gamma(\bar{B} \to X_s\gamma)$*, Phys. Rev. D **56**, 3151 (1997) [hep-ph/9702380].

[59] M.B. Voloshin, *$\mathcal{O}(m_c^{-2})$ nonperturbative correction to the inclusive rate of the decay $B \to X_s\gamma$*, Phys. Lett. B **397**, 275 (1997) [hep-ph/9612483].

[60] A. Khodjamirian, R. Rueckl, G. Stoll and D. Wyler, *QCD estimate of the long-distance effect in $B \to K^*\gamma$*, Phys. Lett. B **402**, 167 (1997) [hep-ph/9702318].

[61] M. Benzke, S. J. Lee, M. Neubert and G. Paz, *Factorization at Subleading Power and Irreducible Uncertainties in $\bar{B} \to X_s\gamma$ Decay*, JHEP **1008** (2010) 099 [arXiv:1003.5012].

[62] T. Ewerth, P. Gambino and S. Nandi, *Power suppressed effects in $\bar{B} \to X_s\gamma$ at $\mathcal{O}(\alpha_s)$*, Nucl. Phys. B **830** (2010) 278 [arXiv:0911.2175].

[63] A. J. Buras and M. Misiak, *$\bar{B} \to X_s\gamma$ after completion of the NLO QCD calculations*, Acta Phys. Polon. B **33** (2002) 2597 [hep-ph/0207131].

[64] M. Czakon, P. Fiedler, T. Huber, M. Misiak, T. Schutzmeier and M. Steinhauser, *The $(Q_7, Q_{1,2})$ contribution to $\mathcal{B}(\bar{B} \to X_s\gamma)$ at $O(\alpha_s^2)$*, JHEP **1504** (2015) 168 [arXiv:1503.01791].

[65] M. Misiak, *QCD challenges in radiative B decays*, AIP Conf. Proc. 1317, 276 (2011) [arXiv:1010.4896];
M. Misiak, $\bar{B} \to s\gamma$ - *Current Status*, Acta Phys. Polon. B **40** (2009) 2987 [arXiv:0911.1651];
M. Misiak, *QCD Calculations of Radiative B Decays*, [arXiv:0808.3134].

[66] M. Misiak *et al.*, *Estimate of* $\mathcal{B}(\bar{B} \to X_s\gamma)$ at $O(\alpha_s^2)$, PRL **98**, 022002 (2007) [hep-ph/0609232].

[67] M. Misiak and M. Steinhauser, *NNLO QCD corrections to the barB* $\to X_s\gamma$ *matrix elements using interpolation in* m_c, Nucl.Phys. B**764** (2007) 62 [hep-ph/0609241].

[68] M. Misiak and M. Steinhauser, *Large-*m_c *Asymptotic Behaviour of* $O(\alpha_s^2)$ *Corrections to* $\bar{B} \to X_s\gamma$, Nucl.Phys. B **840** (2010) 271 [arXiv:1005.1173].

[69] F.V. Tkachov, *A Theorem on Analytical Calculability of Four Loop Renormalization Group Functions*, Phys. Lett. B **100** (1981) 65.

[70] K.G. Chetyrkin and F.V. Tkachov, *Integration by Parts: The Algorithm to Calculate beta Functions in 4 Loops*, Nucl. Phys. B **192** (1981) 159.

[71] S. Laporta, *High precision calculation of multiloop Feynman integrals by difference equations*, Int. J. Mod. Phys. A **15** (2000) 5087 [hep-ph/0102033].

[72] C. Anastasiou and A. Lazopoulos, *Automatic integral reduction for higher order perturbative calculations*, JHEP **0407** (2004) 046 [hep-ph/0404258].

[73] A.V. Smirnov, *Algorithm FIRE – Feynman Integral REduction*, JHEP **0810** (2008) 107 [arXiv:0807.3243].

[74] A.V. Smirnov, *FIRE5: A C++ implementation of Feynman Integral REduction*. Comput. Phys. Commun. **189** (2014) 182 [arXiv:1408.2372].

[75] A. von Manteuffel and C. Studerus, *Reduze 2 - Distributed Feynman Integral Reduction* [arXiv:1201.4330]; C. Studerus, *Reduze-Feynman Integral Reduction in C++*, Comput. Phys. Commun. **181** (2010) 1293 [arXiv:0912.2546].

[76] A. V. Kotikov, *Differential equations method: New technique for massive Feynman diagrams calculation*, Phys. Lett. B **254** (1991) 158.

[77] E. Remiddi, *Differential equations for Feynman graph amplitudes*, Nuovo Cim. A **110** (1997) 1435 [hep-th/9711188].

[78] T. Gehrmann and E. Remiddi, *Differential equations for two loop four point functions*, Nucl. Phys. B **580** (2000) 485 [hep-ph/9912329].

[79] G. 't Hooft and M. Veltman, *Regularization and Renormalization of Gauge Fields*, Nucl. Phys. B44 (1972) 189-213; P. Breitenlohner and D. Maison, *Dimensional Renormalization and the Action Principle*, Commun. Math. **52** (1977) 11;
P. Breitenlohner and D. Maison, *Dimensionally Renormalized Green's Functions For Theories With Massless Particles. 1*, Commun. Math. **52** (1977) 39;

P. Breitenlohner and D. Maison, *Dimensionally Renormalized Green's Functions For Theories With Massless Particles. 2*, Commun. Math. **52** (1977) 55;
For review see, G. Leibbrandt, *Introduction to the technique of dimensional regularization*, Rev. Mod. Phys. **47** (1975) 849.

[80] E. Stueckelberg, A. Petermann, *La normalisation des constantes dans la theorie des quanta*, Helv. Phys. Acta. **26** (1953) 499;
M. Gell-Mann, F. Low, *Quantum electrodynamics at small distances*, Phys. Rev. **95** (1954) 1300;
N. Bogolyubov, D. Shirkov, *Charge renormalization group in quantum field theory*, Nuovo Cim. **3** (1956) 845.

[81] K. G. Wilson, *Nonlagrangian Models Of Current Algebra*, Phys. Rev. **179** (1969) 1499.

[82] W. Zimmermann, *Normal Products And The Short Distance Expansion In The Perturbation Theory Of Renormalizable Interactions*, Annals Phys. **77** (1973) 570.

[83] T. Appelquist and J. Carazzone, *Infrared Singularities and Massive Fields*, Phys. Rev. D **11** (1975) 2856.

[84] B. Grzadkowski, M. Iskrzynski, M. Misiak, J. Rosiek, *Dimension-Six Terms in the Standard Model Lagrangian*, JHEP **1010** (2010) 085 [arXiv:1008.4884].

[85] P. Gambino and U. Haisch, *Complete electroweak matching for radiative B decays*, JHEP **10** (2001) 020 [hep-ph/0109058].

[86] K. Chetyrkin, M. Misiak and M. Münz, *Weak radiative B meson decay beyond leading logarithms*, Phys. Lett. B **400** (1997) 206 [Erratum-ibid. B **425** (1998) 414 [hep-ph/9612313].

[87] K. G. Chetyrkin, M. Misiak and M. Münz, $|\Delta F|$ *Nonleptonic Effective Hamiltonian in a Simpler Scheme*, Nucl. Phys. B **520** (1998) 279 [hep-ph/9711280].

[88] M. Benzke, S. J. Lee, M. Neubert and G. Paz, *Long-Distance Dominance of the CP Asymmetry in* $B \to X_{s,d}\gamma$ *Decays*, Phys. Rev. Lett. **106** (2011) 141801 [arXiv:1012.3167].

[89] F. J. Gilman and M. B. Wise, *Effective Hamiltonian for* $\Delta S = 1$ *Weak Nonleptonic Decays in the Six Quark Model*, Phys. Rev. D **20** (1979) 2392.

[90] C. Bobeth, M. Misiak and J. Urban, *Photonic penguins at two loops and* m_t *dependence of* $BR[B \to X_s l^+ l^-]$, Nucl. Phys. B **574** (2000) 291 [hep-ph/9910220].

[91] L.F. Abbott, *The Background Field Method Beyond One Loop*, Nucl.Phys. B **185** (1981) 189;
L.F. Abbott, *Introduction to the Background Field Method*, Acta Phys.Polon. B **13** (1982) 33.

[92] Pietro Antonio Grassi, *Renormalization of non-semisimple gauge models with the background field method*. Nucl. Phys. B **560** 499, 1999.

[93] M. Misiak and M. Steinhauser, *Three loop matching of the dipole operators for $b \to s\gamma$ and $b \to sg$*, Nucl. Phys. B **683**, 277 (2004) [hep-ph/0401041].

[94] Andrei I. Davydychev, J. B. Tausk, Nucl.Phys. **B397** (1993) 123.

[95] M. Steinhauser, *MATAD: A Program package for the computation of MAssive TADpoles*, Comput. Phys. Commun. **134** (2001) 335 [hep-ph/0009029].

[96] T. Hermann, M. Misiak and M. Steinhauser, *$\bar{B} \to X_s\gamma$ in the Two Higgs Doublet Model up to Next-to-Next-to-Leading Order in QCD*, JHEP **1211** (2012) 036 [arXiv:1208.2788].

[97] C. S. Lim and T. Inami, *Lepton flavor nonconservation and the mass generation mechanism for neutrinos*, Prog. Theor. Phys. **67** (1982) 1569.

[98] K. Adel and Y. P. Yao, *Exact α_s calculation of $b \to s + \gamma$, $b \to s + g$*, Phys. Rev. D **49** (1994) 4945 [hep-ph/9308349].

[99] C. Greub and T. Hurth, *Two loop matching of the dipole operators for $b \to s\gamma$ and $b \to sg$*, Phys. Rev. D **56** (1997) 2934 [hep-ph/9703349].

[100] A. J. Buras, A. Kwiatkowski and N. Pott, *Next-to-leading order matching for the magnetic photon penguin operator in the $B \to X_s\gamma$ decay* , Nucl. Phys. B **517** (1998) 353 [hep-ph/9710336].

[101] M. Ciuchini, G. Degrassi, P. Gambino and G. F. Giudice, *Next-to-leading QCD corrections to $B \to X_s\gamma$: Standard model and two Higgs doublet model*, Nucl. Phys. B **527** (1998) 21 [hep-ph/9710335].

[102] M. J. Dugan and B. Grinstein, *On the vanishing of evanescent operators*, Phys. Lett. B **256** (1991) 239.

[103] A. J. Buras and P. H. Weisz, *QCD nonleading corrections to weak decays in dimensional regularization and 't Hooft-Veltman schemes*, Nucl. Phys. B **333** (1990) 66.

[104] S. Herrlich and U. Nierste, *Evanescent operators, scheme dependences and double insertions*, Nucl. Phys. B **455** (1995) 39 [hep-ph/9412375].

[105] M. Czakon, U. Haisch and M. Misiak, *Four-Loop Anomalous Dimensions for Radiative Flavour-Changing Decays*, JHEP **0703**, 008 (2007) [hep-ph/0612329].

[106] K. G. Chetyrkin, M. Misiak and M. Munz, *Beta functions and anomalous dimensions up to three loops*, Nucl. Phys. B **518** (1998) 473 [hep-ph/9711266].

[107] M. Czakon, Nucl. Phys. B **710** (2005) 485 [hep-ph/0411261].

[108] M. Misiak and M. Münz, *Two-loop mixing of dimension-five flavor-changing operators*, Phys. Lett. B **344** (1995) 308 [hep-ph/9409454].

[109] K. G. Chetyrkin, V. A. Smirnov, *R^* Operation Corrected*, Phys. Lett. B **144** (1984) 419.

[110] P. Gambino, M. Gorbahn and U. Haisch, *Anomalous dimension matrix for radiative and rare semileptonic B decays up to three loops*, Nucl. Phys. B **673** (2003) 238 [hep-ph/0306079].

[111] M. Gorbahn and U. Haisch, *Effective Hamiltonian for non-leptonic $|\Delta F| = 1$ decays at NNLO in QCD*, Nucl. Phys. B **713**, 291 (2005) [hep-ph/0411071].

[112] M. Gorbahn, U. Haisch and M. Misiak, *Three-loop mixing of dipole operators*, Phys. Rev. Lett. **95**, 102004 (2005) [hep-ph/0504194].

[113] M. Misiak, Phys. Lett. B **269** (1991) 161.

[114] A.J. Buras, M. Misiak, M. Münz and S. Pokorski, *Theoretical uncertainties and phenomenological aspects of $B \to X_s\gamma$ decay*, Nucl. Phys. B **424** (1994) 374 [hep-ph/9311345].

[115] A. Kagan, M. Neubert, *QCD Anatomy of $B \to X_s\gamma$ Decays*, Eur. Phys. J. C **7** (1999) 5, [hep-ph/9805303].

[116] Z. Ligeti, I. W. Stewart, F.J. Tackmann, *Treating the b quark distribution function with reliable uncertainties*, Phys. Rev. D **78** (2008) 114014 [arXiv:0807.1926]

[117] J.R. Andersen, E. Gardi, *Radiative B decay spectrum: DGE at NNLO*, JHEP **0701** (2007) 029 [hep-ph/0609250].

[118] F. U. Bernlochner, H. Lacker, Z. Ligeti, I. W. Stewart, F. J. Tackmann and K. Tackmann, *Towards a global fit to extract the $B \to X_s\gamma$ decay rate and V_{ub}*, PoS ICHEP **2010** (2010) 229 [arXiv:1011.5838].

[119] F. U. Bernlochner, H. Lacker, Z. Ligeti, I. W. Stewart, F. J. Tackmann and K. Tackmann, *Status of SIMBA*, arXiv:1101.3310.

[120] F. U. Bernlochner *et al.* [SIMBA Collaboration], *A model independent determination of the $B \to X_s\gamma$ decay rate*, PoS ICHEP **2012** (2013) 370 [arXiv:1303.0958].

[121] I. R. Blokland, A. Czarnecki, M. Misiak, M. Slusarczyk and F. Tkachov, *The electromagnetic dipole operator effect on $\bar{B} \to X_s\gamma$ at $\mathcal{O}(\alpha_s^2)$* , Phys. Rev. D **72**, 033014 (2005) [hep-ph/0506055].

[122] A. Czarnecki and W. Marciano, *Electroweak radiative corrections to $b \to s\gamma$*, Phys. Rev. Lett. **81** (1998) 277 [hep-ph/9804252].

[123] M. Kamiński, M. Misiak and M. Poradziński, *Tree-level contributions to $\bar{B} \to X_s\gamma$*, Phys. Rev. D **86** (2012) 094004 [arXiv:1209.0965].

[124] T. Huber, M. Poradziński and J. Virto, *Four-body contributions to $Brightarrow X_s\gamma$ at NLO*, JHEP **1501** (2015) 115 [arXiv:1411.7677].

[125] A. Ali and C. Greub, *Inclusive photon energy spectrum in rare B decays*, Z. Phys. C **49** (1991) 431;
A. Ali and C. Greub, *A Profile of the final states in $B \to +X_s\gamma$ and an estimate of the branching ratio $BR(B \to K^* + \gamma)$*, Phys. Lett. B **259** (1991) 182;
A. Ali and C. Greub, *Photon energy spectrum in $B \to X_s + \gamma$ and comparison with data*, Phys. Lett. B **361** (1995) 146 [hep-ph/9506374].

[126] N. Pott, *Bremsstrahlung corrections to the decay $b \to s\gamma$*, Phys. Rev. D **54** (1996) 938 [hep-ph/9512252].

[127] C. Greub, T. Hurth and D. Wyler, *Virtual $\mathcal{O}(\alpha_s)$ corrections to the inclusive decay $b \to s\gamma$*, Phys. Rev. D **54** (1996) 3350 [hep-ph/9603404].

[128] A. J. Buras, A. Czarnecki, M. Misiak and J. Urban, *Two loop matrix element of the current current operator in the decay $\bar{B} \to X_s\gamma$*, Nucl. Phys. B **611** (2001) 488 [hep-ph/0105160].

[129] A. J. Buras, A. Czarnecki, M. Misiak and J. Urban, *Completing the NLO QCD calculation of $\bar{B} \to X_s\gamma$)*, Nucl. Phys. B **631** (2002) 219 [hep-ph/0203135].

[130] A. L. Kagan and M. Neubert, *QCD anatomy of $B \to X_s\gamma$ decays*, Eur. Phys. J. C **7** (1999) 5.

[131] K. Baranowski and M. Misiak, *The $\mathcal{O}(\alpha_{em}/\alpha_s)$ correction to $BR[B \to X_s\gamma]$*, Phys. Lett. B **483** (2000) 410.

[132] P. Gambino and U. Haisch, *Electroweak effects in radiative B decays*, JHEP **09** (2000) 001 [hep-ph/0007259].

[133] A. Strumia, *Two loop heavy top corrections to the $b \to s\gamma$ decay*, Nucl. Phys. B **532** (1998) 28 [hep-ph/9804274].

[134] T. van Ritbergen, *The Second order QCD contribution to the semileptonic $b \to u$ decay rate*, Phys. Lett. B **454**, 353 (1999) [hep-ph/9903226].

[135] Z. Ligeti, M.E. Luke, A.V. Manohar and M.B. Wise, *The $B \to X_s\gamma$ Photon Spectrum*, Phys. Rev. D **60**, 034019 (1999) [hep-ph/9903305].

[136] K. Bieri, C. Greub and M. Steinhauser, *Fermionic NNLL corrections to $b \to s\gamma$*, Phys. Rev. D **67** (2003) 114019 [hep-ph/0302051].

[137] A. Ferroglia and U. Haisch, *Chromomagnetic Dipole-Operator Corrections in $\bar{B} \to X_s\gamma$ at $\mathcal{O}(\beta_0\alpha_s^2)$*, Phys.Rev. D **82** (2010) 094012 [arXiv:1009.2144].

[138] M. Misiak and M. Poradziński, *Completing the Calculation of BLM corrections to $\bar{B} \to X_s\gamma$*, Phys.Rev. D **83** (2011) 014024 [arXiv:1009.5685].

[139] S. J. Brodsky, G. P. Lepage and P. B. Mackenzie, *On the Elimination of Scale Ambiguities in Perturbative Quantum Chromodynamics*, Phys. Rev. D **28**, 228 (1983).

[140] K. Melnikov and A. Mitov, *The photon energy spectrum in $B \to X_s + \gamma$ in perturbative QCD through $\mathcal{O}(\alpha_s^2)$*, Phys. Lett. B **620**, 69 (2005) [hep-ph/0505097].

[141] H. M. Asatrian, A. Hovhannisyan, V. Poghosyan, T. Ewerth, C. Greub and T. Hurth, *NNLL QCD Contribution of the Electromagnetic Dipole Operator to $\Gamma(\bar{B} \to X_s\gamma)$* , Nucl. Phys. B **749**, 325 (2006) [hep-ph/0605009].

[142] H. M. Asatrian, T. Ewerth, A. Ferroglia, P. Gambino and C. Greub, *Magnetic dipole operator contributions to the photon energy spectrum in $\bar{B} \to X_s\gamma$ at $\mathcal{O}(\alpha_s^2)$*, Nucl. Phys. B **762**, 212 (2007) [hep-ph/0607316].

[143] H. M. Asatrian, T. Ewerth, H. Gabrielyan and C. Greub, *Charm quark mass dependence of the electromagnetic dipole operator contribution to $\bar{B} \to X_s\gamma$ at $\mathcal{O}(\alpha_s^2)$*, Phys. Lett. B **647**, 173 (2007) [hep-ph/0611123].

[144] H. M. Asatrian, T. Ewerth, A. Ferroglia, C. Greub and G. Ossola, *Complete (Q_7, Q_8) contribution to $\bar{B} \to X_s\gamma$ at $\mathcal{O}(\alpha_s^2)$*, Phys. Rev. D **82** (2010) 074006 [arXiv:1005.5587].

[145] T. Ewerth, *Fermionic corrections to the interference of the electro- and chromomagnetic dipole operators in $\bar{B} \to X_s\gamma$ at $\mathcal{O}(\alpha_s^2)$*, Phys. Lett. B **669**, 167 (2008) [arXiv:0805.3911].

[146] R. Boughezal, M. Czakon and T. Schutzmeier, *NNLO fermionic corrections to the charm quark mass dependent matrix elements in $\bar{B} \to X_s\gamma$*, JHEP **0709** (2007) 072 [arXiv:0707.3090].

[147] D. A. Ross and J. C. Taylor, *Renormalization Of A Unified Theory Of Weak And Electromagnetic Interactions*, Nucl. Phys. B **51** (1973) 125; [Erratum ibid. B **58** (1973) 643].

[148] J. Charles *et al.*, *Current status of the Standard Model CKM fit and constraints on $\Delta F = 2$ New Physics*, Phys. Rev. D **91** (2015) 7, 073007, [arXiv:1501.05013].

[149] http://www.utfit.org/UTfit/.

[150] A. Kapustin, Z. Ligeti and H.D. Politzer, *Leading logarithms of the b quark mass in inclusive $B \to X_s\gamma$ decay*, Phys. Lett. B **357** (1995) 653 [hep-ph/9507248].

[151] H. M. Asatrian and C. Greub, *Tree-level contribution to $\bar{B} \to X_d\gamma$ using fragmentation functions*, Phys. Rev. D **88** (2013) 074014 [arXiv:1305.6464].

[152] H.M. Asatrian, C. Greub, A. Hovhannisyan, T. Hurth, V. Poghosyan, *Reduction of charm quark mass scheme dependence in $\bar{B} \to X_s\gamma$ at the NNLL level*, Phys.Lett. B **619** (2005) 322 [hep-ph/0505068].

[153] V. A. Smirnov, *Evaluating Feynman integrals*, Springer, Berlin, 2004;
V. A. Smirnov, *Feynman Integral Calculus*, Springer, Berlin, 2006;
V. A. Smirnov, *Analytic tools for Feynman integrals*, Springer, Berlin, 2012.

[154] R.E. Cutkosky, *Singularities and Discontinuities of Feynman Amplitudes*, J. Math. Phys. **1** (1960) 429.

[155] R. J. Eden, P. V. Landshoff, D. I. Olive and J. C. Polkinghore, *The analytic S-matrix*, Cambridge University Press, (2002);
N. Nakanishi, *Graph Theory and Feynman Integrals*, Gordon and Breach, New York, (1971).

[156] L. D. Landau, *On analytic properties of vertex parts in quantum field theory*, Nucl. Phys. **13** (1959) 181.

[157] S. Weinberg, *High-Energy Behavior in Quantum Field Theory*, Phys. Rev. **118** (1960) 3.

[158] T. Hahn, *Generating Feynman diagrams and amplitudes with FeynArts 3*, Comput. Phys. Commun. **140** (2001) 418 [hep-ph/0012260].

[159] G. Passarino and M. J. G. Veltman, *One Loop Corrections for e^+e^- Annihilation into $\mu^+\mu^-$ in the Weinberg Model*, Nucl. Phys. B **160** (1979) 151.

[160] O.V. Tarasov, *Connection between Feynman integrals having different values of the space-time dimension*, Phys. Rev. D **54** (1996) 6479.

[161] A.V. Smirnov and A.V. Petukhov, *The Number of Master Integrals is Finite*, Lett. Math. Phys. **97** (2011) 37 [arXiv:1004.4199].

[162] C. Anastasiou and K. Melnikov, Nucl. Phys. B **646** (2002) 220 [hep-ph/0207004].

[163] Gehrmann and Remiddi, *Differential Equations for Two-Loop Four-Point Function*, Nucl. Phys. B **580** (2000) 485 [hep-ph/9912329].

[164] J. Gluza, K. Kajda, and D. A. Kosower, *Towards a Basis for Planar Two-Loop Integrals*, Phys. Rev. D **83** (2011) 045012 [arXiv:1009.0472].

[165] E. Remiddi and L. Tancredi, *Schouten identities for Feynman graph amplitudes; the Master Integrals for the two-loop massive sunrise graph*, Nucl. Phys. B **880** (2014) 343 [arXiv:1311.3342].

[166] K. G. Chetyrkin, M. Faisst, Christian Sturm, and M. Tentyukov, *e-finite basis of master integrals for the integration-by-parts method*, Nucl. Phys. B7 **42** (2006) 208 [hep-ph/0601165].

[167] E.E. Boos and A.I. Davydychev *A method of calculating massive Feynman integrals*, Theor. Math. Phys. **89** (1992) 1052.

[168] V. A. Smirnov, *Analytical result for dimensionally regularized massless on-shell double box*, Phys. Lett. B **460** (1999) 397.

[169] J. B. Tausk, *Non-planar massless two-loop Feynman diagrams with four on-shell legs*, Phys. Lett. B **469** (1999) 225.

[170] T. Binoth and G. Heinrich, *An automatized algorithm to compute infrared divergent multi-loop integrals*, Nucl. Phys. B **585** (2000) 741 [arXiv:hep-ph/0004013].

[171] S. Moch, P. Uwer and S. Weinzierl, *Nested sums, expansion of transcendental functions and multiscale multiloop integrals*, J. Math. Phys. **43** (2002) 3363-3386 [hep-ph/0110083].

[172] S. Laporta, *High precision calculation of multiloop Feynman integrals by difference equations*, Int. J. Mod. Phys. A **15** (2000) 5087 [hep-ph/0102033].

[173] A. Smirnov, V. Smirnov, M. Tentyukov, *FIESTA 2: Parallelizeable multiloop numerical calculations*, Comput.Phys.Commun. **182** (2011) 790 [arXiv:0912.0158];
A. Smirnov, M. Tentyukov, *Feynman Integral Evaluation by a Sector decomposiTion Approach (FIESTA)*, Comput.Phys.Commun. **180** (2009) 735 [arXiv:0807.4129];
A. V. Smirnov, *FIESTA 3: cluster-parallelizable multiloop numerical calculations in physical regions* [arXiv:1312.3186].

[174] E. Remiddi and J. A. M. Vermaseren, *Harmonic polylogarithms*, Int. J. Mod. Phys. A **15** (2000) 725 [hep-ph/9905237].

[175] L. Lewin, *Polylogarithms and associated functions*, North-Holland, New York (1981).

[176] E. Panzer, *HyperInt*, *Algorithms for the symbolic integration of polylogarithms with applications to Feynman integrals*, Comput. Phys. Commun. **188** (2014) 148 [arXiv:1403.3385].

[177] J. Gluza, K. Kajda, T. Riemann, *AMBRE: A Mathematica package for the construction of Mellin-Barnes representations for Feynman integrals*, Comput. Phys. Commun. **177** (2007) 879 [arXiv:0704.2423].

[178] `MB Tools, https://mbtools.hepforge.org`

[179] M. Czakon, *Automatized analytic continuation of Mellin-Barnes integrals*, Comput. Phys. Commun. **175** (2006) 559 [arXiv:hep-ph/0511200]

[180] A.V. Smirnov, V.A. Smirnov, *On the Resolution of Singularities of Multiple Mellin-Barnes Integrals* Eur. Phys. J. C **62** (2009) 445 [arXiv:0901.0386]

[181] T. Seidensticker, *Automatic application of successive asymptotic expansions of Feynman diagrams*, hep-ph/9905298;
R. Harlander, T. Seidensticker and M. Steinhauser, *Complete corrections of $\mathcal{O}(\alpha\alpha_s)$ to the decay of the Z boson into bottom quarks*, Phys. Lett. B **426**, 125 (1998) [hep-ph/9712228].

[182] J. M. Henn, *Multiloop integrals in dimensional regularization made simple*, Phys.Rev.Lett. **110** (2013) 251601 [arXiv:1304.1806].

[183] J. M. Henn, A. V. Smirnov, and V. A. Smirnov, *Analytic results for planar three-loop four-point integrals from a Knizhnik-Zamolodchikov equation*, JHEP **1307** (2013) 128 [arXiv:1306.2799].
J. M. Henn and V. A. Smirnov, *Analytic results for two-loop master integrals for Bhabha scattering I*, JHEP **1311** (2013) 041 [arXiv:1307.4083].
J. M. Henn, A. V. Smirnov, and V. A. Smirnov, *Evaluating single-scale and/or non-planar diagrams by differential equations*, JHEP **1403** (2014) 088 [arXiv:1312.2588].
M. Argeri, S. Di Vita, P. Mastrolia, E. Mirabella, J. Schlenk, et al., *Magnus and Dyson Series for Master Integrals*, JHEP **1403** (2014) 082 [arXiv:1401.2979].
J. M. Henn, K. Melnikov, and V. A. Smirnov, *Two-loop planar master integrals for the production of off-shell vector bosons in hadron collisions*, JHEP **1405** (2014) 090 [arXiv:1402.7078].
Guido Bell and Tobias Huber, *Master integrals for the two-loop penguin contribution in non-leptonic B-decays*, [arXiv:1410.2804];
R. N. Lee, *Reducing differential equations for multiloop master integrals*, [arXiv:1411.0911].

[184] A.I. Davydychev, A. G. Grozin, Phys. Rev. D **59** 054023 (1999) [hep-ph/9809589].

[185] Andrei I. Davydychev, M.Yu. Kalmykov, Nucl. Phys. B **605** 266 (2001) [hep-th/0012189].

[186] P.N. Brown, A.C. Hindmarsh and G.D. Byrne, `ZVODE, http://netlib.sandia.gov/ode/zvode.f` .

[187] A.C. Hindmarsch, `ODEPACK, http://www.netlib.org/odepack` .

[188] D.H. Bailey *et al.* `QD` library, `http://crd-legacy.lbl.gov/ dhbailey/mpdist` .

[189] S. Borowka, J. Carter, and G. Heinrich, *Numerical Evaluation of Multi-Loop Integrals for Arbitrary Kinematics with SecDec 2.0*, Comput. Phys. Commun. **184** (2013) 396 [arXiv:1204.4152];
J. Carter and G. Heinrich, *SecDec: A general program for sector decomposition*, Comput. Phys. Commun. **182** (2011) 1566 [arXiv:1011.5493].

[190] T. Hahn, *CUBA: A Library for multidimensional numerical integration*, Comput. Phys. Commun. **168** (2005) 78.

[191] M. Poradziński, private communication.

[192] M. Misiak, *The $b \to se^+e^-$ and $b \to s\gamma$ decays with Next-To-Leading Logarithmic QCD corrections*, Nucl. Phys. B **393** (1993) 23.

[193] `DiaGen/IdSolver`, M. Czakon, *unpublished*

[194] T. Huber, D. Maitre, *HypExp: A Mathematica package for expanding hypergeometric functions around integer-valued parameters* , Comput. Phys. Commun. **175** (2006) 122 [hep-ph/0507094].

[195] A. Erdelyi (Ed.), Higher Transcendental Functions, vol.1 (McGraw-Hill, New York, 1953); L.J. Slater, Generalized Hypergeometric Functions (Cambridge University Press, Cambridge 1966).

[196] http://functions.wolfram.com/07.31.17.0022.01 .